ED n° 432 : « Sciences des Métiers de l'Ingénieur »

N° attribué par la bibliothèque

T H E S E

pour obtenir le grade de

DOCTEUR DE L'ECOLE NATIONALE SUPERIEURE DES MINES DE PARIS

Spécialité "Energétique"

présentée et soutenue publiquement par
Bernard AOUN

le 13 novembre 2008

MICRO-COGENERATION POUR LES BATIMENTS RESIDENTIELS FONCTIONNANT AVEC DES ENERGIES RENOUVELABLES (MICRO COMBINED HEAT AND POWER OPERATING ON RENEWABLE ENERGY FOR RESIDENTIAL BUILDING)

Directeur de thèse : Denis CLODIC

Jury :

M. B. PEUPORTIER – Ecole des Mines de Paris ..... Président
M. P. STOUFFS – Université de Pau et des Pays de l'Adour ..... Rapporteur
M. G. DESCOMBES – Ecole Nationale Supérieure des Arts et Métiers Rapporteur
M. O. TERZIDIS –SAP centre de recherche CEC Karlsruhe .....Examinateur
M. D. CLODIC – Ecole des Mines de Paris .....Examinateur

Acknowledgements

This thesis is one of the fruits of the followed research work carried out in the Center for energy and processes at the Ecole Nationale Supérieure des Mines de Paris. During the course of my thesis work, many people have been resourceful to help me. Without their guidance, help and patience, I would have never been able to accomplish my thesis. I would like to take this opportunity to acknowledge some of them.

Firstly, I would like to gratefully acknowledge the enthusiastic supervision of Denis Clodic during this work, for his support, his sound advice, and for his confidence on the research direction and guidance, and for the flexibility and responsibility he granted to me.

I would like to express my gratitude to Anne-Marie Pougin, for always being available, and for her proof reading.

I would like to express my gratitude to the examinations board and reporters. I appreciate their patience while reading and evaluating this dissertation.

I would like to give my special thanks to Prof. Georges DESCOMBES, for having given me many valuable comments and great encouragement.

I would like to thank Prof. Pascal STOUFFS for being interested in my work and accepting to be in the jury.

I would like to express my gratitude to Dr. Bruno PEUPORTIER for his support and for accepting to be the president of the Jury.

I acknowledge the group ERGION presented by Dr. Orestis TERZIDIS for its financial support during the development of the experimentation works during the first part of this thesis.

I would like to express my sincere gratitude to Dr. Khalil Khoury, who led me to the research domain of thermodynamics and energy conversion.

Thanks to all of the colleagues in CEP, for their grateful help, and for sharing their work and life experiences.
Rudy, Elie, Georges, Paul, Maria, Stéphane, Elias, Franck, Habib; you make part of my success.

I would like to thank all my close friends from Lebanon, for their continuous moral support.

Last but not least, thanks to Grece, for her love and for always standing by my side and giving me encouragement. Thanks to my parents for their love and support.

Résumé

En français

Micro-cogénération pour les bâtiments résidentiels fonctionnant avec des énergies renouvelables

Introduction

En France, le secteur bâtiment est le plus gros consommateur d'énergie parmi tous les secteurs économiques, avec 70 millions de tonnes d'équivalent pétrole, représentant 43 % de l'énergie totale consommée. Cette énergie consommée entraîne l'émission de 120 millions de tonnes de CO_2 représentant 25 % des émissions nationales de carbone.

Dans le secteur bâtiment, la consommation moyenne annuelle d'énergie est proche de 240 kWh_{ep}/m^2. La nécessité de réduire la quantité de CO_2 émise et l'épuisement progressif des ressources imposent une réduction des consommations moyenne d'énergie. L'objectif fixé par le gouvernement français est d'atteindre 50 kWh_{ep}/m^2.an pour les besoins de chauffage et d'eau chaude sanitaire et de 100 kWh_{ep}/m^2.an pour les besoins totaux.

La problématique générale dans le secteur du bâtiment est liée à la fois à la réduction des gaz à effet de serre et à la réduction des consommations. En conséquence, une forte isolation des murs ne suffit pas pour atteindre l'objectif souhaité, ainsi l'introduction des systèmes de chauffage à haute performance énergétique est indispensable. Ces systèmes peuvent réduire les consommations énergétiques non renouvelable de façon suffisante s'ils fonctionnent avec des énergies renouvelables intermittentes et non intermittentes.

L'objectif de ce travail est d'identifier le potentiel d'intégration de la micro-cogénération fonctionnant avec deux types d'énergies renouvelables dans le secteur bâtiment. Les différentes technologies de micro-cogénération seront comparées afin de choisir celle qui peut s'adapter le mieux à notre application. Ce mémoire présente une étude technique de plusieurs technologies qui peuvent être utilisées, et réalise une conception détaillée d'un système Rankine ainsi que son optimisation énergétique. Une étude économique est réalisée pour identifier le prix actualisé de l'électricité produite pour rendre ce système faisable du point de vue économique.

Chapitre 1. Micro-cogénération dans les bâtiments résidentiels

Le premier chapitre pose la problématique et les enjeux liés aux gisements d'énergie dans le secteur du bâtiment, les méthodes pour limiter les besoins énergétiques liés au chauffage, puis un aperçu des différentes technologies de micro-cogénération adaptées aux bâtiments. L'analyse du potentiel d'utilisation des énergies renouvelables pour la micro-cogénération a été menée du point de vue de l'efficacité énergétique et du point de vue économique.

1.1. Problématique générale et enjeux

Les besoins de chauffage et d'eau chaude sanitaire représentent plus de 80 % des besoins totaux. Pour limiter les besoins de chauffage, la réglementation thermique française est régulièrement mise à jour en vue de réduire drastiquement la consommation énergétique aussi bien des bâtiments neufs que des bâtiments existants.

Pour atteindre les objectifs définis par le gouvernement, de division des émissions de CO_2 par 4 d'ici 2050, un objectif technique est à l'ordre du jour : construire des maisons à énergie positive. Cette solution technique ne peut être réalisée que par une production locale d'énergie pour satisfaire les besoins, et l'électricité produite localement est envoyée sur réseau électrique. La famille de solutions techniques proposées dans cette thèse est celle de la micro-cogénération. En France, l'énergie électrique contient peu de CO_2 car plus de 75 % est d'origine nucléaire. Ainsi la micro-cogénération fonctionnant avec des énergies fossiles peut présenter des émissions de CO_2 supérieures au mix énergétique général. La

micro-cogénération utilisant des énergies renouvelables présente une solution adéquate pour limiter les émissions de CO_2.

1.2. Micro-cogénération

La micro-cogénération est la production simultanée d'énergie électrique et thermique. Elle peut ne pas présenter toujours la solution optimale du point de vue énergétique et environnemental. Les différents facteurs qui affectent la faisabilité des systèmes de micro-cogénération sont :

- la haute efficacité énergétique des grandes centrales de production électrique
- la faible teneur en CO_2 de l'électricité d'origine nucléaire
- les hauts rendements des chaudières à gaz à condensation
- les besoins de stockage thermique et électrique associés aux fluctuations de la demande
- le coût des systèmes de micro-cogénération
- l'absence de technologie mature de micro-cogénération utilisant les énergies renouvelables.

Plusieurs technologies de micro-cogénération sont disponibles sur le marché.

- **Moteur à combustion interne** : c'est une technologie mature déjà commercialisée, le rendement de ces moteurs est relativement basse (~ 26 %) pour les petits modules < 10 kW_{el}. Ces moteurs présentent comme inconvénient la difficulté d'utiliser des énergies renouvelables car ils sont à combustion interne ; seuls les biocarburants peuvent donc être utilisés.

- **Moteur Stirling** : ces moteurs présentent l'avantage d'une combustion externe d'où la possibilité d'utiliser différents combustibles y compris le bois. Ces moteurs sont encore dans la phase de R&D, avec un rendement médiocre comparé à leur performance théorique, et ont un coût assez élevé. Ils constituent une solution très adaptée à notre besoin si ces modules peuvent fonctionner avec des températures basses ~ 200 °C, avec une performance énergétique suffisante.

- **Pile à combustible :** ces technologies sont dans la phase de recherche ; elles peuvent présenter un rendement électrique assez élevé mais sont loin d'être compétitives du fait de leurs prix très élevés.

- **Cycle Rankine Organique :** les cycles Rankine comme les moteurs Stirling présentent l'avantage d'une combustion externe d'où la possibilité d'utiliser une plus grande variété de sources d'énergie. Ce système présente des rendements assez modérés et dépend du niveau de température des sources d'énergie. Par contre, ils peuvent être développés avec des composants déjà disponibles sur le marché à des coûts acceptables.

Le tableau 1.1 présente les différentes caractéristiques des systèmes de micro-cogénération. Le cycle ORC reste le plus convenable pour être utilisé avec des énergies renouvelables à basse température avec un coût acceptable.

Les systèmes de micro-cogénération peuvent être comparés sous trois critères différents : énergétique, environnemental et économique.

Table 1.1 – Systèmes de micro-cogénération disponible sur le marché [PEH06, PAE06a]				
Paramètre	ICE	Pile à combustible	Moteur Stirling	RC–ORC
Puissance électrique (kW_{el})	1-10	0.5-10	1-10	0.5-10
Efficacité électrique (% HHV)	20-40	30-50 PEMFC 40-50 SOFC	10-25 35-50 (potentiel)	10-20
Efficacité de récupération d'énergie (% HHV)	50-60	40-60	40-60	--
Température de la source d'énergie disponible (°C)	85-100	80-100 PEMFC 950-1000 SOFC	200	--
Efficacité globale	80-90	70-90 PEMFC 70-95 SOFC	65-95	--
Puissance de chaleur (kW_{th})	3-30	1-30	3-15	--
Disponibilité (%)	85-98	95	85-90	--
Efficacité à charge partielle	modeste	tres bon	moyenne	--
Coût de maintenance (€/kWh_{el})	0.008-0.012	0.016-0.024	0.005-0.01	--
Emissions	modestes	négligeables	moyennes	--
Cout d'investissement (€/kW_{el})	785-2200	--	--	--
Type de fuel utilisé	Diesel, Gaz	--	Gaz, granules de bois, solaire	Diesel, Gaz, granulé de bois, solaire

a. Impact énergétique

L'économie d'énergie primaire est calculée par l'équation 1.1

$$PE_c = \frac{E_{th}}{\eta_{th}} K_{fuel} + \left(E_{el} - E_{el,mc}\right) K_{el} \qquad (1.1)$$

La figure 1.1 montre une comparaison des différents systèmes de chauffage du point de vue énergétique. Le système de référence est une chaudière à fuel avec un rendement thermique de 80 % et une production électrique de rendement de 0,38 (1/2.58). Les résultats montrent que le système de micro-cogénération fonctionnant avec du bois peut engendrer 30 % d'économie d'énergie primaire. Si le système de micro-cogénération fonctionne avec du bois et de l'énergie solaire, une économie d'énergie de plus de 80 % peut être atteinte. L'économie d'énergie primaire dépend principalement du rendement électrique et thermique, et de la part de l'énergie solaire utilisée.

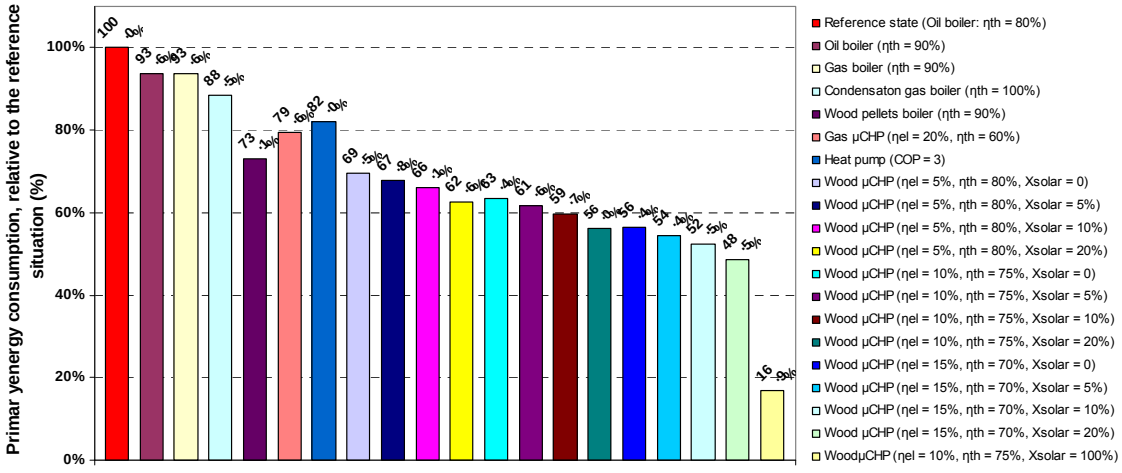

Figure 1.1 – Economies d'énergie primaire pour différents systèmes de chauffage

b. Impact environnemental

Le deuxième critère de sélection des systèmes de chauffage pour les bâtiments résidentiels est un critère environnemental basé sur la quantité de CO_2 émise. La figure 1.2 présente les résultats des émissions de CO_2. La micro-cogénération à bois peut réduire les émissions de CO_2 de plus de 80 % par rapport à une chaudière fioul et peut atteindre 94 %, si l'énergie primaire utilisée est l'énergie solaire. En comparant les différents systèmes étudiés, on peut voir que la pompe à chaleur présente un potentiel élevé de réduction des émissions de CO_2 car le contenu de CO_2 dans l'électricité nucléaire produite en France est très bas et impose donc, du point de vue environnemental, des systèmes de cogénération fonctionnant à base d'énergies renouvelables.

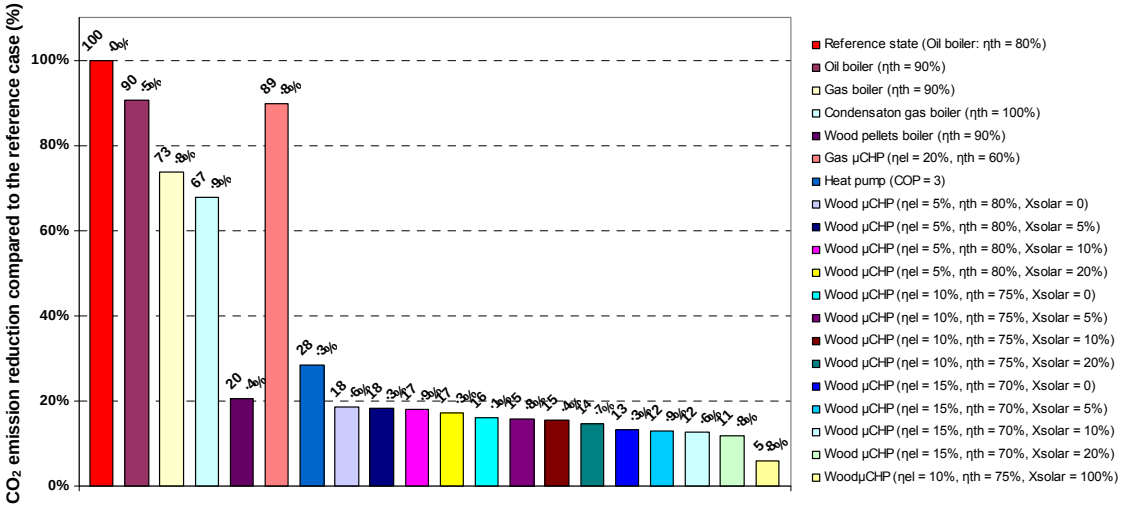

Figure 1.2 – Réductions d'émissions du CO_2 pour différents systèmes de chauffage

c. Impact économique

Le critère économique reste un des critères les plus importants pour la micro-cogénération car, en général, c'est ce critère qui définit la faisabilité ou non de ces systèmes. Une étude a été menée pour calculer le coût d'électricité actualisé d'un système de micro-cogénération et pour comparer les niveaux d'aides financières qui peuvent rendre ce système économiquement viable. Les résultats sont présentés à la figure 1.3. La période de fonctionnement annuel de la micro-cogénération est un paramètre décisif pour la rentabilité du système. A partir de 3 000 heures de fonctionnement annuel, le prix d'électricité devient proche de 40 c€/kWh$_{el,}$. Un accroissement de 10 % du prix de chauffage évité lors de l'utilisation de la micro-cogénération, présente une condition nécessaire qui peut influencer directement l'intégration de ces systèmes dans le marché.

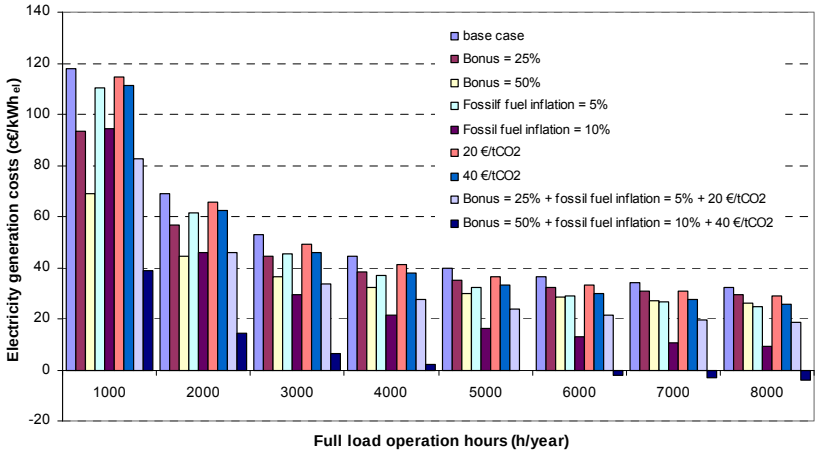

Figure 1.3 – Coût de production électrique actualisé (2007) pour différents systèmes de chauffage

1.3. Micro-cogénération fonctionnant avec des énergies renouvelables

La figure 1.4 présente le schéma de fonctionnement d'un système de micro-cogénération utilisant un cycle Rankine fonctionnant à l'énergie solaire et utilisant la combustion biomasse. Le système comprend trois vannes trois voies qui permettent d'assurer le fonctionnement du système sous trois configurations différentes.

1 – Fonctionnement à l'énergie solaire seule : le fluide caloporteur passe dans les capteurs solaires, et la chaudière à bois est bi-passée.
2 – Fonctionnement avec la combustion bois seule : les capteurs solaires sont bipassés, le fluide caloporteur circule seulement dans la chaudière biomasse.
3 - Fonctionnement hybride : le fluide caloporteur passe dans le capteur solaire pour être préchauffé et circule après dans la chaudière bois pour atteindre la température souhaitée. Les vannes 1 et 2 peuvent être partiellement ouvertes pour faire passer une partie du fluide caloporteur dans les capteurs solaires pour limiter les pertes de charges dans ces capteurs.

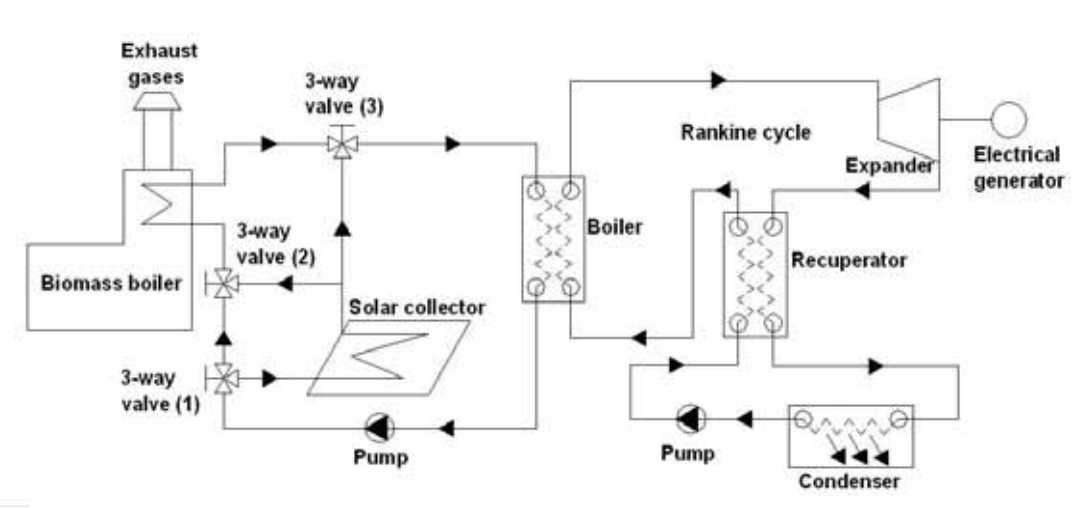

Figure 1.4 – Schéma du principe de la micro-cogénération fonctionnant avec l'énergie solaire et la combustion du bois

Les différents défis techniques qui doivent être surmontés pour mettre ce système en application réelle sont :

- la sélection des différents fluides de travail
- le développement d'une mini-turbine pour les systèmes de micro-cogénération basés sur des cycles Rankine
- une adaptation des échangeurs de chaleur et des chaudières à bois à cette application
- une sélection des capteurs solaires fonctionnant à des températures élevées sans dispositif de suivi du mouvement du soleil.

Chapitre 2. Fluide de travail pour un Cycle Rankine Organique à basse température

Le cycle thermodynamique ainsi que la sélection des différents composants de la micro-cogénération dépendent largement du choix du fluide thermodynamique. Dans ce chapitre, une méthode de sélection des fluides de travail a été développée afin d'identifier les fluides les plus adaptés à cette application. Cette méthode est basée sur des critères énergétiques, environnementaux et de sécurité.

2.1. Méthode de sélection

Différentes études ont démontré que l'utilisation des fluides organiques peut offrir une efficacité comparable à celle obtenue avec la vapeur d'eau lorsque la source chaude est disponible à des niveaux de température modérée. De plus, les fluides organiques sont plus adaptés pour la conception de micro-turbines volumétriques simples.

En analysant une large base de données des fluides thermodynamiques, les fluides les plus convenables sont identifiés comme suit : l'eau, l'hexane, l'isopentane et le R-245fa.

Un modèle a été développé sous Visual Basic et Refprop pour calculer les différents cycles thermodynamiques. Le logiciel comprend des modules qui permettent de dimensionner les composants du système ORC pour comparer les différents fluides de travail.

2.2. Performance du cycle Rankine

Le rendement idéal du cycle Rankine a été calculé pour les différents fluides de travail en considérant une température de condensation de 80 °C, et en variant la température d'ébullition de 100 °C à 180 °C. Les résultats présentés figure 2.1 montrent que les fluides ayant une température critique plus élevée présentent des rendements plus élevés. Les fluides ayant un rendement supérieur à 12 % ont été retenus.

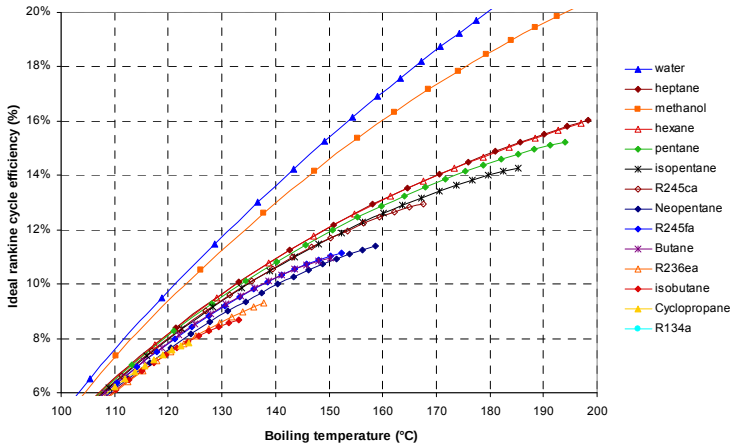

Figure 2.1 – Rendement idéal du cycle Rankine (η_t = 1, η_p = 1, T_{sub} = 10 K, T_{sup} = 25 K si l'eau est le fluide de travail et 1 K pour les différents autres fluides de travail)

a. Sélection des turbines

L'étude menée sur les turbines a montré que deux paramètres principaux : la vitesse spécifique et le diamètre spécifique, influencent les performances énergétiques des turbines. Les calculs montrent sur les figures 2.2 et 2.3 que les fluides à basse température critique sont plus adaptés au développement des turbines à haut rendement car leurs vitesses et leurs diamètres spécifiques se situent dans la bonne plage de fonctionnement. En effet, pour des turbines de puissances mécaniques inférieures à 10 kW, les turbines axiales et radiales restent difficiles à développer car il est nécessaire de faire tourner ces types de turbine à des vitesses très élevées (> 100 000 rpm). Ainsi les turbines volumétriques restent la technologie incontournable pour ces types d'applications et particulièrement les turbines spiro-orbitales.

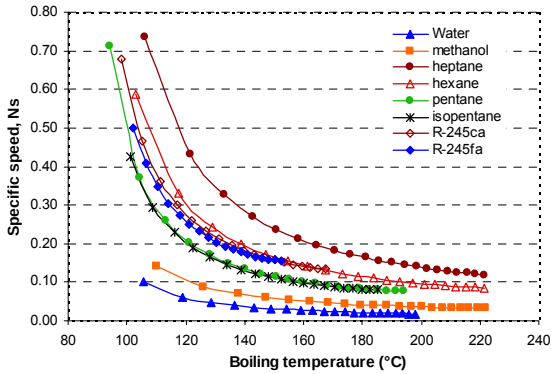

Figure 2.2 – Vitesse de rotation spécifique (N = 3000 rpm, W_{is} = 10 kW)

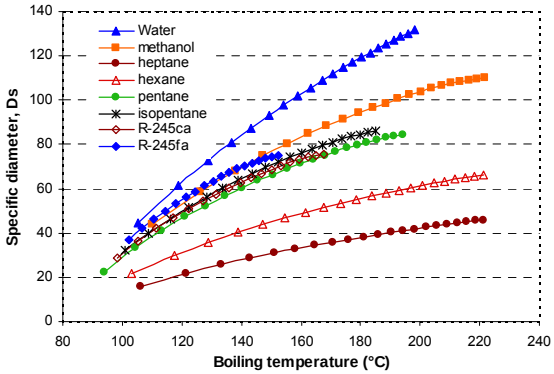

Figure 2.3 – Diamètre spécifique (D = 0,6 m, W_{is} = 10 kW)

b. Sélection des échangeurs

Le surface des échangeurs (bouilleur et condenseur) joue un rôle très important dans le développement des cycles Rankine puisqu'ils influencent le prix total du système. Les calculs menés pour les différents fluides de travail ont montré que les fluides ayant une température critique plus élevée présentent des coefficients d'échange plus élevés et nécessitent donc des surfaces d'échanges inférieures comparativement aux autres fluides. Les résultats présentés dans les figures 2.4 à 2.7 présentent des tendances similaires à ce qui est expliqué ci-dessus.

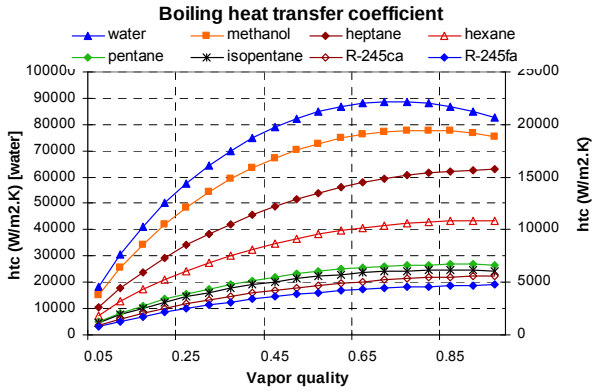

Figure 2.4 – Coefficient d'échange thermique d'ébullition, T_{cond} = 80 °C, G_c = 30 kg/m^2.s, D_h = 4,48 mm.

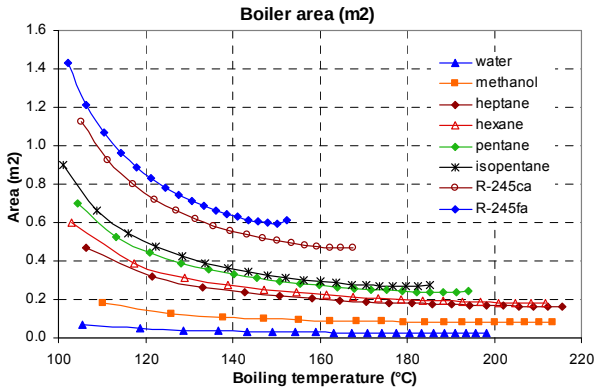

Figure 2.5 – Surface du bouilleur pour différentes températures d'ébullition, G_c = 30 kg/m^2.s, D_h = 4,48 mm.

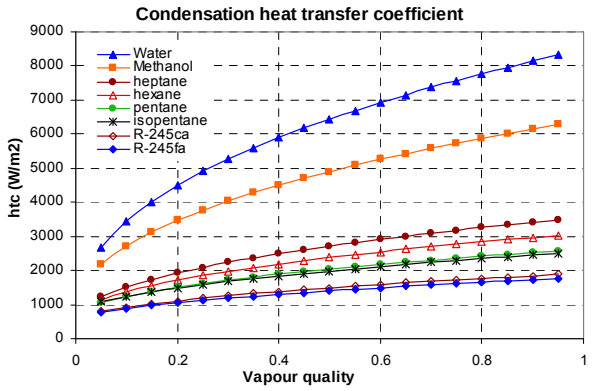

Figure 2.6 – Coefficient d'échange de condensation, T_{cond} = 80 °C, G_c = 30 kg/m^2.s, D_h = 4,48 mm.

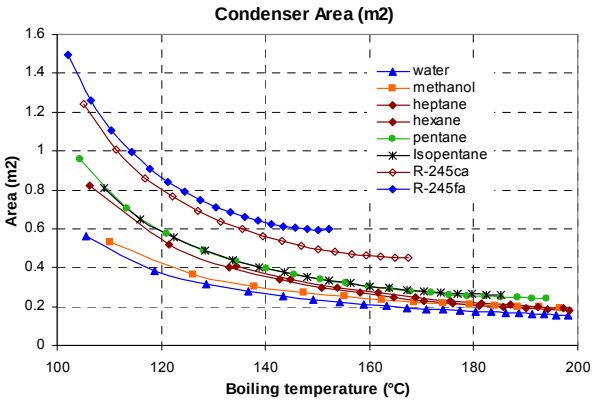

Figure 2.7 – Surface du condenseur pour différentes températures de condensation, T_{cond} = 80 °C, G_c = 30 kg/m^2.s, D_h = 4,48 mm.

c. Sélections des pompes

Les calculs présentés dans les figures 2.8 et 2.9 montrent que les débits volumiques sont relativement bas et les rapports de pression souhaités élevés. Les différentes technologies de pompes cinétiques disponibles sur le marché ne sont donc pas adaptées d'où le recours à des pompes volumétriques comme les pompes à pistons ou à diaphragme. D'après une revue technique des caractéristiques de fonctionnement des différentes pompes volumétriques, les pompes à diaphragme ont été identifiées comme la seule technologie disponible adaptée à cette application.

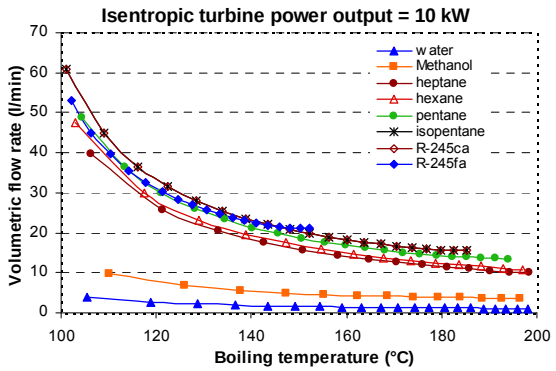

Figure 2.8 – Débit volumique (10 kW)

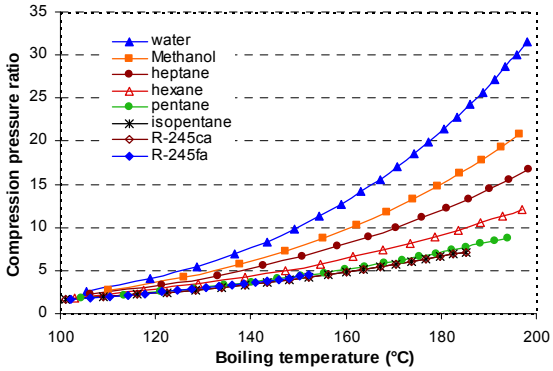

Figure 2.9 – Taux de compression

Chapitre 3. Analyse technologique et expérimentation

Ce chapitre présente les différentes technologies qui peuvent être utilisées et met en évidence les technologies les plus prometteuses pour chacun des composants du système de micro-cogénération : chaudière biomasse, capteur solaire, échangeurs, turbines et pompes. Un banc d'essais a été réalisé pour tester les différents composants d'un cycle Rankine, notamment la turbine, et pour identifier les différents problèmes techniques liés au fonctionnement d'un compresseur volumétrique converti pour fonctionner en mode turbine.

3.1. Chaudière à bois

Différentes technologies de chaudière à bois sont disponibles sur le marché. Ces chaudières sont en général manuellement contrôlable avec des rendements thermiques assez médiocres. Une chaudière à granulés de bois (voir figure 3.1) présente la technologie à la fois la plus efficace et la plus adaptée à notre application car elle présente des rendements assez élevés, qui peuvent atteindre 93 %, avec des échangeurs à condensation intégrés. Ces chaudières présentent l'avantage d'être totalement automatiques.

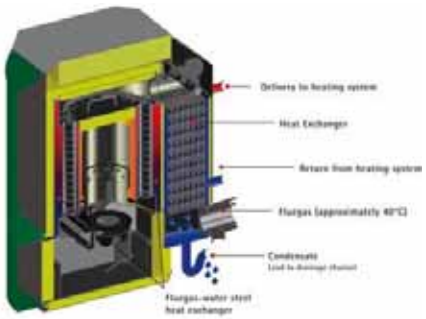

Figure 3.1 – Chaudière à granulés de bois à condensation. [Okefen]

3.2. Capteurs solaires

Les capteurs solaires simples disponibles sur le marché sont conçus pour fonctionner à des niveaux de température de l'ordre de 80 °C. Par contre, pour des niveaux de température plus élevés, les capteurs paraboliques sont utilisés avec un système de suivi du mouvement du soleil. Ce type de capteur présente un rendement élevé même à des niveaux de température de l'ordre de 400 °C. Par contre, ces capteurs présentent des difficultés pour être intégrés dans les bâtiments. Les capteurs à tube sous vide et concentrateurs intégrés (voir figures 3.2 et 3.3) offrent une solution pour des plages de fonctionnement de

température variant de 100 à 180 °C, sans besoin d'un système de suivi du mouvement du soleil. D'autre part, leurs coûts sont bien inférieurs.

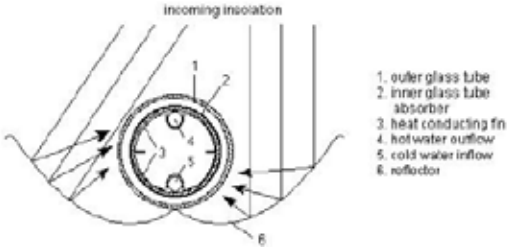

Figure 3.2 – Capteur solaire à tube sous vide avec des réflecteurs à l'extérieur.
Source: CONSOLAR

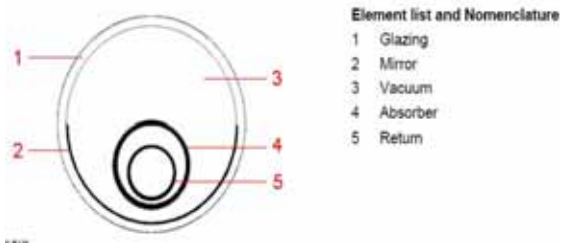

Figure 3.3 – Capteur solaire à tube sous vide avec des réflecteurs à l'intérieur.
Source: SCHOTT

3.3. Pompe

Les pompes volumétriques présentent la technologie la plus adaptée pour cette application. Par contre, seules les pompes à membrane présentées sur la figure 3.4 permettent de pressuriser le fluide à des pressions élevées indépendamment de la viscosité de ce dernier. De plus, ces pompes ne nécessitent aucune lubrification contrairement aux pompes à pistons dont aucune actuellement ne supporte des températures supérieures à 50 °C.

Ces pompes présentent quelques inconvénients car elles sont encombrantes et nécessitent des hauteurs de charges élevées pour éviter tout risque de cavitation.

Le rendement de ces pompes varie entre 20 et 80 % et dépend principalement du débit et du taux de compression.

Figure 3.4 – Pompe à membrane [HYDRACELL].

3.4. Turbine

Les micro-turbines volumétriques sont les seules technologies disponibles sur le marché qui peuvent être utilisées comme organe de détente pour cette application. Mais les performances énergétiques sont assez modérées et les taux de détente et les plages de fonctionnement limités. Toutefois, les turbines volumétriques, bien que non disponibles sur le marché, peuvent être transformées à partir de compresseurs commercialisés en masse.

La figure 3.5 montre deux types de compresseurs (spirale et palette) nécessitant des modifications simples pour être convertis en turbine. La performance de ces compresseurs, en mode compression varie entre 40 et 60 %. Il existe une autre technologie, des moteurs Wankel qui peuvent être transformés pour fonctionner en mode turbine mais avec des modifications significatives spécialement pour l'emplacement des clapets ou des lumières d'entrée et de sortie du fluide.

Compresseur à spirales

Compresseur à palettes

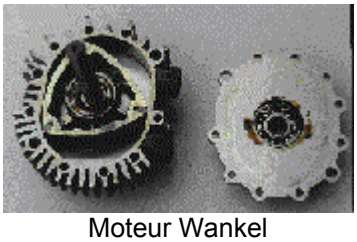

Moteur Wankel

Figure 3.5 – Technologie des compresseurs volumétriques

Une technologie prometteuse de compresseur à spirales sans lubrification, commercialisée par ATLAS-COPCO, peut être convertie avec de légères modifications et peut être transformée en turbine à vapeur. Cette technologie sera testée dans la suite de la thèse pour identifier ses performances en mode turbine et les différents problèmes techniques liés au fonctionnement en mode turbine à des températures variables entre 100 et 180 °C.

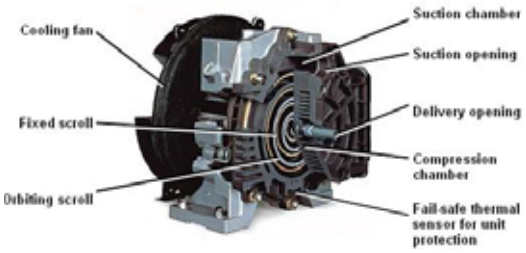

Figure 3.6 – ATLAS COPCO compresseur à spirales sans lubrification

Une solution prometteuse, qui pourra être commercialisée à long terme, est la technologie des turbines comme la turbine Quasiturbine présentée sur la figure 3.5. Cette turbine présente des taux de détente nettement plus élevés que ceux des turbines converties à partir des technologies de compresseurs mais par contre, il reste à résoudre les problèmes de lubrification nécessitant le développement des matières auto-lubrifiantes pour un fonctionnement à la vapeur d'eau.

Figure 3.8 – Quasiturbine

3.5. Echangeur

Le bouilleur et le condenseur utilisés sont des types d'échangeurs à plaques assurant l'échange thermique entre un fluide en phase liquide et un fluide de travail qui passe par les trois phases (liquide, diphasique et vapeur). La technologie des échangeurs à plaques est la technologie la plus adaptée pour cette application. Ce type d'échangeur présente l'avantage d'être très compact, d'approcher la température des deux fluides (~ 1K) et d'avoir un coût acceptable.

Figure 3.9 – Plate heat exchanger [BED00].

L'échangeur intégré dans le cycle organique (récupérateur) est en général de type échangeur tubes / ailettes ou plaques ailetées car l'échange se fait entre un fluide liquide et une phase vapeur. Le coefficient d'échange du fluide en phase liquide est environ 10 fois supérieur à celui de la phase vapeur d'où l'intérêt d'avoir des ailettes du côté vapeur pour assurer un équilibre d'échange entre les deux fluides.

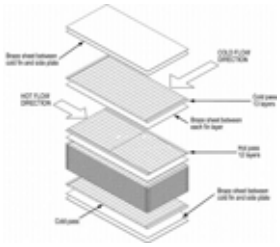

Figure 3.10 – Echangeur à plaques ailettes

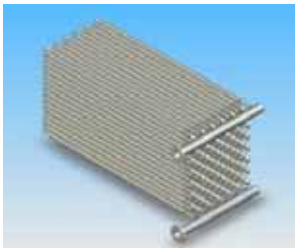

Figure 3.11 – Echangeur à tube ailettes [KAK98]

3.6. Banc de caractérisation de turbine

Pour démontrer la faisabilité d'un cycle micro Rankine et tester plusieurs types de turbines, un banc d'essais a été conçu. Les figures 3.1 et 3.2 présentent ce banc d'essais qui comprend principalement les composants suivants : une résistance électrique, un bouilleur, un condenseur à eau, deux pompes et un frein à courant de Foucault.

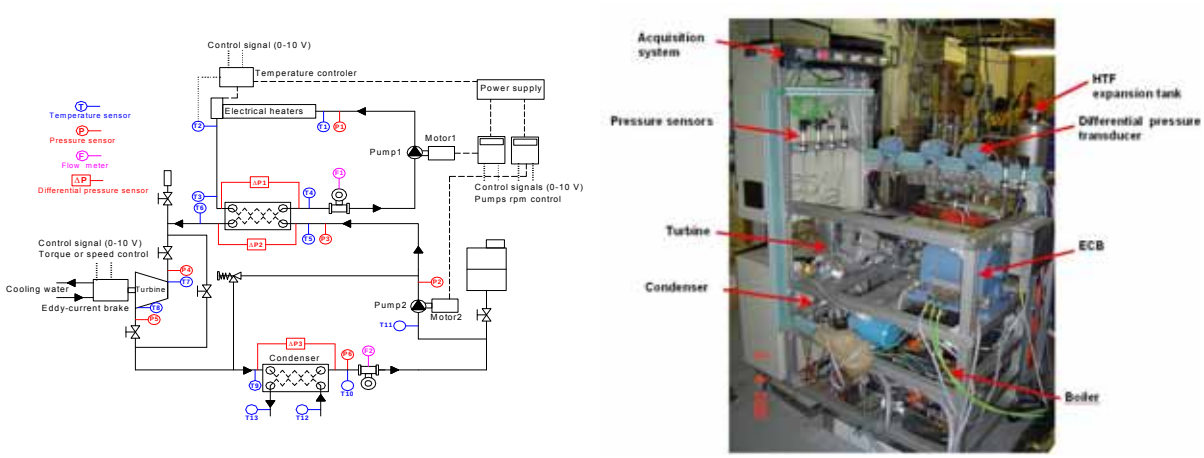

Figure 3.1 – Schéma et photo du banc d'essais des turbines

Les résistances électriques ont été montées pour remplacer et simuler l'énergie fournie par les capteurs solaires et la chaudière biomasse. Une pompe à engrenages à vitesse variable fait circuler le fluide caloporteur (Syltherm 800) à travers les résistances où il est chauffé à une température de 200 °C. A la sortie des résistances, le fluide caloporteur passe à travers le bouilleur où il échange de la chaleur avec le fluide du cycle Rankine (eau).

Une pompe à membrane fait circuler l'eau et la monte à la pression du bouilleur où elle est évaporée et surchauffée. A la sortie du bouilleur, la vapeur d'eau surchauffée se détend dans la turbine et produit l'énergie mécanique. Par la suite, l'eau est condensée dans un condenseur (échangeur à plaques) refroidi par l'eau de ville. Pour mesurer la puissance mécanique générée par la turbine et contrôler sa vitesse de rotation, un frein à courant de Foucault est couplé directement à la turbine testée, afin d'évaluer ses performances sous différents régimes de fonctionnement.

La turbine testée est une turbine spiro-orbitale sans lubrification présentée ci-dessus. La figure 3.2 présente les rendements volumétriques et isentropiques mesurés sur le banc d'essais. Le rendement volumétrique maximal mesuré est de 62 % pour une vitesse de 2800 rpm et pour un taux de détente de 4. Par contre, le rendement isentropique maximal mesuré est de 48 % pour une vitesse de rotation de 2000 rpm et aussi pour un taux de détente de 4.

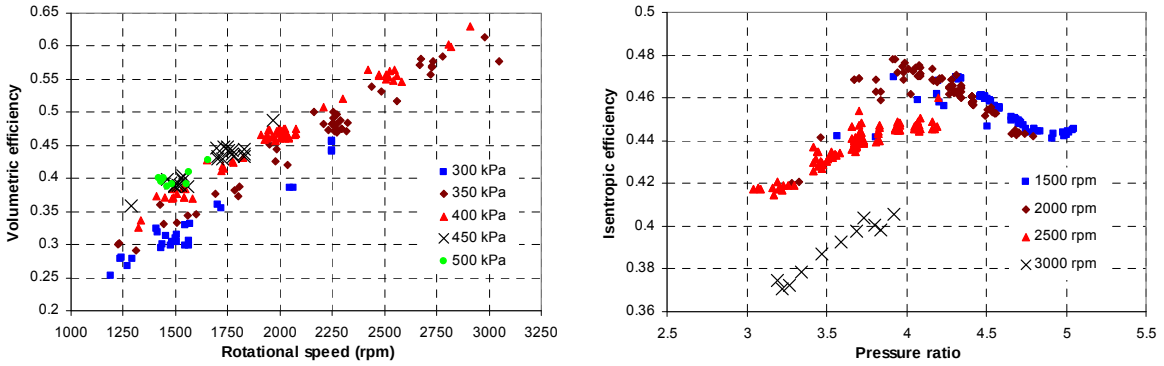

(a) *(b)*

Figure 3.2 – Rendements volumétrique et isentropique mesurés pour différentes vitesses de rotation et taux de détente avec le joint Téflon

Chapitre 4. Conception optimale d'un cycle Rankine fonctionnant à l'énergie solaire et au bois

La conception et le dimensionnement du cycle Rankine organique fonctionnant avec de l'énergie solaire et une chaudière à granulés de bois dépendent principalement du fluide de travail et des paramètres de fonctionnement (température d'ébullition). Les deux paramètres à optimiser sont l'efficacité énergétique et le coût de l'électricité actualisé. Pour calculer la température d'ébullition optimale pour chaque fluide de travail, un outil de calcul a été développé sous Visual Basic couplé à REFPROP.

L'optimisation de la micro-cogénération fonctionnant seulement avec la chaudière bois est faite pour une température d'ébullition variant entre 100 et 180 °C pour les quatre fluides sélectionnés au chapitre 2, afin de calculer l'économie d'énergie primaire et le coût du 1 kWh_{el} actualisé.

Une seconde optimisation a été conduite pour le fonctionnement hybride (granulés bois et solaire). Pour cette optimisation, il y aura 3 paramètres à faire varier : la température d'ébullition, le fluide de travail et la surface des capteurs solaires qui sont représentés dans les résultats comme étant la part d'énergie apportée par le soleil.

Enfin, une étude de sensibilité a été conduite pour identifier les effets de la quantité d'énergie solaire disponible, du coût de fonctionnement du chauffage et de la puissance électrique fournie sur l'économie d'énergie primaire et sur la rentabilité du système.

4.1. Efficacité énergétique

Les résultats du calcul effectué pour la micro-cogénération fonctionnant seulement avec le bois sont présentés dans les figures 4.1 à 4.4. Le rendement électrique de la micro-cogénération augmente lors de l'augmentation de la température d'ébullition. De plus, le fluide qui a la température critique la plus élevée présente les meilleures performances. Par contre, en augmentant la température d'ébullition, des tendances contradictoires ont été observées :

- pour l'eau et l'hexane, le coût d'électricité diminue lorsque la température d'ébullition augmente
- pour les autres fluides, le coût de l'électricité augmente lorsque la température d'ébullition augmente.

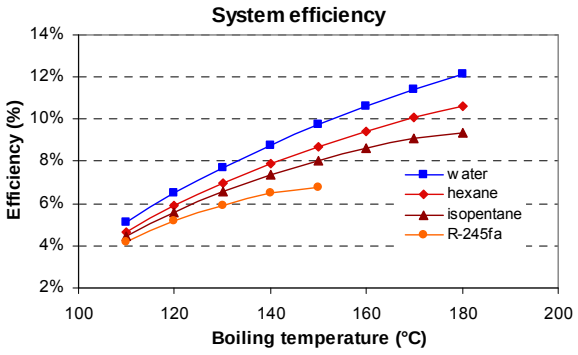

Figure 4.1 – Variation du rendement électrique en fonction de la température d'ébullition et du fluide de travail.

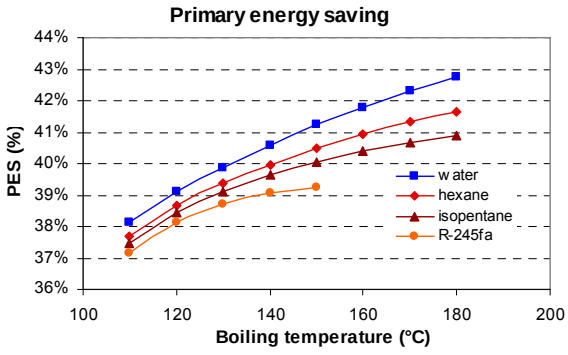

Figure 4.2 – Variation de l'économie d'énergie primaire en fonction de la température d'ébullition et du fluide de travail.

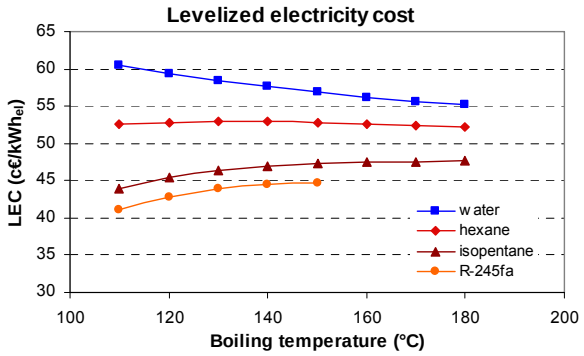

Figure 4.3 – Variation du coût d'électricité actualisé en fonction de la température d'ébullition et du fluide de travail.

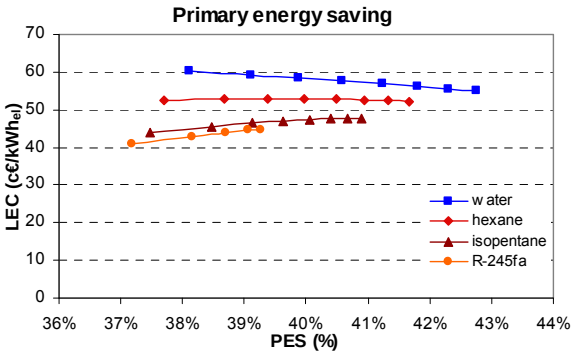

Figure 4.4 – Variation du coût d'électricité actualisé en fonction de l'économie d'énergie primaire et du fluide de travail.

4.2. Fonctionnement hybride

L'optimisation en fonctionnement hybride est complexe comparativement à l'optimisation avec une seule source d'énergie. Un troisième paramètre a été ajouté aux deux paramètres précédents (température d'ébullition et fluide de travail). Ce paramètre est la surface des capteurs solaires présentée sur les graphes par la part d'énergie couverte par l'énergie solaire. Les résultats présentés sur les figures 4.5 et 4.6 montrent que le rendement électrique diminue en augmentant la surface des capteurs solaires car le rendement des capteurs solaires est généralement inférieur à celui des chaudières à granulés de bois. Des résultats similaires ont été obtenus pour les températures d'ébullition et le fluide de travail.

Le prix actualisé de l'électricité augmente en fonction de l'économie d'énergie primaire car la surface des capteurs solaires augmente, ce qui entraîne une augmentation du prix initial du système. Les résultats sont similaires à ceux obtenus précédemment pour les fluides de travail : le fluide qui a la température critique la plus élevée présente le coût de production électrique le plus élevé. D'autre part, la variation du coût de production électrique ne présente aucune tendance générale en fonction des températures d'ébullition, d'où on remarque que chaque fluide de travail présente une tendance différente.

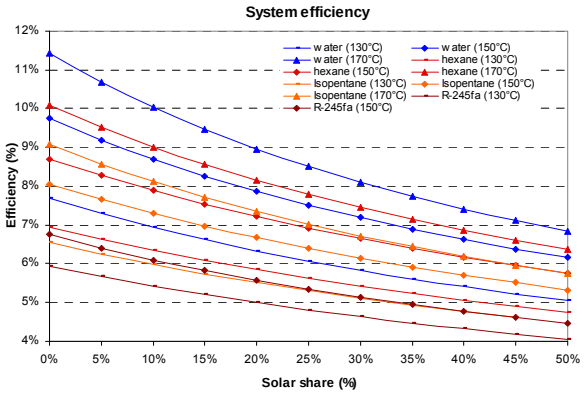

Figure 4.5 – Variation du rendement électrique du système en fonction de la température d'ébullition, du fluide de travail et de la part d'énergie solaire utilisée.

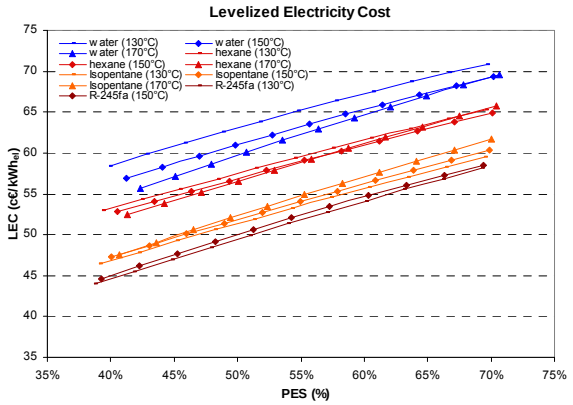

Figure 4.6 – Variation du coût d'électricité actualisé fonction de l'économie d'énergie primaire, température d'ébullition et du fluide de travail.

4.3. Etude de sensibilité

Une étude de sensibilité a été menée pour identifier l'effet de quelques paramètres clés sur les performances et la rentabilité du système. Les résultats montrent (voir figure 4.7) que l'économie d'énergie primaire est proportionnelle à l'énergie solaire globale disponible sur le

site, et le coût d'électricité actualisé est inversement proportionnel à l'énergie solaire globale disponible.

La figure 4.8 présente le coût d'électricité en fonction de l'inflation du coût de chauffage évité. Les résultats montrent que si ce dernier est soumis à une forte élévation du prix à cause de l'inflation du coût de combustion fossile, le prix actualisé d'électricité produite décroit rapidement et elle peut être produite sans aucun surcoût si l'inflation annuelle du coût de chauffage atteint 7 %.

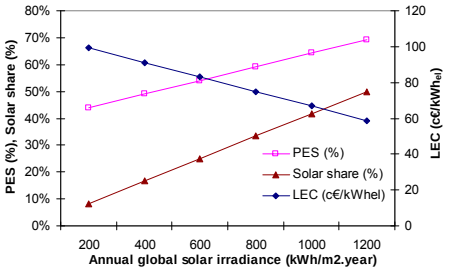

Figure 4.7 – LEC, PES et la part d'énergie solaire fonction du rayonnement solaire global. (A_{sol} = 35 m^2).

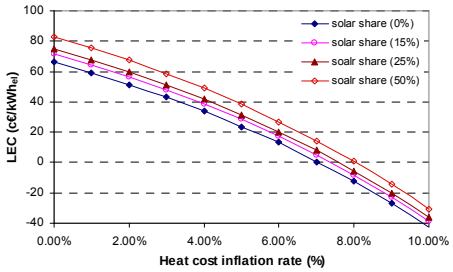

Figure 4.8 – Coût d'électricité actualisé fonction de l'inflation du prix du chauffage évité.

La durée de fonctionnement annuel d'une micro-cogénération présente un paramètre critique pour sa rentabilité économique. La durée de fonctionnement annuel à pleine charge dépend directement de la puissance électrique installée et des besoins thermiques. La figure 4.9 montre qu'en augmentant la puissance électrique de la micro-cogénération le coût de l'électricité augmente car les besoins électrique et thermique annuels du bâtiment restent constants. Par contre, le prix initial de la micro-cogénération augmente. Un optimum de la puissance électrique installée doit être défini ; cet optimum dépend des besoins et des déperditions (cf. chapitre 5).

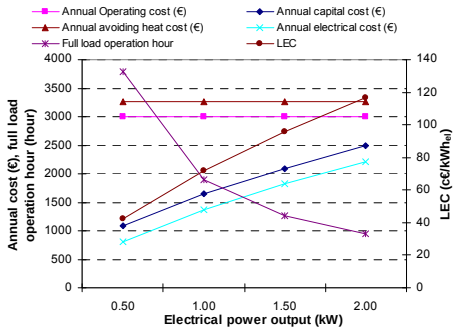

Figure 4.9 – L'effet de la capacité électrique sur le prix de la micro-cogénération et sa durée de fonctionnement annuelle.

Chapitre 5. Simulation dynamique annuelle d'un système de micro-cogénération hybride

Ce chapitre est consacré à la simulation des performances annuelles de la micro-cogénération pour plusieurs types de bâtiments, de volumes de stockage de l'eau chaude pour le chauffage et pour différents cycles Rankine ou organiques. La figure 5.1 présente le système de micro-cogénération couplé à un ballon de stockage d'eau chaude.

Le système est modélisé sous MATALB/SIMULINK pour calculer les différents paramètres de fonctionnements. Un logiciel de simulation des bâtiments multizones COMFIE a été utilisé pour calculer les courbes de charges pour les différents types de bâtiments.

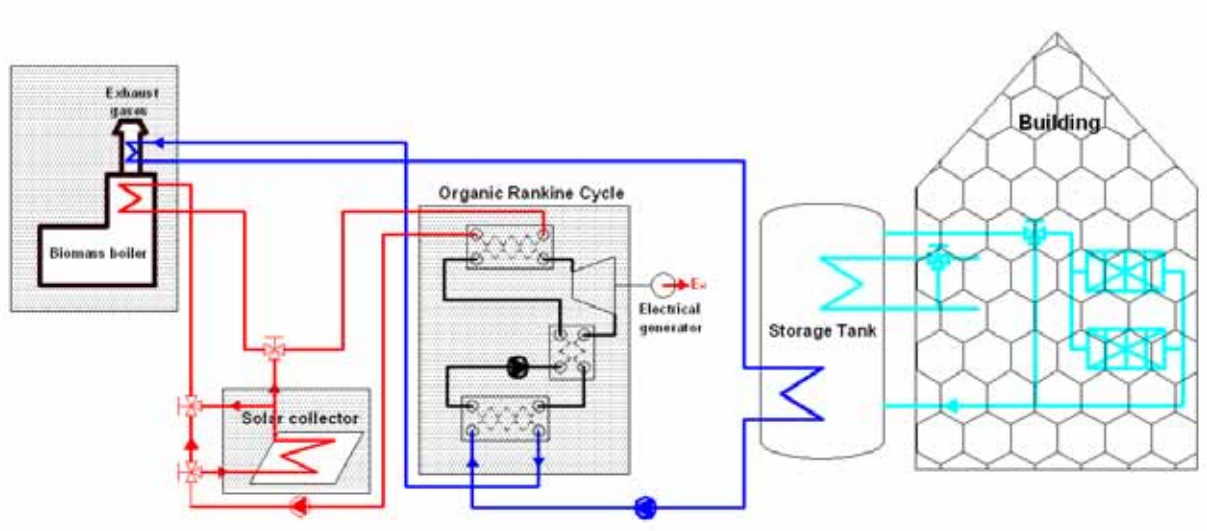

Figure 5.1 – Micro-cogénération pour des bâtiments résidentiels

Pour la simulation des différents cycles Rankine organiques, une optimisation des paramètres de fonctionnement a été menée en fonction des différents types de turbine disponibles sur le marché. Ces paramètres de fonctionnements optimisés seront présentés dans les différentes sections suivantes.

5.1. Cycle vapeur

Les données de calcul pour le cycle à vapeur utilisant des technologies mûres sont indiquées dans le tableau 6.1. Le rendement de la turbine est 50 % et la température maximale du fluide à la sortie de l'évaporateur est fixée à 190 °C.

Tableau 5.1 – Données de calcul (cycle à vapeur utilisant des technologies mûres)	
Température d'ébullition (°C)	100 to 190
Pression du bouilleur (kPa)	47 to 1255
Taux de détente volumique	3.18 – 4.1
Cylindrée de la turbine (cm^3/rev)	52 – 36
Surchauffe à l'entrée de la turbine (K)	25
Sous-refroidissement à l'entrée de la turbine (K)	10
Efficacité globale de la turbine (%)	50
Efficacité globale de la pompe (%)	65

La figure 5.2 montre la puissance électrique et le rendement du cycle Rankine. Les calculs indiquent que le rendement et la puissance augmentent en augmentant la température de bouilleur. D'autre part, la turbine avec le plus grand taux de détente présente les meilleurs rendements.

Le tableau 5.2 présente les paramètres de fonctionnement des cycles Rankine fonctionnant avec des technologies mûres spécifiquement des turbines volumétriques qui sont transformées à partir des compresseurs spiro-orbitaux.

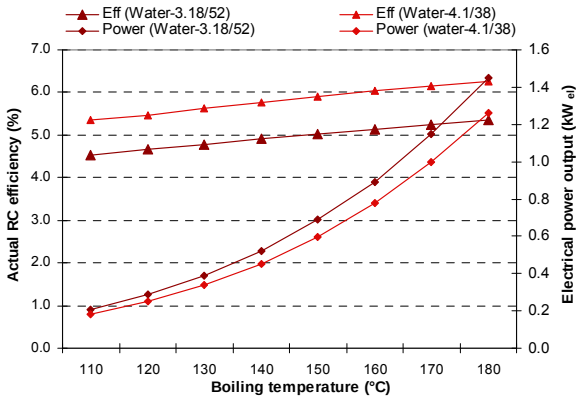

Figure 5.2 – Rendement et puissance électrique du cycle Rankine actuel

Table 5.2 – Paramètres de fonctionnement optimaux		
Technologie disponible sur le marché		
Taux de détente volumique	3,2	4,1
Cylindrée de la turbine	52	38
Température au condenseur (°C)	118	113
Température de bouilleur (°C)	165	170
Pression du bouilleur (kPa)	700	792
Puissance électrique (kWel)	~1	
Rendement du cycle Rankine idéal (%)	10,43	12,35
Rendement du cycle Rankine actuelle (%)	5,06	6,01
Puissance chaleur du bouilleur (kW)	19,77	16,64
Puissance chaleur du préchauffeur (kW)	2,13	1,87
Efficacité thermique de la chaudière (%)	71,4	70
Efficacité globale de la chaudière (%)	79,4	78
Rendement des capteurs solaires (%)	36,62	35,61
Efficacité globale du cycle Rankine (granulé) (%)	3,61	4,2
Efficacité globale du cycle Rankine (solaire) (%)	1,85	2,14
Rapport électricité chaleur	0,047	0,057

Pour identifier le potentiel des technologies futures, les calculs sont répétés en augmentant le rendement de la turbine de 50 % à 80 % et le taux de détente de la turbine sera augmenté pour assurer un fonctionnement entre une température maximale de bouilleur de 190 °C et une température au condenseur de 80 °C.

Les résultats des calculs sont présentés à la figure 5.3. Le rendement du système peut être amélioré pour atteindre 9,5 % et 5,8 % en fonctionnant respectivement avec la chaudière à granulés de bois et l'énergie solaire.

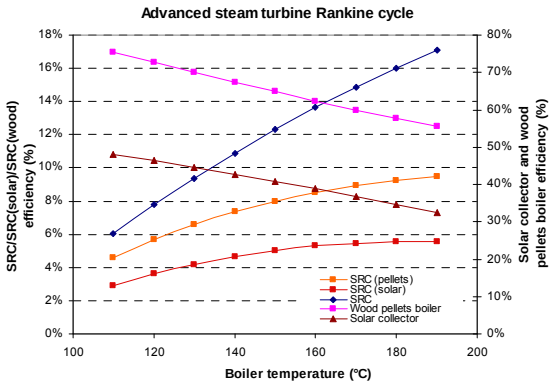

Figure 5.3 – Efficacité des différents composants de la micro-cogénération pour des technologies futures

5.2. Cycle organique

La même méthode est utilisée pour optimiser un cycle Rankine utilisant des fluides organiques. Le tableau 5.3 montre les différents paramètres utilisés pour les calculs des cycles organiques. Le rendement global de la turbine est fixé à 50 % pour les turbines déjà existantes. On peut remarquer une pression dans le bouilleur plus élevée comparativement au cycle à vapeur dû aux propriétés thermodynamiques des fluides organiques.

Table 5.3 – Données de calcul (cycle organique utilisant des technologies mûres)	
Température d'ébullition (°C)	100 to 190
Pression du bouilleur (kPa)	143 to 3500
Taux de détente volumique	2,3 – 4,1
Cylindrée de la turbine (cm^3/rev)	23 – 32
Surchauffe à l'entrée de la turbine (K)	1
Sous-refroidissement à l'entrée de la turbine (K)	10
Efficacité globale de la turbine (%)	50
Efficacité globale de la pompe (%)	65

Les résultats obtenus sont présentés aux figures 5.4 et 5.5. Contrairement aux cycles à vapeur, les rendements des cycles organiques diminuent en augmentant la température au bouilleur puisque le taux de détente est constant. Par contre, la puissance électrique qui peut être générée avec les cycles organiques, est plus élevée par rapport au cycle à vapeur même avec les mêmes dimensions des turbines utilisées.

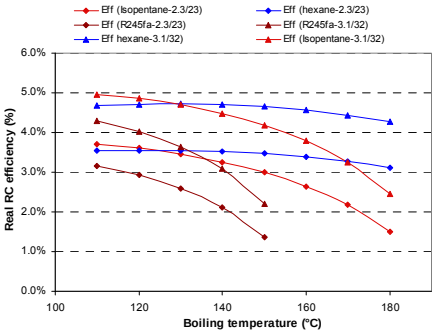

Figure 5.4 – Efficacité réelle du cycle organique

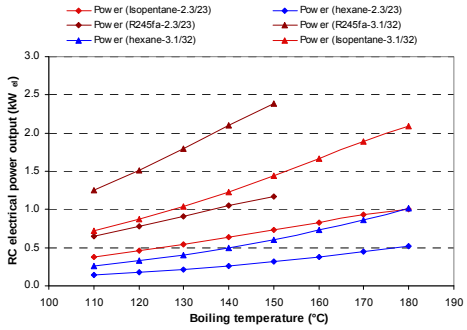

Figure 5.5 – Puissance électrique réelle du cycle organique

Le tableau 5.4 récapitule les résultats obtenus aux figures 5.4 et 5.5 et définit les paramètres de fonctionnement optimaux pour produire 1 kW_{el} avec les rendements les plus élevés.

Table 5.4 – Paramètres de fonctionnement optimaux du cycle organique			
Technologie disponible sur le marché			
Fluide de travail	Hexane	Isopentane	R-245fa
Taux de détente volumique	3,1	2,3/3,1	2,3
Cylindrée de la turbine	32	23/32	23
Température au condenseur (°C)	129	147/80	105
Température de bouilleur (°C)	180	180/128	137
Pression du bouilleur (kPa)	1300	3020/1264	2664
Puissance électrique (kWel)	1	1	1
Rendement du cycle Rankine idéal (%)	9,44	5,24/10,24	6,06
Rendement du cycle Rankine actuelle (%)	4,51	1,59/4,90	2,34
Puissance chaleur du bouilleur (kW)	21,9	62,7/20,4	42,8
Puissance chaleur du préchauffeur (kW)	2,1	6,2/1,05	1,3
Efficacité thermique de la chaudière (%)	75,5	70/77,3	76,7
Efficacité globale de la chaudière (%)	82,7	77,8/81,3	81,3
Rendement des capteurs solaires (%)	36,18	37,04/46,49	45,11
Efficacité globale du cycle Rankine (granulé) (%)	3,40	1,11/3,78	1,79
Efficacité globale du cycle Rankine (solaire) (%)	1,63	0,59/2,27	1,05
Rapport électricité chaleur	0,043	0,014/0,049	0,023

Pour un cycle organique utilisant des technologies futures, les rendements du cycle sont largement améliorés. Les résultats sont présentés à la figure 5.6 où les rendements du cycle ORC peuvent atteindre respectivement 9,5 % et 5 % pour des fonctionnements avec les chaudières à granulés et l'énergie solaire. A noter que ces rendements sont indépendants des puissances électriques du cycle organique, car les technologies des turbines futures sont conçues de façon différente par rapport aux turbines volumétriques.

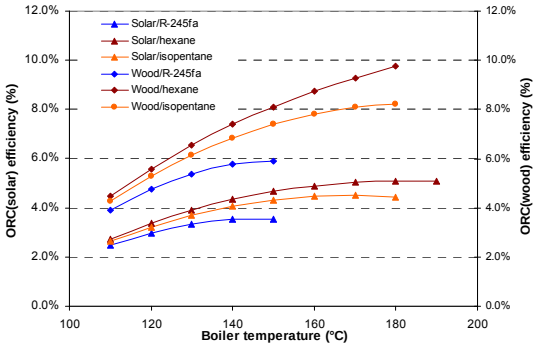

Figure 5.6 – Efficacité du cycle organique pour des futures technologies de turbine

5.3. Résultats des simulations

Les résultats des simulations annuelles sont présentés aux figures 5.7 à 5.9. Les résultats ont montré que le rendement électrique de la micro-cogénération augmente en fonction du volume du ballon de stockage car la durée de fonctionnement continu augmente et ceci en diminuant les intermittences de fonctionnement durant l'année. D'autre part, le rendement électrique augmente pour les bâtiments à haute consommation car la durée de fonctionnement annuelle est plus élevée par rapport aux bâtiments à basse consommation.

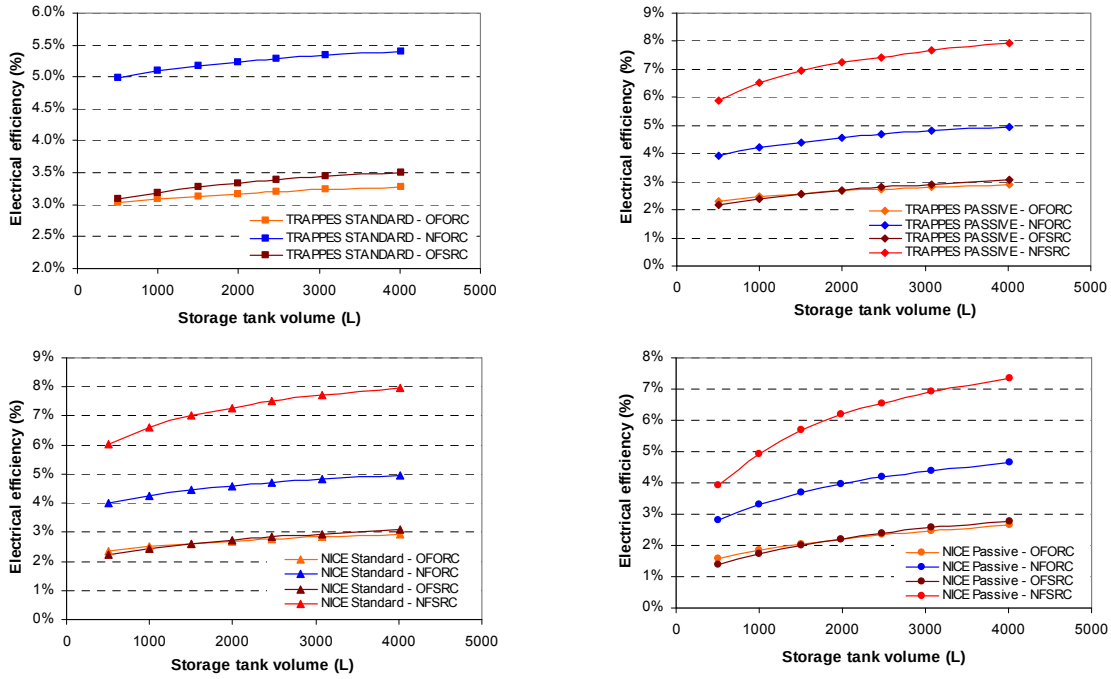

Figure 5.7 – L'effet du volume du ballon de stockage sur le rendement électrique annuel du système pour les différents cycles et types de bâtiments

Le rendement thermique de la micro-cogénération présente des optimums. Ces optimums sont associés à la déperdition thermique dans le ballon de stockage. En augmentant le volume du ballon de stockage, le rendement thermique de la micro-cogénération augmente car il est lié directement au rendement électrique. Par contre, les déperditions dans le ballon

augmentent en augmentant son volume, ce qui entraîne des volumes optimums pour chaque type de bâtiment et pour chaque système de micro-cogénération.

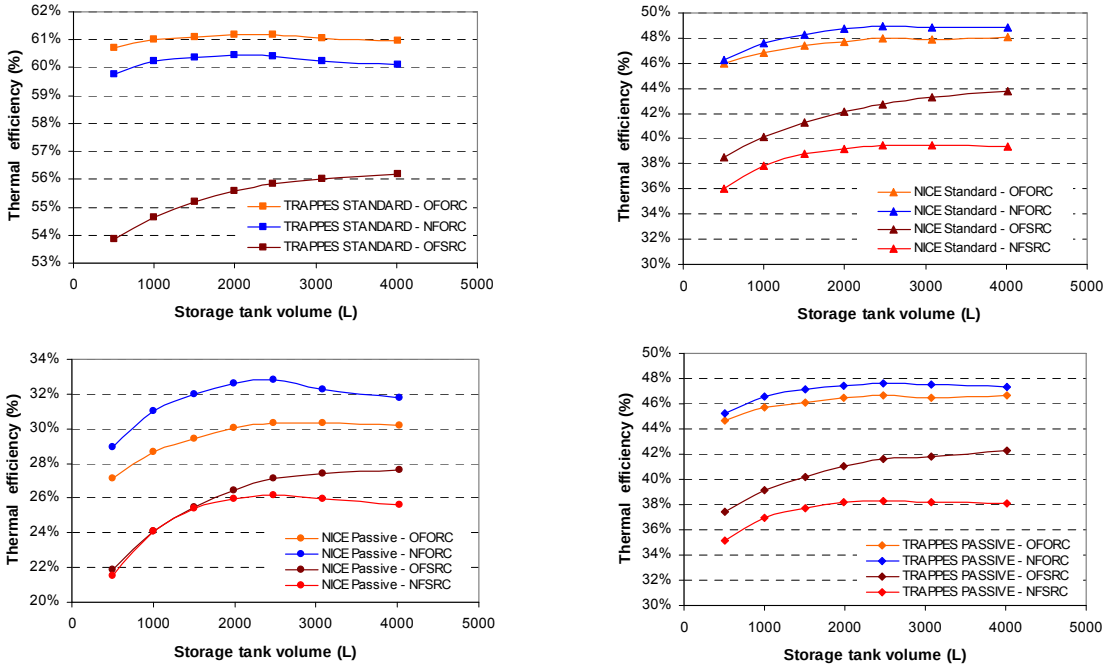

Figure 5.8 – L'effet du volume du ballon de stockage sur le rendement thermique annuel du système pour les différents cycles et types de bâtiments

L'économie d'énergie primaire est le paramètre global à optimiser. Les résultats présentés à la figure 5.4 montrent que, même en atteignant l'optimum du rendement thermique, l'optimum de l'économie d'énergie primaire se situe à des volumes de stockage plus élevés par rapport au volume optimal obtenu pour le rendement thermique. Par contre, compte tenu des grands volumes de ballons obtenus dans les calculs, il est préférable de se fixer au volume optimal obtenu pour les rendements thermiques pour ne pas affecter la rentabilité des systèmes due au prix du ballon de stockage.

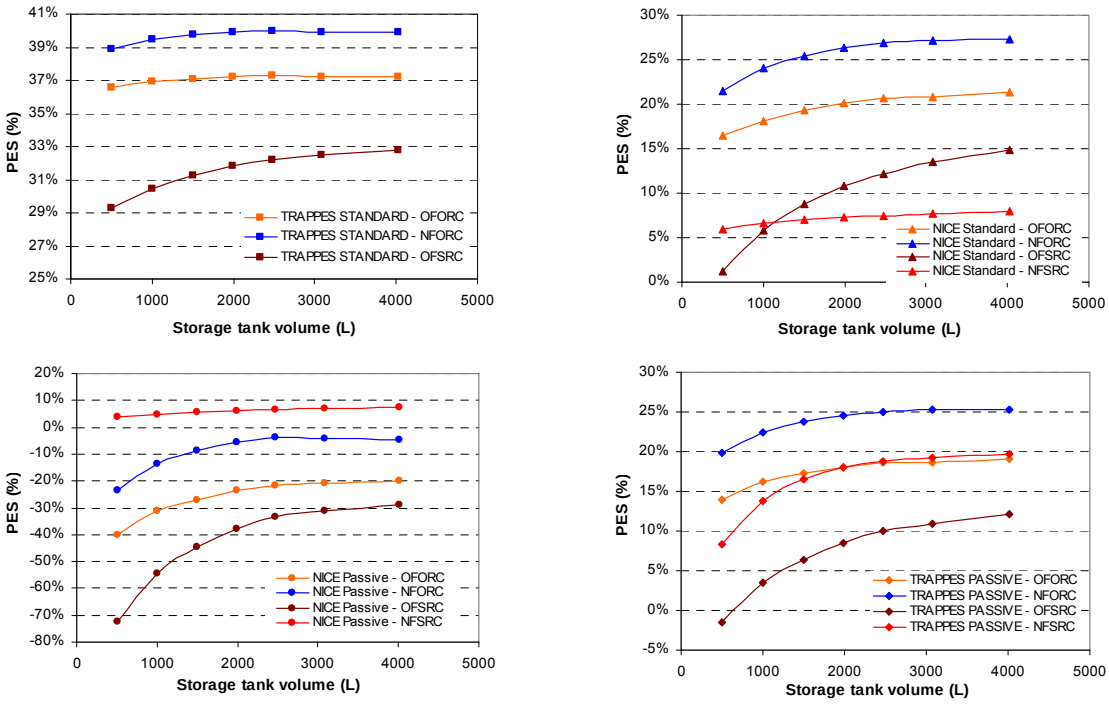

Figure 5.9 – Effet du volume du ballon de stockage sur l'économie d'énergie primaire annuelle du système pour les différents cycles et types de bâtiments. ($\eta_{th,ref}$ = 0,7 and $\eta_{el,ref}$ = 1/2.58)

Conclusions générales et perspectives

Une micro-cogénération fonctionnant avec des énergies renouvelables intermittentes et non intermittentes est une solution prometteuse pour réduire les consommations dans le secteur du bâtiment et atteindre l'objectif de diviser par 4 les émissions de CO_2. Cette micro-cogénération peut présenter des avantages énergétiques et environnementaux pour le secteur du bâtiment puisqu'elle peut assurer plus de 40 % d'économie d'énergie et plus de 80 % de réduction d'émissions de gaz à effet de serre.

Le fluide de travail du cycle Rankine est un paramètre clé pour la conception du cycle puisqu'il affecte les performances énergétiques et économiques du système. Une méthode générale a été développée pour permettre de comparer les différents fluides de travail afin d'identifier les meilleures solutions possibles. L'eau, l'hexane, l'isopentane et le R-245fa ont été identifiés comme étant les fluides les plus convenables.

Une étude technologique a permis d'identifier les technologies les plus adaptées pour chacun des composants du cycle Rankine : chaudière biomasse, capteur solaire, bouilleur, condenseur, récupérateur, pompes et turbine. Les composants les plus adaptés existant sur le marché ont été identifiés. Seule la mini-turbine doit être convertie à partir des technologies de compresseurs volumétriques.

Un banc d'essais a été monté pour tester différents types de turbine. Un compresseur spiro-orbital sans lubrification et dédié à la compression d'air a été testé sur le banc d'essais en tant que turbine à vapeur sans lubrification. Les résultats ont montré que les rendements volumétriques et isentropiques mesurés sont respectivement de 60 % et 48 %.

Une étude économique a été menée pour calculer le prix d'électricité actualisé afin de rendre ce système économiquement faisable. Les résultats ont montré qu'un prix de 40 à 60 c€/kWh_{el} doit être appliqué pour rendre le système de micro cogénération rentable.

Les puissances thermique et électrique de la micro-cogénération à énergies renouvelables présentent un facteur important qui affecte la faisabilité et la rentabilité du système. Une simulation dynamique annuelle a été menée pour mettre en évidence l'effet de la charge thermique, du volume du ballon de stockage et du type de cycle Rankine utilisé pour l'économie d'énergie primaire.

Plusieurs cycles Rankine ont été étudiés en fonction des technologies de turbine utilisées. Quatre cycles de Rankine ont été considérés : un cycle à vapeur utilisant une turbine déjà existante, un cycle organique utilisant une turbine existante avec la possibilité d'utilisation plusieurs fluides de travail et deux cycles Rankine à vapeur et organique utilisant des technologies de turbine qui peuvent être commercialisées dans le futur proche présentant de meilleures performances énergétiques.

L'amélioration de l'efficacité du cycle Rankine nécessite divers progrès technologiques, spécialement le besoin de mini-turbines qui présentent des rendements élevés comparés aux technologies existantes. D'autre part, il est nécessaire de développer un algorithme de contrôle spécifique pour les micro-cogénérations fonctionnant avec deux sources d'énergie, si l'une d'elles est intermittente. Cette stratégie de contrôle doit assurer un fonctionnement plus performant en utilisant toute l'énergie solaire disponible. Ce contrôle est de type adaptatif prédictif.

Contents

Nomenclature

A	Surface Area, Annuity	m^2
C_p	Heat capacity at constant pressure	J/(kg.K)
C	Capital cost	€
C_m, C_{eff}	Thermal capacitance	J/K
CRF	Page 4	
CELF	Constant-escalation Levelization Factor	
D	Diameter	m
C	Capital cost	€
d	Discount rate	
D_h	Hydraulic diameter	m
e	Thermal internal energy per unit mass	J/kg
E	Energy	J
f	Function	
G	Soalr global irradiance	W/m^2
G_c	Mass velocity	$kg/(m^2.s)$
h	Convection heat transfer coefficient, enthalpy per unit mass	$W/(m^2.K)$, J/kg
h_{sl}	Static suction head	m
h_{fs}	Suction frictional head	m
h_{fg}	Latent heat of vaporization	J/kg
h_{sl}	Static suction head	kPa
h_{fs}	Suction frictional head	kPa
K	Primary energy conversion factor	
k	Thermal conductivity	W/(m.K)
L	Mechanical energy	J
L	Length	m
L_c	Distance between the head plates	m
L_h	Distance of the ports at the same height	m
L_v	Vertical length of the fluid path	m
L_w	Horizontal length of the plates	
LMTD	Logarithmic mean temperature difference	K
m	Mass	kg
$\dot{m}$	Mass flow rate	kg/s
M	Molar mass	kg/kmol
Min	Minimum	
N	Rotational speed	rpm
NPSH	Net Positive Suction Head	kPa
NTU	Number of heat Transfer Units	
P	Pressure, Power	KPa, W
p_v	Vapor presser	kPa
PES	Primary Energy Saving	
PR	Pressure Ratio	Kpa
ΔP	Pressure losses	kPa
q”	Heat flux	W/m²
Q	Heat energy	J
$\dot{Q}$	Heat duty	W
r_n	Escalation rate	
s	Entropy per unit mass	J/(kg.K)
t	Time, Thickness	S, m
T	Temperature, Torque	K, N.m
U	Overall heat transfer coefficient	$W/(m^2.K)$
UA	Overall thermal conductance	
v	Volume per unit mass	m^3/kg
V	Volume flow rate	m^3

$\dot{V}$	Volume flow rate	m^3/s
VR	Volume ratio	
x	Vapor quality	
W	Work	J

Greek Letters

Δ	Finite change in quantity	
β	Correction inclination angle	
ε	CO_2 emission factor, heat recovered efficiency	GCO_2/kWh, %
η	Efficiency	
λ	Power to heat ratio	
μ	Dynamic viscosity	Pa.s
ν	Kinematics viscosity	m^2/s
θ	Angle	rad
ρ	Mass density	kg/m^3

Subscripts

a	Ambient
atm	Atmospheric
b	Boiler, beam
c	Cold, kinetic
CHP	Combined heat and power
cond	Condensation
cr	Critical
cyc	Cycle
d	Diffuse
El,elec	Electrical
eq	Equivalent
evap	Evaporator
ex	Exit
h	Hot, heat
hf	Hot fluid
htf	Heat transfer fluid
in	Inlet, input
inv	Investment
is	Isentropic
L,liq	Liquid
lm	Log-mean
m	Mean value
max	Maximum
mc	Micro cogeneration
mes	Measured
nb	Normal boiling
nom	Nominal
out	Outlet, output
p	Pump, primary, port, potential
ph	Preheater
PHX	Plate heat exchanger
pl	part load
rec	Recuperator
ref	Reference
run	Running
s	Isentropic, specific, suction
sat	Saturated
sol	Solar
sub	Sub-cooled
sup	Superheat
t	Turbine

th	Thermal, theoretical
tot	Total
tp	Triple point
turb	Turbine
wf	Working fluid
w	Water, wall
vap	Vapor
v	Vapor
vol	Volumetric

Dimensionless groups

Bo	Boiling number	$Bo = \frac{q}{h_v G}$
Nu	Nusselt number	$\frac{hD}{k}$
Pr	Prandtl number	$\frac{C_p \mu}{k} = \frac{\nu}{\alpha}$
Re	Reynolds number	$\frac{\rho u D}{\mu}$
Re_l	Reynolds number of the liquid phase	$\frac{G(1-x)D}{\mu_l}$

Abbreviation

CFC	Chlorofluorocarbons
CHP	Combined heat and power
COP	Coefficient of performance
CPC	Compound parabolic collector
C.V.	Control volume
DHW	Domestic hot water
ECB	Eddy-current brake
ETC	Evacuated tube collector
EU	European union
GHG	Green House Gases
HCFC	Hydrochlorofluorocarbons
HEX	Heat exchanger
HFC	Hydrofluorocarbons
HOC	Heat of combustion
HRC	Heat recovery factor
HTF	Heat transfer fluid
GWP	Global warming potential
LFL	Lower flammability limit
LFR	Linear Fresnel collector
LHV	Low heating value
MFR	Mass flow rate
Mtoe	Million tons of oil equivalent
Mtpe	Million tons primary energy
NFORC	Near future organic Rankine cycle
NFSRC	Near future steam Rankine cycle
NPSHa	Net positive suction head available
NPSHr	Net positive suction head required
NTU	Heat transfer unit
ODP	Ozone depletion potential
ORC	Organic Rankine cycle

OSORC	Off-the-shelf organic Rankine cycle
OSSRC	Off-the-shelf steam Rankine cycle
PE	Primary energy
PES	Primary energy saving
PHR	Power to heat ratio
PTC	Parabolic trough collector
RC	Rankine cycle
S	Saving
SBORC	Solar biomass organic Rankine cycle
SRC	Steam Rankine cycle
TLV-TWA	Threshold limit value – time weighted average
TPD	Turbine power density
VFR	Volumetric flow rate

General introduction

The building industry in France uses more than 70 135 Mtoe, making this sector one of the biggest consumer of energy among all the sectors of the economy where it represents more than 43% of the total national energy consumption. This sector is responsible of 120 $MtCO_2$ emissions representing more than 25% of national emissions.

Just recently, buildings has become the sector that presents the most promising sector to make significant progress for improvement of energy efficiency and strong decrease of heating needs in order to meet the national commitments with regard to reducing greenhouse gas emissions.

In the building sector, the average annual consumption is currently close to 240 kWh_{pe}/m^2.year. For reducing the CO_2 emissions of 20% at the 2020 horizon the average primary energy consumption of new buildings needs to be reduced to 50 kWh_{pe}/m^2.year of primary energy for heating and domestic hot water (reference Grenelle law).

Moreover Europe has taken the commitment to introduce at least 20% of Renewable energies in the European energy mix so the integration of renewable energies in buildings is winning strategy for building designers.

The main purpose of this thesis is to present the potential of integrating a micro combined heat and power system (micro-CHP) operating on renewable energies (solar and biomass) and the different technical problems, which have to be overcome to put this system in actual application. This study integrates an economical analysis to define the different economical incentives, which have to be applied by the government to improve the economical performance of this system.

The first chapter presents a survey of the different micro-CHP technologies available on the market, which could be converted and adapted to operate with intermittent and non-intermittent renewable energy. It was shown that micro-CHP system based on Organic Rankine Cycle (ORC) operating on renewable energies presents many advantages compared to conventional cogeneration systems, since they could operate with renewable energies while achieving high primary energy savings and reducing significantly CO_2 emissions. On the other hand, this system is not always economically feasible; therefore, a special care has to be taken when designing and dimensioning the micro-CHP system. In addition, the building type should be carefully selected.

The choice of the working fluids of the ORC affects heavily the thermodynamic performance of the Rankine cycle as well as the selection and design of the different components of the system. A selection method has been developed in the second chapter to select the most promising working fluid using different thermodynamic, safety, environmental, and technical criteria. Four different working fluids have been selected as the most promising working fluids for our application. Therefore, the different technical and economical problems, which have to be overcome when operating with these fluids, will be discussed in the following chapters.

The component as well as systems design depend mainly of the working fluids, the required electrical output power and energy source temperature. Therefore, in chapter three a technical analysis has been conducted to identify the most promising technology available on the market that could be used, and the different technical barriers that could be overcome in order to put the system in real application. In addition, an experimental test bench has been designed to test an oil-free vapor scroll expander. This test bench has been able to test a first micro-CHP system prototype.

In the fourth chapter, an economical analysis has been performed to calculate the Primary Energy Saving (PES) and the Levelized Electricity Cost (LEC) when operating with different

working fluids and for different boiling temperatures. This analysis shows the potential of PES achieved by the micro-CHP system on one hand and on the other hand, it shows the LEC which has to be imposed by the government to allow the development and the commercialization of this system from an economical point of view.

In chapter five, a dynamic simulation tool has been developed to simulate the annual performance of the micro-CHP system operating with wood only and on hybrid mode solar and wood. The analyses have been performed to compare different types of buildings, climate conditions, and different micro-CHP systems operating with different working fluids. A special control system has been tested with a hot water storage tank to perform the simulations. The results show that the system architecture and the control system are well suited for operation with wood; however, for hybrid operation mode an advanced predictive adaptive control system is required to improve the performance of the system when operating in hybrid mode.

CHAPITRE 1 – MICRO COMBINED HEAT AND POWER SYSTEM FOR RESIDENTIAL BUILDINGS

1. Context and stakes: Energy policy of the European Union

The development of human activities is increasing the greenhouse effect, which has led to a rise of the Earth surface temperature and risks generating significant change to the world climate. To reduce the Green House Gases (GHGs) emissions of the different countries, which contribute to the global warming effect, the Climate Convention was signed in Rio in 1992 to coordinate actions as part of an international program to forecast, prevent, and limit the causes of climate change and reduces any negative effects. The scope of this convention has been extended by the Kyoto Protocol, which sets legally binding objectives for industrialized nations to reduce their GHG emissions by 2008 – 2012 taking as the reference the emission levels recorded in 1990. To reach the stabilization of GHG emissions around 550 p.p.m., emissions of these gases have to be divided by two by year 2050. Therefore the industrialized countries have to reduce their emissions by four to five times.

The European Union has committed to reduce its greenhouse gas emissions by 8% to 12% by 2008-2012 referred to the 1990 and 20% GHG reduction among EU countries by 2020. To attain these objectives, EU adopts **the directive on the promotion of Electricity produced from renewable energy sources** [DIR01] setting a target of 21% of renewable energy share in electricity production by 2010. The vision of the EU-25 follows the EU's target of 12% renewable energy by 2010. In the vision, the share of the renewable energy by 2030 is 35% and 65% in 2050.

On the other hand, buildings account for more than 40% of the EU's final energy demand and are a major source of GHG emissions, making energy-savings there, a key element of the European climate change strategy. EU efforts to reduce energy consumption in the building sector has introduced the directive on the end-use efficiency and energy services [DIR06], and the 2002 energy performance of building directives (EPBD) [DIR02] providing a common methodology for calculating the energy performance of buildings and for creating minimum energy performance standards in individual member states. The directive applies to new buildings and to existing buildings subject to major refurbishing. In an effort to promote awareness and energy efficiency improvements, member states must ensure that "energy performance certificates" are made available when buildings are constructed, sold or rented out. In public buildings larger than 1,000 square meters, these certificates must be clearly displayed at the main entrance.

The use of combined heat and power (CHP) presents a substantial potential for increasing energy efficiency and reducing environmental impacts. Hence new Community legislative measure concentrates on providing a framework for the promotion of this efficient technique in order to overcome still existing barriers, to advance its penetration in the liberalized energy markets, and to help mobilizing un-used potentials. The EU strategy outlined in the Commission's cogeneration strategy of 1997 sets an overall indicative target of doubling the share of electricity production from cogeneration to 18% by 2010. The European Commission, in its Action Plan [ACT06] on energy efficiency, estimates that meeting this target would lead to additional avoided CO_2 emissions of over 65 Mt CO_2/year by 2010. Emerging micro-CHP technologies in conventional CHP markets could save 19 Mt of CO_2 emissions [MIC02] per year after ten years.

Micro-CHP promises significant economic and environmental benefits to energy suppliers and society at large. The UK government has identified CHP as key components of its CO_2 abatement program and it also represents the most significant individual measure in achieving the European Union's CO_2 reduction targets (150 Mt of a total of 800 Mt) [MIC03].

Many others countries like Germany, The Netherlands, Portugal, and Czech Republic have already micro-CHP units operating on gas, which are currently being installed on a commercial basis [MIC04]. However, in France micro-CHP has not yet found their ways to the commercialization since from an environmental point of view, electrical energy produced by micro-CHPs operating on gas emits more CO_2 (260 gCO_2/kWh_{el} [BIR07]) than the electricity produced by the France electrical grid for building heating (180 gCO_2/kWh_{el}). Therefore, the France political plan is to substitute the fossil fuels by renewable energies. Then micro-CHP operating on intermittent and on intermittent renewable energies can represent a more attractive solution to the French market compared to the conventional micro-CHP operating on gas.

A recent study has been conducted by Amoès [AMO06] to identify the impact of the micro-CHP operating on wood on the greenhouse effect. The results show that integrating a micro-CHP operating on wood in the building sector can reduce emissions of greenhouse gases and reduce the primary energy consumption, increasing the use of renewable energy as well as of local abundant energy as solar and wood, and limiting the peak load of the centralized electricity production. The study shows that integrating a micro-CHP system operating on wood in a residential building is sufficient to rate the building as highly environmentally friendly with a CO_2 emission below 5 kg_{eqCO2}/m^2.year, and in some cases the building can be considered as absorber of CO_2. On the other hand, the study shows that micro-CHP system is not economically feasible for residential houses. However, it is more attractive for apartment buildings from an economical point of view.

2. Energy resources: Building sector in France

In France, the building sector consumes more than 42% (68.2 Mtoe) of the total national energy consumption, which represents the biggest consumer of energy between the different economical sectors. The total CO_2 emissions of this sector represents more than 23% (123 $MtCO_2$) of the national greenhouse gas emission. 66% of the energy is consumed in the residential buildings. The final energy consumption of the building sector distributed by use and final energy is presented in Table 1.1.

Table 1.1 – Building sector consumption for different use and final energy consumption [HER07].

	Area (10^6 m^2)	Electricity consumption (TWh)	Gas Consumption (TWh)	Other (TWh)	Total consumption (TWh)	%
Individual homes	1,782	94.7	96	95	280.2	42.5
Apartment building	884	43.5	81.8	26.8	157.6	24
Residential sector	2,666	138.2	177.8	121.8	437.8	66.5
Tertiary buildings	850	90	72.3	58.9	221.2	33.5
Total building sector	3,516	228.2	250.1	180.7	659	100

The total consumption of the final energy in the residential sector is about 437.8 TWh excluding wood. The different resources of energy used in the residential sector are distributed as follows:

- Gas: 177 TWh (38%).
- Electricity: 138.2 TWh (32%).
- Fuel: 94.6 TWh (22%).
- Coal: 2.3 TWh (<1%).

Wood represents 78 TWh, which correspond to 15% of the overall energy consumption of buildings. The average consumption of the different buildings is about 240 kWh of primary energy for each square meter heated for one year. This value corresponds to the need of heating, domestic hot water, and specific electricity use. The heating consumption in the residential sector represents more than 66% of the total consumption of this sector and accounts also for major parts of CO_2 emissions [HER07].

The energy consumption for heating and domestic hot water in the building sector the is presented in Figure 1.1:

- 100 kWh/m^2.year for buildings built after 2000
- 200 kWh/m^2.year for buildings built between 1975 and 2000, which represent 25% of the building stock
- 375 kWh/m^2.year for buildings built before 1975, which represent 66% of the building stock.

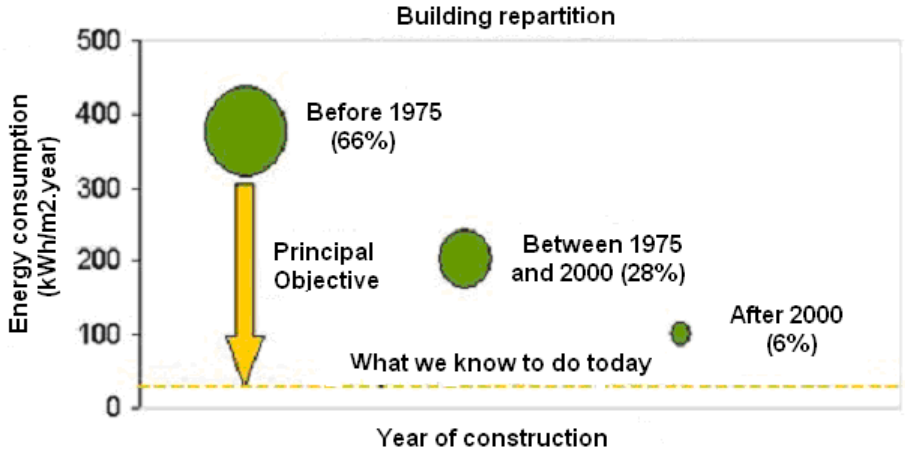

Figure 1.1 – Building repartition depending on their year of construction [AMO06].

The objectives set by the French government are mainly to divide the greenhouse gas emissions by 4 by 2050. The building sector represents a field to invest since it is one of the most important sectors regarding energy consumption. With a call to reduce CO_2 emissions combined with the energy price increase caused by the gradual depletion of resources, the average of primary energy consumption of operational buildings needs to be reduced to approximately 100 kWh/m^2 by 2050, including some 50 kWh/m^2 of primary energy for heating and providing domestic hot water. In France, the development of low energy buildings is one of the ways to fulfill the national objectives of reducing CO_2 emissions by 4 between 1990 and 2050 [LOI05].

For new constructions, several legislations [RTH05] have entered into force. "RT2005" fixes the maximum energy consumption for new buildings depending on their regions, ranging from 130 to 250 kWh/m^2.year according to energy sources, architecture shape, and climate zones. In 2010, a new legislation will enter into force aiming at reducing the energy consumption of buildings; 15% lower than the limit fixed by "RT2005". The objective is to reduce it to 40% by 2020 compared to 2000. However, continually and progressively reducing energy consumption below current legislations allows sustainable policy upon introduction of new legislations.

In Switzerland, 5,800 buildings have been constructed under the "Minergie" label, which guaranties thermal energy consumption lower than 42 kWh/m^2.year. On the other hand, Germany has developed a new concept named "Passivhaus" for homes with heating energy consumption lower than 15 kWh/m^2.year, and with a total primary energy consumption lower than 120 kWh_{pe}/m^2.year [FEI04]. In France, a new label "Effinergie" has been developed, which corresponds to the Suisse label, and allows certifying buildings with the same characteristics as "Minergie". On the other hand, zero or positive energy buildings represent another technical solution to fulfill the national objectives of reducing CO_2 emissions by 4 and increase the share of energy produced by means of renewable energies.

A positive energy building corresponds to a building that produces more energy than it consumes. In order to design such buildings, it is mandatory to work on the reduction of the primary energy consumption of buildings to attain a building with lower energy demand, then producing this energy by intermittent and non-intermittent renewable energy sources.

These performances can be obtained by the combination of various techniques such as bio-climatic design, high insulation level, high performance windows, good air tightness, and heat recovery ventilation. However, going from houses with low energy demand to zero energy building requires producing the energy demand of buildings from available local energy as solar energy, wind, geothermal, wood, etc. Since the building needs heat, electricity and cooling, it is important to develop systems that can ensure the production of these different types of energy. The different techniques adopted to produce electrical, heating and cooling energies locally are listed below.

- Electrical energy: the different techniques available on the market to produce electricity directly in the buildings are photovoltaic solar collectors, wind turbines, electricity generators such as internal combustion engine, gas turbine …
- Heating energy: this energy is in general produced locally by means of boilers operating on various types of energy (oil, gas, wood…); however, solar collectors represent another option to produce the heating energy from free energy sources.
- Cooling: several techniques have been adopted in the last years to produce cooling from renewable energies as cooling from solar energy by means of absorption and adsorption systems without forgetting the different free-cooling systems and ground-to-air heat exchangers.

Recently, Cabinet SIDLER has conducted a study [SID07] to demonstrate the technical feasibility of buildings with low heating demand for French building stocks undergoing refurbishing work. Results show that building with initial consumption of 417 $kWh_{pe}/(m^2.year)$ can be refurbished to attain primary energy consumption varying from 60 to 80 $kWh_{pe}/(m^2.year)$ for a cost varying from 120 €/m^2 to 200 €/m^2 (see Figure 1.2).

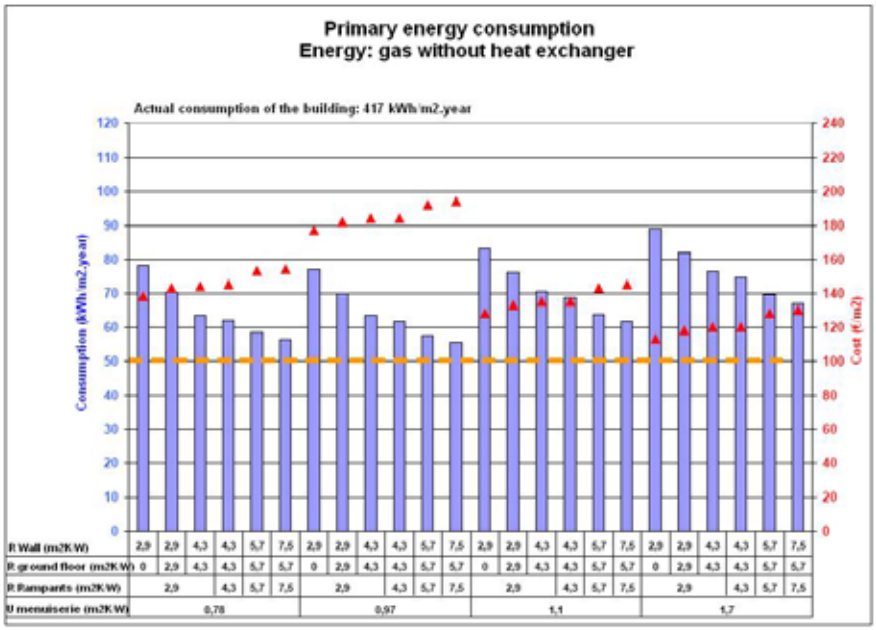

Figure 1.2 – Performance of refurbished buildings heated with gas and ventilated with a mechanical ventilation system without a heat recovery ventilation unit [SID07].

However, reducing the primary energy consumption to a level lower than 50 $kWh_{pe}/(m^2.year)$ for heating needs could not be achieved without integrating a heat recovery ventilation unit. Figure 1.3 shows that buildings undergoing refurbishing work can achieve primary energy consumption for heating needs lower than 50 $kWh_{pe}/(m^2.year)$ for a cost between 150 and 210 €/m^2.

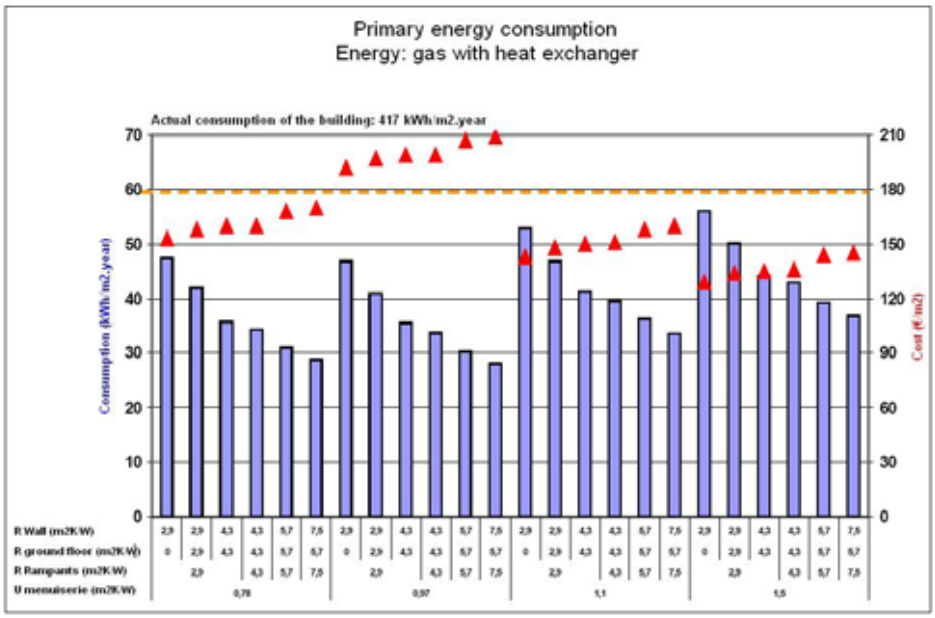

Figure 1.3 – Performance of refurbished buildings heated with gas and ventilated with a mechanical ventilation system with a heat recovery ventilation unit [SID07].

From an economic point of view, if 280 kWh/(m^2.year) of primary energy savings were achieved with a gas price of 0.05 €/kWh, the payback period is estimated at 20 years for a discount rate of 3.5%. Replacing the condensing gas boiler by a micro-CHP operating on renewable energies for the same refurbishing performed in the different type of buildings could achieve higher reduction of primary energy, lower CO_2 emissions, but the economical feasibility should be treated carefully. In this work, the option of replacing conventional heating systems as oil boiler or gas boiler by a micro-CHP system will be highlighted to identify its potential to introduce higher reduction in primary energy consumption and lower CO_2 emissions. The economical feasibility of the micro-CHP system in residential homes could not be justified in all cases; however, for collective apartment buildings these systems can represent an attractive solution towards the use of standard heating system. The different incentives and regulations that have to be imposed by the government will be discussed to improve the economical feasibility of micro-CHP systems. In this chapter, we will establish when micro-cogeneration can be economically beneficial. Therefore, the different costs from the societal perspective will be calculated as subsidies, CO_2 taxes and fossil fuel inflation cost, and the different incentives that the government should include to support the development of the micro-cogeneration systems in the building sector.

3. Micro Combined Heat and Power

CHP is the simultaneous production of electrical or mechanical energy (power) and useful thermal energy from a single energy stream such oil, coal or natural gas. In some cases, the energy source can be provided by solar, geothermal, biomass or other type of intermittent and non-intermittent renewable energy sources. The EU directive [DIR04] facilitates the access to the electrical power for the small-scale CHP units and imposes that tariffs related to the electrical energy produced by these systems have to be set according to objective, transparent, and non-discriminatory criteria. In [DIR04] the maximum power output of the micro-cogeneration units has been set to 50 kW_{el}. However, in France the "*Arrêté" dated 13 March 2002* [ARR02] fixes the power of the installation beneficent from the tariff of purchased electricity to be lower than 36 kW_{el}. The micro-CHP nomenclature will be adopted for units with electrical power output less than 35 kW_{el}. In this thesis, we will only study micro-CHP with electrical power lower than 10 kW_{el}.

There is a growing potential for the use of micro-CHP systems in the residential sector because of their ability to produce both useful thermal energy and electricity from a single or

multiple sources of fuels (see Figure 1.4). In CHP systems, the overall efficiency can increase to 90% especially for micro-CHP systems.

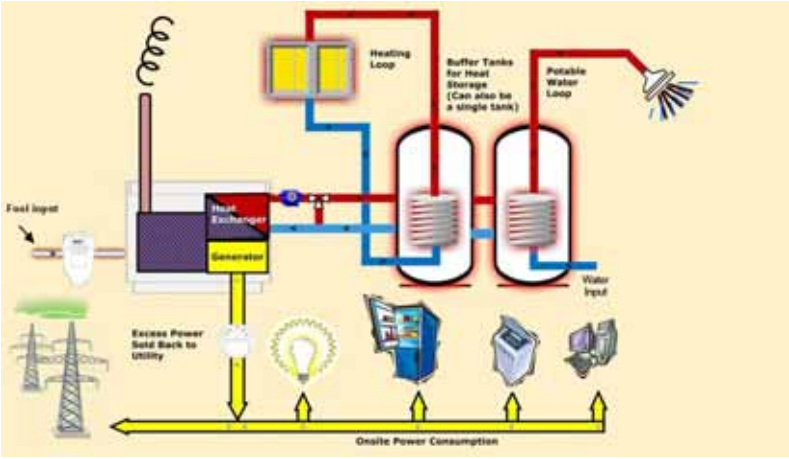

Figure 1.4 – Principle of the cogeneration systems [ENG05].

Micro-CHP might not always be the most energy efficient and/or environmentally friendly solution. The different factors, which affect the economical perofrmance of the micro cogeneration systems, are:

1. High-efficient centralized electricity generation systems are available
2. The electricity production is produced by nuclear power plants with low CO_2 emissions
3. The thermal load is produced by highly efficiency boiler (condensation gas boiler) or with renewable energy (solar energy)
4. Non-coincidence of the thermal and electrical loads necessitating the need for electrical/thermal storage or connection in parallel to the electrical grid
5. Different technologies of small-scale cogeneration seem to be promising but for now the available equipment are found at high prices
6. Absence of micro-CHP systems operating on renewable energy in the market.

These different factors have to be identified in the pre-feasibility study in order to define the profitability of the micro-CHP system. The first two factors depend directly on the country where the system is intended to be installed. The third factor depends on the targeted market either the refurbished or the new housing. These factors help in the first step to identify the most suitable building types where it will be profitable to install a micro-CHP system.

The fourth factor has been partially resolved by the advanced research made in the electronic fields where it is possible nowadays to connect directly the system to give or take electrical energy to or from the grid without the need of electrical storage. However energy storage still represents one of the most difficult issues to overcome for the integration of the micro-CHP systems in the building sector. Since the electricity generation of small systems is less efficient than electricity generation of large-scale generation units, the micro-CHP system is designed first to meet the thermal demand of the building. If the electricity demand of the building is less than the electrical output from the micro-CHP, the electricity surplus will be sent to the utility grid. On the other hand, if the electricity demand of the building is higher than the output of the micro-CHP plant, the lack of electricity is usually covered by taking electricity from the utility grid. Otherwise, to meet the full electrical and thermal demand of a building using micro-CHP, it is usually necessary to install an oversized system in both its electrical and thermal outputs. The over-sizing of the micro-CHP system has many unwanted consequences that will be analyzed in Chapter 4.

The different technologies of micro-CHP will be analyzed to identify the best technology suitable to operate with renewable energies (solar and biomass). Then a technical analysis

will be conducted to identify the best technologies available on the market towards the development of an efficient micro-CHP at acceptable costs.

3.1 Directive promoting micro cogeneration systems in France

Gas micro-CHP systems have been commercialized in Germany and in the United Kingdom where it is very attractive to produce co-generated electricity since the average of CO_2 emissions for electricity production are respectively 641 gCO_2/kWh_{el} and 430 gCO_2/kWh_{el}, which is considered relatively high. In Germany, the most commercialized micro-CHP system is a 5-kW_{el} internal combustion engine [PEH06]. However in the United Kingdom the 1-kW_{el} Stirling engine Whispergen is the most installed system in residential apartments [PEH06].

In France, the average of CO_2 emissions for electricity production is 90 gCO_2/kWh_{el} and 180 gCO_2/kWh_{el} for heating uses. This low average of CO_2 emissions is due to the high share of nuclear power plant (~80%) in the French power production. Due to these low CO_2 emission average values, micro-CHP systems cannot be environmentally justified if they operate with fossil fuels. The development of micro-CHP systems operating with intermittent and non-intermittent renewable energies is a key issue for the integration of these systems on the French markets.

Because of the needs to reduce the primary energy consumption and CO_2 emissions in France, the French government committed itself internationally (signing the Kyoto Protocol in 1997). France adopted the Climate Plan (2004), which gathers the measures to meet the Kyoto targets. Several laws have been adopted (see Appendix 1).

Micro-CHP operating on renewable energy such as biomass or solar energy can answer to energy and environmental requirements:

- Primary energy saving for the consumers
- High potential of CO_2 emission reductions in the building sector
- Use of local abundant energy such as solar and biomass (increasing the biomass consumption (0.2 Mtpe/2007) by six (1.2 Mtpe) by 2015
- Electricity production from renewable energy (“green electricity")
- Reduction of the electrical consumption by the consumers. It is remarkable that people who produce themselves their electricity are more eager to control their electricity consumption.

3.2 Micro-CHP technology

A conversion technology serves to convert chemical and kinetic energies stored within a fuel into “useful” forms of energy (electricity and heat). A number of different conversion technologies have been developed that have possible CHP applications. The conversion process can be based on combustion and subsequent conversion of heat into mechanical energy, which then drives a generator for electricity production (e.g. reciprocating engine, Stirling engines and steam engines). Alternatively, it can be based on direct electrochemical conversion from chemical energy to electrical energy (i.e. fuel cell). These technologies will be presented to identify the most suitable technology to operate with renewable energies with an acceptable capital cost as mentioned previously.

3.2.1 Reciprocating engines

Reciprocating engines are based on conventional piston-driven internal combustion engines. For micro-CHP applications, typically, spark ignition engines are used. The mechanical energy produced by the piston displacement is converted to electricity by an electrical generator. Therefore the exhaust heat as well as the heat from the lubricating oil cooler and the jacket water cooler of the engine are recovered using heat exchangers delivering the heat.

Reciprocating engines operate with less excess air, which leads to higher combustion temperature causing thermal NO_x production. To reduce the amount of NOx released, two possibilities exist: the engine can operate in lean mode with excess air or operate almost at the stoichiometry and use a three-way catalyst.

The electrical efficiency of reciprocating engines, defined as net electricity output divided by natural gas input, depends strongly on the electrical capacity of the system. At sizes less than 10 kW_{el}, efficiency generally does not exceed 26% [ONO04]. Thermal efficiency depends on the system and its level of heat integration (e.g. whether condensing heat is used). Combined electrical and thermal efficiencies (total efficiency) vary between 80% and 90%. Similarly to electrical efficiency, capital costs per kW_{el} depend on the electrical capacity of the system range from (from 2,000 €/kW_{el} to 6,000 €/kW_{el}).

Reciprocating engines are currently available on the market; different companies have already produced systems with electrical power output ranging from 1 kW_{el} to 10 kW_{el}. The market leader is the Germany-based company **Senertec** with a model called Dachs, which generates 5.5 kW_{el} and a thermal capacity of 14 kW. Other companies provide micro-CHP units as **Ecopower** with its 4.7 kWel module. Another interesting development for single-family house applications is Honda's small 1 kW_{el} named **Ecowill**.

3.2.2 Stirling engines

Unlike spark ignition engines, for which combustion takes place inside the engine, Stirling engines generate heat externally, in a separate combustion chamber. Due to the fact that fuel combustion is carried out in a separate burner, Stirling engines offer high fuel flexibility; especially for biofuels and, because of the continuous combustion, lower emissions. Other heat sources, such as solar energy with solar concentrators can be used.

Stirling engines have the potential to reach high total efficiencies. Their electrical efficiencies, however, are only moderate. For small-scale systems, they achieve low electrical efficiency, typically around 10 to 12% [ONO04].

Stirling engines are in between demonstration phases and marketing. There are still field trials being carried out; but initial commercial products are already defined and on the verge of series production. Several modules are available with power range from 0.8 kW_{el} to 10 kW_{el}. **Whispergen** has developed a Stirling engine with electrical power output of 1 kW_{el} and 7 kW_{th} of heat. Several companies [MEC (Microgen), Infinia (STC)] are in the development of a Stirling engine with an electrical power output of 1 kW_{el} and a thermal capacity output from 4 to 40 kW with a corresponding electrical efficiency of 10%. **Sunmachine** has lately developed a module producing from 1.5 to 3 kW_{el} with a corresponding thermal capacity output from 4.5 to 10.5 kW. They pretend to have an electrical efficiency of 20% with a total efficiency of 90%.

3.2.3 Fuel cells

A fuel cell converts the chemical energy of hydrogen and oxygen continuously into electrical energy. The energy incorporated in the reaction of hydrogen and oxygen to water will be partially transformed to electrical energy.

Basically a fuel cell consists of a stack of layers arranged around a central electrolyte: an anode at which the fuel is oxidized; a cathode at which the oxygen is reduced; and bipolar plates, which feed the gases, collect the electrons, and conduct the reaction heat.

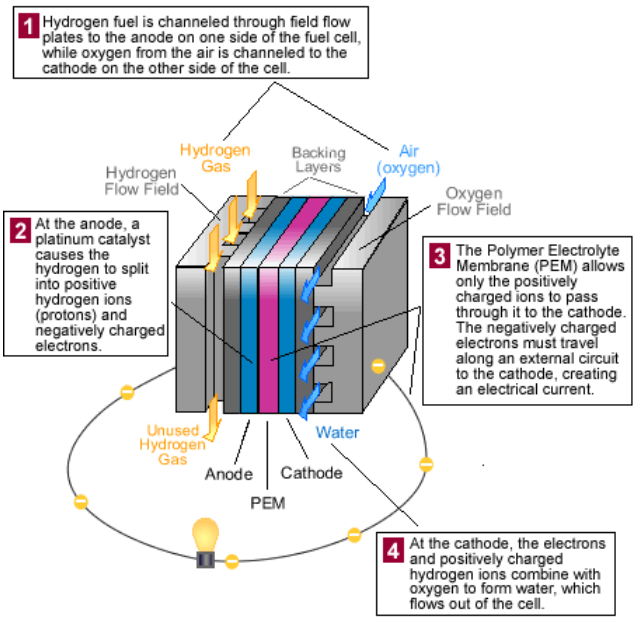

Figure 1.5 – Basic construction of a fuel cell-example Polymer Electrolyte fuel cell [ONO04].

Fuel cell micro-CHP units are either based on Polymer electrolyte Fuel Cells (PEFC; also Proton Exchanger Membrane Fuel Cell, PEMFC), using a thin membrane as an electrolyte and operating at about 80°C, or solid Oxide Fuel Cells (SOFC), which are high temperature fuel cells working at 800°C. Typically natural gas is the available fuel for micro-CHP applications. In short and medium perspectives, a PEMFC in the low power range may reach seasonal electrical efficiency on the order of 28 to 33%; in the long term it is possible to achieve up to 36% for domestic systems. However, it is unclear whether fuel cell systems can achieve the same thermal efficiencies as the competing technologies. The quantity of heat extracted depends mainly on the level of temperature at which the heat is rejected and from the technical feasibility of the heat recovering system since in fuel cells the heat could not be extracted at well-defined points in the system.

Fuel cells are still in the R&D stage. Among the most advanced companies in this sector is **Sulzer Hexis**, marketing a 1-kW_{el} SOFC system with an electrical efficiency between 25% and 30%. **Vaillant** has integrated a plug power PEMFC stack into a heating system with capacities of 4.6 kW_{el} and 7 kW_{th}. The target electrical efficiency of these systems is above 30% [].

3.2.4 Steam and organic fluid engines

Steam or organic fluid engines represent one of the most advanced concepts currently under development. These engines are based on Rankine cycles. Several companies are working on the development of such engines using different types of expanders for the vapor, such as free-piston engine, scroll expanders, or reciprocating engines with different working fluids such as steam or organic fluids.

An Australian company, Cogen Micro, is developing a 2.5-kW_{el} system with a thermal power output of 12 kW_{th}. Energetix Genlec is developing another system with a 1-kW_{el} generator with 10-kW_{th} modulated using a scroll expander with organic working fluids. These systems represent in general moderate electrical efficiency. However, none of these products is commercially available yet.

3.2.5 Micro cogeneration technology findings

To identify the best technology for building application, the different conversion technologies will be compared on the basis of selected criteria:

- Thermodynamic performance (electrical and overall efficiencies, and primary energy saving).
- Economic profitability (capital cost, operating cost, and electricity cost).
- Environmental parameters (CO_2 emissions).

Table 1.2 presents the characteristic of the different micro-CHP technologies.

Table 1.2 – Micro cogeneration technologies available in the market [PEH06, PAE06a].

Parameter range	ICE	Fuel Cell	Stirling engine	RC–ORC
Electrical capacity (kW_{el})	1-10	0.5-10	1-10	0.5-10
Electrical efficiency (% HHV)	20-40	30-50 PEMFC 40-50 SOFC	10-25 Curent 35-50 Possible	10-20
Heat recovery efficiency (% HHV)	50-60	40-60	40-60	N.A.
Temperature of heat available (°C)	85-100	80-100 PEMFC 950-1000 SOFC	200	N.A.
Overall efficiency	80-90	70-90 PEMFC 70-95 SOFC	65-95	N.A.
Thermal output (kW_{th})	3-30	1-30	3-15	N.A.
Availability (%)	85-98	95	85-90	N.A.
Part load performance efficiency?	Good	Best	Better	N.A.
Maintenance cost (€/kWh_{el})	0.008-0.012	0.016-0.024	0.005-0.01	N.A.
Emissions	Low	Lowest	Lower	N.A.
Cost (€/kW_{el})	785-2200	N.A.	N.A.	N.A.
Potential fuel	Diesel, Gas	N.A.	Gas, wood pellets	Diesel, gas, wood pellets, solar

Reciprocating engines are commercially available and produced in large numbers, achieving high electrical and thermal efficiencies, but these systems suffer high maintenance cost, and higher exhaust emissions compared to the other micro-CHP systems. Since the combustion process occurs inside the cylinder limiting the flexibility of fuel use, no renewable energies can be used except bio-fuels and biofuels.

Stirling engine represents the advantage of high fuel flexibility since the combustion is carried out in a separate burner, allowing the use of bio-fuels, wood, and solar radiation. Stirling engine has the potential of achieving high total efficiency, though with only moderate electrical efficiency. These systems are commercialized with high initial cost; the use of solar energy requires a large concentrator mirror since heat input of the Stirling engine should be of high quality to ensure an acceptable electrical efficiency.

Fuel cells are in the R&D phase, with a number of pilot plants currently being tested. They offer the benefit of the highest electrical efficiency and almost zero local emissions. However, it remains unclear if these fuel cell systems can achieve a total efficiency equalizing those promised by competing technologies. Also, the high capital cost of early product generations remains a major challenge to overcome as well as CO_2 emissions related to hydrogen generation.

Vapor expansion machines are still in the R&D phase. Potentially, they offer low emissions and high fuel flexibility, due to their external burner. In addition, some steam engine concepts allow electricity to heat ratios varying from 0.3 to pure heat supply. However, the electrical efficiencies are expected to be low depending on the level of temperature of the heating source.

To develop a micro-CHP system operating with renewable energy as solar energy and biomass, the only two technologies available on the market are the Stirling engine and vapor engines due to their external burner. However, Stirling engine represents a major drawback when operating with solar energy, which is the need of large concentrator mirror to achieve high quality heat in order to ensure good operation of the Stirling engine, and it represents a high capital cost. Therefore, vapor engines seem to be the most attractive technology when operating with multiple-type of fuels at various levels of temperatures. Many works [OLI02, ZHA06 and YAG06] have been done in this field and some demonstrative projects have been carried to build some micro-CHP systems operating on solar energy especially with organic working fluids.

3.3 Potential of Micro-CHP systems for the building sector

The prospects of broad diffusion of innovative micro-CHP technologies depend significantly on their economic profitability. However, before conducting a specific economic study, an analysis will be performed to identify if significant energy and CO_2 savings could be made and to determine the minimum thermodynamic performances required from these technologies to reach significant environmental benefits. Many new technologies are emerging as potential low carbon heat and/or power sources for the building sector, which could be considered as a direct replacement of the standard domestic boilers. Some of the main examples chosen in this study are: heat pumps, gas condensing boiler, and micro-CHP technologies.

In this study seven different heating systems with different thermodynamic performances will be compared to a reference heating system to identify the potential of primary energy and CO_2 emission savings. The different heating systems considered in this study are listed in Table 1.3. For micro-CHPs operating with biomass and solar energy, the different values in brackets correspond to the solar energy share of the total primary energy consumed by the micro-CHP system.

Table 1.3 – Heating system thermodynamic performance.

Heating system	Fuel	η_{el}	η_{th}	η_{tot}
Reference case (boiler)	Oil	0	80	80
Gas boiler	Gas	0	90	90
Condensing boiler	Gas	0	100	100
Wood-pellet boiler	Wood pellets	0	90	90
Heat pump	Electricity	0	COP = 3	COP = 3
Micro-CHP (Vapor engine)	Wood/solar	(5,10,15)/(5,10,20)	85/80/75	85
Micro-CHP (ICE)	Gas	20	60	80
Micro-CHP (Vapor engine)	Solar	10*	75*	85*

* These values correspond to the RC efficiency, which do not include the thermal efficiency of the solar collector because it will not affect the results.

For each configuration, the primary energy saving and CO_2 emission reductions are calculated. To assess the primary energy saving and CO_2 emission reductions, comparisons are made with separate production of heat and electricity (see Figure 1.6). For the reference state, an oil boiler with 80% efficiency is considered. Electricity is bought from the grid. The amount of primary energy needed to produce this electricity is strongly dependent on the technology in use. The conventional values, fixed by the French government for the electricity production efficiency, was 1/(2.58) that corresponds to $\eta_{el,ref}$ = 38.75%. This value integrates the transformation and transport losses, which reflect a realistic value when the electricity is produced by nuclear power plants.

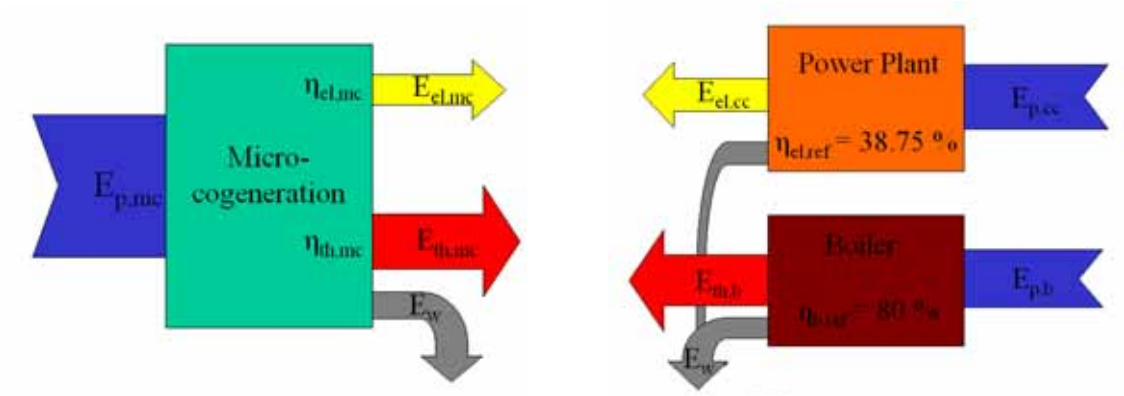

Figure 1.6 – Comparison of thermal and electrical outputs between a CHP engine and a conventional system where the thermal output is generated by a burner and the electricity by a power plant [ISM03].

For a micro-CHP scenario, the operating strategy is determined by the heat demand. Surplus electricity is delivered to the grid. If more electricity is needed than the micro-CHP can deliver, this extra amount of electricity is taken from the grid. To calculate the primary energy use, the electricity sold to the grid is deduced from the total amount produced, using the central power plant efficiency, because the electricity has not been produced by the central power plant. For economic reasons discussed previously, the micro-CHP system will be assumed to cover all the heat needs and will replace totally the conventional boiler.

3.3.1 Energy balance: PES for the micro-CHP application

The primary energy saving has been introduced by the EU cogeneration directive [DIR04] given by Eq. (1.1):

$$PES = \frac{E_{p,ref} - E_{p,mc}}{E_{p,ref}} \tag{1.1}$$

The cogeneration Directive [DIR04] promotes the development of high efficiency cogeneration of heat and power. The cogeneration directive [DIR04] imposes only a PES to be higher than zero (PES>0) for micro-CHP to be classified as high efficiency small-scale cogeneration.

The primary energy saving for a micro-CHP does not depend only on the electrical efficiency of the system, but it depends also on the total efficiency of the micro-CHP system. In some cases, replacing a boiler with high thermal efficiency by a micro-CHP with moderate total and electrical efficiencies cannot achieve primary energy saving. To locate the minimum requirement for a micro-CHP thermodynamic performance to ensure primary energy saving, a calculation procedure will be conducted for the production of 1 kWh of thermal energy to identify its potential for primary energy saving.

The total primary energy required for producing 1 kWh of electrical energy by separate production of heat and power is calculated by Eq. (1.2)

$$E_{p,ref} = \frac{1}{\eta_{b,ref}} + \frac{\lambda}{\eta_{el,ref}} \; [J] \tag{1.2}$$

With

$$\lambda = \eta_{el,mc} / \eta_{th,mc} \tag{1.3}$$

On the other hand, to produce the same heat and power by a micro-CHP system, the primary energy required is calculated by Eq. (1.4)

$$E_{p,mc} = (1+\lambda)/\eta_{tot,mc} \text{ [J]} \tag{1.4}$$

To pursue a primary energy saving Eq. (1.2) and Eq. (1.4) have to ensure the following condition:

$$E_{p,mc} < E_{p,ref} \tag{1.5}$$

Developing the last Eq. will give the following expression:

$$\left(\frac{(1+\lambda)}{\eta_{tot,mc}}\right) < \frac{1}{\eta_{b,ref}} + \frac{\lambda}{\eta_{el,ref}} \tag{1.6}$$

For the French case, the electrical reference efficiency of the power station plant and the thermal efficiency of the reference boiler were assumed to be respectively 38.75% and 80%. Therefore, the primary energy savings due to the production of 1 kW_{th} by means of a micro-CHP system, for different total efficiencies and different power to heat ratio, is presented in Figure 1.7. The results show that when replacing a conventional heat boiler with thermal efficiency of 80% by a micro-CHP system with total efficiency higher than 80%, the micro-CHP exhibits a PES > 0 for the different operating powers to heat ratio. However, when the total efficiency of the micro-CHP system is lower than 80%, then a minimum power to heat ratio is required to exhibit a positive primary energy saving. From the technology review conducted in the previous section, all the micro-CHP systems represent a total efficiency higher than 80% except fuel cell; however, these fuel cells exhibit high power to heat ratio. Therefore, for the French case, all the micro-CHP systems can exhibit positive primary energy saving.

For micro-CHP with Steam engine, the total efficiency is in general higher than 80% when operating with fossil fuels including wood [PEH06]. On the other hand, when operating with solar energy, the total efficiency can decrease to 50% depending on the thermal efficiency of the solar collector, but it still exhibits a positive primary energy saving since solar energy is assumed to be free primary energy (the primary energy conversion factor of the solar energy is equal to zero).

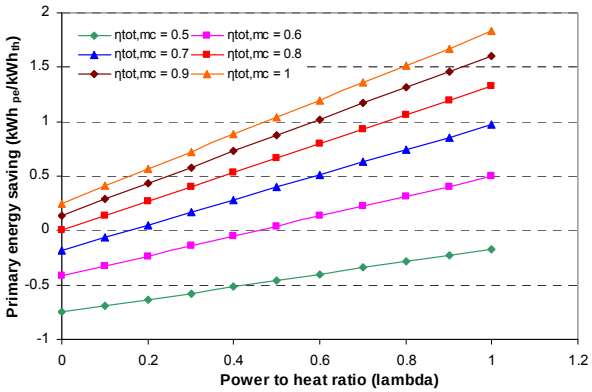

Figure 1.7 – Micro-CHP primary energy saving.

3.3.2 Primary energy saving analysis

The primary energy for the different proposed systems is calculated by the following Eq.(1.7):

$$PE_c = \frac{E_{th}}{\eta_{th}} K_{fuel} + \left(E_{el} - E_{el,mc}\right) K_{el} \tag{1.7}$$

With

$$E_{el,mc} = \lambda E_{th} \tag{1.8}$$

Where E_{th} corresponds to the thermal energy use in the reference building, K represents the different factors (see Table 1.4) used for transforming primary energy to final energy. For a boiler, $E_{el,mc}$ are equal to zero. However, for the heat pump calculation, PE_c is given by the following Eq.(1.9):

$$PE_c = \left(\frac{E_{th}}{COP} + E_{el} \right) K_{el} \tag{1.9}$$

Table 1.4 – Factor used for energy conversion from final energy to primary energy [ARR06a].

Fuel	Gas	Oil	Wood	Electricity
K	1	1	0.6	2.58

Results for the primary energy consumption of the different heating systems units, in relation to the reference case with an oil fired boiler and an electrical energy delivered by the French power plant stations, are shown in Figure 1.8. The heat to power ratio λ is considered to be equal to 4 [] for residential building. As it can be seen, the largest savings for primary energy use are obtained with micro-CHP system operating on solar energy. However, micro-CHP system operating only on solar energy is not feasible due to the variation of the solar energy during the day. Therefore, a back-up energy source is needed to ensure a continuous operation of the system when no solar energy is available. As it can be seen, the primary energy consumption is not 100% since the electricity generated by the micro-CHP can cover only a small part of the electrical energy need.

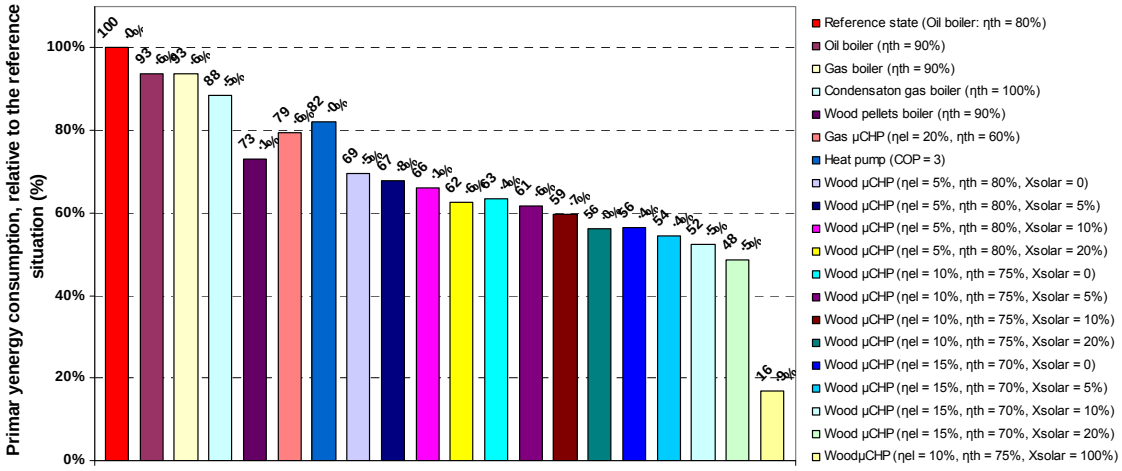

Figure 1.8 – Primary energy consumption for different heating systems.

Otherwise, micro-CHP system operating on biomass energy represents the largest primary energy saving, even when compared to highly efficient boilers such as gas condensing boiler or other technologies of micro-CHP as gas engine.

3.3.3 Environmental impact analysis

In the reference situation, without CHP, a certain amount of CO_2 is emitted through the generation of heat and electricity. CO_2 emissions due to the generation of heat and power have to be evaluated separately. The CO_2 emitted through the generation of heat is calculated for an oil boiler with thermal efficiency of 80% as reference case, CO_2 emissions are assumed to be 300 gCO_2/kWh of burned oil. All emission values due to the combustion of fuel are calculated relatively for the low heating value (LHV). The CO_2 emitted through the

electricity generation strongly depends on the technology. For building application, the electricity is assumed to be produced by the French power plants for period of heat generation (winter period), CO_2 emissions of the average French power plant equal 180 gCO_2/kWh_{el}. However, this value can be higher if we consider that the electricity is produced by combined gas power plant (234 gCO_2/kWh_{el}) or coal fired power plant (800 gCO_2/kWh_{el}), and even if we consider the average of the European power plant with 400 gCO_2/kWh_{el}. The produced CO_2 through the generation of heat for the different types of fuel used are given in Table 1.5.

Table 1.5 – Fuel cost and CO2 emission [ADE05].

	Heating oil	Natural gas	Electricity	Pellets	Solar
CO_2 emissions gCO_2/kWh [LHV]	300	234	180	23	0

CO_2 emissions for electricity and heat generation by the different micro-CHP technologies are calculated. First, the efficiencies allow calculating the necessary amount of valuable energy and its corresponding primary energy. Therefore, the corresponding emissions will be calculated depending on the type of fuel used in the specific micro-CHP system under study.

For heating and cogeneration systems, the CO_2 saving S ($kgCO_2/kWh_{pe}/m^2$.year) is calculated by subtracting emissions associated with the heat and power produced by the cogeneration system to cover all the heating needs of the building and part of its electricity needs, compared to CO_2 emissions emitted by the separate generation systems to cover all the heating and electrical energy needs.

$$S = Em_{CO_2,ref} - Em_{CO_2,c} = \left(\frac{E_{th}}{\eta_{b,ref}} \varepsilon_{fuel,b} + E_{el,i} \varepsilon_{el} \right) - \left(\frac{E_{th}}{\eta_{th,mc}} \varepsilon_{fuel,mc} + E_{el,mc} \varepsilon_{el} \right) \quad (1.10)$$

For heat pumps, the CO_2 savings S will be calculated to take into account the production of heat from electricity given by the following Eq.:

$$S = \left(\frac{E_{th}}{\eta_{b,ref}} \varepsilon_{fuel,b} + E_{el,i} \varepsilon_{el} \right) - \left(\frac{E_{th}}{COP} \varepsilon_{el} \right) \quad (1.11)$$

CO_2 emission reductions compared to the reference case are given by the following Eq.:

$$\Delta S = \frac{S}{Em_{CO_2,ref}} \quad (1.12)$$

Figure 1. shows that the results for CO_2 emissions are quite the same as the results for the primary energy use of micro-CHP operating with biomass and/or solar. It is again the micro-CHP operating on solar energy that presents the best results in term of CO_2 emission reductions, more than 94%, followed by the different micro-CHPs operating on multiple energy solar or/and biomass. The abatements vary between 80% and 90% depending on the micro-CHP electrical efficiency and the percentage of solar energy share. However, the smallest CO_2 emission reduction is obtained by the micro-CHP operating with gas. This is due to the low CO_2 contained in the reference electricity generation system. As mentioned before, these calculations are done, taking into account the electricity produced by the French energy mix, which represents a low CO_2 since more than 80% are produced by nuclear power plants. If the electricity is produced by fossil central power plant systems, the CO_2 saving will gradually rises.

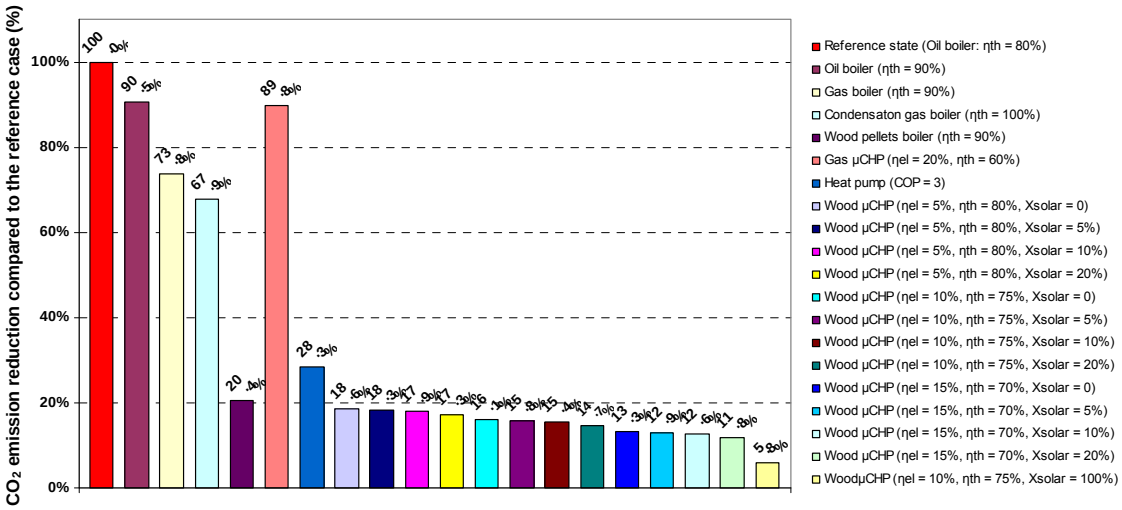

Figure 1.9 – Relative CO_2 reduction for different heating systems.

3.3.4 Economic analysis

The economic viability of micro-CHP systems is critically dependent on the capital cost of the installed system, maintenance costs, and retail prices for the cogeneration system fuel and centrally generated electricity, as well as the purchase electricity price if electricity is sold to the grid.

The economic viability of micro-CHP in the residential sector benefits from the higher retail prices paid by consumers for grid-supplied electricity though currently, the tariff of the electricity imposed by the government is usually lower than the cost of electricity produced by the micro cogeneration systems. Currently this price paid to the producer is usually more than the offset due to the high cost of the cogeneration systems per kW_{el} and kW_{th}. Cogeneration systems are financially more attractive in periods of high electricity prices and low fossil fuel prices. However, for micro-CHP systems operating on renewable energies as wood, it is economically more attractive when it operates in period of high electricity and fossil fuels prices. A special care has to be taken when evaluating the price of wood for the future time since it can be prone to higher inflation rate.

Due to its high specific investment cost, a careful design procedure of cogeneration system is needed in order to define the best sizes of the equipment, considering not only the cogeneration equipment, but also the heat storage devices and the advanced control systems that will forecast the heat requirement and define the optimal control using model based predictive control algorithms [PAE06b].

To overcome the different economic problems hampering the uptake of micro-CHP systems, developments have to be done for decreasing the capital, maintenance and operating costs, and imposing high price for the electricity purchased from micro-CHP operating on intermittent and non-intermittent renewable energy. These factors are discussed briefly below to identify the different sectors where the developments of these systems can be promoted.

- **Capital cost:** Decreasing the capital cost of a system is only feasible when it is possible to pass to the serial production or to develop a new system with off-the shelf components available at low cost. A technical study will be conducted in the following sections to identify the available technologies or components to develop a micro-CHP to limit the costs.
- **Maintenance cost:** Minimizing the maintenance cost is viable only when the different operating components of the system have a long life time and have reached their mature reliability.

- **Operating cost:** The different options to minimize the operating (fuel) costs are to design a high efficient system operating on energies available at low cost or operating on "free" energies. Solar energy represents one of the free energy; however, using this energy affects the capital cost of the system by installing a large surface area of solar collectors that represent a high capital cost. Another possible solution is to operate with wood, which is, in France, an available resource at relatively low cost compared to fossil fuels. However, in 2007 price wood has been subject to a high inflation rate due to a higher demand. Therefore, the lower cost of wood compared to other type of fossil fuels as gas and fuel oil remains under investigation in the near future.

Other factors may help to promote the development of micro-CHP, which can be imposed by the government as:

- Fixing the price of electricity sold to the grid and produced by micro-CHP operating on intermittent and non-intermittent renewable energy to a level higher than the electricity price bought from the grid. Let to the locally producer to decide whatever electricity will be used locally or will be sold to the grid. The owner can decide to purchase all the electrical energy needs from the grid and to sell to the grid all the electrical energy produced by the micro-CHP system by installing separate meters (to be discussed depending on the CO_2 content). The second option is of course more appealing when the selling price of the electricity produced by the micro-CHP system is higher than the price of the electrical energy purchased from the power suppliers.
- Imposing taxes on CO_2 emissions or adopting "Green credits" for systems saving CO_2 emissions.
- Helping the investment -CHP owner by subsidies.

For the economical analysis, the levelized electricity generation costs are calculated by adding up levelized investment, maintenance and fuel costs, and subtracting a credit for avoided heat generation costs. Costs of the different supply options are calculated at 2007 prices including VAT. Inflation of the cost of the fossil fuels is assumed to be 2% per year. Levelized supply costs are calculated with a model. The technical lifetime of the micro-CHP system is assumed to be 10 years. The nominal rate of return for capital is 6%. The prices of wood is given by [ITE07] and assumed to be 5.5 c€/kWh_{th}. The cost of the heat avoided is assumed at 6.3 c€/kWh_{th} for individual apartments and 7.1 c€/kW_{th} for apartment buildings; however, the heat cost delivered by the heat networks varies from 8.8 c€/kWh_{th} to 7.02 c€/kWh_{th} [PRE06].

The maintenance costs and the investment costs cannot be found in the literature since the micro-CHP system operation on wood and solar energy using steam engine does not exist in the market. However, the maintenance costs will be fixed at 50 €/MWh_{el} representing the highest maintenance cost for micro-CHP given by [PEH06]. The investment costs will be also predicted by the different data available for the price of wood boilers and micro-CHP system available. The investment costs depend mainly on the electrical power output and is correlated by Eq. (1.13). This equation is given for steam engines based on Rankine cycle and estimated from cost data collected to pellets boiler and multiplied by 2 for estimated the cost of the total system (boiler and steam engine)

$$C_{inv} = 8151 * \ln(P_{el}) + 12641. \ (€/kW_{el}) \qquad (1.13)$$

Figure 1.10 shows the levelized electricity generation costs as a function of the full load operation hours for different micro-CHP electrical power outputs. The electricity generation costs are significantly higher than electricity purchase costs for households (~ 11 c€/kWh_{el}).

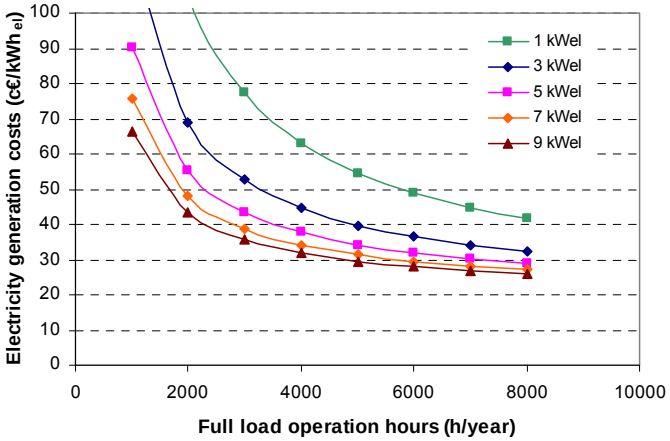

Figure 1.10 – Levelized electricity generation costs (2007 prices with VAT).

Thus, it is not economically feasible to develop a micro-CHP system operating on wood and solar energy based on a steam engine without integration of government subsidies. They can be implemented as follows:

- Payment of a bonus from 10% to 50% of the total capital price to finance the installation of a micro-CHP operating on renewable energies
- CO_2 taxes: 20 €/tCO_2 to 40 €/tCO_2 avoided
- Payment for a bonus or imposing higher electricity costs for electricity produced from renewable energies and fed to the grid. These prices can varies from 15 c€/kWh_{el} to 60 c€/kWh_{el}.

Other economic parameters can be of influence on the levelized electricity generation cost, mainly the high rate inflation of the cost of fossil fuels. Results presented in Figure 1.11 show that the electricity-levelized cost can be attractive only if the different subsidies are applied (Bonus = 50%, fossil fuel inflation cost = 10%, and CO_2 taxes = 40 €/tCO_2). Therefore, micro-CHP systems represent economic benefit only if special tariff of the electricity produced from micro-CHP operating on renewable energy is applied. These tariffs can vary from 30 c€/kWh_{el} to 60 c€/kWh_{el} depending on the different subsidies imposed by the government and the full load operation hours of the system.

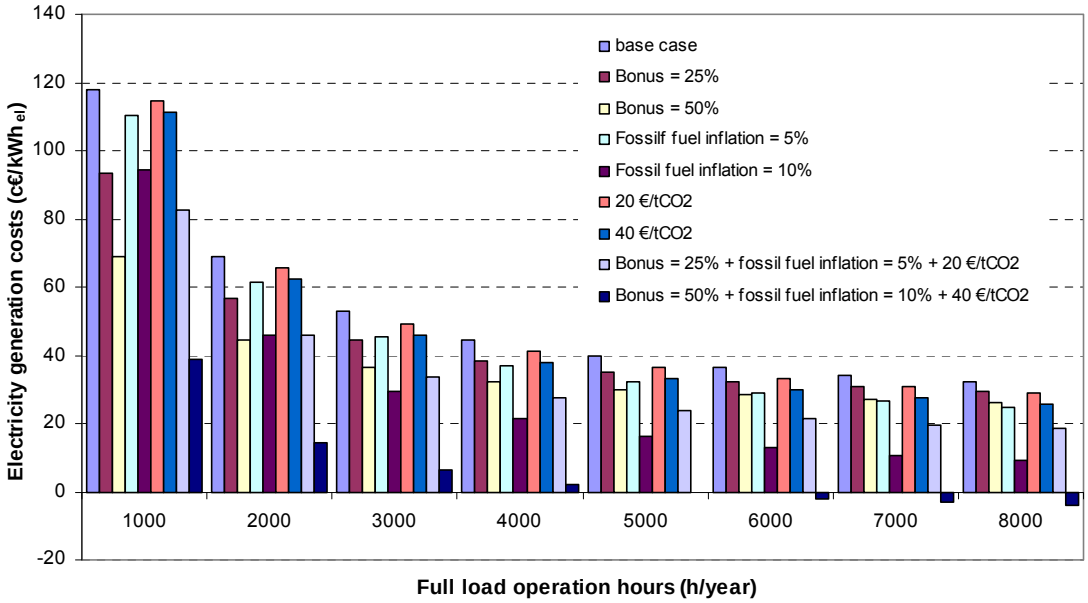

Figure 1.11 – Levelized electricity generation costs (2007 prices with VAT) for different economical politics.

Therefore, a micro-CHP designed for apartment buildings has to be able to deliver all the heating and DHW needs of apartments operating without a supplementary boiler.

3.3.5 Sustainable development

The micro-CHP systems enter in the sustainability development since they have three different effects on economy, environmental, and also socially. The energy economy is exploited by the energy bill reduction, a better profitability of the different investment, increasing the share of electricity decentralization, improving the equilibrium electrical grid and the reduction of the energy dependence of the different countries. Different environmental impacts of the integration of the micro cogeneration system are reduction of emissions of the different pollutants and the CO_2, preserving the reserves of energy, and reduction of the losses in the different electric grid lines and the valorization of the different waste energy. The different social impacts are represented by the increase in local employment (study, maintenance…) and export expertise.

3.4 Dimensioning of a micro cogeneration system (residential and collective)

As demonstrated above, the full load operation hours of the micro-CHP system has the major influence on its economical feasibility. A minimum of 4,000 hours of annual operation is required in order to make the micro-CHP system economically feasible with a purchased electricity cost of 40 c€/kWh$_{el}$ sold to the grid, which represents an acceptable value compared to other renewable energies for electricity production such as photovoltaic (55 c€/kWhel) [ARR06b].

Then to carry out the dimensioning of a micro-CHP system, a typical daily/weekly load curves and annual load curves should be determined. A typical annual load profile is shown in Figure 1.12. However, all the heat demand should be covered by the micro-CHP system to prevent the installation of a backup system that can affect the total cost of the heating system. As shown in Figure 1.12, dimensioning the system for base load requires the installation of a backup system; however, dimensioning at the peak load can affect the annual total-hour operation of the micro-CHP system. Then, finding a compromise between these two options needs a special care on the selection of the electrical power output of the micro-CHP system regarding its power to heat ratio and the volume of the heat storage tank.

The micro-CHP system can be designed to operate at a fix electrical and thermal power output (average) or modulated electrical and thermal power output. The selection of one or the other option depends mainly on the performance of the micro-CHP system at off design operation load.

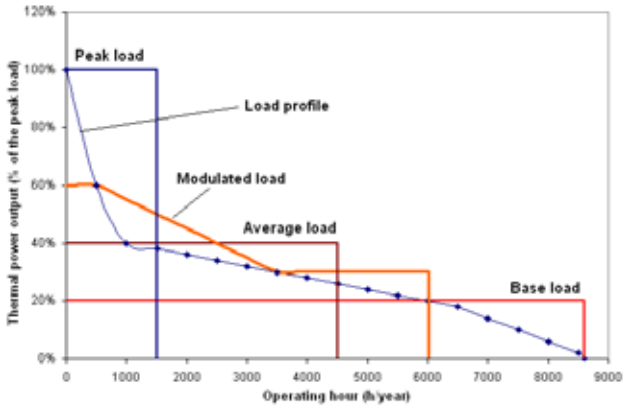

Figure 1.12 – Example of an annual load duration curve profile of the heat demand [KAR05].

The electrical power output of micro-CHP systems depends on the heat and DHW demands in buildings. Otherwise, the insulation level of buildings strongly influences the heat demand.

To identify the best ratio of power output to heat demand, an analysis of different types of buildings in France with different insulation levels and different surface areas representing in general the building France stocks is carried out.

Four cases are studied for single houses (120 m^2) and apartment buildings (1,000 m^2).

- Before 1975: 400 kWh/(m^2.year).
- Base case: 211 kWh/(m^2.year).
- RT2005: 130 kWh/(m^2.year).
- BBC: 50 kWh/(m^2.year).

The different primary energy consumptions and CO_2 emissions related to the energy used in the different types of buildings are represented in Table 1.6. Results show that the PES is about 27% and the CO_2 reduction of 84%. The avoided CO_2 emissions depend on the type of building and the corresponding surface area varying between 1 tCO_2/year and 58.2 tCO_2/year, compared to the reference case. Therefore, from an environmental point of view, the highest CO_2 emission reductions and PES are achieved when these systems are installed in apartment buildings with high primary energy consumption or CHP has to be installed in order to provide heat to high efficient apartment buildings or several single houses with a small heating network.

Table 1.6 – Reference buildings.

	Single house				Apartment building			
Building type	BBC	RT2005	Average	Before 1975	BBC	RT2005	Average	Before 1975
Primary energy (kWh_{pe}/m^2.year)	50	130	211	343	50	130	211	343
Area (m^2)	120				1000			
Heating and DHW load (MWh/year)	2.76	7.19	11.67	18.97	158	97	60	23
Electricity demand (MWh_{el}/year)	0.99	2.5	4.1	6.7	8.2	21.37	34.6	56.3
PES (%)	27	27	27	27	27	27	27	27
Primary energy with µCHP (kWhpe/m^2.year)	31.7	82.4	133.8	217.5	31.7	82.4	134	217
CO_2 emissions ($kgCO_2$/m2.year)	10.12	26.31	42.70	69.4	10.12	26.31	42.70	69.4
CO_2 emission saving (%)	84	84	84	84	84	84	84	84
CO_2 emissions with µCHP ($kgCO_2/m^2$.year)	1.63	4.25	6.89	11.2	1.63	4.25	6.89	11.2
CO_2 emission avoided ($kgCO_2$/year)	1018.8	2647.2	4297.2	6984	8490	22060	35810	58200

Figure 1.13 shows the different full load operation hours depending on the nominal electrical power output of the micro-CHP, the different types of buildings and their corresponding surface areas. As mentioned before, a minimum of 4,000 hours of full load operation is required to achieve an acceptable profitability of the micro-CHP system. For single houses, micro-CHP is not feasible economically, even when the primary energy consumption is very high since the maximum operating hours of the micro-CHP is about 2,600, which correspond to levelized electricity price of 90 c€/kWh_{el} (see Figure 1.10). Therefore, micro-CHP systems are only economically feasible when installed in apartment buildings. Special care has to be taken when dimensioning the micro-CHP system since if the system is oversized, it can reduce the full load operation hours then increase the levelized electricity cost (i.e.: apartment buildings with 130 kWh/m^2.year with a micro-CHP system of 7 kW_{el}, the levelized electricity cost will be 75 c€/kWh_{el}).

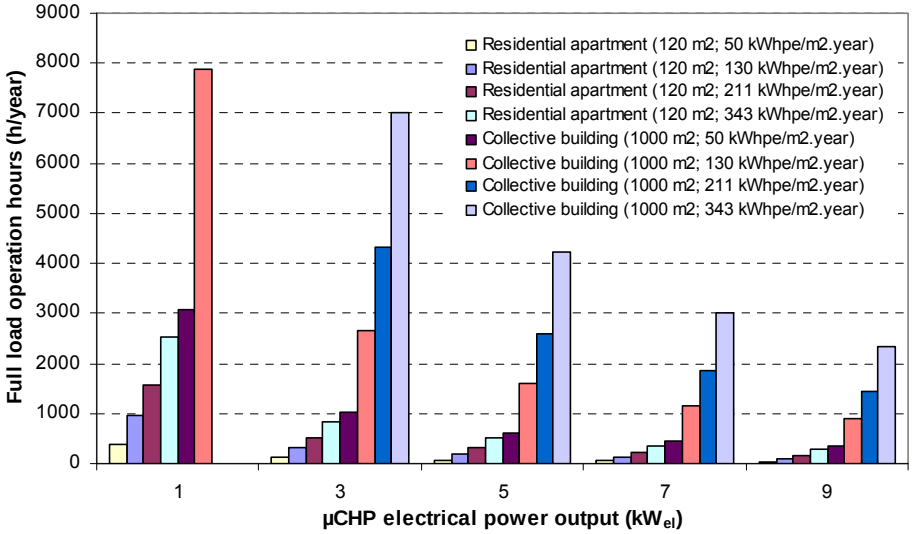

Figure 1.13 – Micro-CHP optimal power output.

Since the power output of the micro-CHP system represents a major impact on the dimensioning of the storage system and its economical feasibility, an advanced analysis has to be conducted to identify the optimum electrical power output and the heat storage volume to seek the minimum payback period of the system. The electrical output will be directly proportional to the thermal power output depending on the power to heat ratio of the micro-CHP system selected.

4. Solar Biomass Organic Rankine Cycle system

From the analysis performed before, a micro-CHP system operating on renewable energies (solar and biomass) shows different advantages compared to conventional heating systems. In this section, a micro-CHP based on a Rankine cycle system operating on solar and biomass energies will be represented with the different technical barriers that have to be overcome to put this system in practical applications.

4.1 Micro CHP: Organic Rankine cycle

The Rankine cycle is a thermodynamic cycle using a phase-change working fluid dedicated to electricity production in large power plant from heat (combustion gases; see Figure 1.14). The Organic Rankine Cycle is a simple cycle and different working fluids are to be chosen depending on the level of temperature.

The ideal Organic Rankine Cycle consists of the four following evolutions (see Figure 1.15):

1 – 2: Isochoric compression by the pump.
2 – 3: Constant pressure heat exchange in the boiler.
3 – 4: Isentropic expansion in the turbine.
5 – 1: Constant pressure heat rejection in the condenser

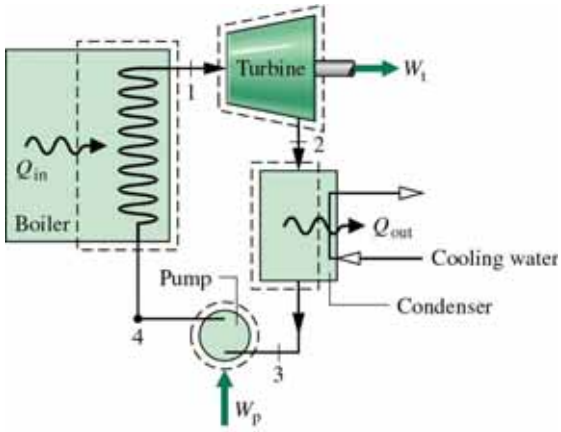

Figure 1.14 – Rankine cycle Layout.

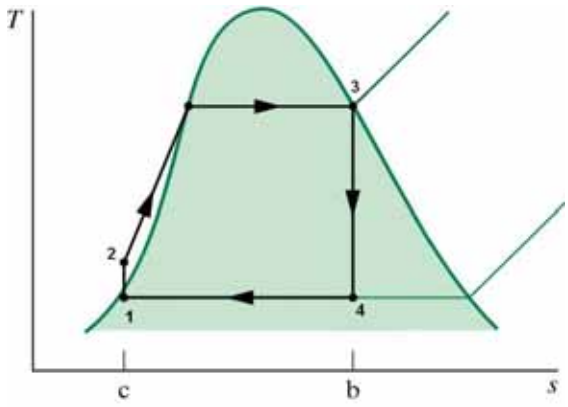

Figure 1.15 – T–S Diagram of an ideal Rankine cycle.

The working fluid enters the pump at state 1 as saturated liquid and is compressed to the boiler operating pressure. The fluid enters the boiler as sub-cooled liquid at state 2 and leaves the boiler as saturated vapor at state 3. Heat is transferred to the fluid at constant pressure. The saturated vapor at state 3 enters the turbine where it expands isentropically and produces work by rotating a shaft connected to an electric generator. The temperature and the pressure of the fluid drop during this process at state 4, where it enters the condenser. The fluid is condensed at constant pressure in the condenser, by rejecting the heat to the cooling media. The fluid leaves the condenser as saturated liquid and then enters the pump to complete the cycle. Some working fluids, especially wet fluids such as water needs to be superheated to increase their thermodynamic efficiency and to reduce the quantity of water droplet at the outlet of the turbine. This cycle is known as Hirn cycle and it is mostly used when high expansion ratio occurs on the turbine.

4.1.1 Energy efficiency

The efficiency of the thermodynamic Rankine cycle (RC) is the ratio of the net work output divided by the net heat input given by Eq. (1.14).

$$\eta_{RC} = \frac{\dot{W}_{net}}{\dot{Q}_{in}} = \frac{\dot{W}_{turbine} - \dot{W}_{pump}}{\dot{Q}_{boiler}} \tag{1.14}$$

The maximum cycle efficiency of the Rankine cycle depends directly on the temperature of the source and sink temperatures. Carnot cycle is the ideal cycle that represents the higher cycle efficiency between the defined source and sink temperatures.

$$\eta_{Carnot} = 1 - \frac{T_c}{T_h} \tag{1.15}$$

The maximum temperature of the heat source T_h depends on the type of energy source (solar or biomass energy). The solar energy can produce heat with maximum temperature of 1500°C [KAL04] with high concentration solar collectors. Otherwise to prevent the complexity of the system and the high cost of the solar collectors, a low concentration ratio of solar collectors is used that can operate with maximum temperature of 200°C. The biomass source is more reliable in controlling the maximum temperature of the combustion since the combustion of the wood-pellet stove occurs at higher temperature ~1100°C [NES04]. The maximum operating temperature of the heat source will be fixed to 200°C even if the available energy from the combustion of wood is slightly higher but this level of temeprature has been fixed to maintain the operation of the system with two sources of energy (solar and wood) in parallel and to limit the problems of high cost materials which have to withstand higher thermal stresses in case of higher temeprature is considered .

For the cold source, the minimum operating temperature for producing hot water is fixed at 65°C. The theoretical maximum cycle efficiency corresponding to a heat temperature of 200°C and a cold sink temperature of 65°C is 28.5%. However, in the real cycle, irreversibilities occur in the different components of the systems. The real cycle efficiency will be significantly lower than 28.5% due to the losses in the turbine, pump, boiler, and condenser.

The total efficiency of the cycle will be the product of the real cycle efficiency by the thermal efficiency of the solar collector or the wood boiler. The performance of the different components of the systems will be analyzed in details in the different chapters of this thesis to identify the most promising technologies of wood boiler, solar collector, and RC to operate for combined heat and power production in residential or collective apartments.

4.2 Intermittent and non-intermittent renewable energies for micro CHP–ORC systems

Since the operation of micro-CHP systems with fossil fuel does not always represent a reduction of CO_2 emissions, the integration of the renewable energy is a key issue to achieve a significant reduction of CO_2 emissions compared to the conventional reference systems as shown in previous sections.

The micro-CHP system operating with the RC represents a major advantage since the heat input to the system can be delivered by several renewable energy sources available globally, solar energy and biomass. The geothermal energy can represent another option but depends on location.

The solar energy is one of the less used renewable energy. This energy represents the advantage to be one of the cleanest energy and it is largely available but it is diluted. This energy is available in the atmosphere as direct and diffusion irradiation to be able to absorb this energy and produce heat with high quality (high temperature > 100°C); it has to be concentrated with adapted technologies of solar collectors available on the market but with high capital cost. On the other hand, the solar energy intensity varies strongly during the day and represents a peak around noon. To fully meet the load demand in buildings with a micro-CHP system operating only on solar energy, over-sizing of solar collectors and of the storage system is necessary. This over-sizing of the two components will affect the total capital cost of the system and it will not be necessarily profitable.

Due to these disadvantages discussed previously, a back-up source of energy is necessary to maintain the operation of the system when no solar energy is available. This second source of energy has to maintain the temperature of the heat source at the desirable temperature to prevent the deterioration of the performance of the RC and to fulfill the heat demand of buildings. Biomass energy represents a suitable solution for the back-up energy source. A number of R&D works have been realized in order to improve energy efficiency of large wood boilers. Wood-pellet boilers with thermal efficiency superior to 90% are commercially available. A technical assessment of the different potential wood boilers will be conducted in the future sections to identify the most suitable solution adapted for the micro-CHP system operating with ORC.

5. Possible configuration of the solar biomass organic Rankine cycle

The system under study is described in Figure 1.16, and is composed of seven components with to two circuits. The first circuit is the Rankine system as described in Section 4.1, including a heat recovery heat exchanger (Hex). The advantages of this Recovery Hex will be discussed in details in the following sections. The second circuit is the heat recovery circuit (HRC) composed of a pump, solar collectors, and wood-pellet boiler with a heat transfer fluid (HTF) circulating in this HRC. Three 3-way valves are integrated in the HRC.

These valves are controlled to operate the system under several configurations. These configurations are as follows:

1. Solar only generation, all the HTF passes through the solar collectors and valve n°3 bypasses the pellet boiler.
2. Biomass only generation, therefore valves 1 and 2 bypass the solar collectors and HTF passes only through the pellet boiler.
3. The Dual solar and biomass operation. Therefore valves 1 and 2 are partially opened to pass a fraction of the mass flow rate (MFR) of HTF through the solar collectors; this MFR1 will be mixed at the outlet of the solar collectors with MFR2 coming directly from the pump to feed the pellet boiler. MFR1 is controlled depending on the available solar energy.

A detailed analysis will be conducted to identify the best operating strategy between the different operational modes in the following chapters.

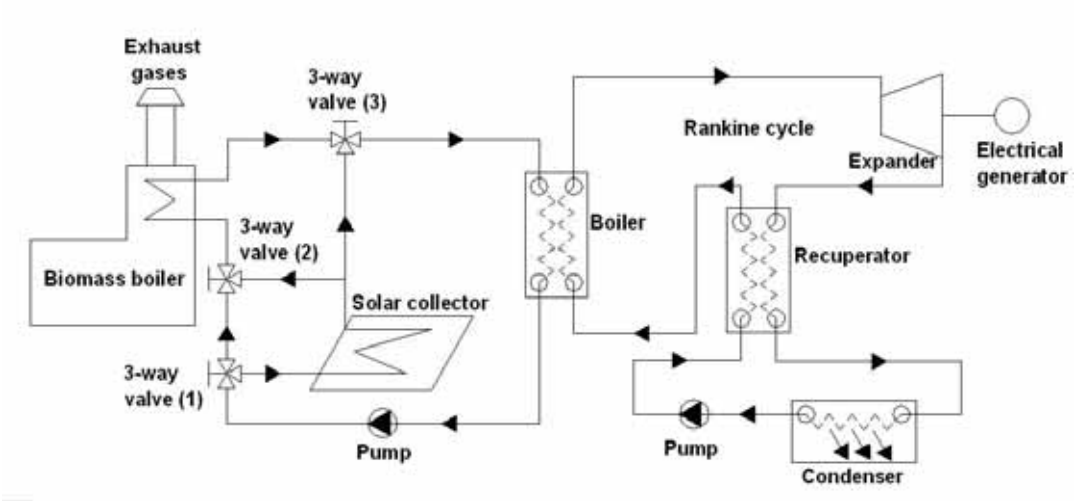

Figure 1.16 – Simplified flow sheet of the proposed SBORC-μCHP system.

6. Technical barriers

Micro-CHPs have the potential to make a significant improvement in primary energy savings and CO_2 emission reductions. The main technical challenges facing the development of these systems are summarized here below.

Working fluid: The selection of the working fluid is a key for the development of the RC meeting all the environmental requirements and ensuring a high-energy performance.

Turbine design: The turbine should be capable of transforming efficiently the recovered heat from the pellet boiler and the solar collectors into mechanical/electrical energy, over a wide range of operation. The turbine operating range depends on the minimum and maximum required heat loads. The turbine should be designed for a wide range of electrical power outputs depending on the thermal heat needs, which vary widely with the type of buildings (low or high insulation) and the surface area of the building.

Heat exchangers: They have to be designed in order to reach a high thermal efficiency with a high degree of compactness to limit the volume of the micro-CHP systems and so prevent the problems related to surface management.

Pellet boiler and solar collectors: The wood boiler and the solar collectors have to be chosen at acceptable costs. Many commercialized solar collectors are suitable for low temperature use. However, the need of solar collectors operating at medium temperature (150°C – 200°C) is still a challenge to overcome. On the other hand, additional tunings are necessary on pellet boilers that have been designed to operate at low temperature (90°C) and so low pressures.

7. Conclusions

In spite of large efforts made by the developed countries to improve the performance of the building sector, high performance cogeneration systems based on renewable energies need to be developed in order to decrease the primary energy consumption in this sector and reduce the global warming effect due to carbon dioxide (CO_2) emissions. Improvements of micro-CHP systems are underway in order to improve their energy performance and profitability.

Because of the large abundance of solar and biomass energies in the world, a specific micro-scale solar wood CHP (SBORC-μCHP) system suitable for generation of electric power and heat for residential building sector will be designed to fulfill all the heating demand while all the generated electrical energy will be directly sent to the grid for economical issues.

The electrical power output of the designed SBORC-μCHP ranges from 1 kW_{el} to 10 kW_{el} suitable for apartment buildings. The SBORC-μCHP should be properly designed in order to ensure good performance (cycle efficiency), low capital, operating and maintenance costs. A compact system has to be designed in order to facilitate its integration in different types of buildings and to limit the heat losses to the surroundings.

The choice of the working fluid affects heavily the thermodynamic cycle and the selection and design of the Rankine system. Therefore, in a first step, different working fluids will be analyzed and the most promising fluids will be selected. Then, a technical assessment will be carried out in order to identify the best available technologies to be used and the technical barriers that must be overcome in order to use the Rankine cycle for combined heat and power generation in the building sector.

The costs of the different components of the RC system have a major impact on the profitability of the system. An optimum design of the different components will be carried out focusing on the dimensioning of the solar collector surface area and the thermal power output of the biomass boiler. Therefore, an optimization algorithm will be developed to identify the optimum design for each working fluid.

A simulation of the micro-CHP system coupled to a building will be performed in the last chapter to identify the effect of the solar collector surface area, the weather data, and the thermal storage volume on the total operating hours of the micro-CHP and its effect on the economical profitability of the system. The simulation will be carried for an apartment building in different regions in France and with different levels of insulation.

References

[ACT06] *Action Plan for energy efficiency: realizing the potential, Communication from the commission, COM (2006) 545 final, Brussels, 19.10.2006.*

[ADE05] ADEME, Note de cadrage sur le contenu CO2 du kWh par usage en France, janvier 2005.

[AMO06] *Amoès, David chénier, "Impact de la micro-cogénération à bois sur l'effet de serre", Rapport d'étude, novembre 2006, www.amoes.com.*

[ARR02] *Arrêté du 13 mars 2002 fixant les conditions d'achat de l'électricité produite par les installations d'une puissance inférieure ou égale à 36 kVA pouvant bénéficier de l'obligation d'achat.*

[ARR06a] *Arrêté du 15 septembre 2006 relatif au diagnostic de performance énergétique pour les bâtiments existants proposes à la vente en France métropolitaine. Ministère de l'écologie du développement et de l'aménagement durable.*

[ARR06b] *Arrêté du 10 juillet 2006 fixant les conditions d'achat de l'électricité produite par les installations utilisant l'énergie radiative du soleil telles que visées au 3° de l'article 2 du décret no 2000-1196 du 6 décembre 2000.*

[BIR07] *J.M. Biren, M. Langlois-berthelot, T. Revial, P. Dumas, Les installations de cogénération sous obligation d'achat, Inspection générale des Fiances N° 2006-M-060-01, Janvier 2007.*

[DIR01] Directive 2001/77/EC of the European parliament and of the council of 27 September 2001 on the promotion of electricity produced from renewable energy sources in the internal electricity market.

[DIR02] Directive 2002/91/EC of the European parliament and of the council of 16 December 2002 on the energy performance of buildings

[DIR04] DIRECTIVE 2004/8/EC OF THE EUROPEAN PARLIAMENT AND OF THE COUNCIL of 11 February 2004 on the promotion of cogeneration based on a useful heat demand in the internal energy market and amending Directive 92/42/EEC.

[DIR06] Directive 2006/32/EC of the European parliament and of the council of 5 April 2006 on energy end-use efficiency and energy services and repealing Council Directive 93/76/EEC.

[ENG05] D. Engle, Micro-CHP plant, 2005, Marathon ecopower micro-CHP, www.marathonengine.com.

[FEI04] W. Feist, First Steps: What Can be a Passive House in Your Region with Your Climate? Passivhaus Institute Darmstadt, 2004. <http://www.passivehouse.com/07_eng/FirstSteps/FirstStep.zip>.

[HER07] Pierre Hérant, "Etat actuel du parc immobilier francais", Colloque national ADEME-CNISF, 2007.

[ITE07] *Institut des bioénergies, ITEBE, 2007. http ://www.itebe.org/portail/affiche.asp?arbo=1&num=305.*

[ISM03] *S. Daoud, Guide de Préfaisabilité pour les acteurs du secteur tertiaire, PME, PMI, mars, 2003.*

[KAL04] *S.A. Kalogirou, Solar thermal collectors and applications, Progress in Energy and Combustion Science 30 (2004) 231–295.*

[KAR05] *Fachinformationszentrum Karlsruhe (ed.), Blockheizkraftwerke, Eine µLeitfaden fur den Anwender, TUV-Verlag GmbH, Koln, 2005.*

[LOI05] *Loi POPE, 2005. Loi n° 2005-781 du 13 juillet 2005 de programme fixant les orientations de la politique énergétique. Journal Officiel de la République Française n°163 of 14 July 2005 (in French).*

[MIC02] *Micromap – Mini and micro CHP – market assessment and development plan, a study supported by European commission save programme, DGTREN, April 2002.*

[MIC03] *Future Cogen Progect, Micro CHP technology & market status, 30 June 2003.*

[MIC04] *Micro-CHP Fact Sheets on the status of micro-CHP technologies and markets in different European countries (2004/5).*
http://www.cogeneurope.eu/

[NES04] *D. Neshumayev, A.Ots, J. Laid, T. Tiikma, Experimental investigation of various turbulator inserts in gas-heated chaneels, Experimental thermal and fluid sciences, 28 (2004) 877–886.*

[OLI02] *A.C. Oliveira, C. Afonso, J. Matos, S. Riffat, M. Nguyen, P. Doherty, A combined heat and power system for buildings driven by solar energy and gas, Applied Thermal Engineering 22 (2002) 587–593.*

[ONO04] *H.I. Onovwionaa, V.I. Ugursalb, Residential cogeneration systems: review of the current technology, Renewable and Sustainable Energy Reviews 10 (2006) 389–431.*

[PAE06a] *M. De Paepe, P. D'Herdt, D. Mertens, Micro-CHP systems for residential applications, Energy Conversion and Management 47 (2006) 3435-3446.*

[PAE06b] *A.D. Paecock, M. Newborough, Impact of micro-combined heat and power systems on energy flows in the UK electricity supply industry, Energy 31 (2006) 1804-1818.*

[PEH06] *M. Pehnt, M. Cames, C. Fischer, B. Praetorius, L. Schneider, K. Schumacher, J.P. Vob, Micro cogeneration towards decentralized energy systems, Springer-Verlag Berlin Heidelberg 2006.*

[PRE06] H. Prévot,J. Orselli, Les réseaux de chaleur, Ministère de l'économie, des finances et de l'industrie, 2006.

[RTH05] Réglementation Thermique 2005, 2006. Arrêté´ du 24 mai 2006 relatif aux caractéristiques thermiques des bâtiments nouveaux et des parties nouvelles des bâtiments. Journal Officiel de la République Française n° 121 of 25 May 2006 (in French).

[SID07] O. Sidler, Rénovation à basse consommation d'énergie des logements en France, Projet « Renaissance » Programme européen Concerto, August 2007.
http://www.enertech.fr/

[YAG06] W. Yagoub, P. Doherty, S.B. Riffat, Solar energy-gas driven micro-CHP system for an office building, Applied Thermal Engineering 26 (2006) 1604–1610.

[ZHA06] X.R. Zhang, H. Yamaguchi, D. Unen, K. Fujima, M. Enomoto, N. Sawada, Analysis of a novel solar energy-powered Rankine cycle for combined power and heat generation using supercritical carbon dioxide, Renewable Energy 31 (2006) 1839–1854.

CHAPITRE 2 – Working Fluid for a Low-Temperature Organic Rankine Cycle

Abstract

A micro Rankine cycle system using wood and solar energies for combined production of electricity and thermal energy is studied. For low power output (< 10 kW), micro Rankine cycle design and its energy performances depend strongly on the properties of the working fluids. Organic fluids present many advantages compared to water for Rankine cycle utilizing low-grade energy as heat input, and particularly for low power output. In this study, the required characteristics of the "ideal" working fluid have been identified. Since such an ideal fluid that fulfills all requirements does not exist, a screening method has been developed to draw a list of the most suited working fluids for the specific application. The screening procedure developed is composed of four different selection phases. The first three phases depend mainly on environmental, safety, and performance criteria. However, the last phase of the screening process requires the evaluation of the thermodynamic and thermophysical properties effect of the working fluids on the design of the different Rankine cycle components.

1. Introduction

In the last years, large efforts have been made to extend the market of micro-cogeneration systems dedicated to produce heat and power for residential and small commercial applications. Micro-cogeneration systems producing heat and power from fossil fuels have been proposed because they could represent a higher global efficiency compared to the conventional electrical production systems when the rejected heat from the Rankine system is used at this low level of temperature and part of supply heat is transformed in electricity through the Rankine system. Moreover micro-cogeneration systems operating on renewable energies can represent an interesting option for sustainable and reliable electricity supply.

The conventional micro-cogeneration systems available on the market are based on such technologies, such as Stirling and reciprocating engines [SIM06]. Researches have been conducted in the last decades to promote the development of other micro-cogeneration technologies based on Rankine cycle operating with organic fluids [FAC05, KAN03, NGU01, YAM01], namely organic Rankine cycle (ORC). This technology offers the opportunity of operating these micro engines with renewable energy.

The organic Rankine cycle is not a new concept and many investigations have been carried out. Research was mainly focused on low-grade heat. Geothermal applications have been investigated [SAL07] and organic working fluid for ORC such as alkanes, fluorinated alkanes, ethers, and fluorinated ethers have been selected for operating temperatures between 100°C (source) and 30°C (sink). Different cycle configurations have been studied depending on the shape of the saturated vapor line in the T-S diagram. Borsukiewicz-Gozdur [BOR07] proposed a method for increasing the power output of a geothermal power plant based on ORC by increasing the flow of geothermal water supplied to the boiler by means of returning the stream of geothermal water from downstream the boiler for a second passage through it. Iqbal et al. [IQB78] proposed a screening procedure to select hydrocarbons for the geothermal binary power plants to quickly identify promising working fluids. On the other hand, Hung [HUN97] shows that the slopes and the shapes of the saturation vapor curve of the fluids have a primary effect on the performance and the architecture of the ORC where the "isentropic" fluids seems to be the most suitable type of working fluid for recovering low temperature waste heat.

ORCs are represented also in waste heat applications. Hung [HUN01] has shown that the efficiency of the ORC depends on two main factors: working conditions of the cycle and thermodynamic properties of the working fluids. Different working fluids have been compared (Benzene, Toluene, p-Xylene, R-113, and R-123). Among these fluids p-Xylene shows the highest efficiency while benzene shows the lowest. However, p-Xylene presents the lowest irreversibilities when recovering high temperature waste heat, while R-113 and R-123 present a better performance in recovering low-temperature waste heat. Wei [WEI07] conducted a performance analysis and optimization of an organic Rankine cycle system using HFC-245fa as working fluid driven by exhaust heat to maximize its recovery in order to improve the system output net power and efficiency. Angelino [ANG00] investigated the use of working fluids such as aromatic hydrocarbons, siloxane, and siloxane mixtures straight chain hydrocarbons, and aromatic perfluorocarbons for waste heat recovery from molten carbonate fuel cell plant. The performance of energy recovery cycles using different fluids is evaluated by means of optimization software for different operating conditions and cycle configurations. LIU [LIU04] analyses the performance of several working fluids of ORC adapted to waste heat applications. The study shows that the presence of hydrogen bond in certain molecules, such as water, ammonia, and ethanol results in a negative slope of the vapor saturation curve in the T-S diagram fluids due to larger vaporizing enthalpy, and is regarded as inappropriate for ORC systems. Chen [CHE06] has conducted a comparative study of the CO_2 transcritical cycle with an organic Rankine cycle and using R-123 as working fluid in waste heat recovery. Results show that the CO_2 transcritical cycle represents a higher performance than R-123 when operating with low-grade waste heat. Another application of using waste heat for micro turbines has been highlighted by [INV06] showing the potential of integrating on ORC bottoming cycle for enhancing the performance of micro-turbines. A specific analysis has been conducted to select the most appropriate fluid capable of satisfying both environmental and technical concerns. Mago [MAG08] shows the potential of using a regenerative ORC using dry organic fluids to convert waste heat to power from low-grade heat sources. The different working fluids studied are R-113, R-245ca, R-123, and isobutene. It was shown that using the regenerator represents a higher thermal efficiency and lower irreversibilities. On the other hand, he has shown that working fluids with high-boiling temperature present better energy performances than working fluids with low-boiling temperature.

Many studies have been carried also to investigate electricity production from solar energy via an ORC. Cong [CON05] conducts a detail analysis for producing mechanical work by an ORC operating on solar energy using R-123 or isobutane and the effect of the thermodynamic properties of the two working fluids on the operating conditions. Yamaguchi [YAM06] investigates the use of CO_2 to produce electricity from solar energy by using vacuum solar collectors. A prototype has been designed and tested in Kyoto, Japan. Mcmahan [MCM06] investigates the use of ORC for electricity production by means of compound parabolic collectors. The effect of the selection of working fluids and the configuration of the ORC on the system performances have been discussed and an additional economic optimization methodology for solar-thermal ORC power plants has been presented.

Other applications have been promoted in the last years for producing power and heat from solid biomass combustion; these power plants use ORC for cogeneration applications. Dresher [DRE06] investigates the use of some organic fluids such as alkybenzenes for power generation and he has identified their thermal efficiency depending on the maximum operating temperature of the system. Marciniak [MAR81] conducts a comparison study of seven working fluids (water, methanol, R-11, R-113, 2-methypyridine/H_2O, Fluorinol 85, and toluene) on the design of an ORC power system in the range of 600–2400 kW. The author shows the disadvantage of using water as working fluid for operating temperatures below 371°C where it becomes less efficient and too expensive. However, other working fluids such as organic compounds can be economically attractive at lower temperatures.

Other work has been conducted in the field of hybrid vehicles where El Chammas [CHA05] shows the potential of integrating an ORC operating on the exhaust gas and cooling circuit permitting to reach higher efficiency in heat conversion to generate electricity. The author proves that dry organic fluids need not to be superheated since the cycle thermal efficiency remains approximately constant when the inlet temperature of the turbine increases. Different working fluids have been compared and three fluids (water, isopentane, and R-245ca) have been selected as potential fluids for ORC onboard operating systems.

The different studies listed before analyze ORC working fluids for a specific application without taking into account the diversity of parameters that affect the design of the ORC main components. However, some authors as Badr [BAD85] have developed a screening method for selecting a working fluid for Rankine cycle engine utilizing low-grade energy as heat input. The proposed method has been established to identify the thermodynamic and thermophysical properties effect of the working fluid on the design of the different components. The screening criteria fixed by the author imposed the selection of three principle fluids R-11, R-113, and R-114 from a list of sixty-eight working fluids. Nowadays, the Montreal Protocol has banned these chlorinated fluids. However, this screening method can be modified and used for organic working fluids such as HFC, alkanes, etc.

In this thesis, a list of potential working fluids is established and a selection method is developed to identify a list of potential working fluids. In general, the screening method depends on different criteria such as environment, safety, performance, and economic issues. The method developed in this thesis will focus on the first three criteria in order to select a working fluid environmentally friendly, representing no toxicity problems, and with high thermodynamic efficiency. However, this method will be extended to study the effect of the working fluid selection on the design of the most critical components of the Organic Rankine cycle. Results of this study aim at identifying a set of working fluids for producing electricity and heat from renewable energy sources for power output lower than 10 kWe.

2. Selection of a working fluid

The working fluid has to fulfill the following requirements.

- **Thermophysical properties**
  - Critical temperature must lie well above the highest operating temperature of the cycle to minimize the irreversibilities generated by heat transfer through a finite temperature difference within the boiler.
  - To keep a small system at an acceptable cost, the boiler pressure should be limited in the range of 2 to 3 MPa.
  - The working fluid condensing pressure should be higher than the atmospheric pressure to avoid leakage of air into the system.
  - The triple point should be below the minimum ambient temperature to ensure that the working fluids will not solidify at any operating temperature or when the system is shut down.
  - On a temperature-entropy diagram, the saturated vapor shape of a working fluid should be nearly vertical, to avoid excessive superheat at the exit of the turbine, which is an exergetic loss.
  - A low value of the heat capacity of the liquid leading to $ds/dT \sim 0$ for the saturated liquid line and a high ratio of the latent heat of vaporization to the liquid heat capacity are favorable. Those properties reduce the amount of heat required to raise the temperature of the sub-cooled liquid to the saturation temperature corresponding to the boiling pressure. The ORC efficiency will be increased. Operating with finite heat

sources, a high heat capacity of the liquid can lead to a higher recovered energy from the heat source and then increases the total efficiency of the cycle.

- The working fluid enthalpy variation in the turbine should be large to increase the efficiency of the thermodynamic cycle and to minimize the flow rate of the working fluid.

- The working fluid density at the inlet of the turbine should be high to keep a small size of the turbine.

- The convective heat coefficient is higher with high thermal conductivity and low viscosity fluids.

- Working fluid liquid and vapor viscosities have to be low to minimize frictional pressure drops and maximize convective heat transfer coefficients.

➢ **Material Compatibility and fluid stability limits**

The working fluids should be non-corrosive to the more common engineering materials used for the different components of the ORC such as pipes, turbine, heat exchangers, and seals. The working fluids should also be thermally and chemically stable at all operating temperatures and pressures.

➢ **Health and safety characteristics**

A working fluid should be non-toxic, and preferably non-flammable.

➢ **Fluid availability and cost**

The fluid selected has to be commercially available from several suppliers at an acceptable cost.

3. List of the possible working fluids potential for organic Rankine cycle

No fluid has been identified to date, which will satisfy all the criteria mentioned above. Using Refprop database version 7.0 [REF07], it is possible to draw a list of working fluids that have been considered as possible candidates or have been used in operational Rankine engines. Selected candidates (CFC, HFC, HCFC, Hydrocarbons…) are listed in Table 2.1 and Table 2.2. Table 2.1 includes some of the thermophysical data of the selected working fluids and Table 2.2 presents their safety and environmental data. Fluids are ranked in those two tables by their critical temperature. These fluids can be grouped in three different categories depending on their vapor saturation curve types (see Figure 2.1) in the temperature-entropy (T-S) diagram. Saturation vapor curve is the most crucial characteristic of a working fluid in an ORC. It affects the fluid applicability, cycle efficiency, and component design in a power-generation system.

The derivative (dT/ds) is primarily a function of the vapor specific heat capacity and, as a consequence, is directly related to the molecule structure of the fluid. For simple molecule, the value of heat capacity ratio γ is relatively high. Those fluids exhibit a negative slope of the saturated vapor line in the T-S diagram and are known as “wet” fluids. As the complexity of the molecule increases, the heat capacity ratio γ decreases, tending to one, and the slope of the saturated vapor line becomes positive (dry fluid). For an ideal working fluid, (dT/ds) tends to the infinity; then the fluid saturation vapor curve tends to be vertical in the T-S diagram, so the name of “isentropic fluid”.

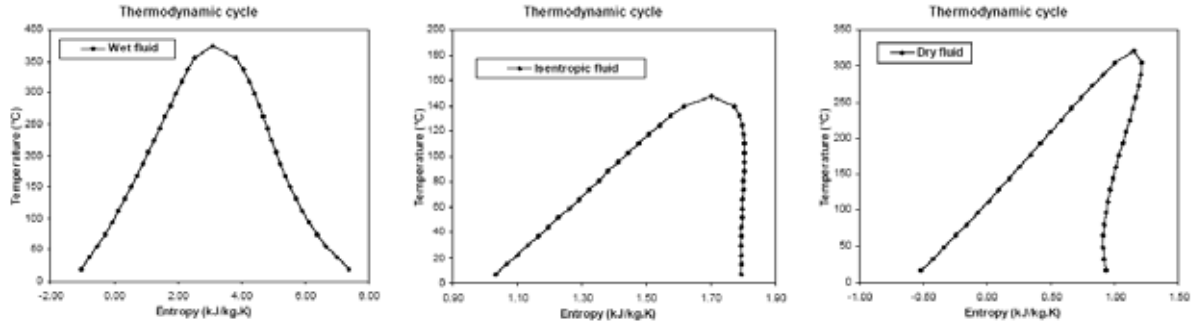

Figure 2.1 – Working fluids type.

- **Dry fluid** with positive slopes (dT/ds). The saturated vapor phase of a dry fluid becomes superheated after isentropic expansion. This type of organic fluid is suitable for turbine design since there is no risk of erosion due to the superheat state at the outlet of the turbine, but part of the energy is lost in the condenser. If this energy is significant, a heat recovery heat exchanger is integrated in the cycle to increase the cycle efficiency. This energy is used to heat the working fluid leaving the pump by minimizing the energy needed at the boiler and then increase the efficiency of the cycle.
- **Wet fluid** with negative slopes usually has low molecular weight (e.g. water and ammonia). The expansion occurs in the two-phase section. Special care has to be taken in the design of the turbine to withstand the liquid droplets. Sometimes superheating of the fluid at the turbine inlet is necessary to avoid high ratio of liquid droplets at the turbine outlet while expanding the fluid.
- **Isentropic fluid** (e.g. R-11 and R-124). Since the vapor expands along a vertical line on the T-S diagram, vapor saturated at the turbine inlet will remain saturated throughout the turbine exhaust without condensation.

Table 2.1 – Some thermophysical properties of the considered fluid.

Fluid name	M (g/mol)	T_{cr} (°C)	P_{cr} (MPa)	T_{tp} (°C)	T_{nb} (°C)	h_{fg} @ 101325 Pa	Saturation dome shape	P_{sat} @ T_{cond} (kPa)
Water	18.02	373.95	22.06	0.01	99.97	2257.44	Wet	47.41
Decane	142.28	344.55	2.10	-73.15	174.15	276.84	Dry	4.08
Nonane	128.26	321.40	2.28	-73.15	150.75	288.65	Dry	9.68
Toluene	92.14	320.73	4.24	-94.15	110.55	361.94	dry	38.88
Octane	114.23	296.17	2.50	-56.78	125.62	302.52	dry	23.30
Benzene	78.11	288.90	4.89	5.55	80.08	394.97	dry	101.06
Cyclohexane	84.16	280.49	4.08	6.32	80.74	356.30	dry	99.10
Heptane	100.20	266.98	2.73	-90.60	98.38	317.21	dry	57.09
Methanol	32.04	240.23	8.22	-97.54	64.48	1101.72	wet	181.11
Hexane	86.18	234.67	3.02	-95.32	68.71	335.24	dry	142.54
R-113	187.38	214.06	3.39	-36.22	47.59	144.45	dry	264.96
R-141b	116.95	206.81	4.46	-103.30	32.05	223.08	dry	421.40
R-11	137.37	197.96	4.41	-110.47	23.71	181.49	isentropic	523.23
Pentane	72.15	196.55	3.37	-129.68	36.06	357.89	dry	368.01
Isopentane	72.15	187.20	3.40	-160.50	27.82	343.71	dry	457.57
R-123	152.93	183.68	3.66	-107.15	27.82	170.34	dry	489.09
R-245ca	134.05	174.42	3.93	-273.15	25.13	201.15	dry	569.63
Neopentane	72.15	160.60	3.20	-16.55	9.49	316.30	dry	736.24
R-245fa	134.05	154.05	3.64	-273.15	14.90	196.88	dry	788.81
Butane	58.12	151.98	3.80	-138.28	-0.55	385.32	dry	1012.15
RE-134	118.03	147.10	4.23	-23.15	6.17	215.22	isentropic	1050.44
R-114	170.93	145.68	3.26	-94.15	3.59	136.05	dry	930.69
R-236ea	152.04	139.29	3.50	-273.15	6.19	165.32	dry	1002.19
R-142b	100.50	137.11	4.07	-130.43	-9.15	222.27	isentropic	1385.73
Isobutane	58.12	134.67	3.64	-159.59	-11.67	366.24	dry	1342.69
Ammonia	17.03	132.25	11.33	-77.66	-33.33	1370.26	wet	4141.97
Cyclopropane	42.08	125.15	5.58	-127.45	-31.48		wet	2528.72
R-236fa	152.04	124.92	3.20	-93.63	-1.44	160.48	dry	1249.12
R-124	136.48	122.28	3.62	-199.15	-11.96	165.99	Isentropic	1576.39
RC-318	200.04	115.23	2.78	-39.80	-5.98	116.87	Dry	1343.44
R-152a	66.05	113.26	4.52	-118.59	-24.02	330.18	Wet	2342.41
R-12	120.91	111.97	4.14	-157.05	-29.75	166.30	Wet	2297.46
R-227ea	170.03	101.65	2.93	-126.80	-16.45	131.55	Dry	1857.39
R-134a	102.03	101.06	4.06	-103.30	-26.07	217.16	Wet	2633.20
Propane	44.10	96.68	4.25	-187.67	-42.09	426.14	Wet	3131.46
R-22	86.47	96.15	4.99	-157.42	-40.81	233.93	Wet	3663.81
Propylene	42.08	92.42	4.66	-185.20	-47.69	439.47	Wet	3723.81
R-32	52.02	78.11	5.78	-136.81	-51.65	382.14	Wet	Supercritical
R-143a	84.04	72.71	3.76	-111.81	-47.24	226.82	Wet	Supercritical
R-218	188.02	71.95	2.67	-160.15	-36.83	105.31	dry	Supercritical
R-125	120.02	66.02	3.62	-100.63	-48.09	164.25	wet	Supercritical
R-41	34.03	44.13	5.90	-143.33	-78.12	489.16	wet	Supercritical
Ethane	30.07	32.18	4.87	-182.80	-88.60	489.79	wet	Supercritical
CO_2	44.01	30.98	7.38	-56.56	-78.40		wet	Supercritical
R-13	104.46	28.85	3.88	-181.15	-81.48	149.47	wet	Supercritical
R-23	70.01	26.14	4.83	-155.13	-82.02	239.55	wet	Supercritical
R-116	138.01	19.87	3.05	-97.15	-78.24	116.59	wet	Supercritical

Table 2.2 – Some thermo-physical properties of the considered fluid [CAL01]

Fluid name	TLV-TWA (ppm)	LFL (%)	HOC (MJ/kg)	Std 34 safety	Atmospheric life	ODP	GWP
Water	none	none	None	A1	--	0	<1
Decane	--	--	--	--	--	--	--
Nonane	--	--	--	--	--	--	--
Toluene	100	--	--	--'/Toxic	--	--	--
Octane	--	--	--	--	--	--	--
Benzene	--	--	--	--'/Toxic	--	--	--
Cyclohexane	--	--	--	--	--	--	--
Heptane	--	--	--	--	--	--	--
Methanol	--	--	--	--	--	--	--
Hexane	--	--	--	--	--	--	--
R-113	1000	none	0.1	A1	85	0.9	6000
R-141b	500	6.40	8.6	--	9.3	0.11	700
R-11	1000	none	0.9	A1	45	1	4600
Pentane	600	1.40	--	--	<<1	0	11
Isopentane	600	1.00	--	--	--	0	--
R-123	50	none	2.1	B1	1.4	0.014	120
R-245ca	--	7.10	8.4	--	5.9	0	640
Neopentane	--	--	--	--	--	--	--
R-245fa	500p	none	6.1	A1p r	7.2	0	950
Butane	800	1.90	49.5	A3	--	0	20
RE-134	--	none	--	--	--	0	--
R-114	1000	none	-3.1	A1	300	0.85	9800
R-236ea	--	none	5.4	--	10	0	1200
R-142b	1000	6.90	9.8	A2	19	0.065	2400
Isobutane	800	1.80	49.4	A3	--	0	20
Ammonia	25	14.80	22.5	B2	--	0	<1
Cyclopropane	--	2.40	--	--	--	0	--
R-236fa	1000	none	--	A1	220	0	9400
R-124	1000	none	0.9	A1	6.1	0.026	620
RC-318	1000	--	--	A1 d	3200	0	8700
R-152a	1000	3.70	17.4	A2	1.4	0	120
R-12	1000	--	-0.8	A1	100	0.82	10600
R-227ea	1000	--	3.3		33	0	3500
R-134a	1000	none	4.2	A1	13.8	0	1300
Propane	2500	2.30	50.3	A3	--	0	20
R-22	1000	--	-12.5	A1	260	0	12000
Propylene	375	2.00	--	B3 r	--	0	20
R-32	1000	13.30	9.4	A2	5	0	550
R-143a	1000	7.10	10.3	A2	52	0	4300
R-218	1000	--		A1	2600	0	7000
R-125	1000	--	-1.5	A1	29	0	3400
R-41	--	--	--	--	2.6	0	97
Ethane	1000	3.20	--	A3	--	0	20
CO_2	5000	--	--	A1	>50	0	1
R-13	1000	--	-3	A1	640	1	14000
R-23	1000	--	-12.5	A1	260	0	11700
R-116	1000	--	--	A1	10000	0	9200

TLV-TWA = ACGIH Threshold Limit Value - Time-Weighted Average, or consistent chronic exposure limit (e.g., OSHA Permissible Exposure Limit, PEL), unless preceded by "C" for TLV-ceiling; LFL = Lower flammability limit (% volume in air), "wff" signifies that the worst case of fractionation may become flammable; HOC = Heat of combustion, ODP = ozone depletion potential (modeled); GWP = global warming potential (for 100 yr integration).

4. Screening method for fluid selection

Finding an ideal fluid that fulfills all the criteria listed previously is practically impossible with all the working fluids listed in Table 2.1 and even with all the working fluids available on the market. To identify the most suitable working fluids, temperatures of the boiler and the condenser have to be known.

The energy source depends mainly on the availability of renewable energy in the different locations where the micro-cogeneration system is installed. Since the heat input of the micro-cogeneration system can be delivered from solar and biomass, then the boiling temperature will be varied from 100°C to 200°C. The maximum temperature is limited to 200°C to be able to operate where low-grade heat only is available (ex: solar energy with solar collector operating temperature lower than 200°C).

On the other hand, the condenser temperature will be fixed around 80°C to ensure that the thermal energy produced by the micro co-generator can be used in heating systems and domestic hot water generation. If advanced heating systems are installed in the building where the heating systems can operate at lower temperature as "low temperature radiator", the condenser temperature can be fixed to values lower than 80°C. The condenser temperature has been fixed at 80°C and the boiler temperature was varied from 100°C to 200°C. The output power of the ORC studied will vary from 1 kW to 10 kW corresponding to output power of micro-cogeneration systems suitable for residential buildings (single house or apartment buildings).

The screening method consists of four different phases represented in Figure 2.2:

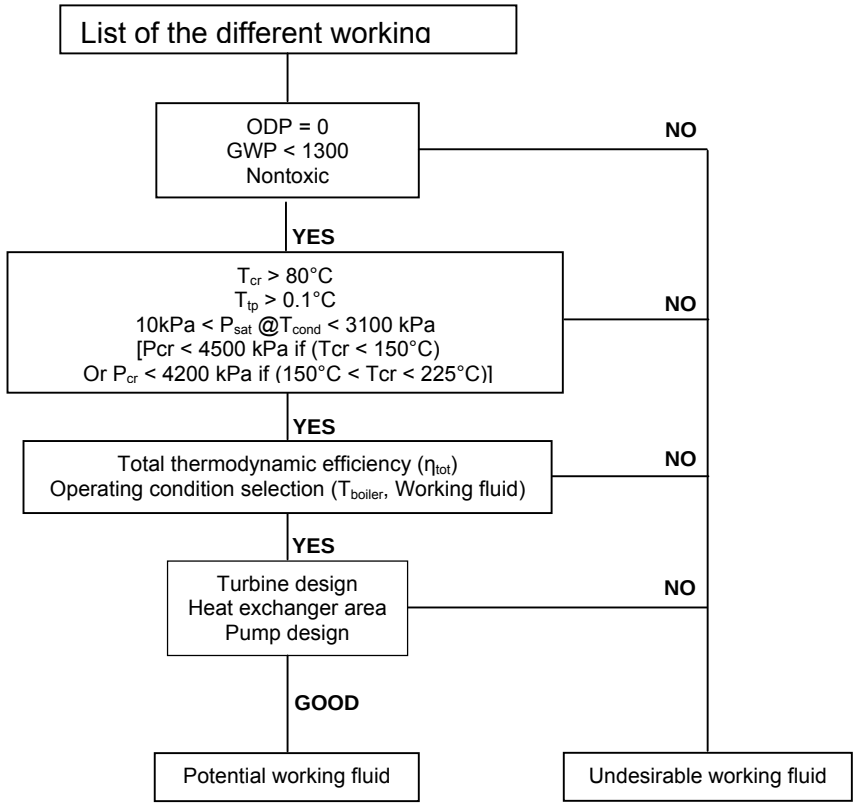

Figure 2.2 – Screening method for fluid selection.

In the first phase, the different candidates are compared using environmental and safety criteria. The working fluid will be rejected in phase 1 if the ODP is higher than zero or GWP > 1300 (corresponding to the GWP of R-134a, which is one of the most used fluid in refrigeration applications). The safety criteria considered are the toxicity and flammability. These criteria are defined by ASHRAE standards [ASH04] as follows.

The safety criteria lead to eliminate high toxic working fluid such as toluene and benzene, which will be eliminated in this phase. All other working fluids will be taken as potential working fluids but special care has to be taken in the designing of the ORC system by limiting the volume of the working fluid in the system or designing an indirect system with different separate loop using heat transfer fluid to carry in and out the heat from the ORC system when the selected working fluid presents high flammability characteristics.

The remaining fluids will be ranked on the basis of their thermodynamic properties in phase 2; the working fluids will be rejected if they do not fulfill the following criteria:

- Working fluid with a critical temperature lower than 80°C.
- Triple point lower than 0.1°C.
- The saturation pressure at the condensing temperature lower than 10 kPa or higher than 3100 kPa (Pressure limited by the mechanical stresses which could be withstand by the condenser technolgy)to eliminate working fluids with low pressure at the condenser to limit the risk of air infiltration or to eliminate working fluids with high pressure at the condenser, which affects the cost of the condenser.
- The critical pressure is higher than 4500 kPa if the critical temperature is lower than 150°C or the critical pressure is higher than 4200 kPa if the critical temperature ranges between 150°C and 200°C. This limitation is imposed by the maximum operating pressure of the brazed plate heat exchanger [SWE08] used for boiler design. This type of heat exchanger is used because it is the most suitable technology available on the market for our application [CHA05].

The remaining fluids will be ranked in phase 3 depending on their thermodynamic cycle efficiency. All fluids with cycle efficiency lower than 8% will be rejected. The working fluids selected for illustrating the screening calculation of phase 3 are: water, heptane, methanol, hexane, pentane, isopentane, R-245ca, Neopentane, R-245fa, Butane, R236ea, isobutane, Cyclopropane, and R-134a. These fluids have not been rejected after phases 1 and 2 of the screening method and the calculation of their thermodynamic efficiency will be performed to identify the most suitable working fluids.

4.1 Organic Rankine cycle performance

The RC [CEN94] is a thermodynamic cycle dedicated to electricity generation from heat (combustion gases) in power plants. RC can be operated on the exhaust gases of different primary systems. In order to have a low initial cost, the Rankine system should be kept as simple as possible.

The ideal Rankine cycle consists of the four following evolutions (Figure 2.4):

1 – 2: Isochoric compression in a pump
2 – 3: constant pressure heat delivery in a boiler
3 – 4: isentropic expansion in a turbine
4 – 1: constant pressure heat rejection in a condenser.

The thermodynamic fluid enters the pump at state 1 as saturated liquid, and is compressed to the operating pressure of the boiler. The fluid enters the boiler as sub-cooled liquid at state 2, and leaves as superheated vapor at state 3. Heat is transferred to the fluid at constant pressure. The superheated vapor at state 3 enters the turbine where it expands isentropically and produces work by rotating a shaft connected to an electric generator. The temperature and pressure of the fluid drop during this process at state 4, where it enters the condenser. The fluid is condensed at constant pressure in the condenser, by rejecting heat to a sink. The fluid leaves the condenser as saturated liquid and enters the pump to complete the cycle. The thermodynamic cycle efficiency is given by Eq. (2.1):

$$\eta_{cyc} = \frac{\dot{W}_t - \dot{W}_p}{\dot{Q}_b} = \frac{(h_3 - h_4) - (h_2 - h_1)}{h_3 - h_2} \tag{2.1}$$

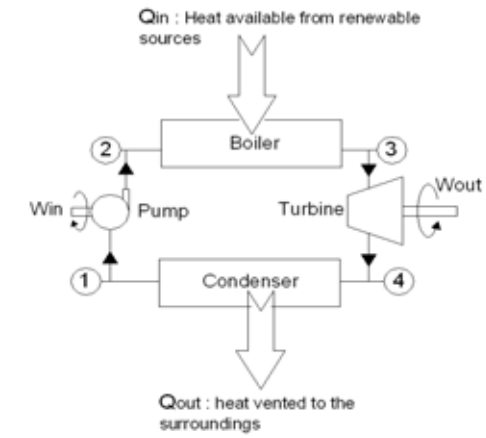

Figure 2.3 – Rankine cycle layout.

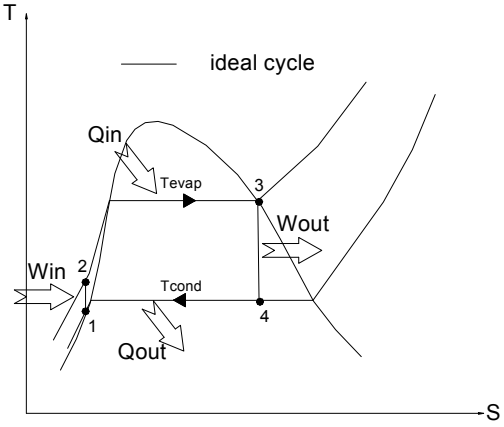

Figure 2.4 – Rankine cycle T-S diagram.

The actual RC differs from the ideal one due to the irreversibility generation in the different components. Two common sources of irreversibilities are fluid friction and undesirable heat loss to the surroundings. Fluid friction causes pressure drop in the boiler, the condenser, and the piping between the various components. The major source of irreversibilities is related to the turbine. The actual expansion process involves frictional effects that increase the entropy, and heat transfers that decrease the entropy (heat loss to the surrounding). Other factors also need to be considered in the analysis of actual RCs where, for example, the liquid must be in the sub-cooled state at the pump inlet in order to avoid the onset of cavitation.

Dedicated software has been developed under Excel and macros calling Refprop 7.0 for the calculation of the thermodynamic properties of the different working fluids. This software allows calculating the ideal Rankine cycle efficiency for different source and sink temperatures. Results are presented in Figure 2. for the selected working fluid. Water and methanol show the highest energy performances followed by the different hydrocarbons with high critical temperatures (heptane, hexane, pentane, and isopentane) and one HFC (R-245ca). Other fluids lay far from the cycle efficiency target set before. However, R-245fa, even if eliminated due to its low efficiency, remains as a candidate since it is commonly used in many operating Rankine cycles [BRA05] and seems to be a promising working fluid even if its cycle efficiency is low compared to other working fluids listed below.

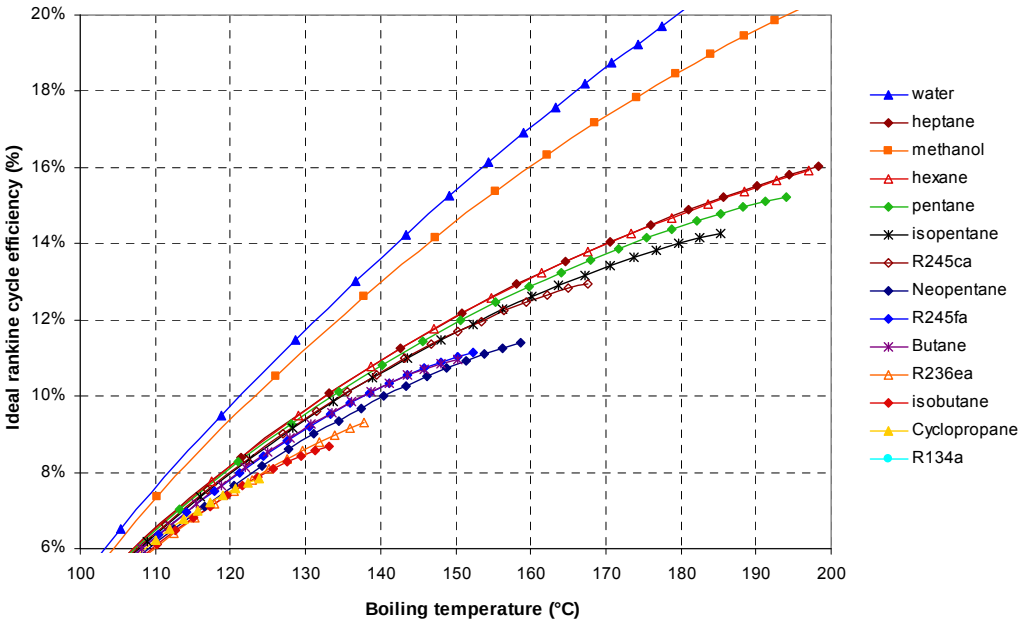

Figure 2.5 – Ideal Rankine cycle efficiency.
(η_t = 1, η_p = 1, T_{sub} = 10 K, T_{sup} = 25 K if water and 1 K for other working fluids).

The potential working fluids screened after the simulations conducted before are represented in the TS* diagram in Figure 2.6. These fluids are divided into two categories: wet fluid (water and methanol) and dry fluids (heptane, hexane, pentane, isopentane, R-245ca, and R-245fa). Figure 2.7 shows the saturation pressure curve for the different potential working fluids for different saturation temperatures.

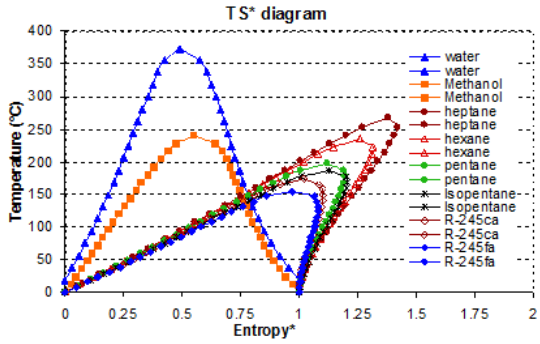

Figure 2.6 – TS Diagram.*

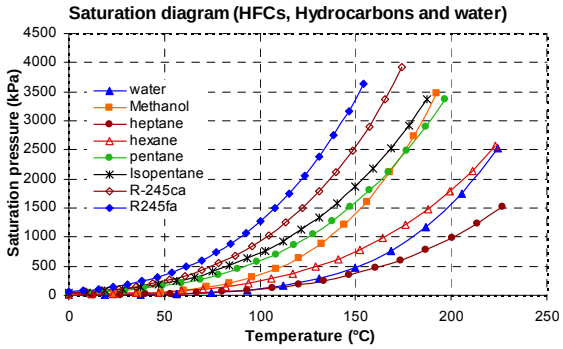

Figure 2.7 – Saturation pressure.

The performance of working fluids in a Rankine cycle system depends not only on their thermodynamic and thermophysical properties, but also on the design of the system components. The selection procedure leading to the selection of the most appropriate working fluid has to be refined through a first design of the main components of the system. The first selection of working fluids will be ranked on the basis of simplified equipment sizing.

In the following section, a comparison between the heat transfer characteristics of the selected working fluids in the boiler and the condenser will be carried out by calculating the heat exchanger surface area for the different boiling temperatures. The effect of the working fluids on the selection of the pump technology will be also studied, as well as on the turbine design.

5. ORC components design - Selection of the most suitable working fluid

5.1 Turbine design

The performance of the expansion device in SRC and ORC systems is one of the major parameters that affect the overall efficiency of the energy conversion. Expanders can be classified into two principal categories: turbines and positive displacement machine known as volumetric expanders. In order to identify the most suitable technology for our application, it is convenient to use the method of similarity and thereby, reducing the number of parameters affecting their performances. Four parameters are sufficient to describe completely the performance of geometrically similar expanders: the Mach number, the Reynolds number at the inlet, the specific speed, N_s, and the specific diameter D_s. Barber [BAR81] discovered that the Reynolds number and the Mach number of the expanding working fluid have only secondary effects on the performance of the turbine. In addition, if the Reynolds number exceeds 10^6. There is no apparent effect on performance. If the Mach number is significantly lower than one, compressibility effects are small and the expander performance can be represented as a function of only two parameters, the specific speed and the specific diameter [LOZ82, LOZ86, MAC81], which are defined respectively by:

$$N_s = \frac{N\dot{V}_{ex}^{1/2}}{\left(\Delta h_{is}\right)^{3/4}} \tag{2.2}$$

$$D_s = \frac{D\left(\Delta h_{is}\right)^{1/4}}{\dot{V}_{ex}^{1/2}} \tag{2.3}$$

The performance characteristics corresponding to different dimensional parameters listed below is given by [BAD84] and shown in Figure 2.8. For a specific flow rate and enthalpy change through the expander, the specific speed is a measure of the rotational speed of the expander-rotor. The specific diameter can be seen as a measure of the size of the machine: it corresponds to the rotor diameter for a rotary machine and to piston diameter for a reciprocating expander. This figure indicates that for various ranges of specific speed, some types of expanders offer better performances than others. Throughout the low specific-speed regime, positive displacement expanders are, efficiency-wise, superior to single stage turbines. Then rotary positive displacement expanders achieve about the same isentropic efficiencies as single-stage turbines at specific diameters, and consequently rotor-tip speeds, which are only one quarter to one third of the values, required for a single disc turbines.

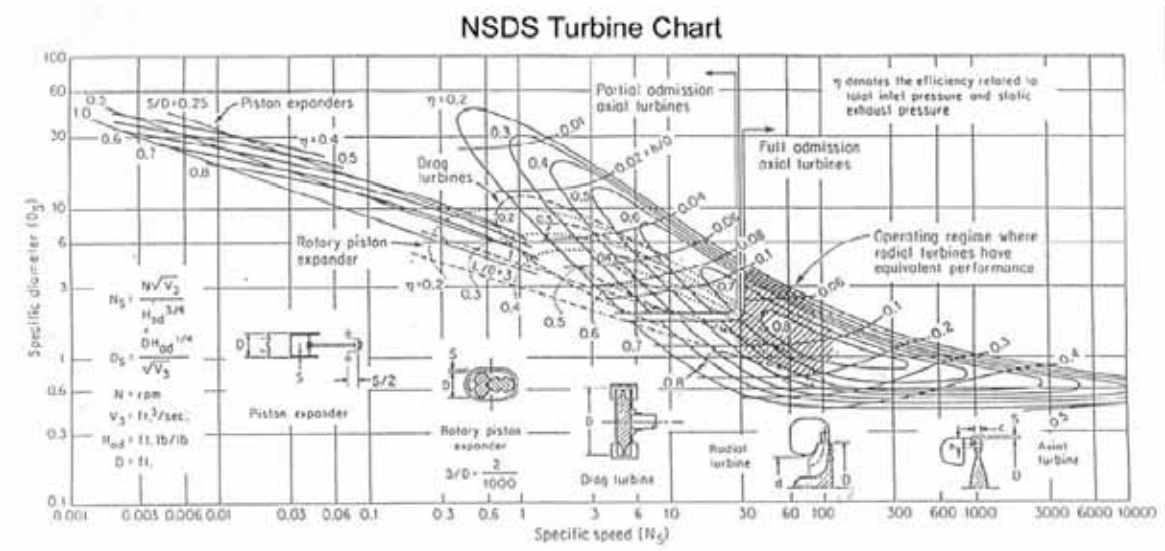

Figure 2.8 – Performance map for different types of expander [BAD91].

The specific speed and the specific diameters are calculated for the different operating boiling temperatures and working fluids for an isentropic power output of 10 kW. The specific speed is represented in Figure 2.9 corresponding to a rotational speed of 3000 rpm. The maximum specific speed is found at lower boiling temperatures corresponding to the low-pressure ratio for hydrocarbon working fluids. On the other hand, the corresponding specific diameters are represented in Figure 2.10 where the minimum specific diameter is found for low-boiling temperatures corresponding to hydrocarbon working fluids.

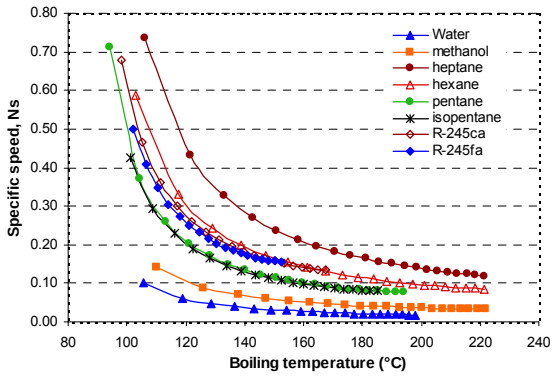

Figure 2.9 – Specific speed
(N = 3000rpm, W_{is} = 10 kW)

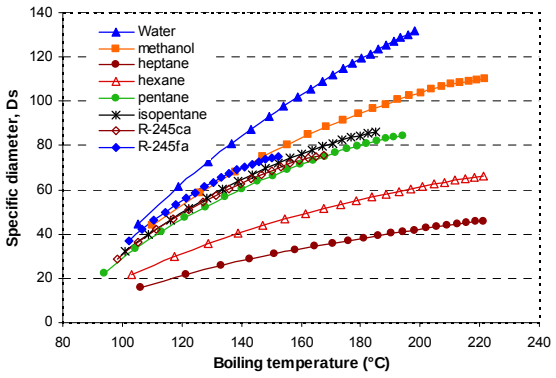

Figure 2.10 – Specific diameter
(D = 0.6 m, W_{is}=10 kW)

Results show that designing a turbine with the different operating conditions listed before with acceptable efficiencies is impossible with the first set of rotational speeds and diameters. The calculated specific speed and specific diameter correspond to design parameters offering low turbines efficiencies (< 20%). To design a turbine with power output

ranging from 1 to 10 kW, none of the conventional turbines would be suitable because of their low efficiencies. Mobarak et al. [MOB78] have shown that designing a turbine to deliver a power range from 1 to 100 kW is not possible with the conventional turbines. However, they have recommended a special design with a ten-stage radial turbine, with a maximum estimated overall efficiency of 71% at 100 kW and 8300 rpm. For lower power output, a higher operating rotational speed is required, which results in mechanical stresses exceeding the allowable strengths of available materials. Problems that may occur regarding the design of the inlet flow passages are due to the supersonic nature of the flow at the inlet. Also, some turbine designs require more than a single-stage expansion (typically from 5 to 10) thus increasing manufacturing difficulties and cost.

After the previous survey, it has been shown that turbines are not particularly suitable devices for low power generation machines. So, volumetric machines remain the more likely candidates. A short survey will be conducted for the different positive displacement machines such as screw, rotary vane, Wankel, and scroll expanders.

- **Screw expanders**

Helical screw machines have been widely used as expansion machines in Rankine cycle systems. These machines offer the advantage of simple architecture compared to multi-stage machines. However, they are used more widely when operating with two-phase expansion process [SMI96], especially in large chillers. These machines represent the disadvantage of being lubricated to ensure a good cooling of the different rotating metal parts and to ensure that there is no internal leakage due to clearance between the screws and the casing. These expanders are more suited for operating with refrigerants where it is possible to ensure a good lubrication with lubricant totally miscible with the desired working fluids. Some screw expanders are used in geothermal power plant. Steidel [STE81] reported the performance of a Lysholm helical screw expander with an isentropic efficiency up to 32.4% with a pressure ratio of 7.1, and a mechanical shaft power output of 32.7 kW. Unfortunately, no data is mentioned in the literature where the screw expanders are used in application with mechanical power output lower than 10 kW.

- **Rotary vane expanders**

Vane expanders represent the advantage of simple construction, reliability, and compactness. A research program has been carried by Badr et al. [BAD91]. The results of the program have shown that the maximum isentropic efficiency that can be achieved is up to 73% at rotational speed of 3000 rpm. The power produced by the vane expander was up to 1.8 kW with R-113 as working fluid. The inlet temperature and pressure of the tested vane expander have been approximately 125°C and 625 kPa. The pressure ratio achieved was 2.79. The major problem encountered when using a rotary vane expander is the achievement of adequate lubrication of the internally rubbing surfaces. The presence of insufficient lubricant results to severe damage on the wear of the components, and results to poor isentropic efficiencies. This problem can be solved by oil injection. However, when using steam as working fluid, the use of lubricant becomes a major barrier with respect to the expander design due to the incompatibility of steam with lubricating oils. Robertson [ROB78] try to solve the lubricant problem by using self-lubricating carbon based components. However, the use of these materials did not reduce the rates of wear of the vanes and stator liner by significant amounts.

- **Wankel engines**

Wankel engine operating as expander is not yet a mature technology. However, some work has been done in this field by Wade [WAD83. He has tested a RE1-11 steam engine. The predicted efficiencies were 60-63%. However, the experimental results show efficiency about 21%. The major problem encountered during the test was the cracking of the rotary inlet valve carbon-seat; this caused excessive steam leakage. Another problem, also associated to the use of the Wankel engine as steam expander, is the lubrication aspect.

- **Scroll expanders**

In the last decades, many researches have been conducted to evaluate the performance of the scroll compressor operating in expander mode. Yanagisawa [YAN01] has investigated the use of a scroll compressor for air expansion; the volumetric and total efficiencies of the tested expander were 76% and 60% respectively with a pressure ratio of 5. A steam scroll expander has been tested by Kim [KIM07]. Results show that the volumetric performance range from 42.3 to 52.1% and the total expander efficiency was nearly 34%. The scroll expander has been designed to operate under a differential pressure ratio of 5.67, a rotational speed of 2317 rpm, and a rated power output of 15 kW. On the other hand, Kane [KAN03] has developed a small hybrid solar power system operating with two superposed scroll expanders. The working fluids for the tested expander were R-123 and R-134a. The first expander operating with R-123 has been designed to generate 5 kW with a built in volume ratio of 2.3. The second expander operating with R-134a was designed to deliver 8 kW for the same built in volume. The expander efficiencies measured up to 68%. Lemort [LEM06] has tested three different types of expanders suitable for recover Rankine cycle. The three compressors present swept volumes of respectively 148, 98, and 60 cm^3, and internal built in volume ratio close to respectively 4.1, 3.1, and 2.6. Results show that the best performances were measured with the expander having the highest built-in volume operating with steam; the isentropic efficiency measured was 55% and the highest delivered mechanical powers are achieved by the same expander around 3 kW.

After the previous survey, it was concluded that positive displacement machines represent the best-suited solution for power generating machines operating at low power output. However, in the range of power output from 1 to 10 kW, the scroll expanders represent the best solution by its operating performance and reliability. On the other hand, the rotary vane expander can represent another option when the required turbine power output is lower than 2 kW. The screw expander has the capability of delivering high power outputs superior to 10 kW. It can be considered the best-suited technology in the range of power when scroll and rotary vane expander cannot operate and when the conventional turbines represent high capital cost due to the need of multistage design. The Wankel engine represents the best technology in the near future, since it offers a wide range of operation with an acceptable performance, but some works has to be conducted to solve the lubrication problems encountered in this engine.

5.2 Heat exchanger design

The research conducted by [CHA05] in the last decades proved the possibility of using plate heat exchanger for boiler and condenser when operating with organic working fluids. The plate heat exchanger (see Figure 2.11) has been selected since it represents high effectiveness with a compact size and volume. The effectiveness of the heat transfer process in the boiler and condenser depends essentially on the mean temperature difference at which the heat is delivered or rejected, and the heat transfer coefficients of the working fluid on the both sides of the heat exchangers.

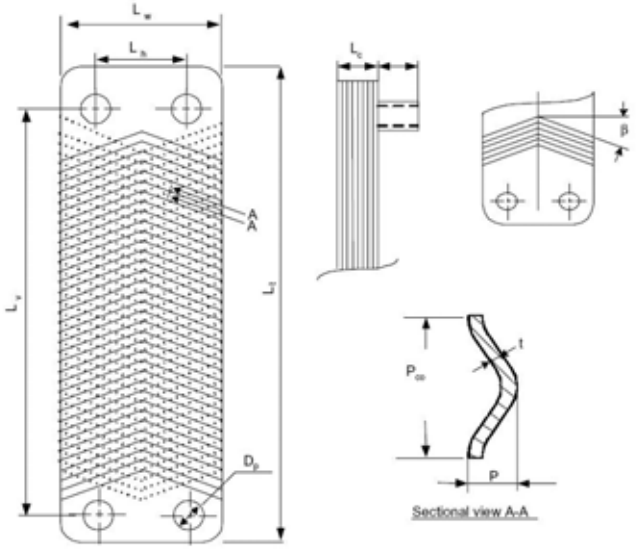

Figure 2.11 – Schematic diagram of brazed plate heat exchanger.

The boiler and the condenser studied are divided into three different sections: a two-phase evaporation or condensation section, a single-phase, a superheat section, and a single-phase sub-cooled section. The boiler and the condenser temperature diagrams are shown in Figure 2.12.

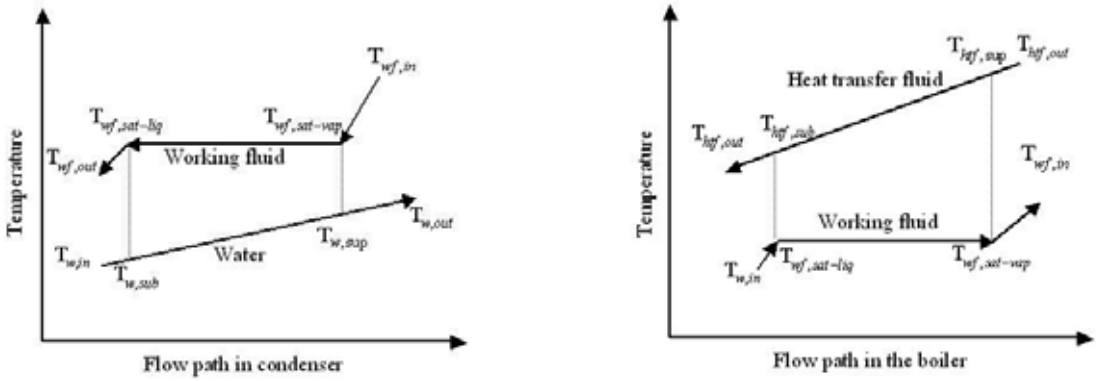

Figure 2.12 – Temperature diagram for the PHEs used boiler and condenser.

The heat exchange power in the boiler and the condenser is calculated by the following equation:

$$\begin{aligned}\dot{Q}_{boiler} &= \dot{m}_{wf}\left(h_{wf,out}-h_{wf,in}\right)=\dot{m}_{htf}Cp_{htf}\left(T_{htf,in}-T_{htf,out}\right)\\ \dot{Q}_{condenser} &= \dot{m}_{wf}\left(h_{wf,in}-h_{wf,out}\right)=\dot{m}_{w}Cp_{w}\left(T_{w,out}-T_{w,in}\right)\end{aligned} \tag{2.4}$$

The surface area of the boiler or the condenser will be the sum of the areas calculated for the different sections of the heat exchanger given by the following equation:

$$A_{tot}=A_{\sup}+A_{sub}+A_{two-phase}=\frac{\dot{Q}_{\sup}}{U_{\sup}\Delta T_{lm,\sup}}+\frac{\dot{Q}_{sub}}{U_{sub}\Delta T_{lm,sub}}+\sum_{i=1}^{n}\frac{\dot{Q}_{two-phase,i}}{U_{two-phase,i}\Delta T_{lm,two-phase}} \tag{2.5}$$

Where ΔT_{lm} represents the log mean temperature difference of the boiler or condenser. Since the heat transfer coefficient of the evaporation and condensation depends mainly of the vapor quality, the two-phase sections have been divided into n sections as shown in Eq. (2.5) and the sum of the areas of the n sections is done to calculate the total heat exchange area of the two-phase section. For a boiler, the log-mean temperature difference is given as

$$\Delta T_{lm}=\frac{\Delta T_1-\Delta T_2}{ln\left(\Delta T_1/\Delta T_2\right)} \tag{2.6}$$

Where the logarithmic temperature difference was typically calculated for the sub-cooled section in the boiler as

$$\left(\Delta T_{lm}\right)_{boiler,sub}=\frac{\left(T_{htf,sub}-T_{w,sat-liq}\right)-\left(T_{htf,out}-T_{wf,in}\right)}{ln\left[\left(T_{htf,sub}-T_{w,sat-liq}\right)/\left(T_{htf,out}-T_{wf,in}\right)\right]} \tag{2.7}$$

The overall heat transfer coefficient for each section is determined from the knowledge of the hot and cold fluid convection coefficients, and appropriate geometric parameters, which it is given by Eq. (2.8):

$$U=\frac{1}{\left(1/h_h\right)}+\frac{1}{\left(1/h_c\right)}+\frac{t}{k_w} \tag{2.8}$$

Where the single-phase heat transfer coefficient h_l was obtained from the *Dittus-Boelter Correlation*:

$$h_l = 0.023\left(\frac{k_l}{D_h}\right)\mathrm{Re}^{0.8}\,\mathrm{Pr}^{0.4} \tag{2.9}$$

The boiling heat transfer coefficient is given by [GAR07], which combines the effect of nucleate and convective boiling in plate heat exchanger, which is valid for a Reynolds range of 2,000<Re_{eq}<10,000.

$$Nu = 1.926\,\mathrm{Pr}_l^{1/3}\,Bo_{eq}^{-0.3}\,\mathrm{Re}_{eq}^{0.5}\left[(1-x)+\left(\frac{\rho_l}{\rho_v}\right)^{0.5}\right] \tag{2.10}$$
$$for\, 2000 < \mathrm{Re}_{eq} < 10000.$$

In this correlation, Re_{eq} and Bo_{eq} are respectively the equivalent Reynolds and boiling numbers, in which an equivalent mass flux is used in their definitions that are given respectively in Eqs. (2.11), (2.12), and (2.13).

$$\mathrm{Re}_{eq} = \frac{G_{eq} D_h}{\eta_l} \tag{2.11}$$

$$Bo_{eq} = \frac{q_w^{"}}{G_{eq} h_{fg}} \tag{2.12}$$

$$G_{eq} = G\left[1 - x_m + x_m\left(\frac{\rho_l}{\rho_v}\right)^{1/2}\right] \tag{2.13}$$

The condensation heat transfer coefficient used is given by [YAN99] and represented in Eq. (2.14) where Re_{eq} and G_{eq} are respectively presented below by Eqs. (2.11) and (2.13).

$$h_{cond} == 4.118\left(\frac{k_l}{D_h}\right)\mathrm{Re}_{eq}^{0.4}\,\mathrm{Pr}_l^{1/3} \tag{2.14}$$

In this study, several parameters are known and are listed in the following:

1. The geometry of the plate heat exchanger is fixed (see Table 2.3): the horizontal length of plates L_v, correction inclination angle "β", and plate thickness "t".
2. The working fluid, the mass flow rate of the working fluids m_{wf}, and the temperature profile of the working fluids calculated for 1 kW of isentropic power output.
3. The pinch point in the boiler or in the condenser (10 K).

Table 2.3 – Geometry and size of the PHEs used in this study.

Parameters	Measures
Distance between the head plates "L_c" (mm)	4.3+2.24*N_t
Distance between the ports at the same height "L_h" (mm)	40
Vertical length of the fluid path between the upper and lower ports "L_v" (mm)	154
Horizontal length of the plates "L_w" (mm)	72
Vertical length of the plates "L_t" (mm)	187
Correction inclination angle "β" (°)	60
Plate thickness "t" (mm)	0.5
Plate material	AISI 316

With the above given values, the total surface area of the heat exchangers, boilers and condensers are calculated. The heat transfer coefficients inside the channels in the boiler

and the condenser are calculated. The overall heat transfer coefficient is then determined from Eq. (2.8). The analysis begins by calculating the mass flux of the working fluids using Eq. (2.4) and the given pinch point temperature, then the temperature profile and the mass flux of the heat transfer fluid or water are calculated. The heat transfer coefficients are calculated for the different sections of the boiler and the condenser with Eqs. (2.9), (2.10) and (2.14).

The heat exchange in the boiler between the heat transfer fluid SYLTHERM 800 [SYL08] and the working fluid occurs along the three different sections described above. Since the highest rate of heat transfer occurs in the stage of two-phase change, then the heat transfer coefficient of the working fluids in this section will have the major influence on the boiler area. Figure 2.13 shows the boiling heat transfer coefficient for the different working fluids varying along the length of the heat exchanger. Water exhibits the highest heat transfer coefficient lying 4 times higher than the heat transfer coefficient of other working fluids. Another result shows that the heat transfer coefficient is directly related to the critical temperature of the working fluids since it is shown that working fluids with higher critical temperature present higher heat transfer coefficient. On the other hand, results show that hydrocarbons present better heat transfer characteristics than HFC and worse characteristics than water. The calculated surface area of the boiler corresponds to 1 kW of isentropic turbine power output; since the area is inversely proportional to the heat transfer coefficient in the boiler, then the results represented in Figure 2. show that the higher the heat transfer coefficient, the smaller the heat exchanger area. Since the isentropic power output of the turbine is always 1 kW, increasing the boiling temperature will increase the efficiency of the Rankine cycle and decrease the heat duty of the boiler. This will result in a lower surface area for boilers operating at high boiling temperatures (see Figure 2.).

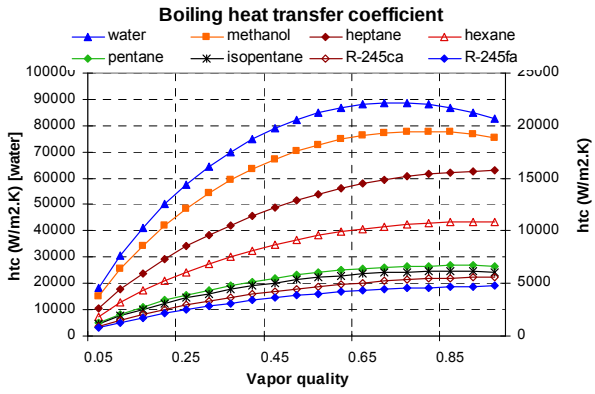

Figure 2.13 – Boiling heat transfer coefficient, T_{cond} = 80°C, G_c = 30 kg/m^2.s, D_h = 4.48 mm.

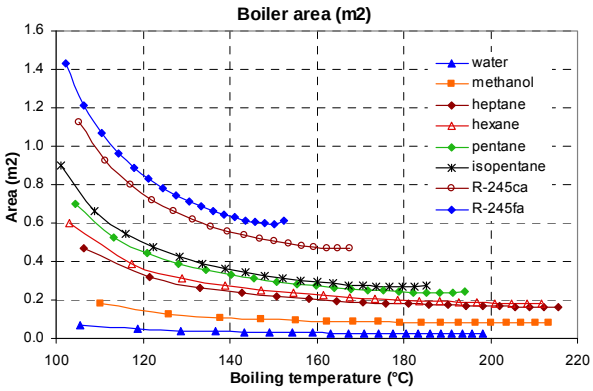

Figure 2.14 – Boiler area for different boiling temperature, G_c = 30 kg/m^2.s, D_h = 4.48 mm.

For the condenser, the condensation heat transfer coefficient (HTC) presents the same tendency as the boiling heat transfer coefficient, which increases while increasing the vapor quality (see Figure 2.). Therefore, the working fluid with the higher critical temperature shows the higher HTC and then exhibits the smaller surface area for the condenser design. Regarding the boiling temperature, the condenser area shows the same tendency as the boiler since when increasing the boiling temperature the surface area of the condenser decreases because the condenser heat exchange capacity decreases when increasing the boiling temperature.

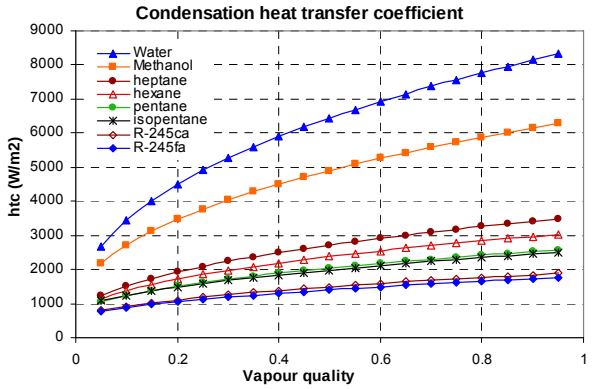

Figure 2.15 – Condensation heat transfer coefficient, T_{cond} = 80°C, G_c = 30 kg/m^2.s, D_h = 4.48 mm.

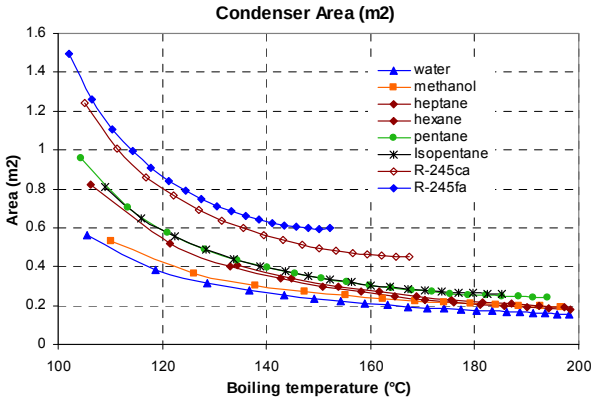

Figure 2.16 – Condenser area for different boiling temperature, T_{cond} = 80°C, G_c = 30 kg/m^2.s, D_h = 4.48 mm.

Regarding only the effect of the heat exchanger area on the design of the ORC, the best suitable working fluid for the ORC corresponds to the working fluid with higher critical temperature (water) and the best operating boiling temperature corresponds to the higher boiling temperature that can be delivered by the heat source (solar collector, wood boiler).

5.2.1 Pump selection

Pumps are divided into two fundamentals types: kinetic or positive displacement. In kinetic displacement, a centrifugal force of the rotating element, called an impeller, "impels" kinetic energy to the fluid, moving the fluid from the suction to the discharge. However, positive displacement uses reciprocating one or several pistons, or a squeezing action of meshing gears, lobes, or other moving bodies, to displace the media from one area into another. The centrifugal pumps differ from the positive displacement pumps by their curves relating pressure and flow. The slope of the centrifugal pump curve is mostly horizontal; when increasing the differential pressure, the flow rate delivered decreases. However, the positive displacement pump curve is mostly vertical; when the flow rate do not depends on the pressure head of the pump. The centrifugal pumps are more used when high volumetric flow rate is desired with low differential pressure [NEL99]. On the other hand, the SRC and ORC pumps should be designed to deliver low volumetric flow rates (< 60 l/min, see Figure 2.17) under high differential pressure (> 5, see Figure 2.18). For turbine isentropic power output lower than 10 kW, the VFR delivered can go down to 0.4 l/min when operating with water as working fluid for 1 kW of isentropic power output under a differential pressure of 7.

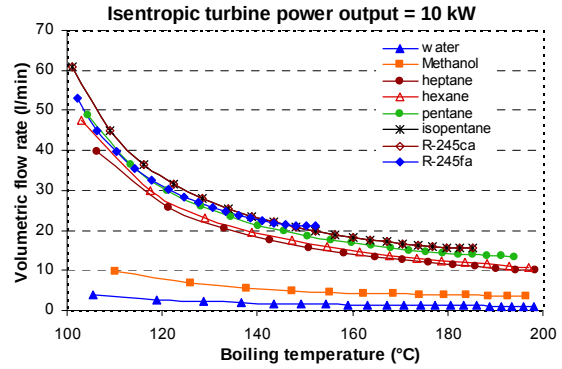

Figure 2.17 – Pump volumetric flow rate (10 kW)

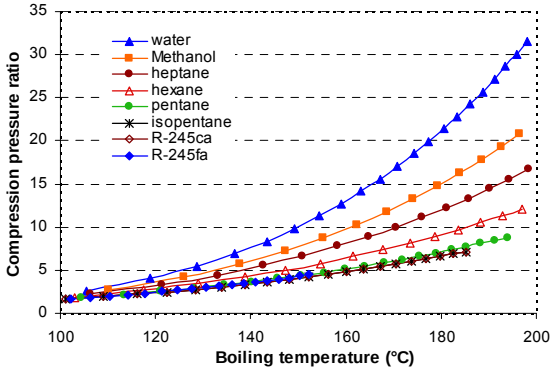

Figure 2.18 – Differential pressure.

However, the selection of the best-suited technology of pumps does not depend only from the VFR and the differential pressure, but it depends also from operating temperatures, inlet pressure, outlet pressure, fluid type, and fluid viscosity. Since the condenser temperature is fixed at 80°C to be able to produce DHW and to fulfill the heating needs of buildings, then

the inlet temperature of the pump will be fixed at 70°C with 10-K sub-cooling to prevent cavitation problems [NEL99]. The ORC pump should be selected in order to handle working fluids with low viscosity (below 0.4 mPa.s see Table 2.4) and still ensure the desired head.

Table 2.4 – Pump inlet–operating conditions.

Fluid	Inlet temperature (°C)	Inlet pressure (kPa)	Viscosity (mPa.s)
Water	70	47.41	0.404
Methanol	70	181.11	0.470
Heptane	70	57.09	0.248
Hexane	70	142.54	0.194
Pentane	70	368.01	0.152
Isopentane	70	457.57	0.152
R-245ca	70	569.63	0.305
R-245fa	70	788.81	0.237

Since the desired differential pressure is higher than a single-stage centrifugal pump can handle, the need of multi-stage design is required to cover all operating conditions of the ORC. However, this option is disregarded because it will represent a high cost and a bulky pump system.

Positive displacement pumps represent the best-suited solution for our application. Not all technologies of positive displacements pump can handle low viscosity (< 1 mPa.s). Gear pumps [VIK03] are almost operating with viscosity higher than 1 mPa.s under limited differential pressure. Diaphragm pumps [HYD08] and piston pumps [SER08] represent almost the only suitable solution for our application, since diaphragm pumps are designed to operate with viscous fluid going down to 0.1 mPa.s under a differential pressure up to 7 MPa. Piston pumps can also handle low viscosity under high differential pressure up to 14 MPa, but some care has to be taken for the operating temperature since some piston pumps cannot handle high-temperature fluids (> 50°C). Table 2.5 shows the characteristics of diaphragm and piston pumps available on the market that can fit all requirements of low VFR and high-pressure ratio for our application.

Table 2.5 – Pump characteristics.

Parameters	Diaphragm pumps [HYD08]	Piston pump [SER08]
Type	G-20/G-03/G-10/G25	R 409.1-13K.1/14/R 409.1-13K.1/28
Temperature (°C)	121	--
Inlet Pressure (MPa)	0.69/1.7/1.7/1.7	--
Outlet pressure (MPa)	7	140/40
Pressure ratio	70	140/40
VFR (l/min)	3.8/11.3/29/76	13/52
Viscosity (mPa.s)	> 0.1	--

5.3 Results

Results show that it is more suitable to operate with higher boiling temperature than high volume ratio to reduce the total surface areas of heat exchangers. However, increasing the volume ratio will decrease the volumetric flow rate of the working fluid and then a smallest pump will be required. Since the efficiencies of the different pumps operating at the different VFRs calculated above present almost the same performance, then the pump effect on the selection of the working fluid will be neglected.

On the other hand, the total area of the different heat exchangers decreases when the selected working fluid presents higher critical temperature. Thus it is almost more suitable to operate with working fluid with high critical temperature to reach the minimum heat exchanger surface area.

However, the main component affecting the design and the performance of the RC and ORC is the volumetric expander, since the selection of the expander will define simultaneously the

volume ratio and the volumetric flow rate of the working fluid at the expander inlet. Then all other parameters will depend only on the selection of the working fluid. To identify the optimal volume ratio, which gives the highest efficiency of the RC or ORC, a calculation has been conducted to show the RC efficiency depending on the VR. Results are presented in Figure 2.19. They show that for low volume ratio (< 5), all working fluids present almost the same efficiency. When increasing the volume ratio, water and methanol reach the highest efficiency followed by the different hydrocarbons, and then HFCs that correspond to the lowest RC efficiency.

The turbine power density is calculated for the different VRs and presented in Figure 2.20. Results for HFCs show different tendencies compared to RC efficiencies, since the highest power density is calculated for HFCs followed by the different hydrocarbons; the lowest power density is calculated for water and heptane.

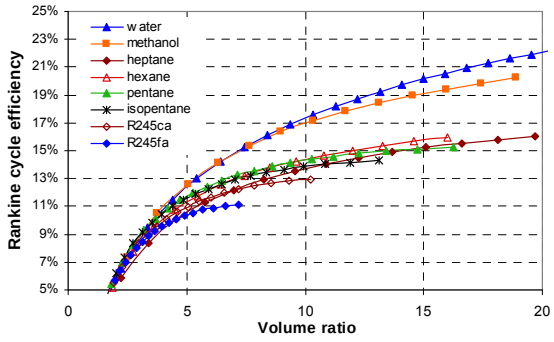

Figure 2.19 – Rankine cycle efficiency.

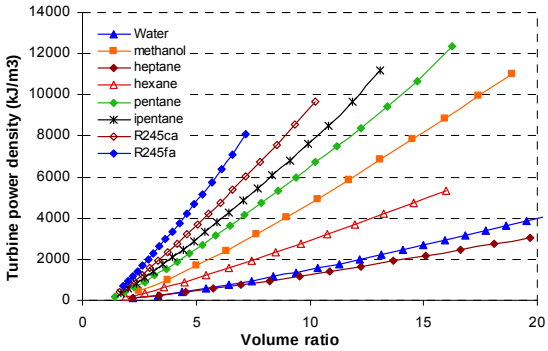

Figure 2.20 – Turbine inlet density.

These results show that there is no unique working fluid that satisfies all requirements set for this application. However, some fluids are more suitable than others.

In a specific application where the micro-cogeneration system is designed to operate with a working fluid with restricted design criteria regarding environmental and safety problems, water seems to be the most promising fluid. However, water presents many disadvantages compared to other working fluids:

- High superheat degree is needed at the turbine inlet to prevent formation of water droplets at the turbine exit and then prevent corrosion problems.
- A well-tight system is needed to prevent air infiltration into the system since the condenser operating pressure is lower than the atmospheric pressure.
- Compared to other working fluids, for the same power output a larger built-in swept volume is required.
- Steam turbine requires an oil-free expander.

If a flammable working fluid is tolerated, then using hydrocarbons can be the first choice after water. Hydrocarbons present the advantage of achieving higher mechanical power output with the same turbine designed to operate with steam. The diversity of hydrocarbons with different critical temperatures presents the advantage of being more reliable in selecting the best working fluids corresponding to different power outputs and required efficiency.

Flammability constitutes a major problem towards the use of hydrocarbons. For micro cogeneration operating in small houses, the use of HFCs can represent an advantage versus the use of water and hydrocarbons since it presents a higher turbine power density but a relative low efficiency compared to other working fluids. The main advantage of using HFCs is the possibility of lubricating the turbine designed with direct injection of oil in the core of the turbine. Many lubricants are available on the markets, miscible with refrigerants when they are used in heat pumps.

In summary, water presents many environmental, safety, and performance advantages. R-245fa is the most suited working fluid when higher output power is required. Isopentane and hexane exhibit relatively high-energy performance when operating with volume ratio ranging from 5 to 12 and a high power density. The selection of one or the other depends on the desired power output and efficiency of the ORC.

5.4 Conclusions

A methodology has been developed to identify promising working fluids for micro-cogeneration system based on an ORC operating with low-grade heat. First identification of criteria has been set up for ideal working fluids. Since no ideal fluid has been identified, a procedure of selection has been conducted in four different phases. The first phase addresses environmental and safety issues; the second phase takes care of operating conditions fixed by the designer, and depends on the application. In the third phase, a calculation of the thermodynamic efficiency is performed for the SRC and ORC cycles to identify a set of potential working fluids. On the fourth phase, a preliminary design of the principal components is conducted to identify the effect of the working fluid on the design. Results show that the selection of the turbine is a key on the design and selection of the best working fluids. Four different working fluids (water, isopentane, hexane, and R-245fa) have been identified as potential working fluids. Selecting the most suitable working fluid depends only from the requirement of the specific application. The designer fixes these requirements at the final stage of the design procedure.

References

[ANG00] G. Angelino , P. Colonna di Paliano, Organic Rankine cycles (ORCs) for energy recovery from molten carbonate fuel cells, in: 35th Intersociety Energy Conversion Engineering, Las Vegas, Nevada, July 24-28, 2000.

[ASH04] ANSI/ASHRAE Standard 15-2004, Safety Code for Mechanical Refrigeration.

[BAD84] O. Badr, P. W. O'Callaghan, M. Hussein, S. D. Probert, Multi-vane expanders as prime movers for low-grade energy organic Rankine-cycle engines, Applied Energy 16 (1984) 129-46.

[BAD85] O. Badr, S.D. Probert, P.W. O'Callaghan, Selecting a working fluid for a Rankine-Cycle engine, Applied energy 21 (1985) 1-42.

[BAD91] O. Badr, S. Naik, P.W. O'Callagen, S.D. Probert, Expansion machine for a low power-output Steam Rankine-Cycle engine, Applied Energy 39 (1991) 93-116.

[BAR81] R.E. Barber, D.E. Prigmore, Solar-powered heat engines, Solar energy Handbook-Chap 22, McGraw-Hill, New York, 1981

[BOR07] A. Borsukiewicz-Gozdur *, W. Nowak, Maximising the working fluid flow as a way of increasing power output of geothermal power plant, Applied Thermal Engineering 27 (2007) 2074-2078.

[BRA05] J.J. Brasz, B.P. Biederman, G. Holdmann, Power production from a moderate – temperature geothermal resources, GRG Annual meeting, Reno, NV, USA, September 25-28, 2005

[CAL01] J.M. Calm and G.C. Hourahan, Refrigerant data summary, Engineered systems, 18 (11): 74-88, November 2001.

[CEN94] Y.A. Cengel, M.A. Boles, Thermodynamics an engineering approach, Second edition, 1994, McGraw-Hill.

[CHA05] R. El Chammas, Rankine cycle for hybrid vehicles, simulation and design of a first prototype, thesis presented at the Ecole des Mines de Paris in 2005

[CHE06] Y. Chen, P. Lundqvist, A. Johansson, P. Platell, A comparative study of the carbon dioxide transcritical power cycle compared with an organic Rankine cycle with R123 as working fluid in waste heat recovery, Applied Thermal Engineering 26 (2006) 2142-2147.

[CON05] C.E. Cong, S. Velautham, A.N. Darus, Sustainable power: solar thermal driven organic Rankine cycle, in: Proceedings of the international conference on recent Advances in Mechanical and materials engineering, Kuala Lumpur, Malaysia, May 30-31, 2005.

[DRE06] U. Drescher, D. Bruggemann, Fluid selection for the Organic Rankine Cycle (ORC) in biomass power and heat plants, Applied Thermal Engineering 27 (2006) 223-228.

[FAC05] J. Facao, A.C. Oliveira, Analysis of a micro-Cogeneration system using hybrid solar/gas collectors, in 4th International Conference on Sustainable Energy Technologies (SET2005), Jinan, China, September 23-25, 2005.

[GAR07] J.R. Garcia-Cascales, F. Vera-Garcia, J.M. Corberan-Salvador, J. Gonzalvez-Macia, Assessment of boiling and condensation heat transfer correlations in the modeling of plate heat exchangers, International journal of refrigeration 30 (2007) 1029-1041.

[HUN97] T.C. Hung, T.Y. Shai, S.K. Wang, a review of organic Rankine cycles (ORCs) for the recovery of low-grade waste heat, Energy 22 (1997) 661-667.

[HUN01] T. Hung, Waste heat recovery of organic Rankine cycle using dry fluids, Energy Conversion and Management 42 (2001) 539-553.

[HYD08] Hydra-cell. Diaphragm pump selection chart, Wanner Engineer, Inc. Minneapolis, USA, 2008, <http://www.hydra-cell.com/product/sealess-pump-selection.html>.

[INV06] C. Invernizzi, P. Iora, P. Silva, Bottoming micro-Rankine cycle for micro-gas turbines, Applied Thermal Engineering 27 (2007) 100-110.

[IQB78] K.Z. Iqbal, H.H. West, K.E. Starling, Hydrocarbon working fluid and operating conditions selection for the conventional geothermal binary cycle, in: Society of Automotive Engineers, Inc. SAE/P-78/75, 1978.

[KAN03] M. Kane, D. Larrain, D. Favrat, Y. Allani, Small hybrid solar power system, Energy 28 (2003) 1427-1443.

[KIM07] H.J. Kim, J.M. Ahn, I. Park, P.C. Rha, Scroll expander for power generation from a low-grade steam source, Proceedings of the IMECHE, Journal of Power and Energy 221 (2007) 705-711.

[LEM06] V. Lemort, I. Teodorese, J. Lebrun, Experimental study of the integration of a scroll expander into a heat recovery Rankine cycle, in: The 18th International Compressor Engineering Conference, Purdue, USA, July 17-20, 2006

[LIU04] B. Liu, K. Chien, C. Wang, Effect of working fluids on organic Rankine cycle for waste heat recovery, Energy 29 (2004) 1207–1217.

[LOZ82] G. Lozza, E. Macchi, A. Perdichizzi, On the influence of the number of stages on the efficiency of axial-flow turbines, ASME Paper 82-GT-43, pp. 1–10.

[LOZ86] G. LOZZA, E. MACCHI, A.PERDICHIZZI, Investigation on the Efficiency Potential of Small Steam Turbines of Various Configurations, Proceedings of the 21st Intersociety Energy Conversion Engineering Conference, August 25-29, San Diego, California, 1986, Paper No. 869312, 1367-1373.

[MAC81] E. Macchi and A. Perdichizzi, Efficiency prediction for axial-flow turbines operating with non conventional fluids, Transaction of the ASME, Journal of Engineering for Power **103** (1981) (October), pp. 718–724.

[MAG08] P.J. Mago, L.M. Chamra, K. Srinivasan, C. Somayaji, An examination of regenerative organic Rankine cycles using dry fluids, Applied Thermal Engineering 28 (2008) 998-1007.

[MAR81] T.J. Marciniak, J.L. Krazinski, J.C. Bratis, H.M. Bushby, E.H. Buycot, Comparison of Rankine-cycle power systems: effects of seven working fluids, 1981, NASA STI/Recon Technical Report N, 82, 26844.

[MCM06] A.C. Mcmahan, Design and optimization of organic Rankine cycle solar-thermal power plants", Thesis presented at the University of Wisconsin-madison in 2006.

[MOB78] A. Mobarak,N. Rafat, M. Saad, Turbine selection for a small capacity solar-powered generator, Solar energy international Progress, Proceedings of the international Symposium, Workshop on solar energy, 16-22 June 1978, Cairo, Egypt, Vol. 3, pp. 1351-67.

[NEL99] L. Nelik, Centrifugal and Rotary Pumps: Fundamentals with Applications, CRC Press LLC, 1999.

[NGU01] V.M. Nguyen, P.S. Doherty, S.B. Riffat, Development of a prototype low-temperature Rankine cycle electricity generation system, Applied Thermal engineering 21 (2001) 169-181.

[RAH06] C. Rahhal, Conception d'une pompe à chaleur air/eau à haute efficacité énergétique pour la réhabilitation d'installations de chauffage existantes, thesis presented at the Ecole des Mines de Paris in 2006.

[REF06] E.W. Lemmon and M.O. McLinden, "Reference fluid thermodynamic and transport properties", NIST standard reference Database 23, Version 7, Beta version 21/13/02.

[ROB78] G.F. Robertson, C.H. Wolgemuth, Experimental and analytical study of friction, leakage and heat transfer in a vane expander, in: Proc. 12th IECEC, 1978, pp. 1430-41.

[SAK98] S. Kakaç, H. Lui, "Heat exchangers: selection, rating and thermal design", published by CRC press LCC, 1998.

[SAL07] B. Saleh, G. Koglbauer, M. Wendland, J. Fischer, Working fluids for low-temperature organic Rankine cycles, Energy 32 (2007) 1210-1221.

[SER08] Seybert & Rahier, Dosiong and feeding solutions,<www.sera-web.de.>

[SIM06] G.R. Simader, R. Krawinkler, G. Trnka, Micro CHP systems: state of the art. Final report of green lodges project for Australian energy agency, Vienna; 2006.

[SMI96] I.K. Smith, N. Stosic, C.A. Aldis, Development of the trilateral flash cycle system Part 3: the design of high efficiency two phase screw expanders. In: Proceedings International of Mechanical Engineering, Part A, 1996, 210(A2), 75-93.

[STE81] R.F. Steidel, R.E. Berger, Performance characteristics of the Lyshlom engine as testes for geothermal applications, in: Proc. 16th IECEC, 1981, Vol. 2, pp. 1334-40.

[SWE08] Brazed plate heat exchanger, Landskrona, Sweden, 2003-2008 SWEP International AB, <www.swep.net>

[SYL08] Dow Chemical Company. Data sheet for SYLTHERM 80, 2008, <http://www.dow.com/heattrans/family/syl800/index.htm>.

[VIK03] Viking Pumps. Comparison chart for all of Viking's pump, Cedar falls, Lowa, 2003, < http://www.vikingpump.com/products/comparison_chart.htm>.

[WAD83] J.D. Wade, R.M. Tompkins, R.M. Brown, G.A. Silvestri, Re1-11 rotary expander engine testing and analysis, in: Proc. 18th IECEC (1983) 636-41.

[WEI07] D. Wei, X. Lu, Z. Lu, J. Gu, Performance analysis and optimization of organic Rankine cycle (ORC) for waste heat recovery, Energy conversion and management 48 (2007) 1113-1119.

[YAM01] T. Yamamoto, T. Furuhata, N. Arai, K. Mori, Design and testing of the Organic Rankine cycle, Energy 26 (2001) 239-251.

[YAM06] H. Yamaguchi, X.R. Zhang, K. Fujima, M. Enomoto, N. Sawada, Solar energy powered Rankine cycle using supercritical CO2, Applied Thermal Engineering 26 (2006) 2345-2354.

[YAN99] Y.Y. Yan, T.F. Lin, Evaporation heat transfer and pressure drop of refrigerant R134a in a plate heat exchanger, Transaction of the ASME, Journal of Heat Transfer 121 (1999) 118-127.

[YAN01] T. Yanagisawa, Y. Fukuta, T. Ogi, T. Hikichi, Performance of an oil-free scroll-type air expander: in: International conference on Compressors and their systems, Paper No. C591/027, London, United kingdom, September 2001, pp.167-174.

CHAPITRE 3 – Design and experimental results of a first Rankine cycle prototype

1. Introduction

Water, isopentane, hexane, and R-245fa have been identified as the most promising working fluids for a Rankine system operating on renewable energies (solar and biomass) for micro-cogeneration applications. In order to improve the system performance and reduce its capital cost, the selection of the different components of the system requires advanced technical assessments to identify the most suitable technologies available on the market that can be easily integrated in the system or slightly modified.

In this chapter, a technical assessment has been carried out in order to identify the technologies to be integrated and the different technical barriers to be overcome in order to disseminate micro-cogeneration systems. Once the technologies are selected, different operating conditions of the Rankine system will be calculated and the optimal design conditions will be defined.

A first experimental test bench has been designed and realized to test some of these components and make a first selection of turbines based on their overall efficiency.

2. Background

The following papers have presented the development of micro cogeneration operating on solar and/or gas energy for different applications. Oliviera et al. [OLI02] have developed a novel hybrid solar/gas system intended to provide cooling/heating and electricity generation for buildings. The system is based on the combination of an ejector heat pump cycle and a Rankine cycle. It is driven by solar energy and supplemented by a gas burner. The main technical improvement concerns the development of a turbo-generator and an ejector. The turbo-generator was developed to supply electrical power output up to 1.5 kW.

Riffat [RIF04] investigates the development of a novel hybrid heat pipe solar collector with a CHP system. The system is based on the integration of a number of innovative components including a hybrid heat pipe solar collector, a turbine, a condenser, a boiler, and pumps. In this study, the system was constructed to operate simultaneously with solar and gas. The main innovation was the development of two types of turbines, one was an impulse-reaction turbine designed to operate at very high rotation speeds, up to 80,000 rpm, and provide electricity output from 1.5 to 3 kW. The other was a gas-driven turbo-alternator, designed to operate at a low rotation speed, around 1000 rpm, with 250-W electricity output.

An ORC has been designed and tested by Yamamoto et al. [YAM01]. The ORC system has been designed to operate with low-grade heat. The working fluids tested are HCFC-123 and water. The experimental test bench was composed of a shell-and-tube heat exchanger for the condenser, electrical heaters for heat generation, and an impulse micro-turbine designed for the study. The maximum cycle efficiency was 1.25% with HCFC-123. This poor efficiency is due to the poor efficiency of the turbine prototype. A micro-CHP system driven by solar and natural gas has been installed and tested for a small-scale application. Two fluids, HFE-301 and pentane, were considered as potential working fluids for this system. Results show that HFE-301 performed better than pentane in terms of actual electrical efficiencies, i.e. 7.6% and 5%, respectively. The prototype was composed of: evacuated glass tube (Thermomax Ltd), brazed-plate heat exchangers (condenser and boiler), an electrical pump with an explosion proof motor was used for HFE-301 and a double diaphragm pump for pentane. The

turbine/generator was designed to deliver 1.5 kW_{el}, the operating rotation speed was 60 000 rpm, and propelled by the radial flow of vapor.

Kane at al. [KAN03] have introduced another new concept. A novel mini-hybrid solar power plant integrating a field of concentrators, two superposed ORC and bio-Diesel engine. The system is designed to produce 15 kW_{el} at the nominal power output. The two turbines used in the experimental test bench were hermetic scroll expander. The ORC efficiency measured was about 13.7% and the overall efficiency when operating with solar energy was about 7.74%.

3. Technical assessment

The micro-CHP system proposed in this thesis is described in Chapter 1, Section 5. The electrical power output ranges from 1 kW_{el} to 10 kW_{el} depending on the heating load of the reference building. From calculations conducted in the previous chapter (Section 4.1), the ORC efficiency was demonstrated to vary from 10% to 16% depending on the working fluid and the boiling temperature. For the calculation of the required heat input, the ORC efficiency will be assumed to be 12% and the thermal efficiency of the wood-pellet boiler to be 90%. Then, the heat capacity of the wood-pellet boiler will vary from 11 kW_{th} to 110 kW_{th}. The thermal efficiency of the solar collector is assumed to be around 40%, and then the required area of the solar collectors will vary from 26 m^2 to 260 m^2 assuming peak overall radiation to be 800 W/m^2.

In this section, a survey covering a large number of available and emerging technologies will be performed. The most promising technologies will be highlighted, for each of the following components:

- Wood-pellet boiler (heat capacity: from 11 kW_{th} to 110 kW_{th}).
- Solar collectors (operating temperature: from 100°C to 200°C).
- Turbine (mechanical power output: from 1 kW to 10 kW).
- Pump (low volumetric flow rate with high pressure head).
- Heat exchangers (boiler, condenser, and heat recovery).

3.1 Biomass combustion technologies

3.1.1 Requirements and technical barriers

The biomass boilers should be designed to deliver heat at higher-level temperature compared to current technologies. The conventional wood boilers available on the market are designed to heat the water for temperature below 95°C. In our application the water will be replaced by a heating media, in general a heat transfer fluid such as “Silicone oil”, heated at temperature higher than 100°C. The heat exchanger integrated in the wood boiler, where the flue gases that heats the heat transfer fluid (HTF), should be capable to withstand high temperatures of the combustion gases. The wood boilers should be controlled based on the thermal load variation of the building. Also, a second heat exchanger could be installed after the first heat exchanger to cool the exhaust gases to a lower temperature to recover additional heat from the flue gases.

The selected wood boiler has to fulfill other environmental requirements. The wood combustion generates high dust emission and filters have to be used to limit particle emissions. The CO emission level depends on the combustion efficiency and also on the type of wood to be burnt. The type of wood has a major impact on the performance, capacity, and pollution of the wood boiler.

3.1.2 Assessments of biomass boiler technologies

Before reviewing the different technologies available on the market for the wood combustion boiler, a survey of the different types of fuel used will be performed. Biomass type fuels have a heat of combustion (HOC) value varying from 15.5 MJ/kg to 16.5 MJ/kg with a typical water content of 15%. Wood contains only 0.5% of ash; but straw contains up to 6%. Table 3.1 shows values characterizing biomass fuel including a comparison to coal. One practical figure: 1000 L of fuel is equivalent to 2.1 tons of wood pellets.

Table 3.1 – Specific weight and calorific value of wood and selected biomass fuels [STE00].

Fuel	Volatiles (%)	HOC (MJ/kg)	Ash (%)	C (%)	O (%)	H (%)	N (%)	S (%)
Straw	80.3	14.2	4.3	44.0	35.0	5.0	0.5	0.1
Wood	85.0	15.3	0.5	43.0	37.0	5.0	0.1	--
Charcoal	23.0	30.1	0.7	71.0	11.0	3.0	0.1	--
Peat	70.0	13.5	1.8	47.0	32.0	5.0	0.8	0.3
Brown coal	57.0	13.6	1-15	58.0	18.0	5.0	1.4	2.0
Mineral coal	26.0	29.5	1-15	73.0	5.0	4.0	1.4	1.0
Coke	4.0	25.9	9-17	80.0	2.0	2.0	0.5	0.8

The combustion process of biomass fuels depends mainly on their moisture content and chemical characteristics as well as HOC and density t (see Figure 3.1). Biomass fuels have to be dried in order to ensure a good storage without losses; biomass fuels with low moisture content are the basis of a high combustion quality especially in small furnaces.

The high volatile gases cause problems for straw and wood combustion. Therefore, it is necessary to perform a combustion process in two different chambers, where the first chamber is used for gasification and the second to burn the gas. Wood furnaces do not work properly in the range below 30% of full power. Heat storage is necessary to cover low heat demand.

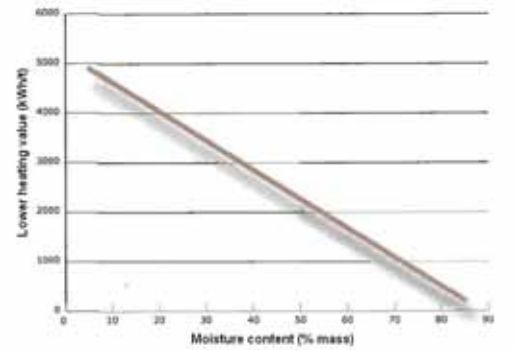

Figure 3.1 – Type of combustion [BOS08].

Combustion of biomass fuels depends not only on the chemical properties but also on the physical structure of organic materials. The physical structure can be influenced by different processing techniques, like milling, cutting, compaction, baling, or pelleting. The different types of processing are shown in Table 3.2 Sawdust is mainly available in wood processing industries and sawmills. It can be utilized in special small stoves with discontinuous charging, in units with automatic fuel charging or in large injection units. Wood ships are in general produced from soft wood, dried to prevent molding; wood humidity has to keep to a value lower than 20%. The most conventional means of wood processing for small voluminous hand-charged stoves are the short rolls or logs and split logs, with length up to 1 m for large size combustion units. Briquettes and pellets are mainly produced from sawdust and bark, and they are generally used in small combustion units where they are more suitable for automated charging. The energy compactness ranges from 40 to 80 kWh/t.

Table 3.2 – Technical characteristics of wood for combustion [STE00].					
Type of wood	Saw dust 	Wood chips 	Wood log 30 – 50 cm length 	Wood logs 100 cm length 	Pellets from saw dust 
Specific weight kg/m^3	120 – 180	160 – 250	250 – 500	300 – 500	400 – 600
Aptitude for short distance transporting	++	++	+	+	++
Aptitude for long distance transporting	+	+	O	+	++
Charging of combustion chamber	Mechanical and by hand	Mechanical and by hand	By hand	By hand	Mechanical and by hand
Possibility of charging by hand	O	O	+	++	+
Automatic control of charging	+	++	-	-	+
Possibility for power regulation	++	++	O	O	++
Notice: ++ = very suitable, + = suitable, O = possible, – = less suitable					

As mentioned before, the biomass combustion systems can be divided into two categories depending on the types of fuel charging: furnaces with discontinuous charging and furnaces with automatic fuel charging. The study of the discontinuous charging furnaces is disregarded since the micro-CHP should operate in fully automated mode. Automated fuel charging is required for a long period varying from three months up to 1 year to ensure a continuity operation of the micro-CHP.

For individual boiler, where low thermal power is required varying from 10 kW to 100 kW, the two main biomass fuel used are pellets and wood chips. Since the furnace thermal capacity output is small, the combustion is more efficient with homogeneous fuels. Since the moisture content of pellets and wood chips is relatively low, a stable combustion process can be achieved with small furnaces allowing the development of adequate furnaces for low thermal capacity output achieving high efficiency (> 90%) with very low pollutant emissions. The use of wood chips needs a special care for the storage techniques since this type of fuel contains a high level of moisture.

Depending on how the pellets are fed into the burner, three types of pellet burner can be distinguished (see Figure 3.2). Some are automatically modulating the capacity from 30 to 100% according to the heat demand. Some manufacturers provide boilers with passages and burners, which are often cleaned automatically by helical screws serving as turbulator vortex generator to improve the heat transfer of the HTF. Ashes from the combustion chamber are also removed without the help of the end user and some manufacturers provide an inbuilt ash compressor that reduces the ash removal times from the boiler to a minimum. The advanced boilers are equipped with an air aspirator for the air supply, and a lambda sensor for optimal combustion and a modulation of the heating capacity. These systems reach high boiler efficiencies up to 94%.

(a) Okofen (b) HARGASSNER (c) ZAEGEL-HELD

Figure 3.2 – Types of pellets burners by there feed principle: (a) Bottom fed burner; (b) horizontal fed burner; (c) top fed burner.

Fuel storage volume can varies from 50 L to more than 500 L depending on the capacity required, the thermal head load and the operating time. Several storage techniques with different air suction process are available (see Figure 3.3). The storage type is defined by the end user depending on the building architecture.

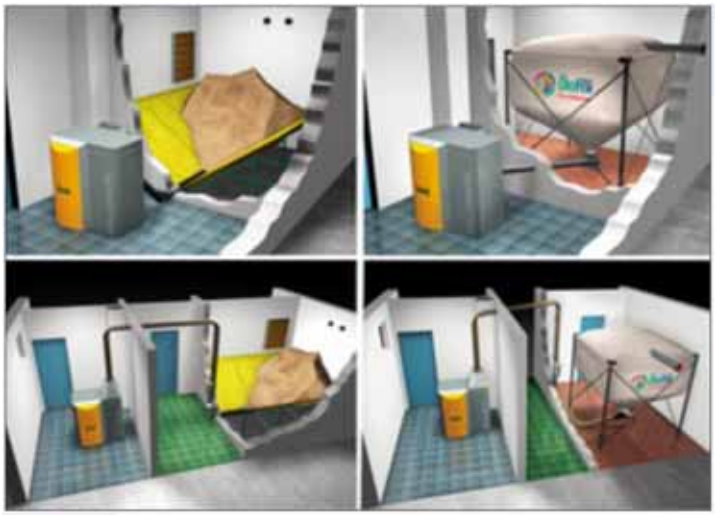

Figure 3.3 – Technique of automatic filling process.

The heat exchanger adopted for the heat transfer from the flue gases to the heating media are in general tube heat exchanger where the flue gases circulate in the tube and the HTF circulates around the tube, alike in the shell-and-tube heat exchanger type placed inside the water volume (see Figure 3.4). In general the tubes are vertically set. However, some models are available with horizontal tubes. Most of heat exchangers contain vortex generators inside the tube to increase heat transfer coefficients on the gas side. Some manufacturers have implemented a second condensing heat exchanger (see Figure 3.5) to extract more energy from the flue gases and so increase the boiler efficiency. Therefore, these boilers can exhibit high thermal efficiency going up to 100%.

Figure 3.4 –Vortex generator heat exchanger [HS France].

Figure 3.5 – Condensing pellet-heating system. [Okefen]

3.1.3 Selection of the wood boiler technology

To ensure good operation of the micro-CHP system with high thermal efficiency, the biomass boiler should be fully automated:

- Regulation of the thermal heat output (from 30% to 100% load).
- Automatic cleaning system of the heat exchangers.
- Automatic ash cleaner or a compressed ash system to minimize the maintenance time interval.
- Automatic combustion regulation system to increase the efficiency of the combustion process and minimize the pollutant emissions.

The condensing heat exchanger is an optional component; it can be implemented in the system if high thermal efficiency is required depending on a cost and benefit decision.

From the different technologies previously reviewed, pellet boiler represents the most suitable solution. Boiler operating on wood chips can represent another option, but some precautions have to be taken for the system design. Pellet boilers are available on the market with different heating capacity outputs ranging from 10 kW to several hundred kW. The standard pellet boilers have to be modified to operate at high temperature of the heat transfer fluid.

3.2 Solar collector

3.2.1 Requirements and technical barriers

The solar collectors should be capable to recover efficiently the solar energy even when at high temperature. Operating temperatures of HTF range from 100°C to 200°C. Synthetic oils can withstand those levels of temperatures at atmospheric operating pressure. The solar collector should handle high flow rate with acceptable pressure drop to minimize the energy consumption of the circulating pump. Moreover, the solar collectors need to be integrated in the architecture of single houses or apartment buildings.

3.2.2 Assessments of plausible solar collector technologies

There are basically two types of solar collectors: non-concentrating or stationary and concentrating. A non-concentrating collector has the same area for intercepting and for absorbing solar radiation, whereas a sun-tracking concentrating solar collector usually has concave reflecting surfaces to intercept and focus the sun radiations to a smaller receiving area, thereby increasing the radiation flux. A large number of solar collectors are available on the market; a review of the various solar collectors currently available will be presented.

Solar collectors are basically distinguished by their motions and their operating temperatures. Their motions can be: stationary, single axe tracking, and two axes tracking. Initially, the stationary solar collectors will be examined. These collectors are permanently fixed in position and they do not track the sun. This type of collectors can be found in three different categories: flat plate collectors (FPC), stationary compound parabolic collectors (CPC), and evacuated tube collectors (ETC).

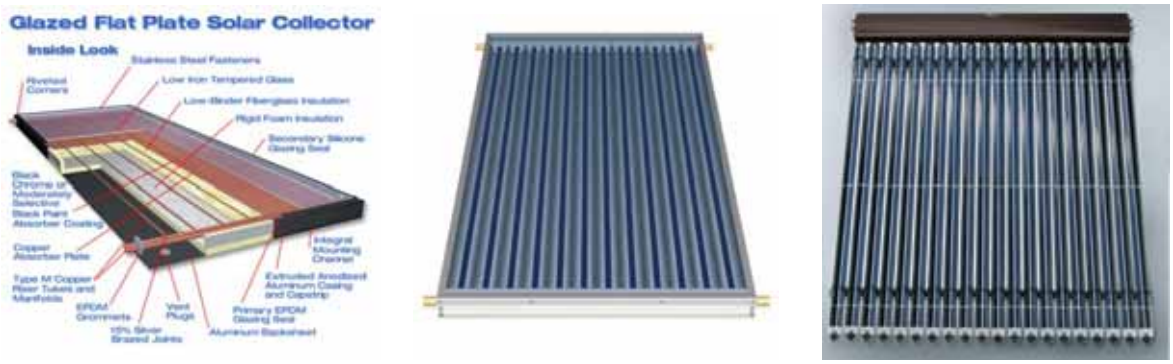

(FPC) source : (CPC) source: SOLARGENIX (ETC) source: VIESSMANN

Figure 3.6 – Stationary solar collectors.

Several flat plate collectors are shown in Figure 3.6. For a FPC, solar radiation passes through a transparent cover, are absorbed by the plates, and then transported by the heat transfer fluid. The “transparent” cover is used both for the green house effect and to reduce the convection losses from the absorber plate through the air layer, between the absorber plate and the glass. FPC is usually in permanently fixed position. FPC is by far the most used type of collector for low-temperature applications up to 100°C. Due to the introduction of highly selective coatings, new FPCs can reach stagnation temperature of more than 200°C. With these collectors good efficiencies can be obtained up to temperatures of about 100°C.

For higher temperatures, double or triple anti-reflective glass is used, and it has been shown by Rommel and al. [ROM03] that the efficiency curve of 2 anti-reflective glass collectors is higher than that of standard flat plate collector. Especially for higher operating temperatures, the advantage of 2 anti-reflective collectors is significant. Figure 3.7 shows the efficiency curves of different flat-plate solar collectors as a function of the mean temeprature of the woking fluid and the insolation. The results show that the flat-plate collector efficiency equipped with 2 or 3 anti-reflector glasses is better than the standard collector efficiency by more than 33%.

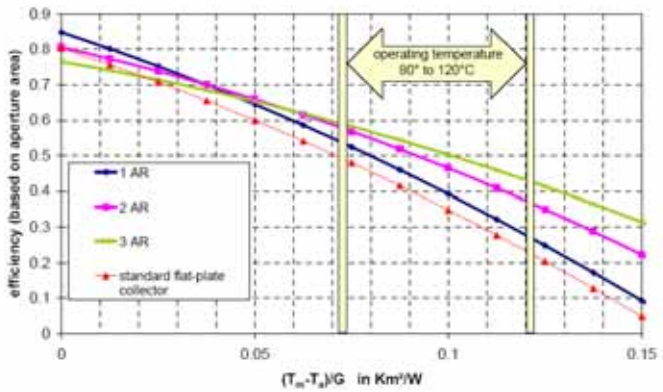

Figure 3.7 – Efficiency curves of a single, double and triple glazed AR collector compared to a standard flat-plate collector with normal solar glass [ROM03].

CPCs are non-imaging concentrators. They have the capability of reflecting to the absorber all of the incident radiation within wide limits. CPCs can accept incoming radiation over a relatively wide range of angles. By using multiple-reflection, all the radiation entering the aperture within the collector acceptance angle finds its way to the absorber (see Figure 3.8). For stationary CPC collectors mounted in this mode, the minimum acceptance angle is equal to 47°.

This angle covers the declination of the sun from summer to winter. In practice, bigger angles are used to enable the collector to collect diffuse radiation at the expense of a lower concentration ratio. Smaller (less than 3) concentration ratio CPCs are of greatest practical interest. These according to [PER85] are able to accept a large proportion of diffuse radiation incident on their apertures and concentrate it without the need of tracking the sun. This type of solar collector has been designed to operate with temperatures higher than the operating temperature of FPC. However, CPCs available on the market are in general suitable for temperatures up to 120°C, but some manufacturers have developed some special CPCs that can operate up to 200°C.

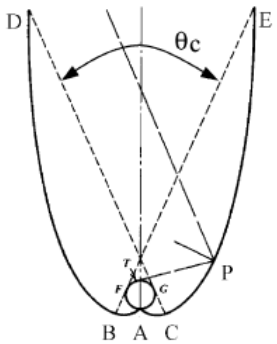

Figure 3.8 – Schematic diagram of a CPC.

Evacuated tube collectors: ETCs are made up of rows of parallel glass tubes connected to a header pipe. Each single tube is evacuated in order to reduce drastically heat losses (no convection). The tubular geometry is necessary to support the pressure difference between the atmospheric pressure and the internal vacuum. Evacuated tube collectors can be classified in two main groups.

- Direct flow evacuated tubes collectors: this collector consists of a group of glass tubes. Inside each tube there is a flat or curved aluminium plate, which is attached to a metal (usually copper) or glass pipe depending on the configuration. The aluminium plate is generally coated with a selective coating such as Tinox. The heat transfer fluid is water and circulates through the pipes, one for inlet fluid and other for outlet fluid. Several types of collectors exist, classified according to the distribution of these pipes.

- **Collectors with concentric fluid inlet and outlet** (glass-metal, see Figure 3.9a): this construction presents the advantage of rotational symmetry. Thus, each single pipe can be easily rotated allowing the absorber fin to have the desired tilt angle even if the collector is mounted horizontally.
- **Collectors with two separated pipes for inlet and outlet** (glass-metal, see Figure 3.9b): this is the traditional type of evacuated tube collector. In some cases the absorber is flat and in other cases it is curved.
- **Sydney type collector** (glass-glass, see Figure 3.9c): this collector consists of two glass tubes bonded together at one end. The inner tube is coated with an integrated cylindrical metal absorber, usually with selective absorbing material.

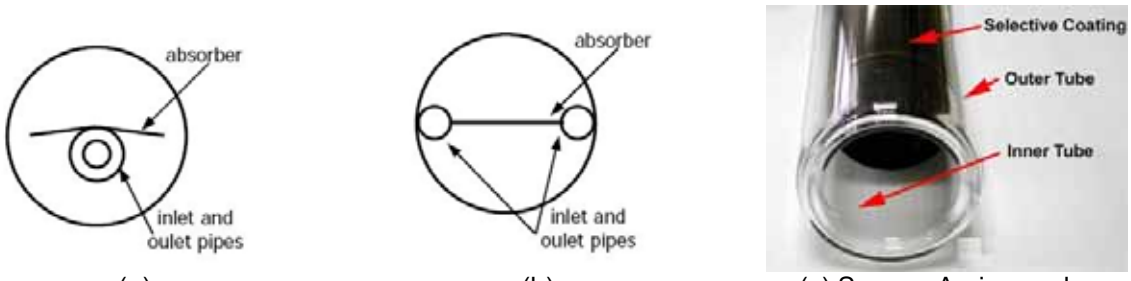

(a) (b) (c) Source: Apricus-solar

Figure 3.9 – Evacuated tube collector types.

Another type of ETC is commercially available and is known as heat pipe evacuated tube collector. This heat pipe is hollow and the space inside is evacuated. Inside the heat pipe the working fluid is purified water and some specific additives.

In the heat pipe, the water is under its saturation pressure and so boils for any additional heat input. The level of temperature is fixed by the heat sink at the condensing part of the heat pipe. As the heat is transferred at the condenser end, the vapor condenses to form a liquid and returns to the bottom of the heat pipe, and the process starts again. Figure 3.10 illustrates this process. This collector must always be mounted with a minimum tilt angle around 25° in order to allow the working fluid of the heat pipe to return to the heat absorber, the boiling end of the heat pipe.

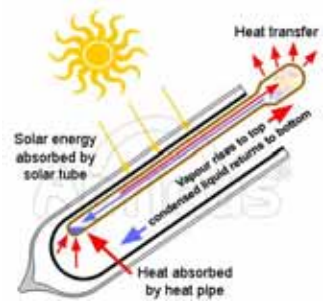

Figure 3.10 – Principle of heat pipe. Source: Apricus-solar.

For high temperature applications, the efficiency of glass-glass tubes can be higher than efficiency of glass-metal tubes. This reliability problem can occur due to the loss of vacuum resulting after a few years of daily contraction and expansion where the seal can fail. It depends on the technical parameters of the collector, and the working and ambient temperatures.

Some evacuated tube collectors include rear-mounted reflectors behind the evacuated tube collectors or inside the glass tube. The external reflectors increase the radiation received by the collector as the radiation that usually passes through the gap between tubes is driven back into the absorber.

ETC has demonstrated that the combination of a selective surface and an effective convection suppressor can result in good performance at high temperatures [KAL03]. The vacuum envelope reduces convection and conduction losses, so the collectors can operate at higher temperatures than FPCs. Like FPCs, they collect both direct and diffuse radiations. However, their efficiency is higher at low incidence angles. This effect tends to give ETCs an advantage over FPCs in daylong performance.

Another type of collector has been developed recently: the integrated compound parabolic collector (ICPC). In this ETC a reflective material is fixed at the bottom of the glass tube

[KAL04]. The collector combines the vacuum insulation and non-imaging stationary concentration into a single unit. Two types of ICPCs are available on the market:

- One is developed by CONSOLAR (see Figure 3.11); the concentrator is fixed outside the glass pipe, and
- The other is commercialized by SCHOTT (see Figure 3.12); a reflector is integrated inside the glass tube.

These collectors could achieve higher temperatures than conventional ETCs since they combine the two technologies of high isolation with a vacuum tube and a higher concentration factor with the reflector integrated. These collectors can operate at temperatures up 250°C.

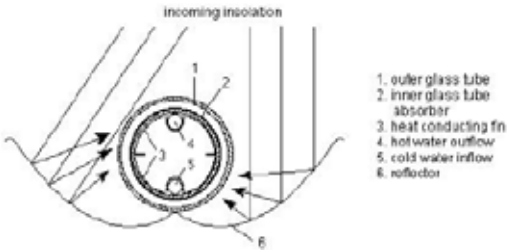

Figure 3.11 – Vacuum tube with external reflector, cross-section. Source: CONSOLAR

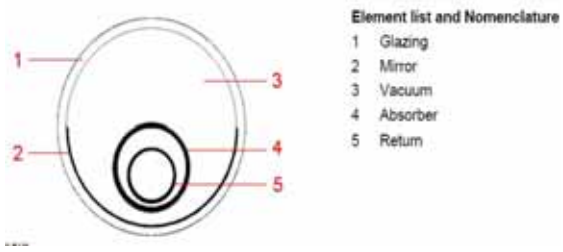

Figure 3.12 – Vacuum tube with internal reflector, cross-section. Source: SCHOTT

When higher operating temperature is desired, highly concentrating collectors can be used [MIL04]. This can be reached if a large amount of solar radiation is concentrated on a relatively small collection area. This can be achieved by interposing an optical device between the source of radiation and the energy-absorbing surface. Concentrating collectors exhibit several advantages compared to FPCs, the mains ones are as follows.

- The working fluids can achieve higher temperatures in a concentrator system compared to a flat-plate system of the same solar energy-collecting surface. This means a higher thermal efficiency that can be achieved because of the small heat loss area relative to the solar absorbing area.
- Reflecting surfaces require less material and are structurally simpler than FPCs. For a concentrating collector the cost per unit area of the solar collecting surface is therefore less than that of a FPC.
- Due to the relatively small area of receiver per unit of collected solar energy, selective surface treatment and vacuum insulation reduce heat losses and improve the collector efficiency.

Their disadvantages are:

- Concentrator systems collect a small portion of diffuse radiation and the collecting efficiency depends on the concentration ratio.
- Some form of tracking system is required to enable the collector following the sun.
- Solar reflecting surfaces may loose their reflectance along the time and may require periodic cleaning and refurbishing.

There are two types of concentrating collectors:

- Parabolic dish solar collectors (see Figure 3.14) with two-axe tracking device to turn in altitude and azimuth; those collectors follow exactly the sun trajectory.
- Parabolic trough collectors (PTC) or Linear Fresnel Reflector (LFR), which are one-axis collectors.

- **Parabolic trough collectors:** PTCs are made of reflective material. A metal black tube, covered with a glass tube to reduce heat losses, is placed along the focal line of the receiver (see Figure 3.13). For these collectors, one-axe tracking is sufficient when it is oriented from south to north and tracking the sun from east to west. PTCs are the most suitable solar technologies to generate heat at temperatures up to 400°C for solar thermal electricity generation or process heat [MIL04].
- **Linear Fresnel reflector:** In this type of collector, large fields of modular reflectors concentrate beam radiation to a stationary receiver at height of several meters. This receiver contains a second-stage reflector that directs all incoming rays to a tubular

absorber. This specific collector has been developed to replace the conventional parabolic trough collector since it is inexpensive due to the planar mirror and its simple tracking system. According to Haberle et al. [HAB03], this type of collector leads to a cost reduction of about 50% for the solar field compared to parabolic trough. This collector can operate with absorber temperatures up to 500°C with a thermal efficiency of 51%.

(PTC)

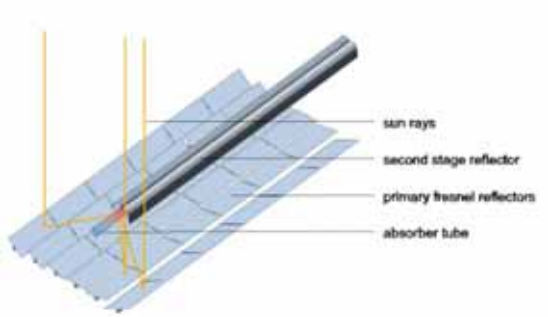

(LFC) source: SOLARMUNDO

Figure 3.13 – Single-axe tracking system.

Parabolic dish reflector, shown in (Figure 3.14), is a point-focus collector that tracks the sun in two axes, concentrating solar energy into a receiver located at the focal point of the dish. The dish structure must track fully the sun to reflect the beam into the thermal receiver. For this purpose, tracking mechanisms are set on two axes. Parabolic-dish systems can achieve temperatures in the range of 650°C.

Figure 3.14 – Parabolic dish reflector [MIL04].

The main advantages of this type of collectors are:

- The collecting efficiency: the highest of all collector systems.
- Concentration ratio in the range from 600 to 2000, and thus they can be used for power conversion systems.
- Modularity: collector and receiver units that can either operate independently or as part of a larger system of dishes.

This type of collectors is mostly used for electrical generation with small engines such as Stirling engines. The disadvantage of this type of collectors is the high capital cost of the collector that needs a sophisticated tracking system. Their integration in the building sector seems unlikely because of cost and foot print issues.

3.2.3 Selection of the solar collector technology

The selection of the solar collectors depends mainly on the operating temperature and its corresponding efficiency. However, the solar collector selected should present easy integration in single house or apartment buildings. Stationary solar collectors present the facility to be integrating into the buildings structure, but not all the solar collector technology can operate efficiently at high temperatures. In the range from 100 to 200°C only, ETC installations are in operation [WEI07]; a CPC vacuum tube collector has been developed by (Micortherm energetietecknik, Germany). This ETC comprises six evacuated tubes produced by Shiroky (Japan) and has been designed to operate with temperatures up to 200°C without the need of tracking system. This type of solar collectors represents the most suitable technology commercially available, which can fulfill all requirements set above. On the other hand, Brunold et al. [BRU94]. have compared three different stationary collectors. Measurement results of collector efficiencies and incident angle modifier have been presented as well as calculated energy gains for three different collectors: a vacuum tube collector (Giordano Ind., France), a CPC vacuum tube collector (Microtherm Energietechnik,

Germany), and a new flat-plate collector using glass capillary as transparent insulation (SET, Germany).

These solar collectors have been tested by the "Solartechnik Prufung Forschung" SPF with respect to the ISO 9806-1.2 Standard "Thermal Performance Tests for Solar Collectors". The thermal efficiency measures were based on absorber and gross area. In our study only thermal efficiency based on gross area will be evaluated since this area might be considered for designing a solar system. The collector data of the solar collector studied is given in Table 3.3.

Table 3.3 – Solar collector data [BRU94].

Solar collector type	Vacuum tube	Vacuum tube (CPC)	Flat plate (TIM)
Manufacturer	J. Giordano Ind.	Microtherm	SET
Gross area (m^2)	1.912	1.191	2.183
Absorber area (m^2)	1.117	1.053	1.740
Weight (kg)	42	17	78
Absorber type	Black-chrome on copper	Metal carbide on copper on glass	Black-chrome on nickel on copper
Absorptance α	0.9	0.93	0.96
Emittance ε	0.05	0.035	0.12
Insulation	Vacuum, 10^{-6} bar	Vacuum, 10^{-6} bar	Glass capillaries

Results of the measured thermal efficiencies are presented in Figure 3.15 with $x=(T_m-T_a)/G$. The FPC shows the highest efficiency for x values up to 0.05 (m^2.K/W), i.e. for high insolation or low temperatures. However, in this range single flat-plate collectors can even perform better, because for low-temperature operations a high transmittance absorptance product (ζα) is of more importance than a low heat loss coefficient. For x values above 0.1 (m^2.K/W), the efficiency of the insulated collector cannot approach efficiencies of the vacuum tube collector. On the other hand, for high values of x when the operating temperature is very high, the vacuum tube (CPC) seems to be the best choice for this application.

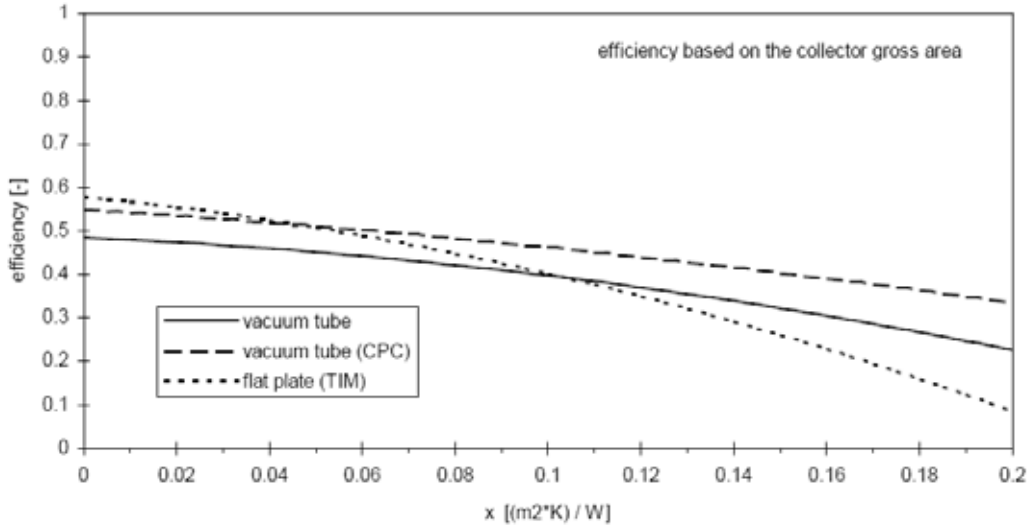

Figure 3.15 – Measured collector efficiency [BRU94].

3.3 Pump

3.3.1 Requirements and technical barriers

A wide variety of pumps is available on the market and selection criteria depends on the application. Nevertheless the MFR and the pressure ratio are for the range of operation the most dominant factors for the selection. Three different types of pumps are of interest.

- Positive displacement pumps: these pumps are more suitable for high pressure with low flow rate.
- Centrifugal pumps: they cover a wide range of applications and are the most commonly used.
- The axial flow pumps are low pressure and high-flow-type pumps.

The pump used for a Rankine cycle should be capable of providing the desired volumetric flow rate with the corresponding pressure ratio and the maximum operating outlet pressure. The pump selected has to operate with high efficiency and for flow rates and pressure ratios that depend on the working fluid selected and the desired power output. In the previous chapter, it has been shown that the volumetric flow rate of the working fluid ranges from 0.1 L/min to 60 L/min (see Figure 3.16). The corresponding pressure ratio varies from 3 to 30. Regarding the low volumetric flow rate with the corresponding pressure ratio, the positive displacement pump represents the most suitable option for SRC or ORC pump. On the other hand, both the ORC and SRC pumps should be capable to withstand low viscosity (below 0.4 mPa.s) and still ensure the desired head, which is only possible with pumps presenting very small clearance between their lobes.

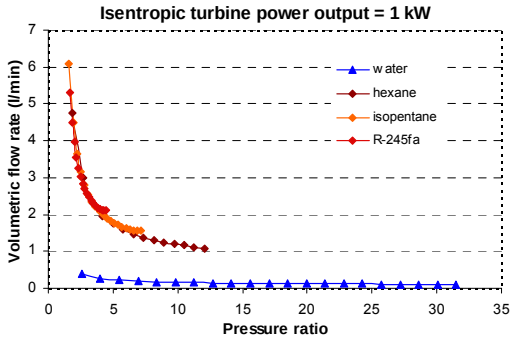

Figure 3.16 – Pump volumetric flow rate. (Turbine power 1 kW)

The pump operates on the condensate leaving the condenser, and thus precautions have to be taken to prevent cavitation problems. Cavitation occurs when the pressure in the liquid drops below the vapor pressure corresponding to its operating temperature, and thus causing the liquid to vaporize. Cavitation could damage the pump. To avoid cavitation problems, the pump should be designed in order that the net suction head available is higher than the design net suction head of the pump for the desired capacity. The net positive suction head (NPSH) is defined as the total head of the pump less the vapor pressure. The available net positive suction head can be calculated as follows:

$$(NPSH)_A = h_{s1} - h_{fs} - p_v \quad (m) \tag{3.1}$$

Where,

h_{sl} (m): static suction head, which is the vertical distance measured from the free surface of the liquid line to the pump center line, plus the absolute pressure at the liquid source.

h_{fs} (m): suction frictional head, which is the pressure required to overcome the resistance in the pipe and fittings.

p_v (Pa): vapor pressure at the corresponding temperature of the liquid

3.3.2 Assessments of possible pump technologies

Positive displacement pump raises the working fluid pressure by decreasing the fluid volume. These pumps can deliver low flow rate with high-pressure output and with a low operating speed. The volumetric flow rate of these pumps is, in general, proportional to their rotating speed. The volumetric pumps are commercially available with different technologies such as external gear, internal gear, piston, screw, vane, and diaphragm… The low viscosity of the

working fluids (< 0.4 mPa.s) represents the main difficulty towards the selection of the Rankine pump. The various plausible positive displacement pump technologies have been assessed as follows.

- **Gear pump**

Different technologies of gear pumps are available on the market and are presented in Figure 3.17. Gear pumps with internal gears; these pumps are used for high viscosity (> 1 mPa.s) applications with a maximum differential pressure of 3.5 MPa. The maximum operating temperature is 260°C. The only identified pump that can handle low viscosity is commercialized by VIKINGPUMP and can handle viscosity down to 0.1 mPa.s with a maximum differential pressure of 1.75 MPa. The maximum operating temperature is 170°C and the volumetric flow rate varies from 0.55 L/min to 4.72 L/min.

(a) (b) (c)

Figure 3.17 – Gear pump technologies. (a) Internal gear pump, (b) external gear pump, (c) micro-pump.

The external gear pumps are designed in most cases for operating fluids with viscosity higher than 1 mPa.s, but with high operating temperatures up to 230°C. This type of pumps will be disregarded in this study because it cannot handle low viscosity fluids.

Micro-annular gear pumps are rotary pumps built with a toothed internal rotor as well as with annular-toothed external rotor, which are slightly eccentric to each other. During rotation of the rotors around their offset axis, the pumping chambers simultaneously increase on the induction side and decrease on the delivery side of the pump. Homogeneous flow rate is generated between the kidney-shaped inlet and outlet. These pumps are very compact and present a low NPSHr (below 1 m of water for some applications) and acceptable cost. They can be used for pressures up 34.5 MPa and temperatures up to 170°C. The maximum differential pressure that can be achieved is about 8 MPa. The maximum volumetric flow rate to be delivered by a micro pump can go up to 12 L/min. The VFR of these pumps is very dependent of the working fluid viscosity. Therefore, the pump pressure and flow capabilities are largely reduced for low viscosity applications (see Figure 3.18). A minimum viscosity is also required to ensure proper lubrication of the mating gears.

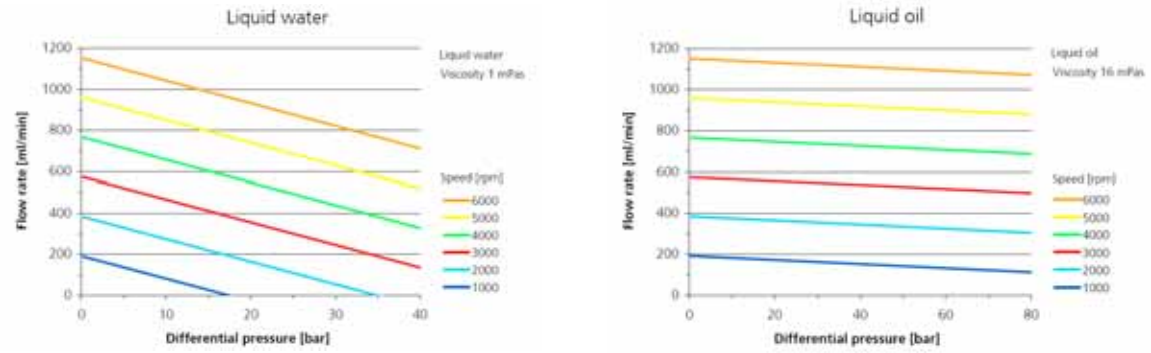

(a) (b)

Figure 3.18 – Micro pump performance for low viscosity (a) and for high viscosity fluids (b) [MICROPUMP].

➢ Vane pump

A rotary vane pump consists of vanes mounted on a rotor that rotates inside a cavity (see Figure 3.19). The sealing is maintained by sliding vanes. All components of the pump are made of 316 stainless steal, except vanes where Carbon-Reinforced Peek is used and carbon graphite for Discs. They are available for volumetric capacity ranging from 0 to 600 L/min, a maximum differential pressure of 1.4 Mpa, and a viscosity down to 0.1 mPa.s. The maximum operating temperature of these pumps lies up to 260°C.

Figure 3.19 – Vane pump layout [VIKINGPUMP].

➢ Diaphragm pump

Diaphragm pumps are available on the market with a wide range of flow rates from ~0 L/min to 140 L/min. The operation principle of the diaphragm pump is presented in Figure 3.20.

Figure 3.20 – Diaphragm pump principal of operation [HYDRACELL].

1. Drive shaft via an electrical motor.
2. Roller bearing, rigid support, immersed in lubricating oil bath.
3. Fixed angle cam, translates rotary motion into linear to the hydraulic cells.
4. Hydraulic cells; displace diaphragms via pressurized oil.
5. Diaphragm, hydraulic balanced, no stress during flexing.
6. Inlet valve assemblies, simple design, allows liquid into pump chamber.
7. Outlet valve assemblies, allow liquid to flow into pressure discharge line.
8. Pressure regulating valve, Controls output pressure and prevents pump overload.

The pumps can be used with pressures up to 17 MPa, temperatures up to 120°C, and for different ranges of volumetric flow rates (see Figure 3.21). Differential pressure of 7 MPa or more can be achieved independently from the fluid viscosity. On the other hand, these pumps are generally heavier and bulkier than gear pumps. They also require high NPSHr (3 m or more). Moreover, this type of pumps does not tolerate cavitation since it could seriously damage the diaphragm (perforation could occur). The maximum suction is limited to 690 kPa, but some special design can ensure higher inlet pressure up to 1.7 MPa.

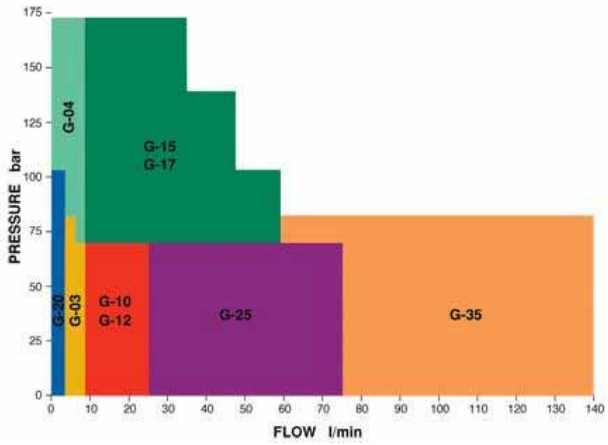

Figure 3.21 – Diaphragm pump flow rate chart [HYDRACELL].

- **Piston pump**

DANFOSS has developed special piston pumps (see Figure 3.22) based on the axial piston principle making the pump very light and compact. The pumps have been designed to ensure water lubrication of all moving parts and thus no oil lubrication is required. The axial piston pumps are designed to operate with water as working fluids, with a volumetric flow rate ranging from 3 to 112 L/min, and with a pressure up to 16 MPa. The only limitation is the maximal operating temperature, limited to 50°C. These pumps are not suitable for Rankine cycle due to the low temperature limitation (<50°C).

Figure 3.22 – Piston pump [DANFOSS]

All piston pumps are designed for long service life. The pump parts are made of stainless steal ensuring high resistance to corrosive and low viscosity fluids. The discharge pressure at continuous operation ranges from 1 to 8 MPa (higher pressure can be designed). The pump size can cover a wide range of volumetric flow rates since the flow is proportional to the rotational speed that can be varied between 700 and 3450 rpm (see Figure 3.23). The design of this piston pump can reduce the pressure pulsation in the discharge line down to 1.5%. Unlike other pump principles, the piston pump can provide almost constant flow regardless of pressure variations. The total efficiency of this type of pumps can goes up to 78% (see Figure 3.24) when operating with discharge pressure lower than 6 MPa and a rotational speed higher than 800 rpm.

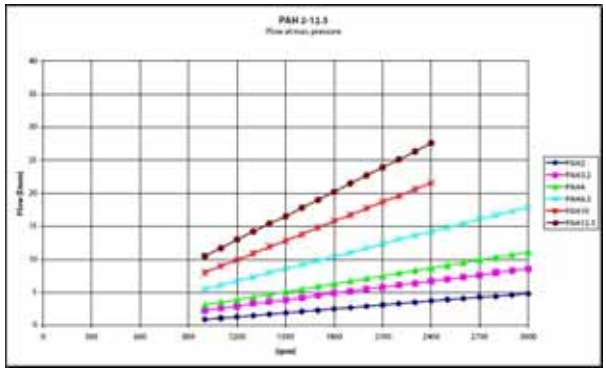

Figure 3.23 – Piston pump flow rate charts [DANFOSS].

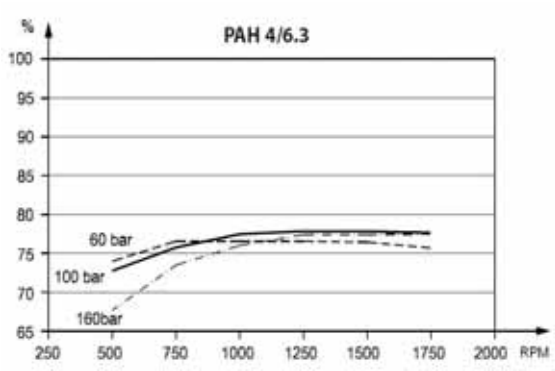

Figure 3.24 – Piston pump efficiency at maximum discharge pressure [DANFOSS].

3.3.3 Findings

Today, diaphragm pump appears to be the most promising concept for handling low viscosity fluid under high differential pressure. The main drawback of diaphragm pumps is the need of a high NPSHr, therefore the need of a 10-K sub-cooled liquid at the pump inlet. On the other hand, this type of pumps presents a high volume and mass compared to the other types.

The piston pump seems to be more attractive than diaphragm pumps by avoiding the cavitation problem but they are not available on the market yet with operating temperature higher than 50°C. The micro pump presents the advantage of higher compactness and lower NPSHr. However, these pumps can be used only with viscous fluids when the differential pressure required is high.

3.4 Heat exchangers

3.4.1 Requirements and technical barriers

The SBORC-µCHP system includes three different heat exchangers: boiler, condenser, and possibly a recovery heat exchanger (named recuperator). Selection of heat exchangers takes into consideration the specific operating conditions of each heat exchanger.

For all heat exchangers, compactness and high heat exchange coefficients are two essential criteria; they offer easy building integration and high overall energy efficiency. The boiler should be capable to withstand high operating pressure, up to 4.5 MPa depending on the working fluids, with a maximum operating temperature of 225°C.

The condenser has to be able to withstand high volumetric flow rates of working fluids that can be operating at low pressure since the condensing temperature is fixed at 80°C. The recuperator is designed to transfer efficiently the heat from a working fluid in gas phase to a working fluid in liquid phase, having similar mass flow rate but different heat capacities and heat transfer coefficients.

3.4.2 Assessments of possible heat exchanger technologies

Compact heat exchangers (CHEXs) offer high heat transfer coefficients and large surface areas with a small footprint making them the most suitable to fulfill all the defined criteria. The different plausible technologies are described here below.

- **Plate heat exchangers:** they are commercially available with different construction materials. Four types of plate heat exchangers exist: plate and frame, partially welded, brazed and welded plate heat exchangers.

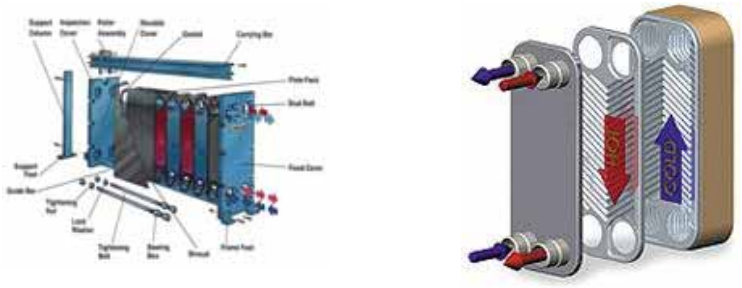

Figure 3.25 – Plate heat exchanger [BED00].

The frame and plate heat exchanger are constructed from a number of pressed, corrugated metal plates compressed together into a frame. These plates are provided with gaskets, partly to seal the spaces between adjacent plates and partly to distribute the media between the flow channels. The most common plate material is stainless steel. The plates can be constructed from stainless steel (AISI304, 316), titanium, incoloy, and hastelloy. When there is a risk of corrosion, some companies offer heat exchangers with nonmetallic materials. The gaskets are commonly made from Nitril rubber, hypalon, viton, neoprene, and EPDM. The operating temperature of the metals plates range from -35°C to 200°C. Design pressures up to 2.5 MPa can be tolerated. Heat transfer areas range from 0.02 m^2 to 4.45 m^2 (per plate). Flow rates of up to 3,500 m^3/hour can be accommodated in standard units, rising to 5,000 m^3/hour with a double port entry. The minimum temperature difference between the hot and cold streams could be as low as 1 K and this minimum temperature difference could be located at the inlet or the outlet of the heat exchanger depending on the configuration adopted for heat exchange (co-current or counter-current). Approach temperatures (defined as the minimum temperature difference) as low as 1 K are feasible with plate and frame heat exchangers.

The partially welded heat exchangers have alternating welded channels and gasket channels. The advantage of welding the plate pairs is that, except for a small gasket around the ports, other materials are eliminated. The operating conditions are the same as the plate and frame heat exchanger; this type of heat exchanger is more used for the evaporation and the condensation of refrigerants because they limit refrigerant leaks.

The brazed plate heat exchanger consists of a pack of pressed-plate brazed together, thus completely eliminating the use of gaskets. The frame can also be eliminated. These heat exchangers have heat transfer capacities up to 600 kW. Plate materials are usually made of Stainless steal. Copper brazed units are available for temperatures up to 225°C and a maximum operating pressure of 3 MPa, but copper braze may produce an incompatibility with some working media. Nickel brazed units are available for temperatures up to 400°C and maximum operating pressures of 1.6 MPa. The brazed-plate type is also sold on the refrigeration/heat pump market for evaporators and condensers (water-cooled), but it is also suitable for process water heating, heat recovery, and district heating systems. Brazed-plate heat exchangers can also be used as desuperheaters, sub-coolers, economizers, and oil coolers. The introduction of nickel-brazed units has allowed brazed units to be used in the process industries, for duties such as de-mineralized water-cooling and solvent condensation.

The welded plate heat exchanger consists of a pack of pressed-plate welded together, thus this heat exchanger cannot be dismounted. This heat exchanger can be made from a wide range of metal materials, provided that they can be welded and cold-formed. Plate materials include stainless steel, high temperature steel, copper and alloys, nickel and alloys, Hastelloy and titanium. Depending on the material used, the welded-plate heat exchanger can operate at temperatures up to 900°C and in cryogenic applications down to -200°C. The broad application area of the welded-plate heat exchanger is: waste gas heat recovery, cryogenic applications, and heat transfer between corrosive materials.

- **Plate-fin heat exchanger**

Plate-fin heat exchangers consist of two passages, with the cooling fluid in one passage and the warming fluid in the other. The brazed-plate-fin heat exchanger consists of an embossed sheets stacking, called fins, separated by plane sheets called parting sheets, and closed on the sides by side bar (see Figure 3.26). An exchanger block consists of a great number of interdependent layers (see Figure 3.).

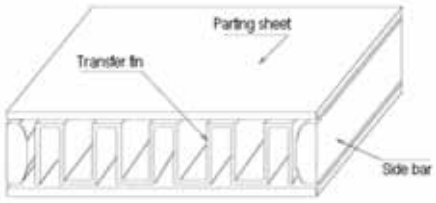

Figure 3.26 – A fluid passage [THO00]..

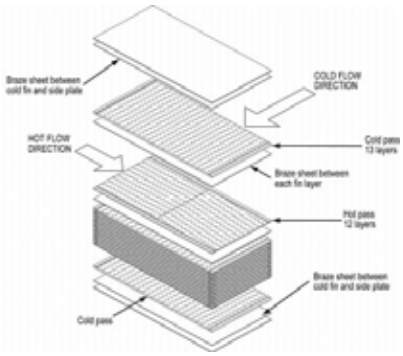

Figure 3.27 – Core structure of the PFHEX [THO00]..

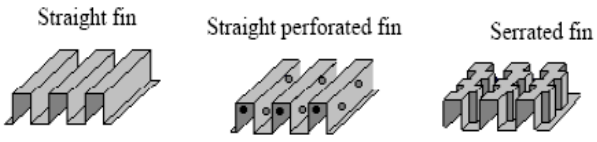

Figure 3.28 – Different geometries of fins [THO00].

The flow direction of each of the fluids relative to one another may be counter-current, co-current or cross-flow. These heat exchangers are available with numerous types of fin corrugations, each with their own characteristics (see Figure 3.28).

These heat exchangers are made of aluminum when maximum operating temperature lies below 200°C with a maximum operating pressure of 1 MPa. This type of heat exchanger is most used in applications such as air separation, hydrocarbon separation industrial and natural gas liquefaction. For higher temperature applications or when aluminum is not acceptable, stainless steel (temperature up to 650°C) or copper materials can be used. Some titanium units have been developed where they can tolerate temperatures approaching 550°C. For very high temperatures (T>1200°C such as gas turbine heat recovery with low pressure applications < 0.4 MPa), a ceramic-plate-fin heat exchanger has also been developed.

- **Micro-channel heat exchangers**

Micro-channel heat exchangers refer to compact heat exchangers where the channel size is around 1 mm or lower. These heat exchangers have been developed for severe environment such as offshore platforms. The most common one is the printed circuit heat exchanger developed by HEATRIC Company. Channels are manufactured by chemically etching into a flat plate. The plates are stacked together and diffusion bonded; these heat exchangers can support pressure up to 50-100 MPa and temperature up to 900°C. Diffusion-bonded heat exchangers are constructed from flat metal plates into which fluid flow channels are either chemically etched or pressed (see Figure 3.29). For each fluid, the required configuration of channels on the plates is governed by the temperature and pressure-drop constraints for the heat exchange duty and the channels can be of unlimited variety and complexity. Fluid contact can be counter-flow, cross-flow, co-flow or a combination of these to suit the process requirements. The typical size of channels is 1.0 by 2.0 mm (see Figure 3.30), and the plate size can be up to 1.2 x 0.6 m.

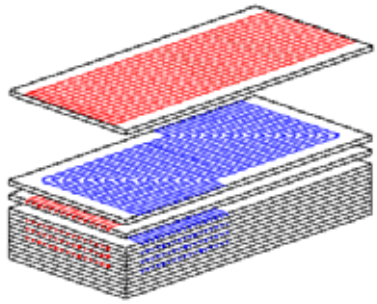

Figure 3.29 – Plate stacking prior to diffusion bonding [TON04].

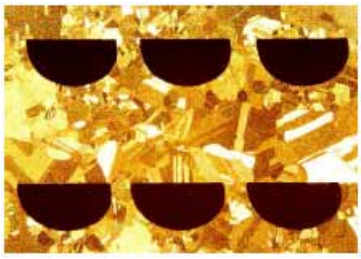

Figure 3.30 – Section through diffusion bonded core [TON04].

A variety of materials, including stainless steal, titanium, nickel, nickel alloys can be used. These heat exchangers present high densities, 650 to 1300 m^2/m^3 and are appropriate for operating pressures from 50 to 100 MPa and temperatures from 150 to 800°C. They are used extensively in offshore oil platforms as compressor after cooler, gas coolers, cryogenic processes… The main advantages of these heat exchangers are high pressure/strength, flexibility in design, and high effectiveness.

- **Plate-and-shell heat exchangers**

Plate-and-shell heat exchangers feature an outer shell enclosing circular plates welded into pairs. The cooling medium flows on the shell side between the pairs of plates. As a plate is more thermally efficient than a tube, this structure achieves a significantly higher level of heat transfer. The construction of a plate-and-shell heat exchanger involves welding together, in pairs, circular plates of a similar surface form and material to those of plate-and-frame heat exchangers. The plates are then located inside a shell, as shown in Figure 3.31.

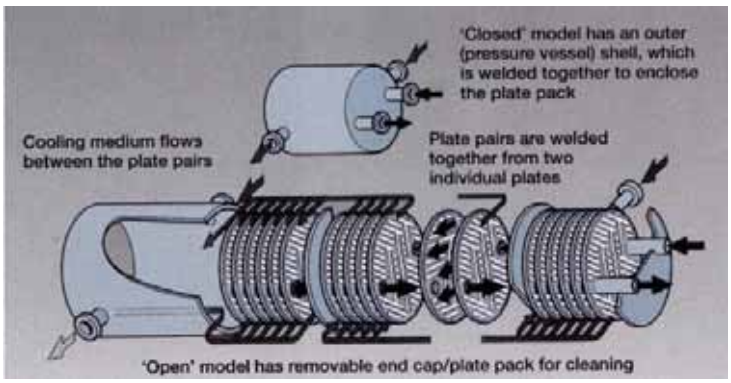

Figure 3.31 – General arrangement of a plate and shell heat exchanger [BED00].

Current plate-and-shell heat exchanger models accommodate up to 600 plates in a shell 2.5 m long with a 1-m diameter. Plate-and-shell heat exchangers are available with a heat transfer surface area of up to 500 m^2. Standard materials that can be used are titanium B265, Avesta 254 SMO, and AISI 316. The shell can be made of St 35.8 or AISI 316 or other materials, such as Hastelloy or nickel, if necessary. The maximum operating temperature of a plate-and-shell heat exchanger is 900°C, and maximum working pressure is 10 MPa.

- **Tube-fin heat exchangers**

Tube-fin heat exchangers are constructed from a row of tubes with different types of fins (see Figure 3.32). In a tube heat exchanger, round and rectangular tubes are most common, although some elliptical tubes are also used. Fins are in general used on the outside; they are attached to the tubes by a tight mechanical fit, tension winding, adhesive bonding, soldering, brazing, welding or extrusion. The fins can be plain, wavy, or interrupted. Tube-fin heat exchanger is most used in a gas-to-liquid exchanger where the heat transfer coefficient on the liquid side is generally one order of magnitude higher than on the gas side. On the other hand, if the pressure is high for one fluid, tubes are more economical. The highest temperature is limited by the type of bonding, chosen materials, and material thickness.

Tube-fin heat exchangers are used when one fluid is at higher pressure and/or has significantly higher heat transfer coefficient than the other fluid stream. These heat exchangers are used extensively as condensers and evaporators in air condensing and refrigeration applications, as condenser in electrical power plants, as oil cooler in propulsive power plants, and as air-cooled exchangers in process and power industries.

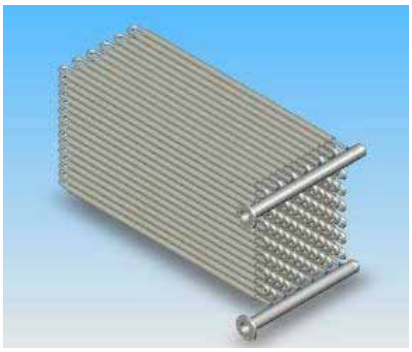

Figure 3.32 – Tube fin heat exchanger [KAK98].

- **Spiral heat exchangers**

Spiral heat exchanger is constructed of two metal strips rolled around a center core forming two concentric spiral channels (see Figure 3.33). Usually, these channels are alternately welded, ensuring that the hot and cold fluids cannot intermix. This heat exchanger can be optimized for the process concerned by using different channel width. Channel width is

normally 5 to 30 mm. Plate width along the exchanger axis may be 2 m, as can the exchanger diameter, giving heat transfer areas up to 600 m^2.

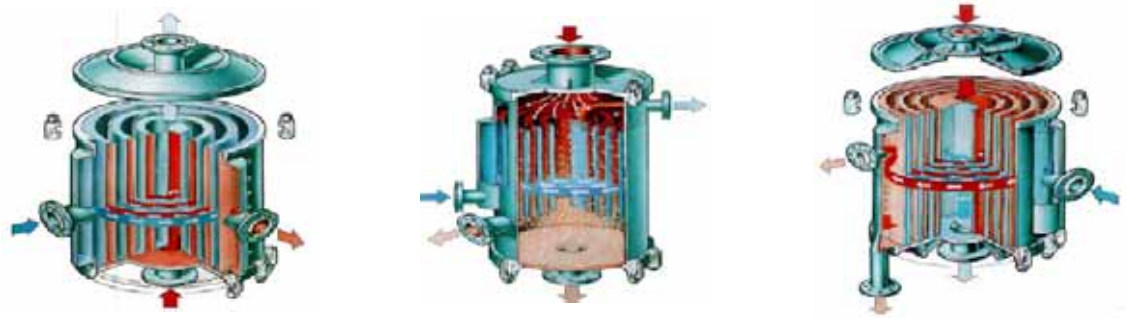

Figure 3.33 – Spiral heat exchanger configurations: full counter-current flow (a), One medium in cross-flow while the other is in spiral flow (b), Combination design (c) [BED00].

Spiral heat exchanger tends to be self-cleaning. The smooth and curved channels result in a lower fouling tendency with fluids containing particles. Each fluid has only one channel and any localized fouling will result in a reduction in the channel cross sectional area causing a velocity increase to scour the fouling layer. This self-cleaning effect yields to reduce operating costs particularly when the unit is vertically mounted.

Typically, the maximum design temperature is 400°C set by the limits of the gasket material. Special designs without gaskets can operate with temperatures up to 850°C. Maximum design pressure is usually 1.5 MPa, with pressures up to 3 MPa with specific designs. These heat exchangers are most used in chemical industries as condensing applications, in particular condensing under vacuum.

3.4.3 Findings

The selection of the most suitable technology of heat exchanger depends on the operating conditions such as operating pressures and temperatures, cost, fouling, and material compatibility.

For liquid-phase change heat exchangers (boiler and condenser), if the operating pressure is limited to less than 2.5 MPa and temperature is lower than 225°C, brazed-plate heat exchanger constitutes one of the most adequate solutions. If higher temperature or pressure is required fully welded plate-heat exchanger could be the choice, depending on the design criteria. However, for liquid-gas heat exchanger (recuperator), the heat transfer coefficient of the gas side is 1/10 to 1/100 of that on the liquid side. Therefore, for a thermally balanced design to obtain an overall heat coefficient of the same magnitude on each fluid side of the heat exchanger, fins are required to increase the gas side surface area. Thus, the common heat exchangers used for liquid-to-gas heat exchanger are the extended surface and tubular, plate-fin heat exchanger. If the operating temperature and pressure could be tolerated with aluminum plate-fin heat exchanger, then this type of heat exchanger could be used since it represents a compact solution and an acceptable cost.

Cost represents a very important factor for selecting heat exchanger type. In general plate-heat exchangers have a lower total cost than the different heat exchangers types when stainless steel, titanium and other highly quality materials are used. Since tubes are more expensive than extended surfaces, and the heat transfer surface area density of tubular core is in generally much lower than that of an extended surface, plate-fin heat exchangers are less expensive than tubular heat exchangers for the same duty.

Fouling and material compatibility present a secondary effect on the selection of the heat exchanger type since the different fluids used in our system presents a low fouling level. Moreover, plate-heat exchanger and plate-fin heat exchanger can be designed from the most available non-corrosive materials.

From the survey conducted above, it is concluded that plate-heat exchanger represents the most suitable technology for boiler and condenser, and plate-fin heat exchanger for recuperator. Special attention should be paid to fouling, when designing the heat exchanger; low mass velocity should be avoided.

3.5 Selection of the different type of expanders

3.5.1 Requirements and technical barriers

As mentioned before in the previous chapter, volumetric expanders have been identified as one of the few technologies capable of providing high expansion ratios and an acceptable performance over a wide range of operations, without the need of a sophisticated design that can affect the turbine cost and so the system cost. The turbine operating range depends on the required thermal and electrical power outputs. The designed turbine should be capable to withstand high pressures (up to 2.5 MPa) and high temperatures up to 200°C. The geometric design parameters of the different turbine technologies depend mainly on the electrical power output, working fluid, inlet temperature, and pressure. The main parameters that affect the cycle efficiency and the electrical power output are the swept inlet volume and the built in volume ratio presented respectively in Figure 3.34 and Figure 3.35.

For the same required power output, a larger turbine is needed if the selected working fluid is water compared to other working fluids (see Figure 3.35). These results show that for a given turbine selected with a constant built-in volume and swept inlet volume, higher power output can be generated when operating with organic fluids compared to water. On the other hand, results show that the power density of the turbine increases when increasing the turbine inlet pressure (see Figure 3.34); this is due to the higher inlet density at the turbine inlet.

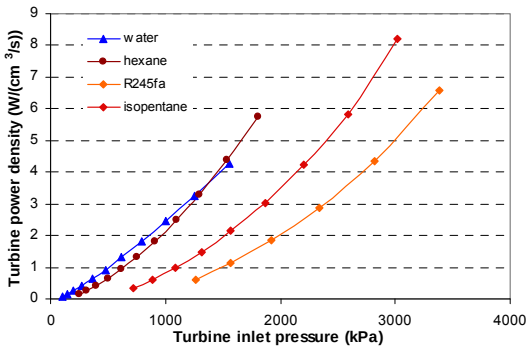

Figure 3.34 – Turbine power density, T_cond = 80°C.

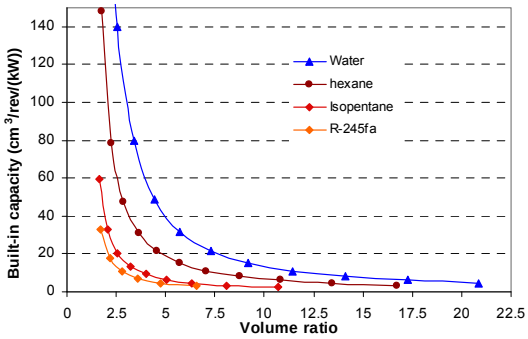

Figure 3.35 – Turbine built-in suction volume, T_cond = 80°C.

3.5.2 Assessment of the plausible turbine technologies

Volumetric turbines operating under the different operating conditions, as defined in Chapter 2, are difficult to be designed or found on the market. Otherwise, many volumetric compressors readily available on the market could be converted to operate as expanders with a few modifications. The different technologies of compressors that can be converted to operate as turbine have been presented in the previous chapter. Scroll compressors, vane compressors and Wankel engines have been identified as technologies that can most likely be used in micro-CHP system.


Scroll expander


Rotary vane expander

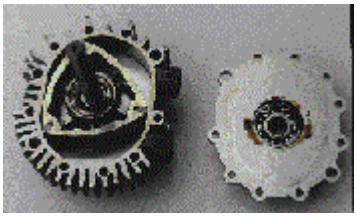
Wankel engine

Figure 3.36 – Possible compressor technologies.

Rotary Vane expander: the expansion process is obtained between the cylinder wall and the vanes slotted into the rotor, the center of which is located eccentrically in the cylinder casing. The vane expander operating at low speed has played an important role in industry for low-temperature applications [BAD91a]. This expander presents the advantages of low cost, good reliability, and compactness; however, its energy performances are poor. Vane expanders have initially been used for air motor with overall efficiency ranging from 25 to 35%. The major source of power losses is internal fluid leakage and the performances depend strongly on the location of the inlet and exhaust ports. A state-of-the-art design of rotary vane expander can results in high overall efficiency, up to 80%, providing careful control of the tolerances of vanes as well as appropriate port timings. Performances of multi-vane expander have been evaluated by different researches. Eckard [ECK75] has described the tests of a multi-vane expander operating with R-11; the maximum overall efficiency measured was 80% at 800 rpm. The overall efficiency remains high, over the speed range from 400 to 2200 rpm. The maximum power output was 4.1 kW with overall efficiency of 70% at 1800 rpm. Badr et al. [BAD85] tested a multi-vane expander with R-113 with inlet temperature and pressure of 110°C and 523 kPa. The pressure ratio obtained was about 4. The maximum power measured was 1.8 kW with a corresponding overall efficiency of 50%.

This compressor is originally lubricated with oil (or other viscous fluid), and then operating this type of compressor in expansion mode without lubrication can affect strongly its performances. Therefore, a lubrication system has to be designed to ensure an efficient lubrication of the different mechanical parts to limit the losses due to the friction and to prevent the deterioration of its volumetric efficiency due to high internal leakage rate. For the different tests reported below, the lubrication system consists of mixing from 5% to 10% mass of lubricant with the working fluid, but this high percentage of lubrication could hamper the energy performance of the thermodynamic cycle, thus 5% is the maximum mass ratio that could be tolerated. The lubricant oil is totally miscible with the working fluid, and then the lubricant will circulate with the working fluid in the expander. The injection process of oil occurs by pressure difference between the boiler and the turbine. A small amount of high-pressure lubricant/working fluid mixture is extracted from the bottom of the boiler and injected in the expander core.

Scroll expander: Scroll compressors are available on the market with two different options: lubricated and oil free. The lubricated scroll compressors are more used in refrigeration, heat pumps, and air conditioning systems. These compressors can operate with high pressures (up to 2.5 MPa). However, these compressors present relatively low built-in volume ratio (around 2.3).

Kane at al. [KAN03] have developed a small hybrid solar power system operating with a two-staged ORC. The system includes hermetic scroll expanders operating with R-123 and R-134a, with a lubrication system developed for the specific application. The scroll expanders used for this system are respectively a 5-kW scroll expander operating with R-123 with a corresponding discharge volume of 53 cm^3/rev, and a built-in volume of 2.3. However, the other scroll expander operates with R-134a with a corresponding discharge volume of 72 cm^3/rev and a built-in volume of 2.3. Two lubrication systems have been designed: the first system operates with a circulating pump where the oil is separated from the working fluid at the outlet of the turbine and then the oil is injected back at the inlet of the turbine. The

second system is a simplification of the first system: the pumps are eliminated and an oil separator has been installed at the boiler exit to recover the oil to be injected inside the hollow expander shaft using the pressure difference.

Lubrication can limit the development of volumetric turbine, so oil-free scroll compressor represents another interesting solution: the scroll compressor can be converted to operate in expansion mode without the need of any lubrication system. An oil-free scroll compressor developed by ATLAS-COPCO (see Figure 3.37) is readily available on the market with a built-in volume ratio of 3.2 and with discharge volumes ranging from 21 cm^3/rev to 52 cm^3/rev. This compressor is capable to operate at high temperatures around 200 °C. However, a major drawback of this compressor is its sealing design where some leakage occurs between the suction volume and the surroundings (see Figure 3.38). Such leakage is of little importance for air compression, but could not be tolerated for R-245ca due to environmental impact. Therefore, this turbine will be used only for steam expansion, and for a maximum turbine inlet pressure of 1 MPa.

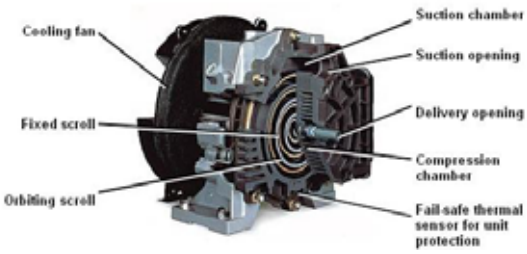

Figure 3.37 – ATLAS COPCO oil free scroll compressor.

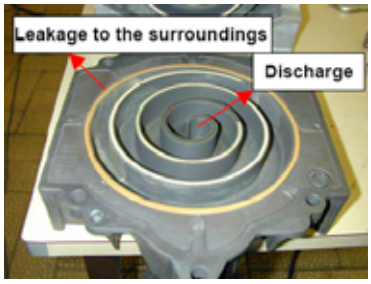

Figure 3.38 – Fixed scroll of the ATLAS COPCO oil free compressor.

Wankel engines have been designed for automotive applications since they represent a simple design of the rotary system, more compact than reciprocating engines, and cheaper to manufacture. However, to convert the Wankel engine to operate as steam expander, basic design changes are desirable [BAD91b]; in order to operate as a vapor engine, the inlet and exhaust ports need to be relocated. The relocation of the inlet and exhaust ports defines the inlet suction volume and the built-in volume ratio. For a good operation of the Wankel steam expander, adequate lubrication of the rubbing surfaces is necessary. If the lubrication is ensured by direct injection of oil and working fluid, studies have demonstrated that oil injection into the expander inlet resulted in an emulsion at the exhaust and cannot be controlled. Solid lubrication can be used as an alternative option. Solid lubricants present some disadvantages, as they are sometimes difficult to feed or replenish. Their useful life is limited, they can present different expansion coefficients from those of metals, and losses of clearance may occur. Some solid lubrication is achieved using graphite, molybdenum disulphide and polytetrafluoroethylene (PTFE), but actually no such systems are in practical uses.

Today, the Quasiturbine efficiency is theoretically identical to the one of a positive displacement engine with a geometric compression ratio of about 10/1, running without intake cut-off. A Quasiturbine steam engine (see Figure 3.39), which is superficially similar to the Wankel engine, is available as a pre-commercialized prototype. However, a large effort is needed for improving its energy efficiency, and for solving lubrication and corrosion problems.

Figure 3.39 –Quasiturbine steam engine.

3.5.3 Findings and turbine market prognosis

Oil-free scroll expander appears to be the best promising concept among the assessed technologies, regarding its reliability and acceptable expansion ratio. Such compressor

requires some modifications in order to operate in expansion mode. Moreover, this expander does not need any lubrication system, which can complicate the system design and affect the thermodynamic performances of the SRC or ORC.

On the other hand, this type of expander cannot be used with organic fluid or refrigerants because leakage is not tolerated when flammable or high GWP fluid is used. Therefore, the selection of the most suitable technology depends on the required power output and the selected working fluid.

However, scroll expanders are far from being the ideal solution for a SRC or ORC turbine, regarding their limited expansion ratios, limited operating pressures and temperatures, and their relatively poor efficiencies (40% to 60%). Moreover, these turbines cover a small range of possible operating conditions.

Increasing demands for efficient micro turbines could spur the micro-CHP suppliers or other expander and compressor manufacturers to develop in the near future, more performing products capable of meeting a larger range of operating conditions. Efficiencies of about 80% or more could be achieved. Recently, FREEPOWER has developed a micro turbine based on two-stage inflow turbine with high rotating speed to produce electrical power output of 6 kW, which can presents a major impact towards the development of highly efficient micro-CHP systems.

4. Rankine system experimental test bench

A specific test bench has been developed at the Center for Energy and Processes. The test bench is designed to characterize several turbine technologies in order to identify the most suitable technology for micro-CHP systems based on SRC or ORC operating on solar energy and wood-pellet boiler. In order to simplify the design of the test bench, the solar collectors and the wood-pellet boiler have been replaced by an electrical heater to simulate the heat source. The main objective of this characterization test bench is to test several types of expanders and evaluate their energy performances. The volumetric and isentropic efficiencies of the tested turbines are measured and the optimum operating conditions are identified. In the field of the work conducted in this thesis, only an oil-free scroll expander operating with steam has been tested.

The steam test bench comprises an electrical heater, a boiler, the expander itself, a condenser and two variable speed pumps (see Figure 3.40 andFigure 3.41). Moreover, the expander shaft is directly coupled to an Eddy current brake (see Figure 3.42).

The Eddy current brake imposes the rotation speed of the expander, which can be fixed by an external controller. The electrical heater used in the test bench simulates the heat source. A gear pump circulates a heat transfer fluid (SYLTHERM 800) through these electrical heaters where it will be heated to a defined temperature selected by the operator. A power control unit controls the power supplied to the electrical heaters and so the outlet temperature of the HTF. A frequency converter controls the speed of the gear pump and so the HTF volumetric flow rate (VFR). At the outlet of heaters, the HTF flows through the boiler where it will exchange its energy with the working fluid (water) of the Rankine system. At the boiler outlet, the cooled HTF is pumped by the HTF pump.

A high-pressure diaphragm pump (pump 2) pressurizes and circulates the water inside the boiler. A frequency converter controls the speed of the diaphragm pump and so the water volumetric flow rate (VFR). The water is preheated, evaporated, and then superheated in the boiler. At the boiler outlet, the superheated steam expands through the turbine and produces mechanical work. The water leaving the turbine is condensed in a water-cooled condenser before reaching the diaphragm pump suction.

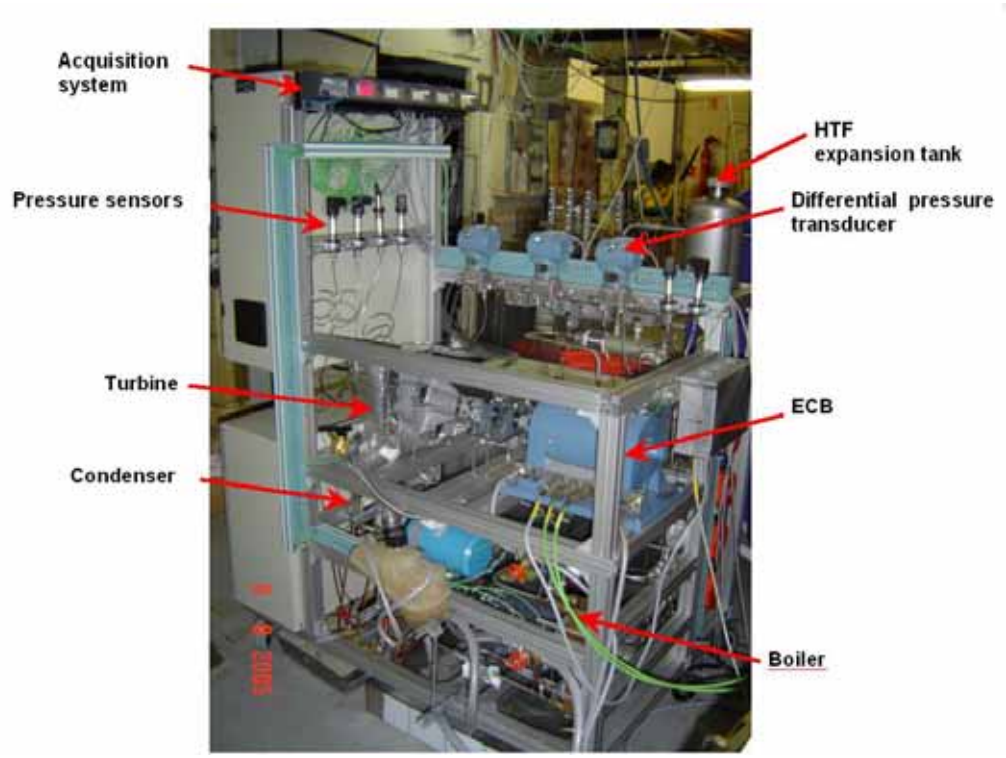

Figure 3.40 – Turbine characterization test bench.

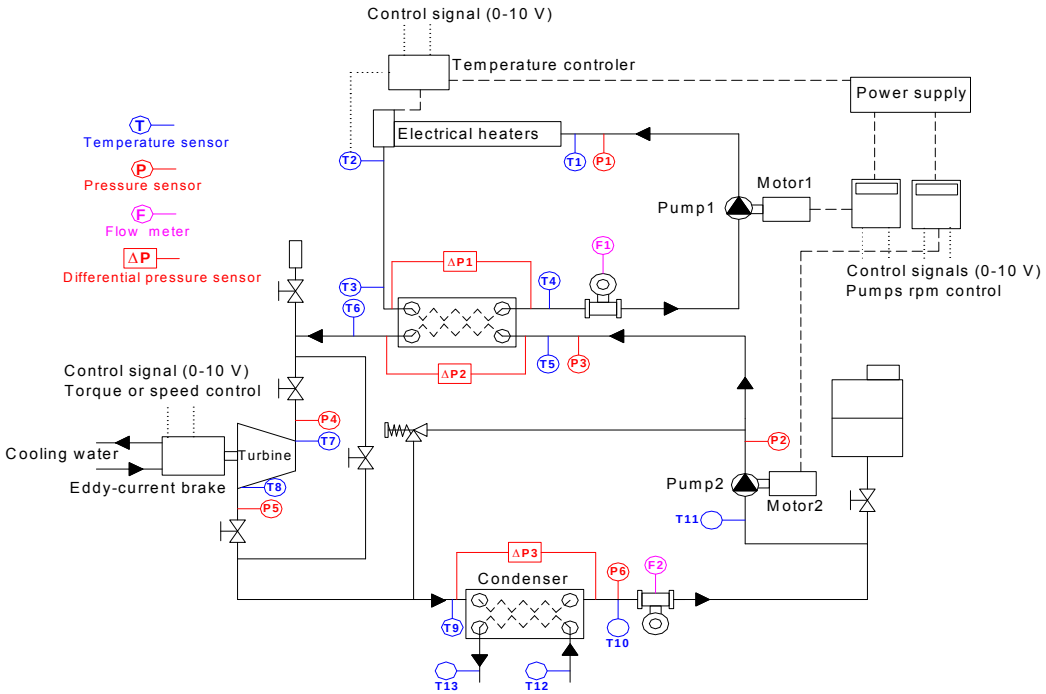

Figure 3.41 – Layout of the test bench.

Note: On this test bench, the electrical generator has been replaced by an Eddy-current brake (ECB) in order to ensure a precise control of the turbine torque and/or speed. This ECB transforms the turbine mechanical work into heat dissipated by a water-cooling circuit.

Temperature and pressure are measured at the inlet and outlet of the scroll expander. The mechanical power output is calculated by measuring simultaneously the rotational speed and the torque developed at the expander shaft by the Eddy current brake. The VFR of the water is measured also by an electromagnetic flow meter. In the experiments, the scroll expander is operating at room temperature under various head pressures and rotation speed conditions.

Figure 3.42 – Turbine and eddy current brake coupling.

4.1 Design and dimensioning of the mock up

The expander selected is originally an oil-free open drive scroll compressor (see Figure 3.43) that has been converted to operate in expander mode. The rated power and the nominal flow rate of the compressor are respectively 1.5 kW and 160 L/min at 1920 rpm, 2.2 kW and 240 L/min at 2720 rpm. Its operating efficiency in compression mode has been reported by [YAN99] and in air expansion mode by Yanagisawa et al. [YAN01]. The main dimensions of the expander are: wrap height: 23.5 mm, wrap thickness: 4.5 mm, wrap pitch involutes: 20.5 mm, involute angles at starting and ending point of wrap: 0.31 and 7.25 π rad. The expander ideal intake and exhaust stroke volumes are 31.5 and 100.1 cm^3/rev, respectively. The built-in volume ratio of the turbine is 3.18 and the built-in expansion ratio is 5.05 for air as a working fluid. The only modification implemented on the original scroll compressor was removing the cooling fan. The high-pressure steam is supplied to the discharge port of the compressor, which leads to the reverse rotation of the machine, namely the turbine operation.

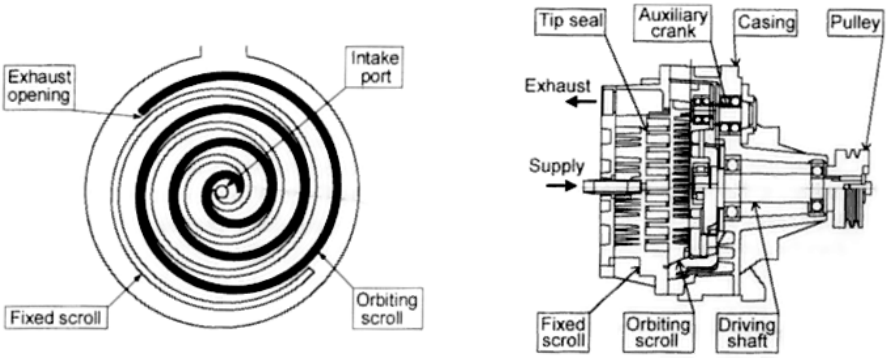

Figure 3.43 – Structure of the experimental scroll expander.

Yanagisawa et al. [YAN99] show that the volumetric and total efficiencies of the compressor are 87% and 56% respectively under the conditions of discharge pressure 700 kPa (gauge) and rotation speed 2720 rpm. On the other hand, Yanagisawa et al. [YAN01] show the performance of the same compressor but in air expansion mode to be respectively 76% and 60% for volumetric and total efficiencies, which occurs under the conditions of having a pressure supply of 650 kPa and a rotation speed of 2500 rpm. The dominant factor lowering the efficiency was the mechanical losses accompanying the orbiting motion, but the leakage loss through the radial clearance between wraps becomes more significant as the rotation speed decreases.

The theoretical pressure change in the expansion chamber is analyzed taking into account the change of the chamber volume. For air, the equation of state of an ideal gas is adopted

to calculate the theoretical pressure ratio with a constant adiabatic expansion exponent γ. However, the theoretical expansion ratios of steam in the superheat and the two-phase regions are calculated with the equation of state available in REFPROP 7.0 [LEM02]. The expansion process is modeled as an isentropic expansion with a constant volume ratio in a closed control volume. The theoretical expansion ratio is calculated by Eq. (3.2).

$$PR = \frac{P_{in}}{P_{out}} = \frac{P_{in}}{f\left(\rho_{out}, s_{out}\right)} = \frac{P_{in}}{f\left(\rho_{in}/VR, s_{in}\right)} \tag{3.2}$$

The theoretical mass flow rate depends mainly on the density at the scroll expander inlet. The latter depends on the inlet pressure and the steam temperature. The theoretical mass flow rate is calculated using Eq. (3.3).

$$\dot{m}_{s,th} = \rho_{s,in} N V_{s,th} = \rho_{s,in}\left(T_{s,in}, P_{s,in}\right) N V_{s,th} \tag{3.3}$$

Where N is the rotation speed, $V_{s,th}$ is the chamber volume when the expansion chamber is closed, and $\rho_{s,in}$ is the inlet density of the vapor. The isentropic power output can be calculated from an equation based on the first law of thermodynamics for an open control volume with steady state operation and without heat transfer to the surroundings. The isentropic power output of the scroll expander is calculated by Eq. (3.4).

$$W_{is} = \dot{m}_{s,th}\left(h_{turb,in} - h_{turb,out,is}\right) = \dot{m}_{s,th}\left[h\left(P_{in}, T_{in}\right) - h\left[\left(\rho_{in}/VR\right), s_{\text{in}}\right]\right] \tag{3.4}$$

The theoretical study shows that the theoritical pressure ratio of the scroll expander operating with vapor (~3.9) is lower than the ideal pressure ratio with air expansion (~5). Figure 3.44a shows the corresponding inlet and outlet temperatures of the steam for the different boiler pressures. By fixing the condenser pressure at 100 kPa to limit the steam leakage from the scroll expander to the surroundings at the exit port, the corresponding boiling temperature will be 144°C with a boiling pressure of 400 kPa. Obviously, the highest boiler pressure gives the highest mechanical power. In fact, the vapor density increases with the pressure and thus the MFR expanding via the turbine increases while increasing the boiler pressure. But since the condensing pressure is fixed to 100 kPa, the maximum power output, which could be delivered by the vapor scroll expander, is around 780 W for an inlet pressure of 400 kPa and a rotation speed of 3000 rpm at the ideal pressure ratio of 3.9.

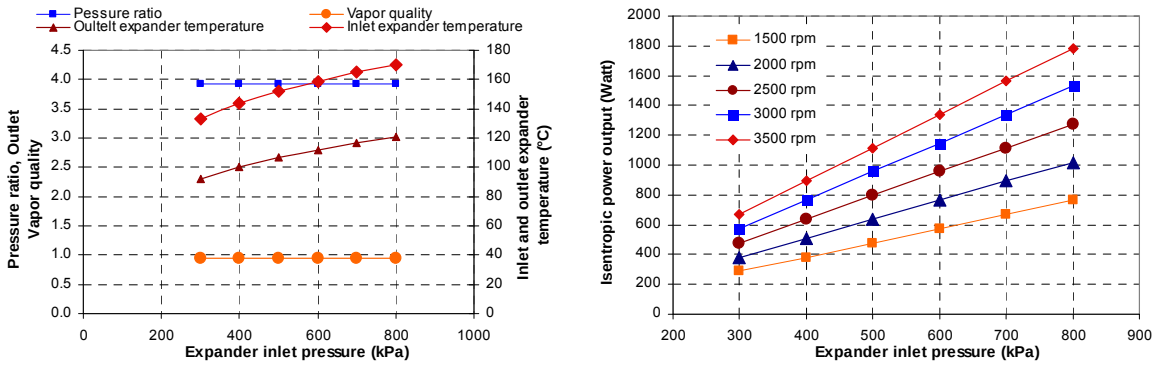

(a) (b)

Figure 3.44 – (a) Evolution of the pressure ratio, outlets vapor quality, and turbine outlet temperature.(b) Theoretical power output corresponding to different inlet pressures and operating rotation speeds.

The sizing of the test bench is based on the mechanical power output that can be delivered by the scroll expander. Therefore, the turbine operating pressure should range from 300 kPa to 600 kPa. To ensure the reliable operation of the tests under the different operation conditions, the test bench has been designed at the maximum operating pressure allowable, fixed to 600 kPa to limit the inlet temperature of the turbine below 180°C. The different

operating conditions under the different operating pressures are presented in Figure 3.45. The ideal Rankine cycle efficiency at the maximum operating pressure (600 kPa) is around 10.4%, the corresponding mass flow rate is around 4.8 g/s.

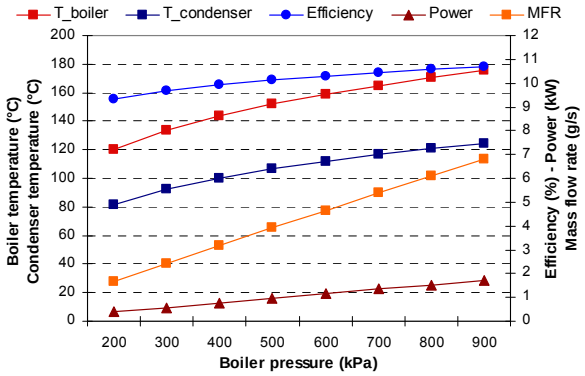

Figure 3.45 – Test bench operating parameters.

The different operating conditions presented here after correspond to the ideal Rankine cycle design. However, the real Rankine cycle operating conditions are evaluated by fixing the turbine and the pump efficiency to 60% and 65% respectively. The different real operating conditions are listed in Table 3.4. The corresponding efficiency of the Rankine cycle is around 6.2% with a corresponding working fluid MFR around 5.82 g/s. The boiler heat duty is around 13.9 kW. The maximum temperature at the turbine inlet is 183°C. The vapour quality at the turbine exit is 0.99. All test bench components will be dimensioned based on these conditions.

Table 3.4 – Design parameters of the Rankine cycle.

	Ideal cycle	Real Cycle
Turbine inlet pressure (kPa)	600	600
Turbine power output (Watt)	1150	860
Pump power input (Watt)	2.18	3.35
Cycle efficiency (%)	10.30	6.16
Turbine volumetric efficiency (%)	100	80
Turbine global efficiency (%)	100	60
Pump efficiency (%)	100	65
Working fluid mass flow rate (g/s)	5.82	7.56
Inlet pump volumetric flow rate (L/min)	0.365	0.47
Boiler heat capacity (kW)	11.12	13.9
Condenser heat capacity (kW)	9.97	13.04
Pressure ratio	3.93	3.93
Boiling temperature (°C)	158.8	158.8
Condensation temperature (°C)	111.9	111.9
Vapor quality at the exit of the turbine	0.94	0.99
Turbine inlet temperature (°C)	183.3	183.3
Rotational speed (rpm)	3000	3000

4.2 Design of the heat source system

Electrical heaters used in the test bench simulate the CPC collectors and the wood-pellet boiler used in the real system. Considering 30% of safety factor, then the electrical capacity required is 13.9*1.3 = 18 kW. Electrical heaters should be capable of providing up to 18 kW of heat. Temperatures ranging between 160°C and 200°C are anticipated. VULCANIC electrical heaters (see Figure 3.46) present a wide range of immersion and inline heaters capable of fulfilling the desired requirements.

Figure 3.46 – VULCANIC electrical heaters.

4.3 Rankine pump design

The Rankine pump design specifications are presented in Table 3.5. The desired pump should provide a volumetric flow rate of about 0.47 L/min under a differential pressure of 390 kPa. The maximum operating pressure and temperature at the pump inlet are respectively 153 kPa and 100°C.

Table 3.5 – Pump specification.

Working fluid	Water
Water inlet temperature (°C)	100
Water outlet temperature (°C)	100
Volumetric flow rate (L/min)	0.47
Pump head (kPa)	390

Hydra-cell pumps are capable of handling low-viscosity fluids at high differential pressures. They can operate with operating temperatures up to 120°C. F/G-20-G model shown in Figure 3.47 can deliver a maximum flow of 0.76 L/min with maximum operating speed of 1750 rpm. The maximum inlet pressure permissible is 700 kPa, and the maximum outlet pressure is 7000 kPa for metallic heads and 1700 kPa for non-metallic heads. The major disadvantage of this type of pumps is that they require high net positive suction head (NPSHr) reaching up to 3.5 m of water for the F/G-20-G. 10-K sub-cooling is required at the pump inlet to avoid any pump cavitation. When operating with 0.47 L/min of volumetric flow rate, the F/G-20-G pumps operate at 800 rpm (see Figure 3.47). According to the manufacturer data sheets, its overall efficiency and electric power are respectively 67% and 55 W.

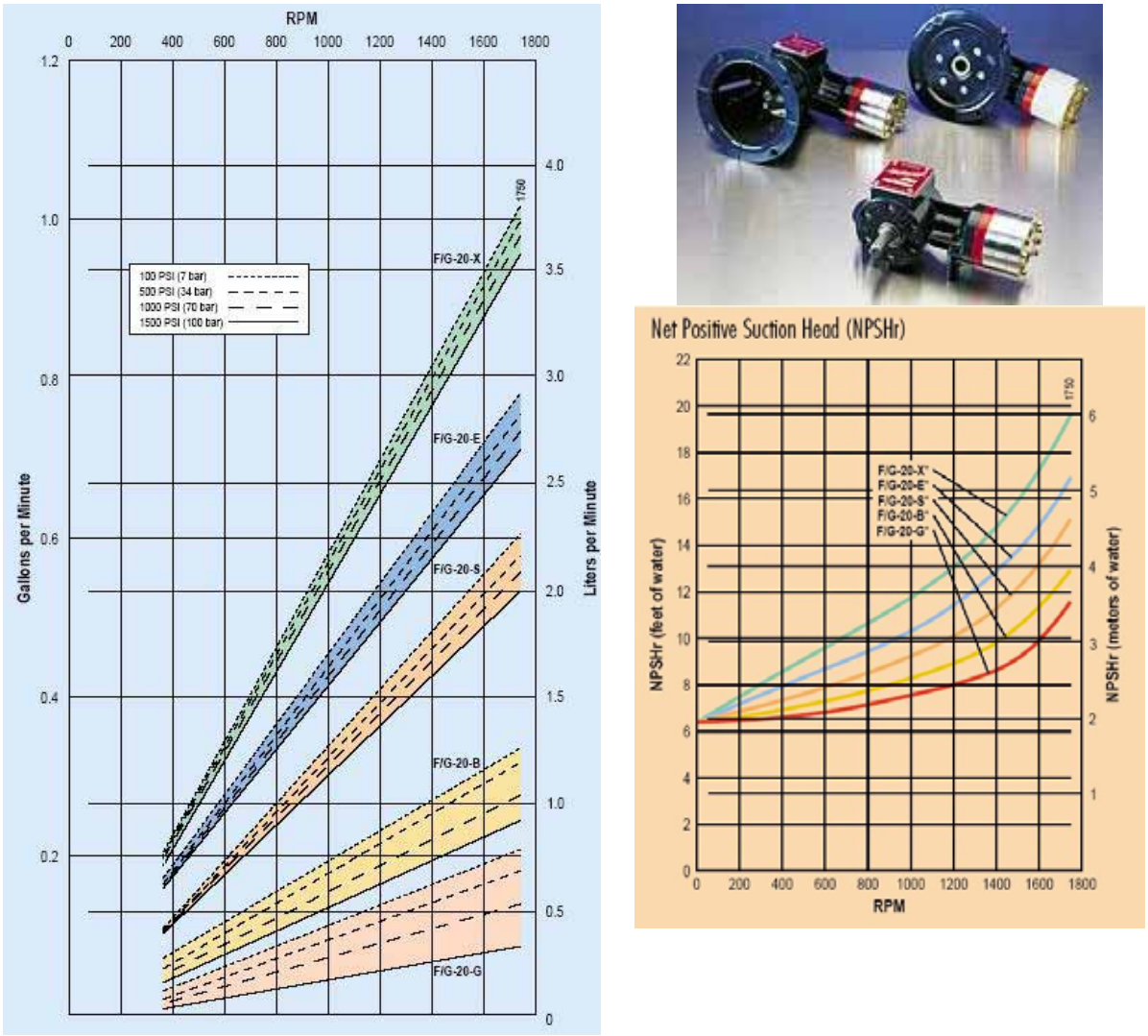

Figure 3.47 – Hydra cell pump series F/G-20.

4.4 Design of heat exchangers

➢ Boiler design

The boiler should be designed to transfer heat from a single-phase liquid fluid, a heat transfer fluid – Syltherm 800, to a two-phase fluid (Rankine fluid – Water). Syltherm is a silicone-based fluid that will be used for recovering the heat generated by the electrical heaters (see Figure 3.) in the test bench, or the CPC collectors and the pellet boiler in the real system.

The brazed-plate heat exchanger (Figure 3.48) technology is chosen. El Chammas [CHA05] has developed a specific software program for a steady-state simulation of a brazed-plate heat exchanger working as boiler. The boiler specification sheet is given in Table 3.6. The water enters the evaporator in liquid state (T = 100°C, P = 600 kPa). The water mass flow rate is 7.56 g/s. The desired output temperature is fixed at 183°C (superheat vapor).

Figure 3.48 – Brazed Plate heat exchangers [SWEP].

Table 3.6 – Boiler specification.	
working fluid	Water
Heat duty (kW)	18
Water inlet temperature (°C)	90
Water outlet temperature (°C)	183
Water inlet pressure (kPa)	600
Water flow rate (L/min) – (g/s)	0.47 – 7.56
HTF inlet temperature (°C)	Design parameter (190°C)
HTF outlet temperature (°C)	Design parameter (170°C)
HTF MFR (g/s)	Design parameter (0.5 kg/s)

Table 3.7 presents the geometrical characteristics of the selected brazed-plate evaporators based on Syltherm mass flow rate and thermo-physical properties corresponding to SWEP B8–brazes plate Evaporators. The basic material of CBHEx (compact brazed heat exchangers) is AISI 316 stainless steel, brazed with pure copper. The only two parameters that can be varied are the number of plates and the stamp pattern (chevron angle).

Table 3.7 – Brazed plate evaporator geometrical characteristics.	
L_c = Core height (mm)	71.5
Length (mm)	310
$L_v - D_p$ = Core effective length (mm)	278
L_w = Core width (mm)	72
Number of plates	30
t =Plate thickness (mm)	0.5
β = Chevron angle	45°
D_p = Inlet port size (mm)	16

The maximum operating temperature of the electrical heaters (200°C) fixes the HTF maximum inlet temperature below 200°C at 190°C. Therefore, the HTF mass flow rate will be calculated ensuring a 5-K minimum temperature difference at the liquid saturated point (pinch point see Figure 3.49).

The temperature profile from the simulation results is presented in Figure 3.49. Syltherm enters the evaporator at 190°C (at 278 mm effective length), exchanges about 18 kW with mainly boiling water, and exits the evaporator at 184.7°C. The water enters the evaporators at 100°C and 600 kPa (sub-cooled liquid). At the exit of the heat, the water is in the superheat vapor state (26°C superheat).

Figure 3.50 presents the water and Syltherm heat transfer coefficients. The water heat exchange coefficient presents large discontinuities related to the transition from the sub-cooled liquid state to the two-phase state, and from the two-phase state to the superheated vapor state. These discontinuities originate the perturbations observed along the surface temperature profile (Figure 3.49). The pressure drop occurs in the heat exchanger for the water and the heat transfer fluid sides are respectively 0.9 kPa and 19 kPa.

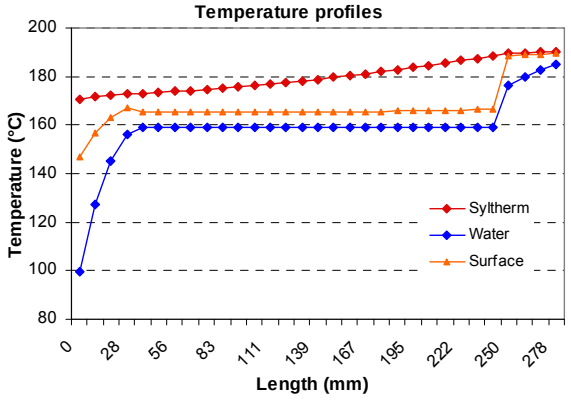

Figure 3.49 – Temperature profiles.

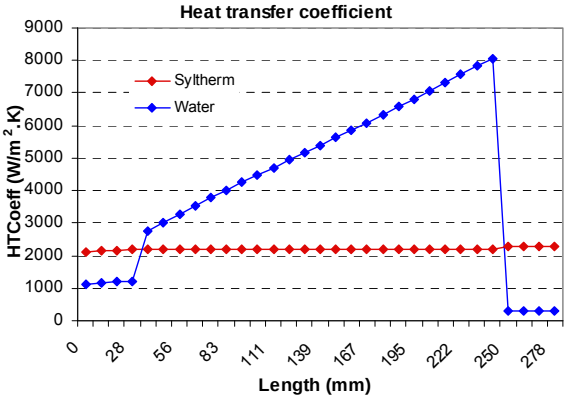

Figure 3.50 – Heat transfer coefficients profiles.

4.5 Condenser design

The condenser specification sheet is summarized in Table 3.8. The cooling water enters the condenser at 100 kPa and 40°C. The desired hot water temperature at the condenser exit is 75°C. The working fluid (steam) enters the heat exchanger in the saturated vapour state (T= 110°C, P = 148 kPa) and leaves the condenser with a sub-cooling of 10 K (T_{exit} = 100°C).

Table 3.8 – Condenser specification sheet.	
Heat duty (kW)	16.9
Working fluid (steam) inlet temperature (°C)	110 – saturated vapor
Working fluid (steam) outlet temperature (°C)	100
Working fluid (steam) Water pressure (kPa)	148
Working fluid (steam) flow rate (L/min) – (g/s)	0.47 – 7.56
Cooling water inlet temperature (°C)	40
Cooling water outlet temperature (°C)	75
Cooling water flow rate (L/min) – (g/s)	6 – 100

Table 3.9 presents the geometrical characteristics of the selected brazed-plate condenser, which is a SWEP of the B5 series.

Table 3.9 – Brazed plate boiler geometrical characteristics.	
L_c = Core height (mm)	26.7
Length (mm)	187
L_v – D_p = Core effective length (mm)	154
L_w = Core width (mm)	72
Number of plates	10
t =Plate thickness (mm)	0.5
β = Chevron angle	45°
D_p = Inlet port size (mm)	16

Figure 3.51 presents the temperature profile of the working fluid (steam) and the cooling fluid (water) as a function of the condenser effective length. The cooling water enters the condenser at 40°C, exchanges about 15.4 kW with water, and exits the condenser at 75°C. The water enters the condenser at 106°C and 148 kPa. At the condenser outlet, the working fluid temperature is 90°C (~23 K sub-cooled). Figure 3.52 presents the cooling water and the

condensing steam heat transfer coefficients. The steam condensing heat exchange coefficient presents large discontinuities related to the transition from the two-phase state to the sub-cooled state. The cooling water and the working fluid (steam) pressure drops are 380 Pa and 0.3 Pa, respectively.

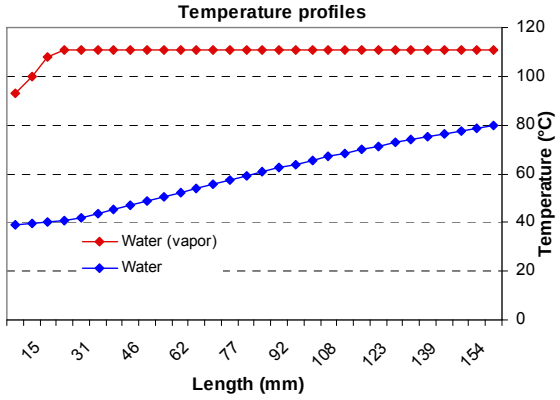

Figure 3.51 – Temperature profiles.

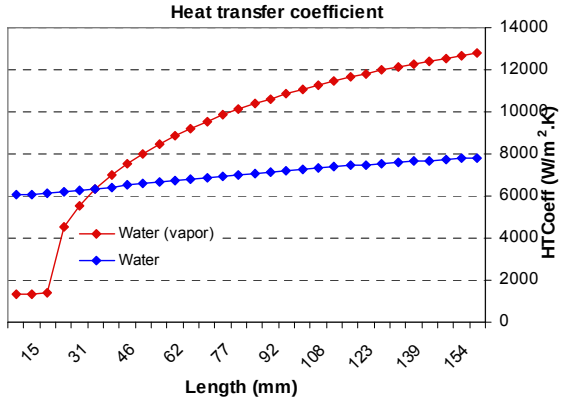

Figure 3.52 – Heat transfer coefficients profiles.

4.6 Design and selection of the heat transfer fluid pump

The Syltherm pump specification sheet is summarized in Table 3.6. The desired pump should provide a flow of about 37.5 L/min (0.5 kg/s) under a differential pressure of 50 kPa. The pressure drop in the evaporator is 19 kPa. The remaining pressure drop takes place in the electrical heaters, the pipe length, and the different connections.

Table 3.6 – Syltherm Pump specification sheet.	
Syltherm inlet temperature (°C)	170
Syltherm outlet temperature (°C)	170
Syltherm volumetric flow rate (L/min)	37.5
Syltherm flow rate (kg/s)	0.5
Pump head (kPa)	50
Pump efficiency (%)	60
Electrical consumption (W)	52

Gear pumps are capable of meeting a large range of flow and viscosity requirements, under high operating temperatures. Figure 3.53 presents the NP series gear pumps. The NP-22/6 can deliver 38.40 L/min at 1500 rpm. The maximum operating temperature is 320°C.

Figure 3.53 – Maag pump series NP.

4.7 Data acquisition

The test bench is equipped with various measuring transducers. Table 3.10 indicates the measuring apparatuses: standard thermocouple K, pressure transmitters, differential pressure transmitters, flow meter, and eddy current brake. All measurements are transmitted to a computer via Field point modules. The interface is written with CVI/Lab windows allowing acquisition of all the data and recording them in the computer. Software named "Thermoblend" (based on Refprop 6) was used to calculate the thermodynamic properties of the working fluids (water).

Table 3.10 – Instrumentation.

	Name	Description	Range
Turbine	T	Turbine torque	0 – 20 N.m
	rpm	Turbine rotation speed	0 – 30,000 rpm
	P	Turbine mechanical output power	12 kW
HTF	T1	HTF temperature at the inlet of the electrical heaters	Thermocouple type K
	T2	HTF temperature at the outlet of the electrical heaters	Thermocouple type K
	T3	HTF temperature at the inlet of the boiler	Thermocouple type K
	T4	HTF temperature at the outlet of the boiler	Thermocouple type K
	P1	HTF pressure downstream of the electrical heaters	0 - 500 kPa
	ΔP1	HTF pressure drop at the boiler	0 - 25 kPa
Rankine cycle	F1	Liquid water volumetric flow rate	0 – 2 Lpm
	T5	Water temperature at the evaporator inlet	Thermocouple type K
	T6	Water temperature at the evaporator outlet	Thermocouple type K
	T7	Water temperature at the turbine inlet	Thermocouple type K
	T8	Water temperature at the turbine outlet	Thermocouple type K
	T9	Water temperature at the condenser inlet	Thermocouple type K
	T10	Water temperature at the condenser outlet	Thermocouple type K
	T11	Water temperature at the pump inlet	Thermocouple type K
	T12	City water temperature at the condenser inlet	Thermocouple type K
	T13	City water temperature at the condenser outlet	Thermocouple type K
	P2	Water pressure at the pump outlet	0 - 3000 kPa
	P3	Water pressure at the boiler inlet	0 - 3000 kPa
	P4	Water pressure at the turbine inlet	0 - 3000 kPa
	P5	Water pressure at the turbine outlet	0 - 500 kPa
	P6	Water pressure at the pump inlet	0 - 500 kPa
	ΔP2	Water pressure drop at the boiler	0 - 25 kPa
	ΔP3	Water pressure drop at the condenser	0 - 25 kPa

The eddy-current brake (ECB) is ideal for applications requiring high speeds, and provides increasing torque as the speed increases, reaching peak torque at the rated speed. The dynamometer has a low inertia as result of small rotor dynamometer. Brake cooling is provided by a water circulation system, which passes inside the stator to dissipate heat generated by the braking power. The WB MAGTROL eddy-current dynamometers (see Figure 3.54) have accuracy ratings of ± 0.3% to 0.5% full scale, depending on size and system configurations.

Mounted on the test bench, the WB 65 Series Dynamometer is particularly adapted for motors rotating at high speeds, up to 30,000 rpm. The ECB mounted on the characterization test bench is the 2 WB 65. The rated power of this ECB is 12 kW. The torque speed curve of this ECB is shown in Figure 3.55.

Figure 3.54 – MAGTROL WB Eddy-current dynamometer.

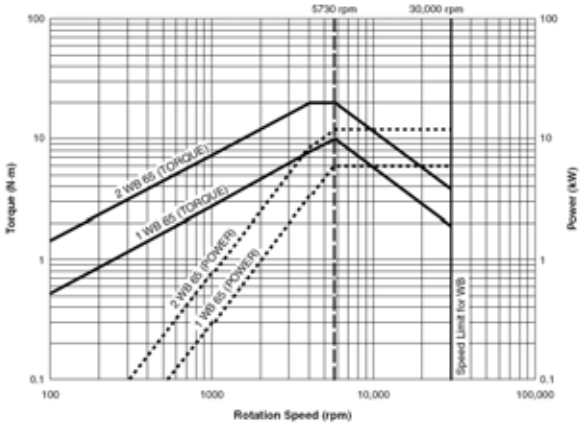

Figure 3.55 – WB torque–speed–power curves.

5. Characterization of the scroll turbine: Dry vapor expansion device

The test program aims at identifying the operating parameters of a scroll expander associated to a micro-CHP system in order to reach the highest energy performances. First the condenser pressure is fixed to the atmospheric pressure to limit the leakage from the expander exhaust to the atmosphere through the tip seals. Another advantage of setting this temperature to 100°C is to ensure the production of co-generated heat at high temperature for heating application. Tests have been performed for boiling pressure from 300 to 500 kPa (water saturation temperature ranging between 133°C and 143°C). The maximum superheat of the steam at the expander inlet is 50 K. The expander rotation speed is limited at 3500 rpm.

Tests are performed to determine the volumetric and isentropic efficiencies of the scroll expander and the mechanical power output. The volumetric efficiency is an important parameter to assess the performance of the expander and is defined as the ratio of the theoretical volume flow rate to the practical volume flow rate as defined by Ziwen [ZIW93]. (The volumetric efficiency defiend below is the inverse of the filling factor)

$$\eta_{vol} = \dot{V}_{s,th} \big/ \dot{V}_{mes} \tag{3.5}$$

Two primary factors affect the volumetric efficiency. The first parameter is the leakage from the inlet port to the suction chamber, which increases the vapor mass flow rate in the expander. The other factor is the throttling effect due to the inlet suction port, which results in a charging pressure lower than the nominal suction pressure then a lower vapor mass flow rate enters the expander suction volume. When the effect of leakage exceeds the throttling effect, the volumetric efficiency as defined in Eq. (3.5) is greater than 100%.

The isentropic efficiency is defined by Eq. (3.6) representing the ratio of the real expansion process to the ideal expansion one, where there is neither resistance losses and pressure losses during the charging and discharging processes nor loss along the expansion process.

$$\eta_{is} = \left(h_{in,turb} - h_{out,turb}\right) \big/ \left(h_{in,turb} - h_{out,turb,is}\right) \tag{3.6}$$

Many parameters affect the isentropic efficiency such as:

- Charging pressure lower than the nominal suction pressure due to the actual pressure losses in pipes and in expander ports.
- The pressure after expansion could be slightly higher than the condensing pressure: so a part of the steam remains in the discharge pocket and flows backward into the expander.
- Leakage occurs between the wraps and the tips along the expansion process.
- Heat losses from the scroll expander chambers to the surroundings across the body of the expander.

All these factors result in a reduction of the isentropic efficiency.

6. Tests and results

Two series of tests have been performed for measuring volumetric and isentropic efficiencies. The first series of tests has been performed with the original gasket of the scroll compressor. Results of volumetric and isentropic efficiencies are presented respectively in Figure 3.56a and Figure 3.56b. The volumetric efficiency increases gradually with the rotation speed because the leakage flow decreases. The isentropic efficiency increases with the pressure ratio and with the rotation speed as shown in Figure 3.56b. For rotation speeds higher than 2500 rpm, results are limited to some test points because the capacity of the test bench reaches its maximum heating capacity and then it was not possible to increase the pressure ratio or the inlet pressure of the turbine. The maximum isentropic efficiency measured is about 48%, which corresponds to several operating conditions.

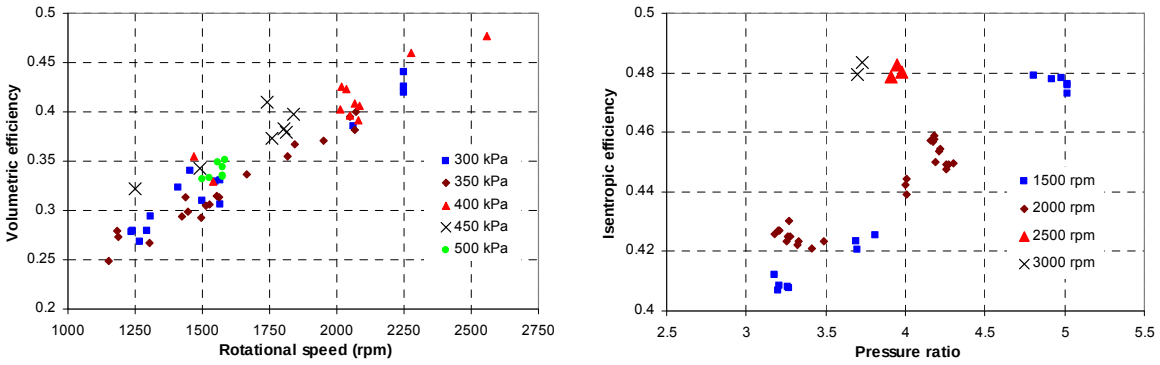

(a) (b)

Figure 3.56 – Evolution of the measured volumetric and isentropic efficiencies with the rotational speed for different operating pressure ratios with the original gasket, (a) Volumetric efficiency, (b) Isentropic efficiency.

Since the maximum measured volumetric efficiency (~46%) lies below the predicted efficiency (76%), which is measured with air expansion, the original gasket has been replaced by Polytetrafluoroethylene (PTFE), gasket. The PTFE has been selected because of its adequacy for high temperature applications (about 190°C) and its lubricating properties. The PTFE gasket was hand made with a larger width than the original gasket to limit the axial clearance and reduce the leakage flow. Results obtained with the new designed gasket are presented in Figure 3.57a and Figure 3.57b.

The volumetric efficiency measured with the new gasket design, presents the same tendency as the previous measurements since it mainly increases while increasing the rotational speed and exhibits a maximum value of 62% at rotational speed of 2750 rpm and pressure ratio of 4. Results show that the volumetric efficiency has been improved by the change to the higher width Teflon gasket, which limits the leakage flow. However, the isentropic efficiency exhibits an optimum value of pressure ratio corresponding to the ideal pressure ratio of the scroll expander and for rotational speed of 2000 rpm.

Improving the volumetric efficiency of the scroll expander has allowed extending the measurement of the isentropic efficiency to cover a wide range of operating conditions as seen in Figure 3.57b. The tendency of the isentropic efficiency shows that for each operating rotational speed, the optimum isentropic efficiency exhibits nearly the ideal expansion ratio, which represents the local optimum. On the other hand, the overall optimum isentropic efficiency now occurs at rotational speed of 2000 rpm and an expansion ratio of 3.8 close to the theoretical expansion ratio (~ 4).

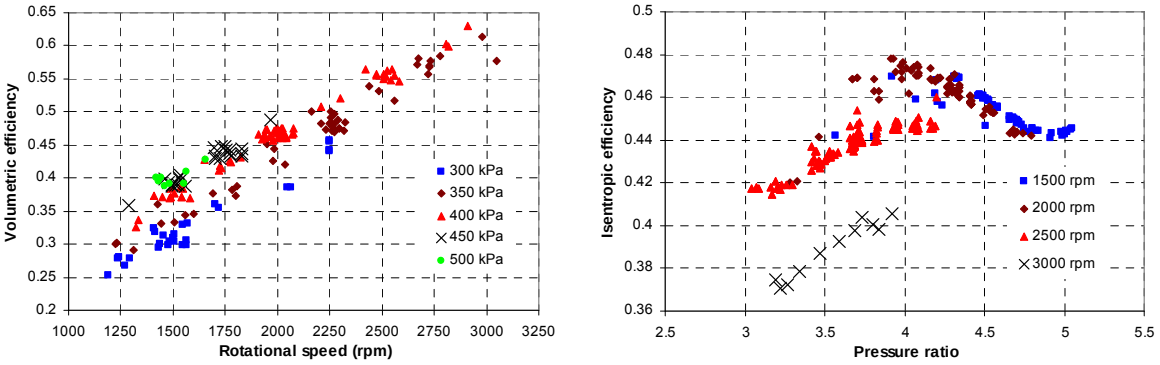

(a) (b)

Figure 3.57 – Evolution of the measured volumetric and isentropic efficiencies with the rotational speed for different operating pressure ratios with the Teflon gasket, (a) Volumetric efficiency, (b) Isentropic efficiency.

Results show that the maximum volumetric efficiency (~63%) occurs at 2850 rpm and a pressure ratio of 4. However, the optimum isentropic efficiency (48%) occurs at 2000 rpm and a pressure ratio of 3.8. The isentropic efficiency is less sensitive to the rotation speed compared to the volumetric efficiency. The optimum global efficiency is reached at a pressure ratio of 3.8 and rotation speed around 2500 rpm with corresponding volumetric and isentropic efficiencies of 55% and 48% respectively.

The mechanical power output measured for the PTFE gasket is presented in Figure 3.58. At optimum operating conditions, the mechanical power delivered by the expander is about 450 W. However, a higher mechanical power is measured for higher expansion ratio and rotation speed, but these operating points do not correspond to the higher overall efficiency. As presented in Figure 3.58, the maximum power delivered by the expander comes close to 500 W for 3000 rpm and to an expansion ratio of 3.6 but, at these operating conditions, the volumetric and isentropic efficiencies measured are respectively 60% and 38%.

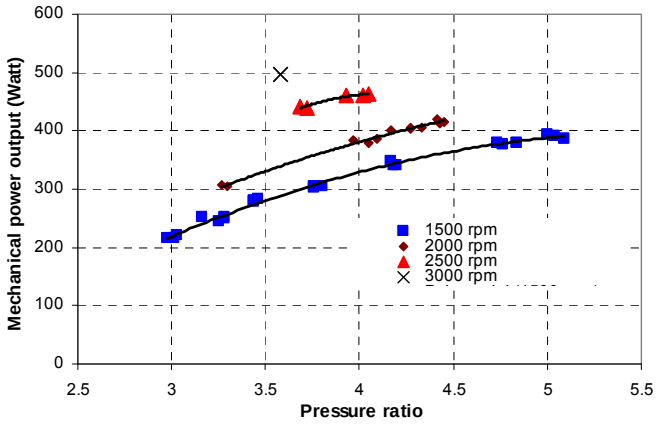

Figure 3.58 – Evolution of the measured mechanical power output with the pressure ratio for several operating rotational speeds with TEFLON gasket.

This is mainly due to the steam high operating temperature that results in metal expansion and could lead to larger axial and radial clearances and so larger throttling losses. In addition, for the same operating temperature, the steam presents a lower viscosity than air, and therefore larger internal leakages and throttling losses are expected to occur under the same differential pressure.

As shown in Figure 3.58, the turbine mechanical power output tends to increase while increasing the turbine expansion ratio and rotation speed. However, on this test bench, the maximum power for rotation speeds higher than 2500 rpm could not be measured, except one point presented for 3000-rpm rotation speed.

When comparing the performance of the vapor scroll expander to the same scroll expander operating with air, the expander performance is higher for air expansion than for steam expansion. When the expander operates at optimum conditions, the maximum achieved volumetric efficiency is about 62% with vapor and 76% with air.

The performance of an oil-free scroll compressor, converted to operate as oil-free vapor scroll expander, has been evaluated and compared to previous results obtained as expander operating with air expansion. Results of this study are summarized below.

An oil-free scroll compressor has been successfully converted to operate as oil-free vapor scroll expander at high inlet temperature range from 130°C to 180°C. The main objective of this study is to integrate this scroll expander in micro-cogeneration systems operating on Rankine cycle system.

The volumetric and isentropic efficiencies of the tested expander were 62% and 48% respectively under the conditions of inlet pressure of 350 kPa, pressure ratio of 3.5 and rotation speed of 2000 rpm.

The main losses are due to the high leakage flow due to high temperature operation and low viscosity of the steam. Also, the mechanical losses present a major impact on the expander efficiency.

The main modification applied to the original scroll compressor was the replacement of the original gasket by a PTFE gasket designed to operate at high temperature.

The effects of the steam viscosity and temperature on the scroll expander performance have to be evaluated. A physical modeling has to be developed in the future to study the viscosity effect on the leakage flow rate and of the temperature on the clearance due to the thermal stress deformation.

7. Conclusions

In this chapter, the most promising technologies to be used, for manufacturing each of the following components of the SWORC-μCHP: wood-pellet boiler, solar collector, boiler, turbine, pump, condenser, and recuperator have been identified.

Biomass boiler: Wood-pellet boiler has been identified as the most promising technology since this type of boiler represents high thermal efficiency (>90%) and their thermal capacity could be modulated to follow the thermal load variation. Besides, this type of boilers is fully automated and could operate continuously without the need of human intervention.

Solar collector: Evacuated tube solar collector with integrated reflector is used for absorbing the solar energy. This type of solar collector technology is selected since it can operate at high temperatures varying from 100°C to 200°C with acceptable thermal efficiency. Moreover, this type of solar collector needs no mechanical system for sun tracking. In addition, it represents a compact design easy to integrate in buildings at acceptable costs.

Boiler and condenser: Brazed-plate heat exchanger is the most suitable technology for boiler and condenser since it presents compact design, high heat transfer coefficient, and acceptable cost. This type of heat exchanger could handle pressures up to 2.5 MPa at 225°C and 4.5 MPa at 150°C. If higher operating conditions are required, fully-welded plate-heat exchanger could be used.

Recuperator: Plate-fin heat exchangers are used as recuperator since they offer compact design. This type of heat exchanger is used especially when two working fluids present significantly different heat transfer coefficients. Therefore the area on the side of the working fluid with low heat transfer coefficient is increased by fins to reach a balance of the total heat transfer coefficient from the two sides of the heat exchanger. If the operating pressure of one of the two fluids is very high, tube-fin heat exchanger could be used where high-pressure working fluid with will be circulated in the tube side.

Pump: A pump adapted to the Rankine cycle could be a diaphragm pump when the process fluid presents low viscosity. 10-K sub-cooling is required to avoid pump cavitation. A gear pump could be used if the working fluid is mixed with a lubricant. In general, the overall efficiency of diaphragm pumps is very low (~ 20%).

Turbine: Today, different types of volumetric expanders could be used as scroll expander: Wankel engine and rotary vane expander. However, these expanders present moderate energy performances since they are not designed to operate in expander mode. On the other hand, designing a completely new turbine presenting a higher efficiency and meeting

exactly the desired operating range would be very costly and require a very long development time. Therefore, in this study it was demonstrated that an oil-free scroll compressor could be converted to operate as oil-free scroll expander with an overall efficiency up to 50%. For other working fluids, several researches have shown that using lubricated scroll compressor in lubricated scroll expander mode leads to an acceptable efficiency. For the near future, the Wankel engine could represent a potential solution where efficiencies of about 70% or more could be achieved.

Except the Rankine turbine, all other components are “off-the-shelf components” that could be custom designed to meet a wide range of capabilities. The Rankine turbine will be converted from available small compressors.

After identifying and testing the different components available on the market and that could be used for the proposed system development, data available from the manufacturers will be used in the next chapter to identify the optimum design and operating parameters depending on thermodynamic and economic optimum operating conditions.

References

[BAD85] O. Badr, S.D. Probert, P.O'Callaghan, Performances of multi-vane Expander, applied energy (1985) 207-234.

[BAD91a] O. Badr, S. Naik, P.W. O'Callaghan, S.D. Probert, "Expansion machine for a low power output steam Rankine cycle engine", Applied energy 39 (1991) 93-116.

[BAD91b] O. Badr, S. Naik, P.W. O'Callaghan, S.D. Probert, Wankel Engines as steam Expanders: Design Considerations, Applied energy 40 (1991) 157-170.

[BED00] A.M. Bredesen, J. Pettersen, R.L. Hoggen, Guide to compact heat exchanger – Module 2.1, September 2000.

[BOS08] J. Bossard, Le chauffage à partir de la filière bois, CVC N° 851 Januray/February 2008.

[BRU94] S. Brunold, R. Frey, U. Frei, A comparison of three different collectors for process heat applications, SPIE 1994.

[CHA05] R. El chammas, D. Clodic, "Combined cycle for hybrid vehicles", SAE internationnal (2005) 01-1171.

[ECK75] S.E. Eckard, Multi-vane expander as prime mover in low-temperature solar or waste-heat applications, Proceedings of the 1975 IECEC, August 1975, No. 729048, pp. 249-254.

[HAB03] A. Häberle, C. Zahler, H. Lerchenmüller, M. Mertins, C. Wittwer, F. Trieb, J. Dersch, "The Solarmundo line focusing fresnel collector. Optical and thermal performance and cost reductions. Power-Gen Europe, 2003.

[KAK98] S. Kakac, H. Liu, Heat exchangers section, rating and thermal design, copyright by CRC Press LLC, 1998.

[KAL03] S.A. Kalogirou, "The potential of solar industrial process heat applications", Applied energy 76 (2003) 337-361.

[KAL04] S.A. Kalogirou, "Solar thermal collectors and applications" Progress in energy and combustion science 30 (2004) 231-295.

[KAN03] M.Kane, D.Larrain, D. Favrat, Y. Allani, Small hybrid solar power system, Int. J. Energy, (2003), vol. 28, p. 1427-1443.

[LEM02] E.W.Lemmon, M.O.McLinden, Reference fluid thermodynamic and transport properties, NIST standard reference Database 23, (2002), Version 7, Beta version 21/13/02.

[MIL04] D. Mills, "Advances in solar thermal electricity technology", Solar energy 76 (2004) 19-31.

[OLI02] A.C. Oliviera, C. Afonso, J. Matos, S. Riffat, M. Nguyen, P. Doherty, A combined heat and power system for buildings driven by solar energy and gas, Applied thermal engineering 22 (2002) 587-593.

[PER85] M. Pereira, Design and performance of a novel non-evacuated 1.2x CPC type concentrator. Proceedings of Intersol Biennial Congress of ISES, Montreal, Canada, vol. 2.; 1985. p. 1199–204.

[RIF04] S.B. Riffat, X. Zhao, A novel hybrid heat-pipe solar collector/CHP system—Part II: theoretical and experimental investigations, Renewable Energy 29 (2004) 1965–1990.

[ROM03] M. Rommel, Dr. A. Gombert, J. Koschikowski, A. Schäfer, Y. Schmitt, Which improvements can be achieved using single and double AR-glass covers in flat plate collectors, ESTEC 2003, Freiburg, Germany.

[STE00] A. Strehler, Technologies of wood combustion, Ecological Engineering 16 (2000) S25–S40.

[THO00] B.Thonon, E.Breuil, Compact Heat Exchangers Technologies for the HTRs Recuperator Application, IAEA-TECDOC—1238, pp:149-160, California, November 2000.

[TON04] P. Tochon, C. Mauget, F. Pra, The use of Compact Heat Exchangers technologies for the HTRs recuperator application per proper design, 2nd International Topical Meeting on high temperature reactor technology, Beijing, China, September, 2004.

[WEI07] W. Weiss, Solar heat for industrial Processes, IEA SC – task 33, IEA SolarPACES – task IV, Newsletter No. 3, January 2007.

[YAM01] T. Yamamoto, T. Furuhata, N. Arai, K. Mori, Design and testing of the Organic Rankine cycle, Energy 26 (2001) 239–251.

[YAN01] T.Yanagisawa, Y. Fukuta, T.Ogi, Hikichi, Performance of an oil-free scroll-type air expander: Proc. of the ImechE Conf. Trans. On compressors and their systems: 167-174, (2001).

[YAN99] T.Yanagisawa Y.Fukuta, T.Ogi, Performance of an oil-free scroll-type air compressor: Proc. of the ImechE Conf. Trans. On compressors and their systems: 279-287, (1999).

[ZIW93] X. Ziwen, The characteristics of systems with rotary vane expander for converting low-grade heat into power, PhD Thesis, Xi'an Jiao Tong University.

Websites (Components suppliers company)

Okofen	*http://www.pelletsheizung.at/*
Hargassner	*http://www.hargassner.at/*
Zaegel-held	*http://www.zaegel-held.com/*
Solargenix	*http://www.solargenix.com/*
Viessmann	*http://www.viessmann-us.com/*
Consolar	*http://www.consolar.de/*
Schott	*http://www.schott.com/*
Vickingpump	*http://www.vikingpump.com/*
Hydracell	*http://www.hydra-cell.com/*
Danfoss	*http://www.danfoss.com/*
Vulcanic	*http://www.vulcanic.com/*
Swep	*http://www.swep.net/*
Magtrol	*http://www.magtrol.com/*
Apricus-solar	*http://www.apricus.com/*
Solarmundo	*http://www.solarmundo.de/*
Freepower	*http://www.freepower.co.uk/index.htm*

CHAPITRE 4 – Optimum design of a solar pellets Organic Rankine Cycle system

Abstract

Residential micro-CHP systems have been introduced recently in different European countries and they are expected to diffuse more and more. In France, the adoption of micro-CHP systems operating on renewable energies, such as wood for the building sector, is one of the options to achieve the environmental targets set by the French government. In this paper, a hybrid solar-wood micro-CHP system based on Organic Rankine Cycle (ORC) is presented. A mathematical model has been developed to calculate the Primary energy saving (PES) and the Levelized electricity cost (LEC), which are used as the objective functions to be optimized. The choice of the working fluids and the boiling temperatures can greatly affect the objective functions, which are measured by the system capital cost and the cycle efficiency. Using this model, an investigation was conducted to analyze the effect of the working fluid choice and the boiling temperature on the PES and LEC. In addition, the effect of the solar field on the PES and the LEC were analyzed. Furthermore, a sensitivity analysis was elaborated in order to show how the objective functions would vary due to changes of some key parameters as the heat cost, electrical capacity of the system, and the solar energy availability.

1. Introduction

In the recent years, the consumption of fossil fuels has been increasing and the burning of fossil fuel is said to be a major contributor to global warming and air pollution. Besides the environmental problems, the oil price fluctuates considerably reaching as high as 120 $ in April 2008. Such a high price hampers the economic growth of any oil importing country. France plans to reduce the reliance on fossil fuels by increasing the share of renewable energies. July 2005 law [LOI05] sets ambitious targets: an increase of 50% in the production of electricity from renewable energy sources by 2010.

On the other hand, the building sector in France consumes more than 42% of the total national energy consumption corresponding to 23% of the national CO_2 emissions [HER07]. Therefore, the development of low-energy buildings is one of the ways to fulfill the national objectives of reduction by 4 of the CO_2 emissions by 2050 [LOI05]. Then, it is pertinent to explore renewable energies for the production of electricity and heating by means of high efficient systems.

Cogeneration, also known as CHP (combined heat and power), is a well-known high efficient approach to generate electricity and heating from single or multiple fuel sources. Therefore, associating a CHP plant operating on renewable energies will represent an attractive solution. Nowadays, companies such as Solo and Sunmachine have developed parabolic mirrors to operate Stirling engine on solar energy. Furthermore, Sunmachine has developed a small Stirling engine (~ 3 kW_{el}) operating on wood pellets, which is the only micro-CHP system operating on renewable energies available on the market.

Several cases [COC06, PAE06 and PRA06] have been investigated in European countries on micro-CHP to verify the interest of these systems technically as well as economically. Recently, Chenier [CHE06] has conducted an economical and environmental study identifying the effect of the integration of micro-CHP system operating on wood in the residential sector. It was demonstrated that micro-CHP system for apartment buildings is more economical than for residential homes and can contribute to the reduction of CO_2 emissions on the building sector.

On the other hand, it is not always economically feasible to use low-grade heat sources for conventional CHP system. Most of the renewable energy sources, for example solar and biomass, are considered low-grade heat sources because the heat energy supplied is significantly lower compared to that of fossil fuel. The use of ORC for micro-CHP applications operating on solar or/and gas energy has been investigated by several researchers [OLI02, RIF04a, RIF04b, ZHA06, YAM01 and YAG06]. Therefore, in this study, the use of hybrid solar-wood energy for sustainable power and heat production using the Organic Rankine Cycle (SWORC-μCHP) is proposed.

The selection of the working fluid is critical to achieve high-thermal efficiencies as well as optimum utilization of the available heat source. Also, organic working fluids must be carefully selected based on safety and technical feasibility. A number of studies [HUN97, MAG08, CHA05, LIU04, MAD07 and WEI07] have demonstrated that the working fluid selection and the boiling temperature have major influence on the performance of the ORC system. The selection of the different working fluids for ORC operating at low power output (from 1 to 10 kW_{el}) has been the subject of a previous research study [AOU08a]. Four working fluids have been identified as potential working fluid (water, hexane, isopentane, and R-245fa) for the proposed system. A review of the system components has also been performed to identify the most suitable technologies for heat exchangers, pumps, and expander.

In addition, there are many barriers to overcome before significant penetration of the micro-CHP in the building sector. The operation of micro-CHP system is subject not only to the variation of load demands, but also to the fuel prices and tariff policies. Therefore, it is necessary to develop a rational method of determining system sizes and operational strategies throughout the year. Different studies have focused on the operation strategies of the micro-CHP system. Ren et al. [REN08] have developed a model to calculate the optimal CHP capacities coupled to an optimum size of storage tank for heat storage. Results show that each heating scenario presents an optimal tank capacity for each electrical CHP capacity. On the other hand, Damshala [DAM00] has previously demonstrated the superiority of economic optimum condition compared to thermodynamic optimum operating condition. Furthermore, Kane et al. [KAN00] have conducted a thermo-economic analysis of a hybrid solar-fossil combined power plant presenting the optimum configuration of the power plant based on pinch technology principles coupled with a mathematical optimization algorithm. A sensitivity analysis based on the relative size of the solar field has been performed to calculate the levelized electricity price, solar share, and the internal rate of return.

Thus, it was shown that the feasibility of the micro-CHP system depends mainly on the capital cost and on the value of energies delivered by the unit: electrical and thermal energies. The operational variables, such as boiling temperature, working fluid, and solar collector surface area at each state of the system, should be determined in order to optimize the thermodynamic efficiency. Economical optimization should be performed including capital costs of the different components.

2. SWORC-μCHP system description

The system is composed of two different cycles as shown in Figure 4.1, namely Solar Pellets Thermal Cycle (SPTC) and Organic Rankine cycle (ORC). SPTC uses heat transfer fluid to complement solar thermal energy and the energy produced from the combustion of wood pellets is transferred to the ORC. There are four main components in the SPTC, pump to circulate the fluid in the cycle, solar collector to recover solar energy, wood-pellet boiler to generate the additional energy needed when the solar energy does not provide all the heat required by the ORC, and a heat exchanger (boiler) to transfer heat to the ORC. In the SPTC, three-way valves are introduced in the system to regulate the volumetric flow rate of the heat transfer fluid entering the solar collectors depending on the admissible pressure

drop and the available solar energy. These valves allow the system operating under several configurations. These configurations are as follows.

4. Solar only generation, all the HTF passes through the solar collectors and valve n°3 bypasses the pellet boiler.
5. Wood only generation, therefore valves 1 and 2 are used to bypass the solar collectors and HTF passes only through the pellet boiler.
6. The Dual solar and wood operation. Therefore valves 1 and 2 are partially opened to deliver a fraction of the HTF mass flow rate (MFR) through the solar collectors; this MFR n°1 will be mixed at the outlet of the solar collectors with MFR n°2 coming directly from the pump to feed the pellet boiler. MFR1 is controlled depending on the available solar energy.

In the ORC, there are four main components and an additional optional component. The four main components are: turbine to convert internal energy to mechanical work, condenser to produce hot water for heating needs or domestic hot water, pump to circulate the working fluid from the condenser to the boiler, and boiler to absorb heat energy from the SBTC. The optional component is an internal heat exchanger (recuperator), which is commonly used when dry fluid is the working fluid to recover the energy available in the working fluid leaving the turbine at high temperature and is still in superheated vapor. This recuperator is introduced in order to improve the ORC efficiency by using waste heat at the turbine outlet to preheat the working fluid at the pump outlet (see Figure 4.1).

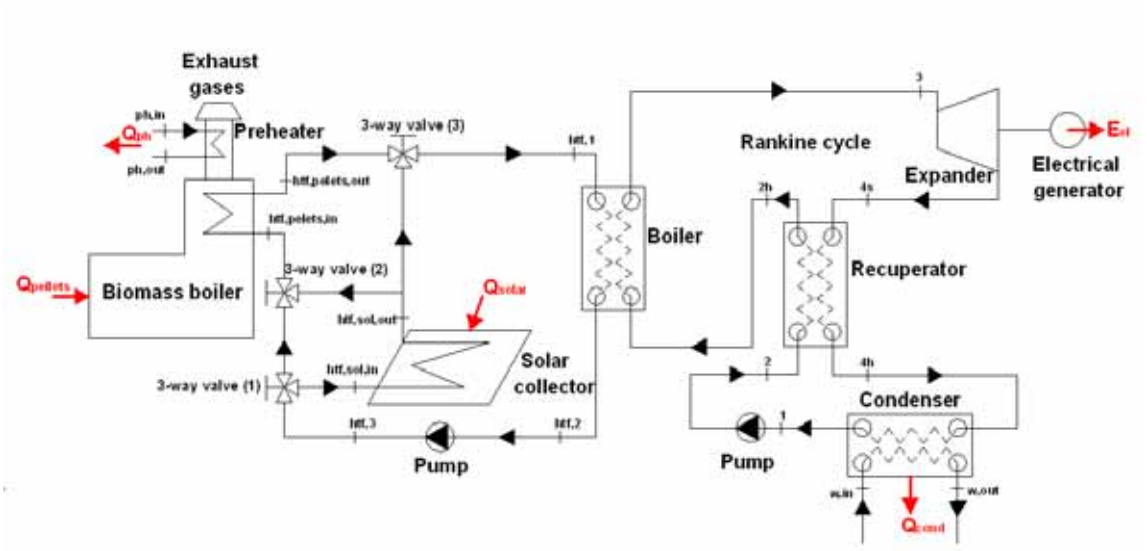

Figure 4.1 – A simple diagram of SBORC-µCHP.

3. Mathematical formulation

3.1 Primary energy savings

The thermodynamic performance of the micro-CHP system depends not only on the electrical energy but also on the total efficiency of the micro-CHP system. Therefore, a parameter, which can couple the electrical efficiency to the total efficiency, is required to better optimize the micro-CHP thermodynamic performance. Therefore, the primary energy savings introduced by the European cogeneration directive [DIR04] given in Eq. (4.1) will be used as the thermodynamic function to be optimized.

$$PES = \frac{E_{p,ref} - E_{p,mc}}{E_{p,ref}} \tag{4.1}$$

To assess the primary energy savings, comparison is made with the separate production of heat and electricity. For heating, a 90% efficiency gas-condensing boiler is considered. The electricity is assumed to be produced by the French power plants, and then the efficiency of the electricity production is given by [ARR06] to be (1/2.58). The PES developed is calculated by Eq. (4.2).

$$PES = \frac{\left(\frac{E_{el}}{\eta_{el,ref}} + \frac{E_{th}}{\eta_{th,ref}}\right) - \left(K_{sol}E_{solar} + K_{pellets}E_{pellets}\right)}{\left(\frac{E_{el}}{\eta_{el,ref}} + \frac{E_{th}}{\eta_{th,ref}}\right)} \quad (4.2)$$

K_{sol} and $K_{pellets}$ are the conversion factors from final energy to primary energy respectively for solar and wood energies. It is noted that the system reaches thermodynamic optimum conditions when the value of the PES attains its maximum values because the PES depends mainly from the eelctrical and thermal efficiency of the thermodynamùic cycle.

3.2 Levelized electricity cost

The levelized electricity cost (LEC) has been used as an economic function of the model to minimize the electricity cost that has to be imposed by the government to favor the development of micro-CHP systems and to make these technologies economically attractive. The fuel cost over any period of time represents the running cost of the micro-CHP plant. The turn over is the income from selling the electricity power at the spot market and the income from the cost of the heat avoided to be produced by a local boiler or bought from a heating network. The economic function to be minimized is given by Eq. (4.3).

$$Min\left\{A_{sold}^{elec} = A_{inv}^{CHP} + A_{run}^{CHP} - A_{sold}^{heat}\right\} \quad (4.3)$$

The annual system investment costs of the micro-CHP plant are described in Eq. (4.4). System capital cost is calculated according to annualized capital cost. Annualizing capital is a mean to spreading the initial cost of an option across the lifetime of that option while accounting for the time value of money. The cost of capital is annualized as if it were being paid off as a loan at a particular interest of discount rate over the lifetime of the option. The results are a future value cost or constant annual cost of capital.

$$A_{inv}^{CHP} = C_{inv}^{CHP}\left[d(1+d)^n/(1+d)^n - 1\right] = C_{inv}^{\mu CHP}(CRF) \text{ (€/year)} \quad (4.4)$$

The terms in the square bracket is the capital recovery factor (CRF), the investment cost of the system is calculated according to the cost of the main components of the system. The total investment cost is given by Eq. (4.5).

$$C_{inv}^{\mu CHP} = C_{inv}^{turb} + C_{inv}^{cond}A_{cond} + C_{inv}^{rec}A_{rec} + C_{inv}^{boiler}A_{boiler} + C_{inv}^{pump}A_{boiler} + C_{inv}^{pellets,boiler}P_{pellets,boiler} + C_{inv}^{sol}A_{sol} \quad (4.5)$$

Annual running cost for micro-CHP plant is calculated by Eq. (4.6). The running cost is composed of the fuel and the maintenance costs. The fuel cost is calculated with the total fuel consumption over the year multiplied by the levelized fuel price. The maintenance cost is neglected in this study due to the lack of available data in the literature.

$$A_{run}^{CHP} = E_{pellets}C_{pellets}CELF \quad (4.6)$$

CELF represents the constant-escalation levelization factor, which is used to express the relationship between the value of the expenditure at the beginning of the first year (P_0) and an equivalent annuity (A), which is called a levelized value. The CELF depends on both the

effective annual cost of money, or discount rate, and the nominal escalation rate r_n given by Eq. (4.7).

$$CELF = \frac{k\left(1-k^n\right)}{1-k} CRF$$
$$k = \frac{1+r_n}{1+d} \tag{4.7}$$

The levelized annual cost of the heat provided by the SWORC-μCHP is considered as heat produced by heat networks. Therefore, the cost of the heat avoided is considered to be 7.1 c€/kW_{th} for collective residence [PRE06]. The annual cost of the heat avoided is given by Eq. (4.8).

$$A_h^{CHP} = C_h \left(E_{cond} + E_{ph}\right) CELF \tag{4.8}$$

The Levelized Electricity Cost (LEC) approach including capital investment, operating and product cost is used to characterize the economic viability. Therefore, the LEC is the objective function of the economical model. To reach the economic optimum conditions the LEC has to attain minimum values. The LEC is calculated according to Eq. (4.9).

$$LEC = \left(A_{inv}^{CHP} + A_f^{CHP} - A_h^{CHP}\right) \Big/ E_{el} \tag{4.9}$$

4. Formulation of the problem

The purpose of this investigation is to determine the optimum operating conditions of the SWORC-μCHP system operating with solar and wood energy. Most of the time, the system is optimized to operate at its highest thermodynamic performances, represented here by the function PES. Often, operating at maximum thermodynamic efficiency requires large size heat exchangers, which are non-practical and uneconomical due to the high capital cost of those components.

In order to circumvent this problem, the system is economically optimized, based on minimization of the costs and maximization of the PES. It is important to note that the maximum primary energy saving can be achieved when the system operates only on solar energy since this energy is considered as free energy. However, to be able to operate this system only on solar energy, a large surface area of solar collectors is required. Therefore, a significant impact of the solar field area can be shown on the SWORC-μCHP capital cost. Therefore, the surface area of the solar collector should be carefully designed in order not to hamper the economic performances of the system.

In this section, the formulation is presented for both types of optimization, thermodynamic optimization and economic optimization. The formulation of this problem is based on the following assumptions.

1. The micro-CHP system operates under steady state conditions; the pressure losses due to friction in the different heat exchangers are neglected.
2. All the components of the ORC are considered adiabatic; however, a thermal efficiency of 95% has been considered to take into account the losses to the surroundings for the ORC system.
3. The working fluid at the expander inlet is assumed to be at the saturated vapor conditions except for water where a superheat of 25 K has been considered to prevent the formation of liquid droplets at the outlet of the expander.
4. The boiler and the condenser are designed to operate with a constant DT between the HTF and the working fluid.

5. The lifetime of the different components is 15 years and the discount rate is 6%. The micro-CHP unit operates 3000 hours per year. The inflation rate of the fuel cost is assumed to be 2% for the cost of pellets and for the cost of heat generation.
6. The total efficiency of the expander is 75% and for the efficiency of the working fluid pump is 65%.

An iterative numerical technique method was used to optimize the objective functions. During the optimization procedure, the thermodynamic objective function is maximized and the economic objective function is minimized. This optimization procedure is performed by varying the different decision variables such as boiling temperature, working fluids, and solar collector surface area to identify the optimum values of the decision variables.

The numerical calculations were carried out for a net power of 1 kW_{el} with a cold source temperature of 40°C for the simulation of the cold-water temperature that could varied from 40°C to 75°C. representing the average temperature of a storage tank for heating system. The boiling temperature will be varied from 100°C to 200°C. Heat and mass balance across the devices and efficiencies of the different components are calculated as given below.

The mass flow rate of the working fluid for different output net power is calculated by Eq. (4.10).

$$\dot{m}_{wf} = \frac{\dot{W}_{net}}{\eta_t \left(h_3 - h_{4s}\right) - v_1 \Delta P / \eta_p} \tag{4.10}$$

The heat supplied to the boiler is calculated by Eq. (4.11)

$$\dot{Q}_b = \dot{m}_{wf} \left(h_3 - h_{2h}\right) \tag{4.11}$$

The heat rejection at the condenser is calculated by Eq. (4.12)

$$\dot{Q}_{cond} = \dot{m}_{wf} \left(h_{4h} - h_1\right) \tag{4.12}$$

The outlet temperatures of the internal heat exchanger (recuperator) are calculated using the epsilon-NUT method for heat exchanger analysis.

$$\dot{Q}_{rec} = \varepsilon \dot{Q}_{rec,\max} = Min\left[\left(h_{2h} - h_2\right); \left(h_{4s} - h_{4h}\right)\right] \tag{4.13}$$

In order to determine the solar energy and the pellets boiler capacity required it is necessary to calculate the temperature profile of the HTF in the different components since the thermal efficiency of the solar collectors and the wood pellets boiler depends mainly on the operating profile temperature of the HTF. First, the temperature profile in the boiler will be determined as shown below. The temperature of the HTF at the inlet of the boiler is calculated by Eq. (4.14).

$$T_{htf,1} = T_3 + \Delta T_1 \tag{4.14}$$

The temperature of the HTF at the saturation temperature of the working fluid is given by Eq. (4.15)

$$T_{htf,sat-liq} = T_{wf,sat-liq} + \Delta T_{pinch} \tag{4.15}$$

Therefore, the mass flow rate of the of the HTF is calculated by Eq. (4.16)

$$\dot{m}_{htf} = \frac{\dot{m}_{wf} \left(h_3 - h_{2,sat-liq}\right)}{Cp_{htf} \left(T_{htf,1} - T_{htf,sat-liq}\right)} \tag{4.16}$$

The outlet temperature of the HTF fluid is then calculated using the energy balance applied to the boiler.

$$T_{htf,2} = T_{htf,1} - \frac{\dot{m}_{wf}\left(h_3 - h_2\right)}{\dot{m}_{htf} Cp_{htf}} \tag{4.17}$$

After calculating the mass flow rate and the temperature profile of the HTF in the boiler, the thermal efficiency of the solar collectors and the wood pellets boiler will be calculated as follows. The solar collector thermal efficiency is defined as the ratio of the rate of useful thermal energy leaving the collector, to the useable solar irradiance falling on the aperture area. Simply stated, collector efficiency is given in Eq. (4.18)

$$\eta_{sol} = \frac{\dot{Q}_{useful}}{GA_{sol}} = \frac{\dot{m}_{htf,sol} c_{p,htf}\left(T_{sol,out} - T_{sol,in}\right)}{GA_{sol}} \tag{4.18}$$

The solar collector thermal efficiency depending on the different solar collector parameters is given by Brunold et al. [BRU94] and calculated using Eq. (4.19)

$$\eta_{sol} = \eta_0 - k_1\left(T_m - T_a\right)/G - k_2\left(T_m - T_a\right)^2/G \tag{4.19}$$

Where the outlet temperature of the solar collector is calculated using the energy balance applied to the solar collector

$$T_{htf,sol,out} = T_{htf,sol,in} + \frac{\eta_{sol} GA_{sol}}{\dot{m}_{htf,sol} Cp_{htf}} \tag{4.20}$$

In order to determine the fraction of the HTF flow rate that goes into the solar collector, an optimal temperature difference is imposed to the solar collector, based on the maximum allowable VFR given by the manufacturer. The thermal efficiency of the wood pellets boiler depends on the temperature of the HTF at the inlet of the boiler and its corresponding part load performances. The thermal efficiency of the wood pellets boiler is calculated using the different equation defined in the method adopted in the thermal regulation “RT2000” [RTH00]. The thermal efficiency of the wood pellets boiler is given in Eq. (4.21).

$$\eta_{pellets,boiler} = \frac{\dot{Q}_{pellets,boiler}}{\dot{Q}_{pellets,boiler} + \dot{Q}_{pellets,boiler-losses}} \tag{4.21}$$

The heat losses are calculated by Eq. (4.22).

$$\dot{Q}_{pellets,boiler-losses} = \frac{\dot{Q}_{pellets} - \dot{Q}_{pellets,pl}}{\dot{Q}_{pellets,nom} - \dot{Q}_{pellets,pl}}\left(\dot{Q}_{pellets,nom,losses} - \dot{Q}_{pellets,pl,losses}\right) + \dot{Q}_{pellets,pl,losses} \tag{4.22}$$

The nominal load losses and the part load operation losses are calculated respectively by Eqs. (4.23) and (4.24).

$$\begin{aligned} &\dot{Q}_{pellets,nom,losses} = \left(\frac{100 - \eta_{pellets,nom}}{\eta_{pellets,nom}}\right)\dot{Q}_{pellets,nom} \\ &\eta_{pellets,nom}\left(T_{htf,pellets,in}\right) = \eta_{pellets,nom}\left(T_{test,nom}\right) + 0.1\left(T_{test,nom} - T_{htf,pellets,in}\right) \end{aligned} \tag{4.23}$$

$$\begin{aligned} &\dot{Q}_{pellets,pl,losses} = \left(\frac{100 - \eta_{pellets,pl}}{\eta_{pellets,pl}}\right)\dot{Q}_{pellets,pl} \\ &\eta_{pellets,pl}\left(T_{htf,pellets,in}\right) = \eta_{pellets,pl}\left(T_{test,pl}\right) + 0.1\left(T_{test,pl} - T_{htf,pellets,in}\right) \end{aligned} \tag{4.24}$$

Where $T_{test,nom}$ and $T_{test,pl}$ are respectively the nominal load and the partial load temperatures used to evaluate the thermal efficiency at the nominal and partial load operation. In order to determine the inlet temperature of the HTF entering the wood-pellet boiler a mass and energy balance is applied at the mixing point 3-way valve (2).

$$T_{htf,pellets,in} = \frac{\dot{m}_{htf,sol,out} Cp_{htf} T_{htf,sol,out} + \left(\dot{m}_{htf} - \dot{m}_{htf,sol,out}\right) Cp_{htf} T_{htf,2}}{\dot{m}_{htf} Cp_{htf}} \tag{4.25}$$

To complete the economical analysis, the technologies of the different components used have to be identified. Therefore, the different components of the SWORC-μCHP considered in this analysis are boiler and condenser of the brazed plate technology. A scroll expander is used as a turbine since it is the most common technology of turbine used for low power output system [AOU08b, LEM06 and KAN03]. Evacuated tube CPC collector is used as solar collector since they can operate up to 200°C without the need of a special solar tracking system. A wood pellets boiler is used as biomass boiler since it represents a high thermal efficiency and is fully automated.
The surface area of the different heat exchangers has been calculated. Therefore, the overall heat transfer coefficient for each section of the boiler and the condenser is determined using the hot and cold fluid convection coefficients and appropriate geometric parameters, which it is given by Eq. (4.26).

$$U = \frac{1}{\left(1/h_h\right)} + \frac{1}{\left(1/h_c\right)} + \frac{t}{k_w} \tag{4.26}$$

The total boiler or condenser heat exchanger surface areas are given by Eq. (4.27).

$$A_{tot} = A_{\sup} + A_{sub} + A_{two-phase} = \frac{\dot{Q}_{\sup}}{U_{\sup}\Delta T_{lm,\sup}} + \frac{\dot{Q}_{sub}}{U_{sub}\Delta T_{lm,sub}} + \sum_{i=1}^{n} \frac{\dot{Q}_{two-phase,i}}{U_{two-phase,i}\Delta T_{lm,two-phase}} \tag{4.27}$$

Numerical correlations are used to calculate the heat transfer coefficients in the condenser and boiler are listed below. The single-phase heat coefficient h_l was obtained from the Dittus-Boelter correlation:

$$h_l = 0.023\left(\frac{k_l}{D_h}\right)\mathrm{Re}^{0.8}\,\mathrm{Pr}^{0.4} \tag{4.28}$$

The boiling heat transfer coefficient, h_b is calculated using the correlation [GAR07],

$$Nu = 1.926\,\mathrm{Pr}_l^{1/3}\,Bo_{eq}^{-0.3}\,\mathrm{Re}_{eq}^{0.5}\left[\left(1-x\right)+\left(\frac{\rho_l}{\rho_v}\right)^{0.5}\right] \qquad for\ 2000 < \mathrm{Re}_{eq} < 10000. \tag{4.29}$$

Where

$$\mathrm{Re}_{eq} = \frac{G_{eq} D_h}{\eta_l}$$
$$Bo_{eq} = \frac{q''_w}{G_{eq} h_{fg}} \tag{4.30}$$
$$G_{eq} = G\left[1 - x_m + x_m\left(\frac{\rho_l}{\rho_v}\right)^{1/2}\right]$$

The condensation heat transfer coefficient, h_{cond} for all the working fluid is evaluated using Dittus-Boelter correlation

$$h_{cond} = 4.118\left(\frac{k_l}{D_h}\right)\mathrm{Re}_{eq}^{0.4}\,\mathrm{Pr}_l^{1/3} \tag{4.31}$$

Therefore, the cost of the plate heat exchanger used as boiler and condenser are estimated from the different data collected from the manufacturers. The cost has been correlated as follows

$$\begin{aligned} &C_{inv}^{PHX} = C_{inv,1}^{PHX}\ln\left(A_{PHX}\right) + C_{inv,2}^{PHX} \\ &if\left(C_{inv}^{PHX} < 200\right); C_{inv}^{PHX} = 200 \end{aligned} \tag{4.32}$$

For the recuperator, the area of the heat exchanger is calculated from the effectiveness of the heat exchanger, which represents the ratio of q over q_{max} is given by Eq. (4.33).

$$q_{\max} = C_{\min}(T_{h,i} - T_{c,i}) \tag{4.33}$$

Where C_{min} is the minimum of $(mC_p)_c$ and $(mC_p)_h$, while $T_{h,i}$ and $T_{c,i}$ represent temperatures of the hot and the cold streams entering the heat exchanger. The number of heat transfer units NTU for a counter flow heat exchanger [KAK98] is given by Eq. (4.34).

$$NTU = \frac{1}{1-C^*}\ln\left(\frac{1-C^*\varepsilon}{1-\varepsilon}\right) \tag{4.34}$$

The overall thermal conductance is calculated using Eq. (4.35)

$$UA = NTUC_{\min} \tag{4.35}$$

Therefore the cost of the recuperator can be expressed as a function of the overall thermal conductance [ESD92].

$$C_{inv}^{rec} = C_{inv,1}^{rec}\left(UA_{rec}\right) \tag{4.36}$$

For the preheater, the cost of the additional condensing boiler is included in the total cost of the wood pellets boiler. According to [BEJ96], the cost equation of an equipment item (C_Y) at a given capacity or size (expressed by the variable X_Y) could be calculated when the cost of the same equipment item (C_X) at different capacity or size (expressed by X_W) is known by Eq. (4.37).

$$C_Y = C_X\left(\frac{X_Y}{X_W}\right)^{\alpha} \tag{4.37}$$

For thermal process equipment, the scaling exponent is usually inferior to one. This factor is in general obtained from an estimating cost chart established by the manufacturers. In the absence of cost information, an exponent of 0.6 can be used. This approach is known as the six-tenth rule. The capital cost of the scroll compressor that is used as scroll expander depends on the built-in volume ratio (VR) and swept volume (V_s). Therefore, the cost equation of the scroll expander is given by Eq. (4.38).

$$C_{inv,Y,W}^{turb} = C_{inv,X,V}^{turb}\left(\frac{VR_W}{VR_V}\right)^{0.6}\left(\frac{V_Y}{V_X}\right)^{0.6} \tag{4.38}$$

The cost of the wood pellets boilers depends mainly on its thermal capacity. Therefore, the cost information has been established and collected from the different data delivered by the

manufacturers of this type of boilers. Therefore, the cost of the wood pellets boiler has been correlated as follows:

$$C_{inv}^{boiler} = C_{inv,1}^{boiler} Q_{pellets} + C_{inv,2}^{boiler} \quad (4.39)$$

4.1 Solution procedure

For the design and optimization of a thermal system, it is convenient to identify two types of independent variables: decision variables and parameters variables [BEJ96]. The decision variables may be varied in optimization studies but the parameters remain fixed in a given application. All other variables are dependent variables. Therefore, their values are calculated from the independent variables.

To be able to establish the solution procedure, it is convenient to identify first the different decision variables to be varied and the different parameters to be kept constant. The different independent parameters that can be varied are the boiler temperature, the condensing temperature, the superheat at the inlet of the turbine, the sub-cooled at the inlet of the pump, the DT at condenser and the boiler, the mass flow rate of the working fluid, the mass flow rate of the HTF, the mass flow rate entering the solar collector, the solar collector surface area, the exit temperature of the wood pellets boiler and the working fluids.

Therefore, it is important to distinguish the decision variables of minor importance that could be excluded from this optimization study from the main variables. Then the variable of minor importance will be considered as fixed parameters selected with reasonable values. The main decision variables are listed here after.

- Rankine fluid boiling temperature: high boiling temperatures are desirable since they offer high Rankine cycle efficiencies and enable the decision of smaller turbines. However, raising the system temperature is not always feasible because of cost issues affecting the design of the different components of the Rankine cycle especially the design of the expander that could not tolerate high operating temperatures and pressures. In addition raising the boiling temperature will slightly decrease the thermal efficiency of the solar collectors and the wood pellets boiler.
- Working fluid: the selection of the working fluid has a major impact on the performance of the ORC and on the design of the main components of the Rankine cycle. Therefore, working fluid could have a major impact on the capital cost of the system and it is more important when conducting the economical optimization.
- The solar collector surface area: Increasing the collector surface area will increase the primary energy saving, however, a large surface area could affect the total capital cost of the system and it will affect strongly the economic performance of the system.

Several parameters such as superheat at the turbine inlet, sub-cooling at the inlet of the pump, condensing temperature, minimum DT at the boiler and the condenser, and the mass flow rate of the heat transfer fluid have been considered as fixed parameters. They are fixed in the optimization study since they have a minor influence on the performance of the micro-CHP system. They are represented in Table 4.1.

Table 4.1 – Parameters	
Condensing temperature	80°C
Turbine efficiency	75%
Pump total efficiency	65%
Condenser minimum DT	10 K
Boiler minimum DT	10 K
ΔT_1	10 K
Superheat at the inlet of the turbine	1 K (25 K if water)
Sub-cooling at the inlet of the pump	10 K
Recuperator efficiency	0.8

The procedure adopted in this study is a reverse resolution technique where first the electrical power output of the Rankine cycle is fixed and then the total required heat duty is calculated. Therefore, the MFR of the working fluid is calculated using Eq. (4.10) for a fixed (1 kW_{el}) electrical power output. Resolving simultaneously Eqs. (4.11) to (4.13), the required boiler and condenser thermal duties are calculated and therefore the RC efficiency. After calculating the required heat capacity of the boiler, the HTF MFR and the temperature profile are calculated using Eqs. (4.14) to (4.17) by fixing the minimum ΔT_{pinch} and the temperature different ΔT_1 in the boiler. Then the HTF MFR passing through the solar collector is estimated depending on the solar collector surface area. The HTF outlet temperature leaving the solar collector is calculated using Eqs. (4.19) and (4.20). The HTF temperature at the inlet of the wood pellets boilers is calculated using Eq. (4.25) and therefore the thermal efficiency of the wood pellets boiler is calculated using Eqs. (4.21) to (4.24). After identifying all thermodynamic parameters, the thermodynamic objective function PES is calculated using Eq. (4.2).

On the other hand, the economic function LEC is calculated simultaneously with the thermodynamic function PES by estimating the cost of the different components. The cost evaluation is valid in real terms (constant cost 2007) and a real discount rate of 6% has been assumed. A constant real wood-pellet price of 5.5 c€/kWh has been considered. The cost of heat avoided was assumed to be 7.1 c€/kWh_{th} and the lifetime of the micro-CHP is assumed to be 15 years. All cost data have been collected from the different equipment suppliers (see Appendix B). The cost of the solar collector was fixed to 500 €/m^2 including the cost of the HTF system. The full load operation of the system was assumed to be 3,000 hours per year.

5. Analysis and results

The performance of the system is evaluated for different boiling temperatures and working fluids when operating with wood pellets. The electrical efficiency and primary energy savings are calculated for different operating conditions. Afterwards, the economic performance (LEC) is calculated for different boiling temperatures and working fluids. Therefore, the LEC is established depending on the achieved PES. After evaluating the performance of the system operating on wood pellets, the dual mode operation solar-wood is studied. The system electrical efficiency is calculated for several boiling temperatures, working fluids, and solar collector surface areas. Afterwards, the effect of the solar collector surface area on the LEC is evaluated to establish the relationship between the PES achieved by the system and the corresponding LEC.

5.1 Performance analysis

The performance of the system has been calculated for several working fluids and for several boiling temperatures with different operating modes (wood only and dual mode wood-solar). Results (seeFigure 4.2) show that the system electrical efficiency increases with the increment of the boiling temperature when operating on wood boiler. Results are consistent for all working fluids considered in this study. Results show that water presents the best performance among all working fluids with a maximum electrical efficiency of 12% for a boiling temperature of 180°C when operating on wood energy. Hexane shows the best performance among the organic fluids. R-245fa shows the worst performance because it represents the lowest critical temperature with a maximum electrical efficiency of 6.5% at 150°C.

On the other hand, the primary energy savings are presented in Figure 4.3 showing the same tendency as the electrical efficiency of the system, because it is directly related to the electrical efficiency (see Eq. (4.2)). Therefore, the maximum PES could be achieved with water as working fluids and operating at high boiling temperature (~180°C).

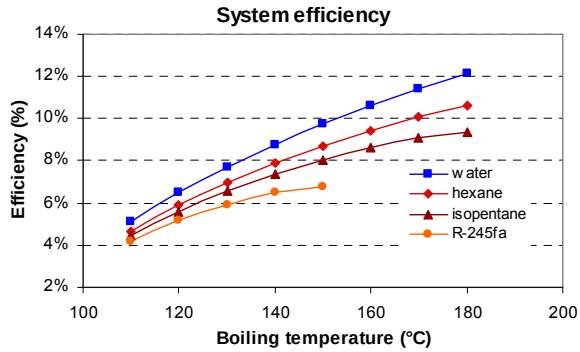

Figure 4.2 – Variation of the system electrical efficiency as a function of the boiler temperature and the working fluid.

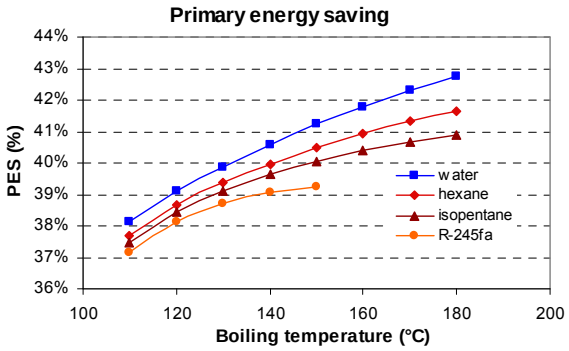

Figure 4.3 – Variation of the primary energy saving as a function of the boiler temperature and the working fluid.

The levelized electricity cost calculated for the same operating parameters listed below shows a different tendency compared to electrical efficiency and PES. Therefore, the LEC increases while increasing the boiling temperature of R-245fa and isopentane whereas it decreases for water and hexane. This opposite tendency is mainly due to the system low electrical efficiency when operating with R-245fa and isopentane. Therefore, the customer gain (measured by marginal revenue) does not exceed his costs (measured by marginal cost). Otherwise, for the same level of boiling temperature, working fluids with the higher critical temperature present the higher LEC.

Figure 4.5 shows LEC as a function of PES. It was shown that, for the same primary energy savings, the working fluid with the lowest critical temperature shows the lowest electricity cost. However, the maximum primary energy savings for some working fluids are limited to their maximum electrical efficiency (ex: R-245fa could not achieve more than 39.5% of PES because the maximum boiling temperature is limited to its critical temperature). To achieve higher primary energy savings, it requires utilizing some working fluids with higher critical temperature even if the electricity cost will be higher (see Figure 4.).

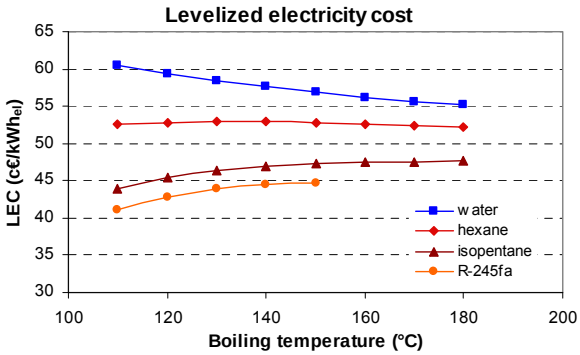

Figure 4.4 – LEC variation as a function of the boiling temperature and the working fluid.

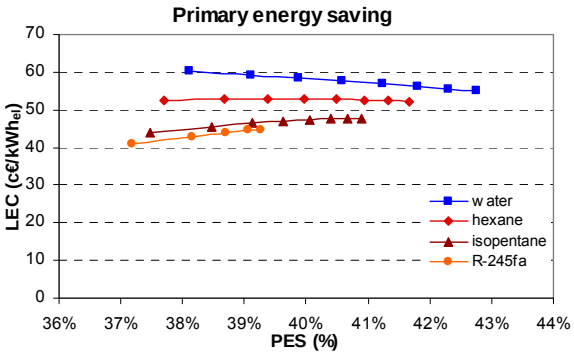

Figure 4.5 – LEC variation as a function of the PES and the working fluid.

5.2 Dual operation analysis

Results presented previously for the system operating on wood energy show that for higher PES a higher boiling temperature is required for working fluids. However, the economic performance shows a different tendency compared to the thermodynamic performance as shown in Figure 4.5. Increasing the PES could result in the LEC increase for R-245fa and isopentane, whereas the LEC decreases for water and hexane.

Operating in hybrid mode solar-wood could lead to different results. A parametric study has been conducted to evaluate the effects of the working fluid, boiling temperature, and the solar energy share on the system performance.

Figure 4.6 shows the system efficiency as a function of the different parameters fixed above. The system efficiency decreases when increasing the solar energy share, and this applies for the different working fluids and boiling temperatures. The system efficiency decreases since the thermal efficiency of the solar collectors (~40%) is, in general, lower than the thermal efficiency of the wood-pellet boilers (~ 80%). Similar results have been observed for the system efficiency as a function of the boiling temperature, where it has been shown that the system efficiency increases while increasing the boiling temperature, even in hybrid mode operation. These results are applicable for all working fluids.

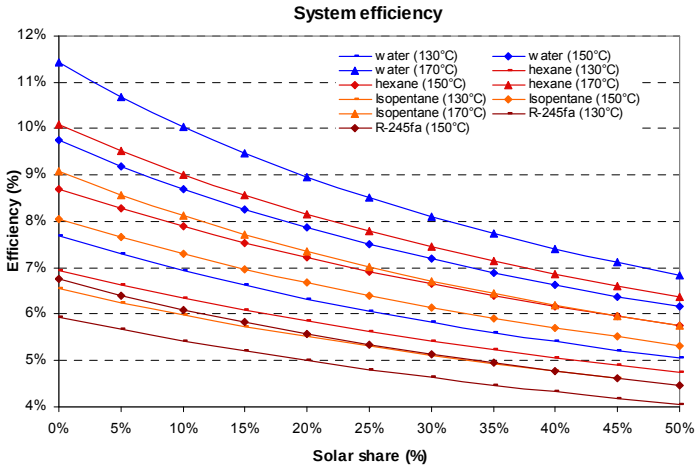

Figure 4.6 – Variation of the system electrical efficiency as a function of the boiler temperature, working fluid, and solar energy share.

For the PES, same results as shown previously are obtained regarding the direct relation between the system efficiency and the PES: increasing the system efficiency would lead to the PES increase when operating on wood only.

For LEC, at high solar energy share, the system operating with water shows the same LEC with two different boiling temperatures (see Figure 4.7). This result is mainly due to the lower thermal efficiency of the solar collectors and the wood -pellet boiler when operating at higher boiling temperature. For higher solar energy share (>50%), results for water and hexane show similar tendency as that of R-245fa and isopentane since the LEC decreases when increasing the boiling temperature.

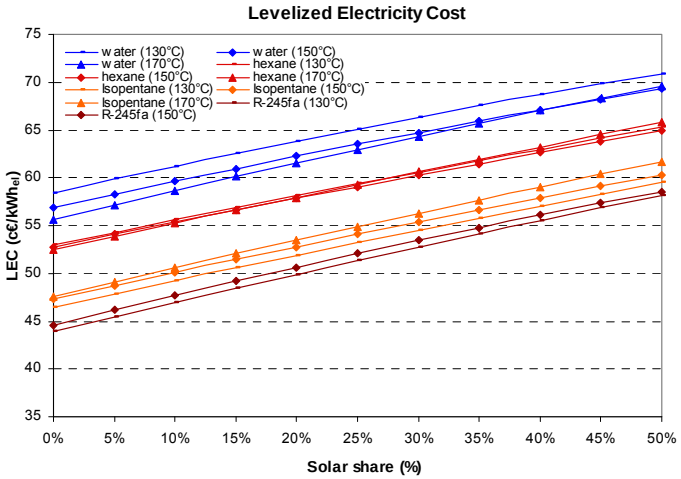

Figure 4.7 – Variation of the LEC with the boiler temperature, working fluid and solar energy share.

Figure 4.8 shows the LEC as a function of the PES. The LEC increases with increase in the solar energy share and then the PES. This result is mainly due to the higher solar collector surface area and so a higher investment cost that affects directly the electricity cost. The LEC for hybrid mode operation shows similar tendency compared to wood operation since the LEC increases when operating with working fluids at higher critical temperature. For water and hexane, the LEC decreases when increasing the boiling temperature and increases when operating with R-245fa and isopentane.

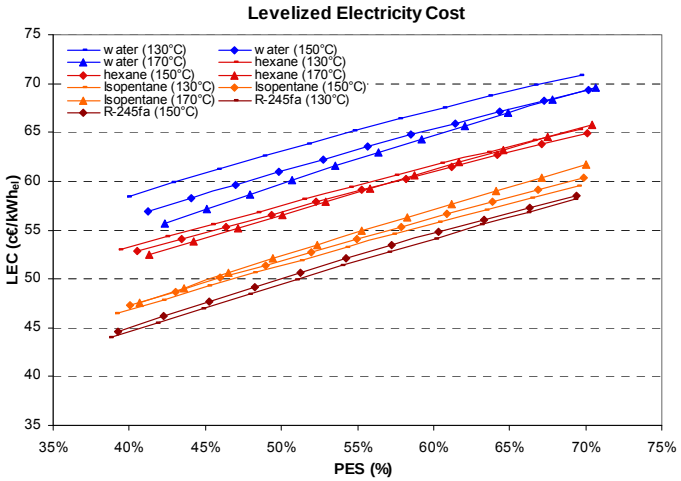

Figure 4.8 – Variation of the LEC as a function of the PES, boiler temperature and working fluid.

6. Sensitivity analysis

The sensitivity analysis improves understanding the influence of the different key parameters on the decision of adopting micro-CHP systems for building applications. In this study, sensitivity analysis has been performed on global solar irradiance, cost of heat generation, and electrical capacity of the micro-CHP system.

6.1 Global solar irradiance

The global solar irradiance depends mainly on the location where the micro-CHP system is installed. The solar global irradiance impacts on the thermodynamic and economic system performance. Since the PES is sensible to the availability of solar energy since, then when higher solar energy is available, higher PES savings are gained. Similar impact will be seen on the economic performance. A location where solar energy is more abundant implies that for the same surface area of solar collector the consumption of the fuel “wood pellets” will be lower because the share of solar energy will be higher.

Figure 4.9 shows the variation of the PES, LEC, and the solar share as a function of the global irradiance energy available. Results have shown that for locations where higher solar energy is available for the same solar collector surface area, the PES is higher and the solar share is higher corresponding to a lower LEC. Therefore, it is economically more attractive to install the systems operating on dual mode solar and wood in areas where solar energy is abundant. In areas where the solar energy availability is lower than 200 kWh/m^2.year, the solar share could go down to less than 10%, the achieved PES would be very close to the system operating without solar collectors, and the LEC could rise up to 90 c€/kWh$_{el}$, which could result in a major impact on the system profitability. Therefore, the solar collector surface area has to be well dimensioned according to the solar energy availability.

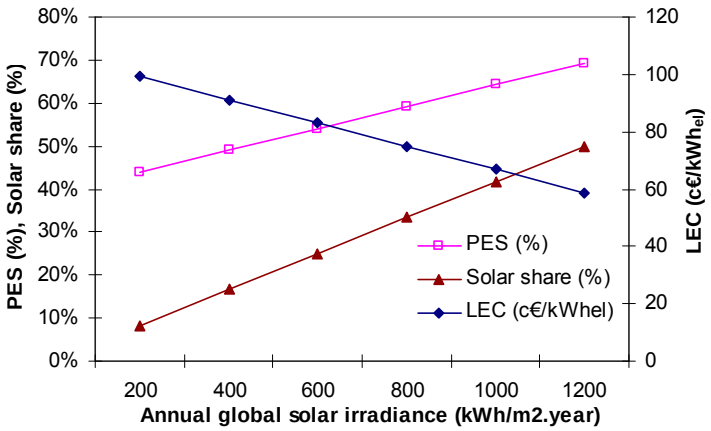

Figure 4.9 – LEC, PES and Solar share according to the global solar energy availability (A_{sol} = 35 m^2).

6.2 Heating price inflation rate

Since the micro-CHP system operating on wood aims at replacing conventional boilers operating on fuel or gas, the cost of heat produced by the competing boilers has a major impact on the system profitability.

Figure 4.10 shows the electrical cost calculated when the heat has been subjected to different scenarios of price escalation.

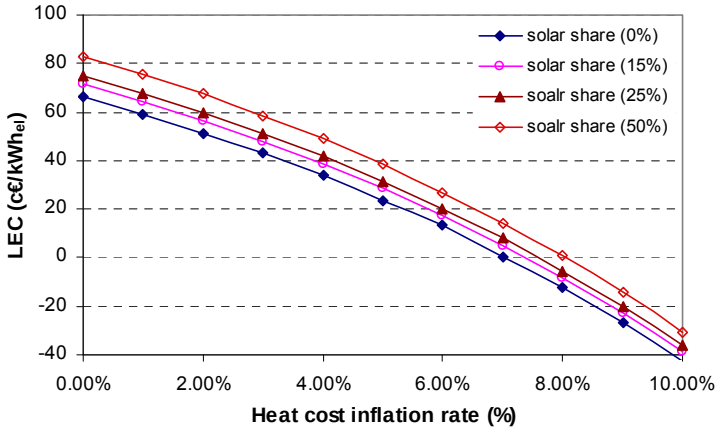

Figure 4.10 – Levelized electricity cost as a function of the heat cost inflation rate.

The base case was assumed to be a 1-kW_{el} system operating with R-245fa at boiling temperature of 150°C. Three different sizes of solar fields have been considered as a function of various solar shares. The levelized electricity cost is very sensitive to the cost of the heat avoided. It can be seen in Figure 4.10 that if the heat produced is subjected to inflation rate higher than 6%, the LEC of 20 c€/kWh_{el} could be sufficient to make the micro-CHP system attractive, even with a surface area solar collector covering 25% of the energy needed. If the price of heat avoided is subjected to a higher inflation rate than 6%, the micro-CHP system could be economically feasible without imposing a special tariff for electricity produced from renewable energy.

6.3 Electrical capacity of the micro-CHP system

The system size affects the economy of residential micro-CHP systems. A small thermal capacity enables longer operation hours during the year and improves the annual performance of the micro-CHP systems due to the lower intermittence operation, which leads to higher efficiency. A larger system will lead to a short intermittence operation with a

higher number of on/off operations, which leads to a low efficiency due to losses occurring during the transient phase. It is always more convenient to operate with an under-dimensioned system compared to the maximum power required, coupled to a storage tank that will provide the extra heat required for the peak load period.

The electrical capacity variation of the micro-CHP system operating on wood pellets only shows that increasing the system electrical power output will lead to increasing the annual electrical cost since it would produce more electricla energy for the same operating period. Increasing the annual electricity cost will lead to increase in the LEC generated by the micro-CHP system. This is due mainly to increase in the micro-CHP system annual capital cost where both the annual operating and avoiding costs remain constant.

As seen in Figure 4.11, the number of hours at full load will decrease when increasing the electrical power output of the micro-CHP system. The maximum annual full load operation of the micro-CHP system is 8760 hours. Therefore, decreasing the electrical power output of the micro-CHP system is limited to fixed values, which corresponds to the ratio of the annual heat load demand divided by the micro-CHP system thermal capacity and multiplied by the power to heat ratio of the micro-CHP system.

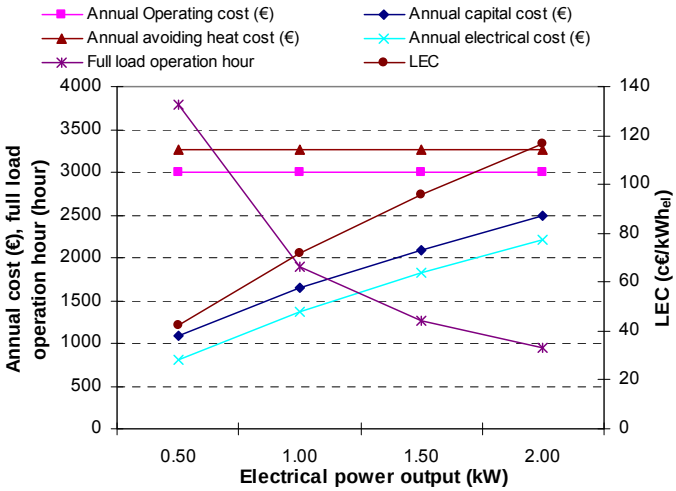

Figure 4.11 – Effect of the electrical capacity of the micro-CHP system on energy cost structure and running time.

When dimensioning a system to provide a constant annual heat load, an under-dimensioned system will lead to higher economical performance. The minimum capacity of the micro-CHP system is limited since the system has to provide the annual energy load with 8760-hour maximum operation.

7. Conclusions and perspectives

It can be concluded that an optimized capacity of the micro-CHP system is based on a trade-off between the long operation time and fulfilling only the thermal needs of the buildings.

In this study, a mathematical model has been developed to calculate the PES and the LEC of a micro-CHP system operating on wood and solar energy. The model has been developed to determine the effect of the different operating parameters on the thermodynamic and economic performances of the micro-CHP system. According to the sensitivity analysis, the following conclusions can be drawn.

- The main parameters affecting the micro-CHP system performance are the boiling temperature, working fluids, and the solar collector surface area.
- The thermodynamic performance increases while increasing the boiling temperature. In addition, working fluids with higher critical temperature show higher thermodynamic performances.

- The economic performance of the system shows a different tendency compared to the thermodynamic performance: increasing the boiling temperature could improve the system performance if water or hexane were used as working fluids, whereas it will deteriorate its economical performance if R-245fa or isopentane were used.
- Increasing the solar collector surface area will lead to an increase of the PES and the LEC.

A balance has to be made between the thermodynamic performances that could be achieved with an acceptable LEC. However, it was shown from the sensitivity analysis that the system is more economically feasible when installed in locations where the solar energy is more abundant and where the cost of heat avoided could be the subject of a major cost inflation.

On the other hand, the economical feasibility is sensitive to the micro-CHP capital cost, which is proportional to the micro-CHP electrical power output. In a future work, an optimization procedure should be performed to define a balance between the electrical power capacity of the micro-CHP system, power to heat ratio, storage tank volume, heat load demand, and the location. This work will be treated in next chapter.

References

[AOU08a] B. Aoun, D. Clodic, "Working Fluid for a Low Power-Output Organic Rankine Cycle" to be published in International Journal applied thermodynamics (Refer to chapter 2).

[AOU08b] B. Aoun, D. Clodic, "Theoretical and experimental study of an oil-free scroll type vapour expander", Proc. of 19th Int. compressor eng. Conf. at Purdue, 2008.

[ARR06] Arrêté du 15 septembre 2006 relatif au diagnostic de performance énergétique pour les bâtiments existants proposes à la vente en France métropolitaine. Ministère de l'écologie du développement et de l'aménagement durable.

[BRU94] S. Brunold, R. Frey, U. Frei, A comparison of three different collectors for process heat applications, SPIE 1994.

[CHE06] David chénier, "Impact de la micro-cogénération à bois sur l'effet de serre", Rapport d'étude, Amoès, Novembre 2006.

[COC06] J. Cockroft, N. Kelly, A comparative assessment of future heat and power sources for the UK domestic sector, energy conversion and management 47 (2006) 2349-2360.

[DAM00] P.R. Damshala, "Thermodynamic analysis of a CHP system by iterative Numerical technique" Ashrae (2000) NE, Atlanta.

[DIR04] DIRECTIVE 2004/8/EC OF THE EUROPEAN PARLIAMENT AND OF THE COUNCIL of 11 February 2004 on the promotion of cogeneration based on a useful heat demand in the internal energy market and amending Directive 92/42/EEC.

[ESD92] ESDU International Ltd, "Selection and costing of heat exchangers", London, 1992.

[GAR07] J.R. Garcia-Cascales, F. Vera-Garcia, J.M. Corberan-Salvador, J. Gonzalvez-Macia, Assessment of boiling and condensation heat transfer correlations in the modeling of plate heat exchangers, International journal of refrigeration 30 (2007) 1029-1041.

[HER07] P. Herrant, Eat actuel du parc immobilier français, Colloque national ADEME-CNISF, novembre 2007.

[HUN97] T.C. Hung, T.Y. Shai, S.K. Wang, "A review of organic Rankine cycles (ORCs) for the recovery of low-grade waste heat", Energy 22 (1997)661-667.

[KAK98] S. Kakaç, H. Lui, "Heat exchangers: selection, rating and thermal design", published by CRC press LCC, 1998.

[KAN00] M. Kane, D. Favrat, K.Ziegler, Y. Allani, "Thermodynamic analysis of advanced solar-fossil combined power plants", International Journal applied thermodynamics 3 (2000) 191-198.

[KAN03] M. Kane, D. Larrain, D. Favrat, Y. Allani, "Small hybrid solar power system", Int. J. Energy, vol. 28 (2003) p. 1427-1443.

[LEM06] V. Lemort, I. Teodoreset, J. Lebrun, "Experimental study of the integration of a scroll expander into a heat recovery Rankine cycle", Proc. of 18th Int. compressor eng. Conf. at Purdue, 2006.

[LIU04] B.T. Liu, K.H. Chien, C.C. Wang, "Effect of working fluids on organic Rankine cycle for waste heat recovery", Energy 29 (2004) 1207–1217.

[LOI05] Loi POPE, 2005. Loi n° 2005-781 du 13 juillet 2005 de programme fixant les orientations de la politique énergétique. Journal Officiel de la République Française n°163 of 14 July 2005 (in French).

[MAD07] H.D. Madhawa Hettiarachchi, M. Golubovic, W.M. Worek, Y. Ikegami, "Optimum design criteria for an Organic Rankine cycle using low-temperature geothermal heat sources", Energy 32 (2007) 1698–1706.

[MAG08] P.J. Mago, L.M. Chamra, K. Srinivasan, C. Somayaji, "An examination of regenerative organic Rankine cycles using dry fluids", Applied Thermal Engineering 28 (2008) 998–1007.

[OLI02] A.C. Oliveira, C. Afonso, J. Matos, S. Riffat, M. Nguyen, P. Doherty, "A combined heat and power system for buildings driven by solar energy and gas", Applied Thermal Engineering 22 (2002) 587-593.

[PAE06] M. De Paepe, P. D'Herdt, D. Mertens, Micro-CHP systems for residential applications, energy conversion and management 47 (2006) 3435-3446.

[PRA06] B. Praetorius, L. Schneider, Micro cogeneration: Towards a decentralized and sustainable German energy system, 29th IAEE International Conference, Potsdam, 7-10 June 2006.

[PRE06] H. Prévot, J. Orselli, "Le réseaux de chaleur", Rapport pour le ministère de l'économie et de l'industrie, 2006.

[REN08] H. Ren, W. Gao, Y. Ruan, "Optimal sizing for residential CHP system" Applied thermodynamic Engineering 28 (2008) 514-523.

[RIF04a] S.B. Riffat, X. Zhao, "A novel hybrid heat pipe solar collector/CHP system - Part I: System design and construction », Renewable Energy 29 (2004) 2217–2233.

[RIF04b] S.B. Riffat, X. Zhao, "A novel hybrid heat-pipe solar collector/CHP system - Part II: theoretical and experimental investigations", Renewable Energy 29 (2004) 1965-1990.

[RTH00] Règle Th-C, arrêté du 1er décembre 2000 portant approbation des méthodes de calcul Th-C, modifié et complété par l'arrêté du 22 janvier 2004.

[WEI07] D. Wei, X. Lu, Zhen Lu, J. Gu, "Performance analysis and optimization of organic Rankine cycle (ORC) for waste heat recovery", Energy Conversion and Management 48 (2007) 1113–1119.

[YAG06] W. Yagoub, P. Doherty, S.B. Riffat, "Solar energy-gas driven micro-CHP system for an office building", Applied Thermal Engineering 26 (2006) 1604-1610.

[YAM01] T. Yamamoto, T. Furuhata, N. Arai, K. Mori, "Design and testing of the Organic Rankine Cycle", Energy 26 (2001) 239–251.

[ZHA06] X.R. Zhanga, H. Yamaguchia, D. Unenoa, K. Fujimab, M. Enomotoc, N. Sawadad, "Analysis of a novel solar energy-powered Rankine cycle for combined power and heat generation using supercritical carbon dioxide", Renewable Energy 31 (2006) 1839-1854.

CHAPITRE 5 – A year-round dynamic simulation of a hybrid wood-solar ORC system

1. Introduction

In the previous chapter, an optimization study has been performed identifying the optimum operating parameters of the SWORC-μCHP. The parameters that affect slightly the system thermodynamic and economic performances have been identified. Results have shown that the boiling temperature, working fluids, and the solar collector surface area have the major impacts on the system performances. It was shown that it does not exist a single optimum for the thermodynamic and the economic performances. Therefore, a balance has to be found between the optimal thermodynamic operating parameters and the economic operating parameters.

In this chapter, a year-round dynamic simulation is performed for the different systems, building types, and locations. MATLAB/SIMULINK, PLEAIDE/COMFIE [PEU90], and REFPROP 7.0 [REF06] simulation tools are used to model and analyze the performance of the hybrid solar-wood ORC system.

First, the mathematical model description of the whole system is presented as modeled under the SIMULINK environment, without the building model sub-system developed under the COMFIE/PLEAIDE, a program dedicated for multi-zone building dynamic simulation.

Then, two Rankine cycle systems are proposed:

- the first is composed of off-the-shelf components
- the second is a potential system, with more efficient components that could be commercialized in the near future.

The year-round simulation will be performed to identify the effect of those two Rankine systems on the overall operation of the system when installed in a real house. The primary energy saving potential of the residential micro-CHP systems depends mainly on the system sizing, especially the capacity of the micro-CHP prime movers. If the capacity of the micro-CHP prime movers is underestimated, the effect of introducing the system becomes relatively small, and if they are overestimated, the economical feasibility decreases. For residential buildings, the thermal energy demand fluctuates seasonally and hourly, so it is necessary to take into account the variation of heat demand to establish annual operational strategies. In addition, an operation strategy needs to integrate the availability of the solar energy and its seasonal and hourly fluctuations. Therefore, it is necessary to develop a rational method of determining system size and operational strategies throughout the year.

To take into consideration the effect of prime movers, a reverse technique has been adopted where micro-CHP prime movers will be fixed and several heat load demands will be varied depending on the residential building insulation level and the corresponding location. Therefore, for each residential building selected, different simulations will be conducted taking into account the two Rankine systems, the location, the storage tank volume, and the solar collector surface area.

2. Description of the hybrid solar-wood micro-CHP system

The system is divided into five sub-systems (see Figure 5.1): the solar collector, the wood-pellet boiler, the Rankine cycle, the hot water storage tank, and the building represented by its thermal needs. The wood-pellet boiler is used to supply the heat to the Rankine cycle system as a main energy source of the system. The solar thermal collector is used as a

second source of energy, whose availability depends on the location and the daytime. The solar energy could be considered, as the main energy source when the energy delivered by the solar collectors covers more than 50% of the total required energy.

For a stable operation of the system, a hot storage tank is included. The thermal energy generated by the preheater and the condenser is delivered to the hot water stored in the storage tank via a heat exchanger. A second heat exchanger is integrated in the hot storage tank to produce domestic hot water at a constant temperature. The regulation of the temperature of the domestic hot water is maintained by a three-way valve, controlled by a temperature sensor by changing the ratio of hot water and cold water mixed by the valve. However, the water stored in the tank is circulated in the hydrolic network to deliver the space heat required. The temperature of the hot water entering the different radiators will be controlled by a three-way valve depending on the ambient temperature.

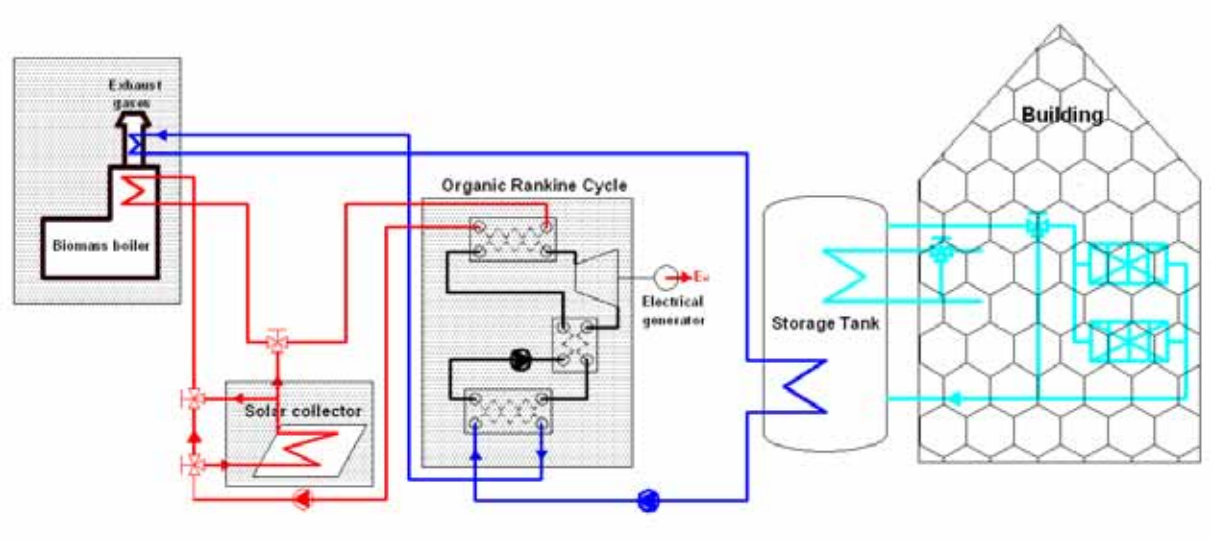

Figure 5.2 – Wood-Solar micro-CHP system in a residential building.

In Chapter 3, the possible technologies to be used and the technical barriers to overcome in order to introduce the Rankine system into practical application have been identified. Except for the Rankine turbine, all other components are off-the-shelf components and could be custom designed to meet a wide range of output powers.

The plate heat exchangers made of stainless steal and copper brazed appear to be the most suitable technologies to be used as boilers and condensers. The Rankine pump is a diaphragm pump that could handle a wide range of flow capabilities with no viscosity restriction.

The solar collectors are evacuated tube collectors with integrated parabolic mirror with low concentration ratio. These types of solar collectors are most suitable for application with temperatures ranging from 120°C to 180°C. A fully automated wood-pellet boiler is selected since it represents a high thermal efficiency with the capabilities of cooling exhaust gases at low temperatures (~ 100°C) and extracting available heat from the exhaust gases.

Because micro turbines, designed for a small-scale Rankine cycle, are difficult to find on the market, the Rankine cycle turbine is converted from available volumetric compressor technologies. These turbines will not be able to cover all the mechanical output powers required by the micro-CHP system and these turbines will be limited in their maximum operating pressures and temperatures, in addition to their flow capabilities and expansion ratios. The maximum output power of these turbines and their corresponding efficiencies will be discussed in details in following sections.

2.1 Micro-CHP led control strategy

In this chapter, the heating led control dispatch strategy (the system will be controlled depending on the thermal needs) is adopted coupled to a large storage tank. This method consists of decoupling the heat load demand and fluctuation from the operation of the micro-CHP system. The thermal energy generated by the micro-CHP system is fully stored in the storage tank; therefore, when the storage tank is at its maximum temperature of 75°C the micro-CHP system is turned off. The micro-CHP system is turned on only when the storage tank temperature is lower than 55°C. The storage tank is considered "empty" or "full" depending on the storage tank temperature. In this study, the tank maximum temperature is fixed at 75°C and the minimum temperature at 55°C. The generated electricity can be delivered to the grid or used locally. It depends on the operator strategy based on economical criteria discussed in Chapter 1.

3. Simulation of a hybrid solar-wood micro-CHP system coupled to a building using MATLAB/SIMULINK software

In this study, the PLEIADE-COMFIE [PEU90] and MATLAB/SIMULINK simulation tools are used to model and analyze the performances of the hybrid solar-wood micro-CHP system. PLEIADE-COMFIE is a dynamic simulation program developed at the CEP and dedicated to the dynamic simulation of multi-zone buildings. MATLAB/SIMULINK is a mathematical environment capable to handle dynamic simulations. Recently, a special tool SIMBAD (Simulator of building and devices) has been developed under this environment including different standard components for heating and ventilation simulation systems. This toolbox with other existing toolbox (Neural network, fuzzy logic, and optimization) offers a very powerful and efficient tool for the application listed above. SIMBAD has a modular structure that it is widely used for analysis of time dependent systems, such as solar and hydraulic systems. The whole system is modeled in SIMULINK environment, and it is divided into five sub-systems: the solar collector subsystem, the wood-pellet boiler sub-system, the Rankine cycle subsystem, the storage tank model, and the heating and domestic hot water load (see Figure 5.1).

The following sections describe the detail of the hybrid solar-wood micro-CHP system, as shown in Figure 5.3, followed by the simulation model of the components. Several simulations for one year will be performed to compare different operating conditions. Two types of buildings and locations will be considered for the simulations, representing various heating and domestic hot water loads. Two different Rankine cycles (SRC and ORC) will be compared based on their performances and their applicability from a technical point of view. In addition, the effect of the hot storage tank volume and solar collector surface area on the system annual performance will be evaluated.

3.1 Hybrid Solar-Wood micro-CHP system model description

Simple thermal systems can be simulated using mathematical model that consists in developing simple mathematical equations that can be solved analytically. However, complex thermal systems, such as the SWORC-μCHP system previously described, cannot be simulated using only such simple mathematical models. The reasons include incomplete models, model complexity, and component interdependency. Some of the input data and functions required for the dimensioning models, particularly for the turbine model, are not available. A complex numerical thermo-hydraulic model should be developed for the steady-state simulation of the system.

Furthermore, steady state design cannot fulfill all requirements for the simulation objectives. The ORC is designed with a simple steady state model since there is no regulation imposed to the expander operation. In the SPTC, the complexity of the control system and the high inertia of the thermal components require a dynamic model to predict the performance of the components and effects of the interaction between controllers.

The easiest way to obtain information on the dynamic behavior of the thermal and power system generation system requires simulating the evolution of the significant parameters. Any thermal and power system can be considered as a set of elements and hence could be sub-divided into blocks known as the “compartment approach”. For example, the fundamentals blocks of a thermal and power system include a boiler, a pump, a turbine, and valves.

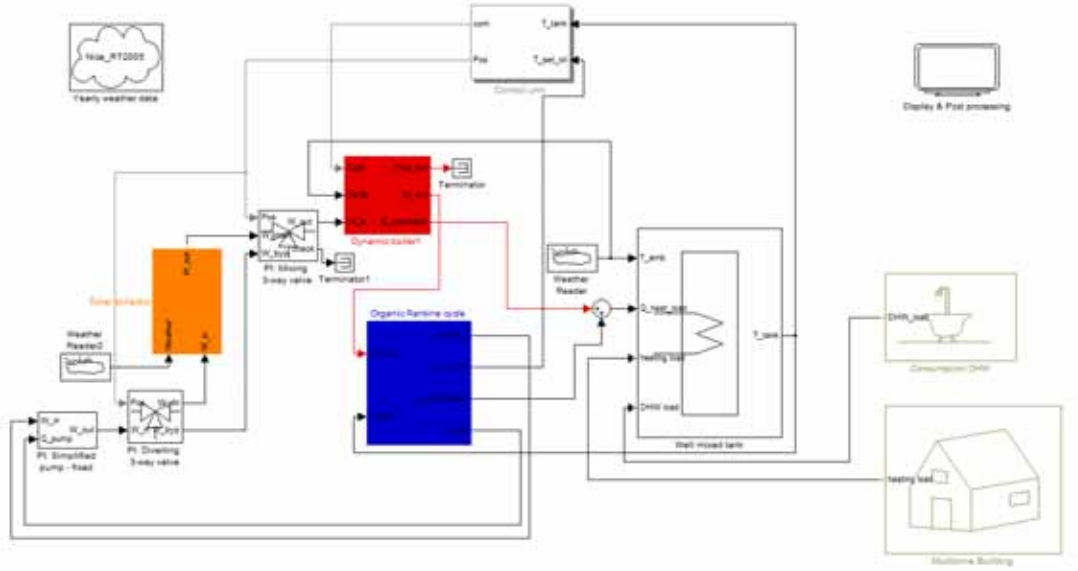

Figure 5.3 – Flowchart of the simulation software.

Along this thesis a computer program code COGENSIM (Cogeneration simulator) has been developed to simulate a thermal and power generation system by means of customized blocks. Any given block is modeled by a lumped formulation of conservation equations [ARP66].

Using the above elements, the evolution of the parameters is given by solving the mass and energy conservation equations. The mass and thermal energy balances are implemented as a block equation for each component of the system. In order to write these equations, each block is modeled as an unsteady open system, and the mechanical energy balance is written as a loop equation. More specifically, the thermal loop behavior operating in an unsteady mode comes from the simultaneous solution of the fluid flow and the thermal problems.

The fluid flow problem consists of determining the mass flow rate and pressure losses in each block (block represents a component such as solar collector or wood boiler). Following the above procedure, neglecting the mass accumulation in each block, the equation of the fluid flow problem may be written in the following form.

For the m_{th} block, the net mass flow rate must be zero:

$$\sum_{k=1}^{K} \dot{m}_{k,m} = 0 \tag{5.1}$$

In order to determine the mass flow rates through every component, Eq. (5.1) has to be written for every system block.

The thermal problem consists of determining the temperature values at the outlet of the blocks of the system. As for the fluid problem, the application of the above procedures leads to the thermal energy balance equation being written as follows for the m_{th} block.

$$\sum_{m=1}^{M} \dot{m}_{k,m} \left(e_{p,k} + e_{c,k} + c_p T_k \right)_m + \frac{\partial}{\partial \tau} \int_{V_m} \rho e dV = \frac{dQ_m}{d\tau} - \frac{dL_m}{d\tau} \tag{5.2}$$

In general, the contributions due to the kinetic and potential energies are small in comparison with the enthalpy term in the context of the present work and may be neglected. Since the problem is time-dependent, the time derivative of the total energy in the m_{th} block is calculated on the basis of the well-mixed condition [HOL88]. Based on those assumptions, the integral in Eq. (5.2) can be calculated as follows:

$$\frac{\partial}{\partial \tau}\int_{V_m} \rho e dV = C_m \frac{dT_{o,m}}{d\tau} \tag{5.3}$$

Where C_m is the effective thermal capacitance of the m_{th} block. Assuming the well-mixed condition, in Eq. (5.3) the temperature considered in the time derivative is the outlet temperature of the m_{th} block. For the nodes of the Rankine system, the effective thermal capacitance is considered negligible.

Therefore, after establishing mathematical models of different components, the final system of non-linear differential equations is solved using MATLAB. In order to gain an easy introduction of the equations in the code, the graphical opportunities given by Simulink are used. Also for a thermal and power system with a small number of components, the non-linear system of ordinary differential equations (ODEs) described above can only be solved numerically. Simulink solves the set of ODEs numerically through an algorithm of Explicit Fixed-Step Continuous Solver like Runge-Kutta and Implicit Fixed-Step Continuous Solver, which use a combination of Newton's method and extrapolation from the current value to compute the value of a model state at the next time step.

The HVAC toolbox SIMBAD (Simulator of building and Devices) has been developed within the MATLAB/SIMULINK environment. This toolbox with other existing toolboxes (Neural network, fuzzy logic, optimization) offers a very powerful and efficient tool for the application listed below.

The toolbox is made up of 11 groups of models and utilities and 1-group examples of installations with various HVAC heating or cooling system. Models are developed either completely in the SIMULINK block diagram language, in MATLAB code or in compiled C-code. Source codes of modules written in C-Language or MATLAB language are provided. The open structure of the models enables users to modify them and adapt the models.

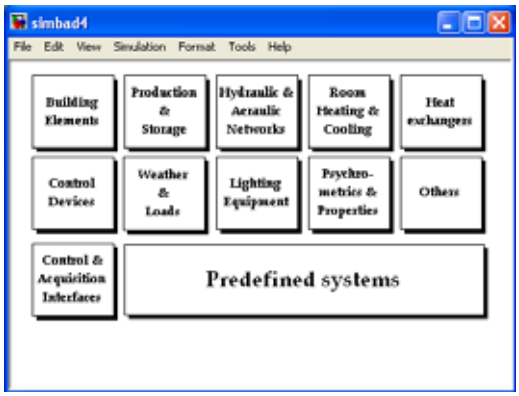

Figure 5.4 – SIMBAD library.

All toolbox models are implemented using the graphical Simulink environment, so the user can understand the physical phenomena taking place in the component.

3.2 Solar collector model

The solar collector selected is assembled by the German microtherm energietecknik GmBH, and comprises six vacuum tubes produced by Shiroky (Japan) as described in Chapter 3. The collector has a gross area of 1.191 m^2 and a weight of 17 kg. The simulation model is based on a lumped capacitance model proposed by Perers and Karlson [PER93]. It considers separate incident angle modifiers for direct and diffuse solar radiation. These modifiers are variables in the model and are estimated from experimental data. The useful heat gained by the solar collector is calculated from the heat balance in the solar collector given by Eq. (5.4).

$$\dot{q}_{sc} = \dot{m} c_p \left(T_{out} - T_{in}\right)$$
$$\dot{q}_{sc} = \eta_0 K_{\theta b}(\theta) G_b + \eta_0 K_{\theta d}(\theta) G_d - c_1 \left(T_m - T_a\right) - c_2 \left(T_m - T_a\right)^2 - c_{eff} \frac{dT_m}{dt} \quad (5.4)$$

Where the collector parameters are η_0, $K_{\theta b}(\theta)$, $K_{\theta d}(\theta)$, c_1, c_2 and c_{eff}. The incidence angle dependence $K_{\theta b}(\theta)$ for beam radiation is conveniently modeled with the standard b_0 equation for some collector design. However, the collector considered in this work is optically nonsymmetrical. Therefore, the biaxial incident angle modifiers $K_{\theta b}(\theta)$ and $K_{\theta d}(\theta)$ have been measured and are defined as follows:

- $K_{\theta b}(\theta)$ is the incident angle modifier referred to the angle varying between the collector normal and its longitudinal axis.
- $K_{\theta b}(\theta)$ is referred to the angle given by the normal direction and the transverse direction.

For a vacuum tubular collector, the longitudinal direction is determined by the axis of the tubes, while it is given by the length for a flat plate collector. Therefore the incidence angle modifier of the selected solar collector is given by [BRU94] and presented in Figure 5.5.

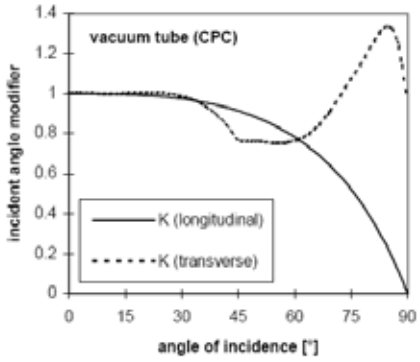

Figure 5.5 – Incidence angle modifier functions for the solar collector tested.

Figure 5.6 shows the different model layers of the solar collector that are implemented for the calculation of the solar irradiance and the thermal model of the solar collector. On the other side, Figure 5.7 shows the graphical interface, which is used to define the different characteristics of the solar collector: surface area, heat loss coefficient, mass and initial conditions.

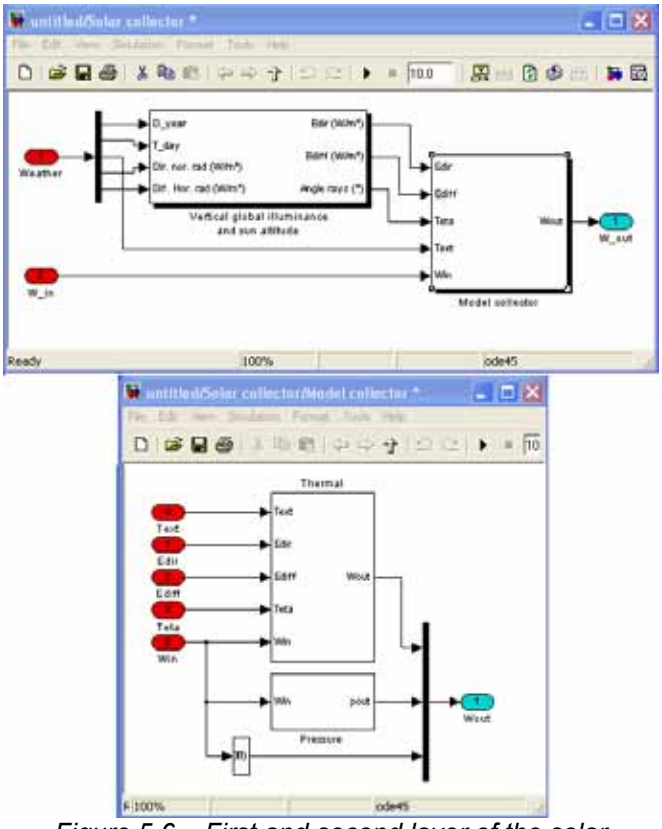

Figure 5.6 – First and second layer of the solar collector model.

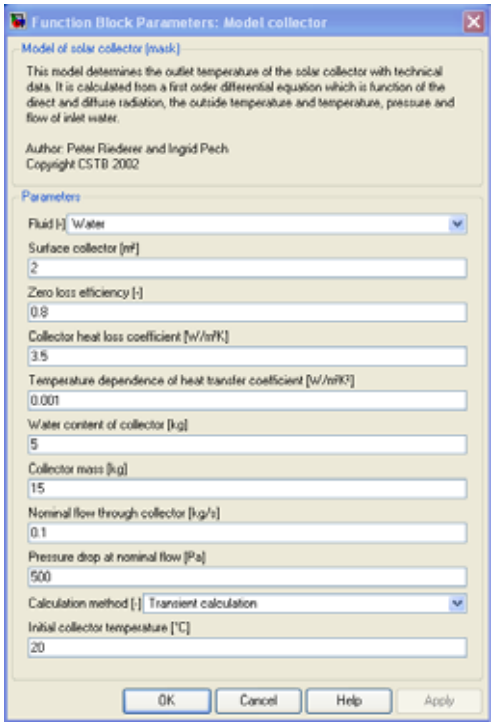

Figure 5.7 – The user-interface for the solar collector.

The different parameters of the solar collector used in the simulation program are listed in Table 5.1 given by [BRU94].

Table 5.1 – Solar collector parameters.	
Solar collector type	Vacuum tube (CPC)
η_0	0.547
c_1	0.651
c_2	0.003

3.3 Wood-pellet boiler model

Wood-pellet boiler models have been under investigation by Nordlander [NOR04], he has developed a mathematical model for the simulation of a Pellet stove with liquid heat exchanger. This model has been implemented in TRNSYS known as type 210 and validated by different measurements. The model has been developed to simulate a biofuel stove with liquid heat exchanger to deliver energy to the ambient air and to a liquid stream. The model incorporates two thermal masses for modeling the dynamic behavior of the stove. The model takes into account the start and stop sequence since in these phases a non-negligible part of energy is delivered and possibly a major part of the emission of harmful substances may be emitted.

The model developed has not been validated for a pellet burner integrated with a boiler. The combustion part of the model is probably good enough, but the two-node model of the thermal masses may be too simplified for modeling the heat losses to the room, the heating of the liquid and the dynamics of the boiler.

Therefore, to be more realistic, only the combustion model has been used for the simulation of the wood-pellet combustion in our model (see appendix C). Therefore, the dynamic model of the boiler (see appendix D), which is available in the library of the SIMBAD tool, has been modified to include the combustion model developed by Nordlander [NOR04].

The dynamic model of the boiler allows calculating the water outlet temperature in dynamic conditions. In addition, this model takes into account the heat losses from the boiler to the surroundings in both standby and operation modes, and it allows to calculate the outlet temperature of the exhaust gases. A heat exchanger has been added to the boiler model to recover the energy available in the exhaust gases if the temperature of the exhaust gases is higher than 100°C and this is mainly possible due to the higher operating temperature of the heat transfer fluid which is a function of the boiling temperature of the working fluid in the Rankine cycle. This heat exchanger has been dimensioned to allow a cooling of the exhaust gases to almost 100 °C.

3.4 Thermodynamic cycle model

A numerical model has been developed, using MATLAB coupled to REFPROP 7.0, in order to simulate the Rankine thermodynamic cycles operating with different working fluids. This model has been integrated as a subsystem in the simulation tool.

The development numerical model (see Figure 5.8) takes as input data, the working fluid, both condenser and boiler operating temperatures, the sub-cooling at the pump inlet and the superheat at the turbine inlet and the electrical output power. The turbine total efficiency, including both isentropic and mechanical efficiencies and the pump overall efficiency should be also provided as input data.

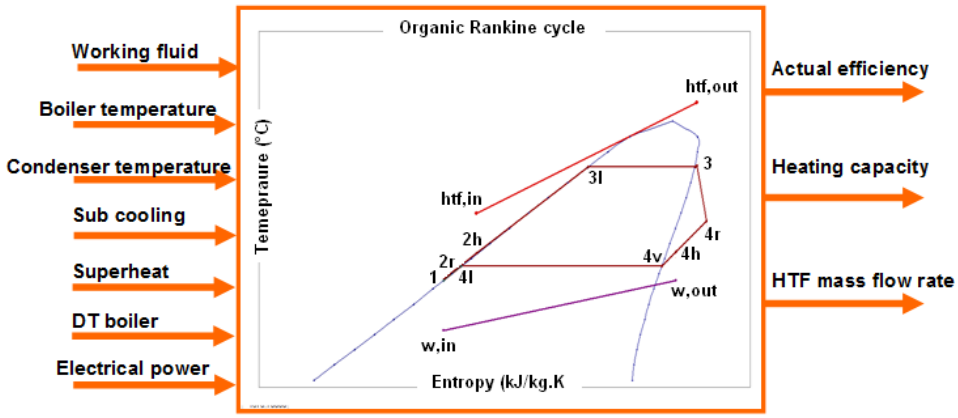

Figure 5.8 – Thermodynamic cycle model.

The mathematical formulations of the ORC components are described as follows: the mass flow rate of the working fluid is calculated by dividing the net work by the turbine work minus the pump work given by Eq. (5.5).

$$\dot{m}_{wf} = \frac{\dot{W}_{net}}{\left(\eta_t \left(h_3 - h_{4s}\right) - \left(h_2 - h_1\right)/\eta_p\right)} \tag{5.5}$$

The pump work is calculated by multiplying pressure change with the working fluid volume at the pump inlet and given by Eq. (5.6).

$$W_p = \nu_1 \left(P_2 - P_1\right)/\eta_p \tag{5.6}$$

The heat rejected by the condenser is obtained by calculating the enthalpy difference and multiplying it by the working fluid mass flow rate (MFR) (Eq. (5.7)).

$$\dot{Q}_{cond} = \dot{m}_{wf} \left(h_{4r} - h_1\right) \tag{5.7}$$

Heat received through the heat exchanged from the HTF to the ORC working fluid is found also by multiplying enthalpy difference by the working fluid MFR.

$$\dot{Q}_{boiler} = \dot{m}_{wf} \left(h_3 - h_{2p}\right) \tag{5.8}$$

For dry working fluids, the working fluid is still superheated at the turbine outlet as shown in chapter 2. Recovery is introduced to improve energy efficiency of the ORC system by utilizing the available heat at the turbine outlet to preheat the working fluid at the boiler inlet through a heat exchanger. The heat transferred by this internal heat exchanger is calculated by Eq. (5.9).

$$\dot{Q}_{preheater} = \varepsilon Min\left\{\left(h_{4r} - h_{4v}\right); \left(h\left(T_{4r}, P_{boiler}\right) - h_1\right)\right\} \tag{5.9}$$

Eqs. (5.10) and (5.11) are used to model the ideal Rankine cycle and actual efficiencies:

$$\eta_{RC,ideal} = \frac{W_{t,ideal} - W_{p,ideal}}{Q_{boiler}} = \frac{\left(h_3 - h_{4is}\right) - \left(h_2 - h_1\right)}{h_3 - h_{2h}} \tag{5.10}$$

$$\eta_{RC,actual} = \frac{W_{t,actual} - W_{p,actual}}{Q_{boiler}} = \frac{\left(h_3 - h_{4r}\right) - \left(h_{2r} - h_1\right)}{h_3 - h_{2h}} \tag{5.11}$$

The heat transfer fluid mass flow rate has been calculated by applying the heat balance equation to the boiler and fixing the pinch point (the minimum temperature difference at the

saturation liquid state of the working fluid) at 10 K. Therefore, the mass flow rate required will be generated by the ORC model as an output parameter (see Chapter 2).

3.5 Thermal storage model

A short-term thermal storage is one of the key components of solar domestic hot water systems and systems associating domestic hot water and space heating generation, called combi-systems. Storages for this kind of application are often equipped with heat exchangers that are located inside the hot storage tank. This type of thermal storage is used in our CHP system to prevent short on-off operation of the micro-CHP.

Generally, in a solar system, the thermal storage is charged via a heat exchanger since the working fluid of the collector loop is usually a mixture of water and MPG (mono-propylene-glycol).

For the simplicity of the analysis of the storage tank and to reduce the calculation time, a fully mixed storage tank [DIN02] is considered for the calculation. In this model, it is assumed that the bulk of liquid stored in the tank has a uniform temperature (no stratification), which changes along the time as a result of the energy balance variations in the storage tank due to the charge and discharge processes and due to the heat losses to the surroundings. The model representing this thermal balance is given by Eq. (5.12).

$$MC_p \frac{dT_{\tan k}}{dt} = \sum_{i=1}^{N} \dot{Q}_i - U_{ext} A_{ext} \left(T_{\tan k} - T_a \right) \qquad (5.12)$$

Eq. (5.12) is solved numerically for the initial temperature condition equal to the average temperature of the liquid in the tank. In this equation M is the mass of water in the tank, A is the heat loss surface area, and U is the overall heat transfer coefficient. Characteristics of the storage tank are given in Table 5.2.

Table 5.2 – Storage tank characteristics.

Parameters	Value
Volume (l)	500 – 4000
Thickness of insulation (m)	0.05
Initial temperature (°C)	71
Conductivity of the insulation material (W/m.K)	0.025

4. Building model

Houses considered for the simulation are built by the company LES AIRELLES that has completed the construction for the first labeled passive houses in France (see Figure 5.9). These houses are composed of two attached houses, of 132-m^2 SHON[1] surface each, and their design is in compliance with the Passivhaus standard.

Figure 5.9 – LES AIRELLES houses.

These houses have been initially designed to be heated with small heat pump with hot water production. The cooling is achieved by a ground-to-air heat exchanger coupled to a heat recovery ventilation unit to minimize heat losses. In this study, houses geometric data will be used for thermal simulations, for different levels of insulation, and for two different locations Nice and Trappes, which are considered in the climate zone H3 and H1 respectively.

[1] Surface hors-œuvre nette

4.1 Building description

Houses are composed of two attached two-story dwelling units, of 132-m^2inhabitable area each, designed for a family of four persons. Other than the house, they comprise a garage, a terrace, a balcony, and a garden. Rooms are identical in each house: a hall, an office, a living room and a kitchen downstairs, and three bedrooms, one bathroom, and a sitting room upstairs. The orientation is the same for both dwellings. Two different levels of insulation have been considered to comply with the French thermal regulation, RT2005 and the label BBC-EFFINERGIE. Figure 5.10 and Figure 5.11 show the ground floor and the first-floor plan respectively.

Figure 5.10 – Lay-out of the ground floor.

Figure 5.11 – Lay-out of the first floor.

Energy performances of the same building (dimensions, orientation, timber structure) have been calculated with different levels of insulation and air tightness set according to the reference level defined by RT2005 thermal regulation. The description of standard building envelope characteristics and thermophysical properties of building materials require input parameters, and are presented in Table 5.3 and Table 5.4 for standard and BBC building respectively. The construction components of the building consist of external walls and roof. The exterior wall has a wood structure with polystyrene and cellulose. The main difference between the constructions of the exterior wall of the two building types is the insulation thickness. The BBC building roof is made of gypsum board and cellulose, and that of the standard building is made of cellulose; the insulation thickness is not similar. The slab is made of concrete and polystyrene (on crawl space).

The standard building windows are double glazed with external blinds; the BBC house windows are triple glazed. The standard building external doors are made mainly of wood whereas those of the BBC building are polystyrene insulated.

Table 5.3 – Characteristics of the standard building envelope materials.

Building components	Material	Thickness (cm)	Thermal conductivity (W/m.K)	U-value ($W/m^2.K$)
Exterior wall	Wood Polystyrene Cellulose	1 13 2.5	0.23 0.05 0.36	0.35
Slab	Concrete Polystyrene Concrete Gypsum	15 14 10 5	1.75 0.04 1.75 1.70	0.27
Roof	Cellulose Gypsum	22.5 1.3	0.05 0.36	0.2
	Description		Solar factor	U-Value
Windows	Double-glazed		0.66	1.8
External doors	Wood		0	1.5

Table 5.4 – Characteristics of the BBC building envelope materials.				
Building components	Material	Thickness (cm)	Thermal conductivity (W/m.K)	Thermal capacity (kJ/kg.K)
Exterior wall	Wood Polystyrene Cellulose	1 38 2.5	0.23 0.05 0.36	0.12
Slab	Concrete Polystyrene Concrete Gypsum	15 20 10 5	1.75 0.04 1.75 1.70	0.19
Roof	Cellulose Gypsum	40 1.3	0.05 0.36	0.11
	Description		Solar factor	U-Value
Windows	Triple-glazed		0.52	0.71
External doors	Wood		0	0.78

The thermal bridges considered here for the standard building are 0.4 W/m.K for the edge concrete slab, plus a standard heat loss of 0.5 W/m.K multiplied by the building perimeter, representing all the thermal bridges. A 0.6-vol/h air infiltration has been considered for the simulation.

For the BBC building, a thermal bridge of 0.1 W/m.K for the edge of the concrete slab and attic floor has been considered. A 0.58-vol/h air infiltration has been measured from a blowing door test under a differential pressure of 50 Pa.

4.2 Weather data

Local weather information is required as input for the dynamic building and solar collector model. For instance, the solar radiation and convection by the surrounding air are the dominant factors of building heat transfers. Inputs for the building simulation are ambient temperature, solar radiation, wind speed, and humidity. The meteorological annual data of Nice and Trappes are used in simulations. These data are an average of 10 years of measurements and they are readily available to be used in a computer simulation.

Figure 5.12 shows the annual temperature profile of Nice and Trappes; the maximum and minimum temperatures in Nice are respectively 30.3°C and 3°C. However, in Trappes the maximum and minimum temperatures are respectively 31.8°C and -5.9 °C. Throughout the year, Trappes is a colder area compared to Nice and higher heating demands are required in this area.

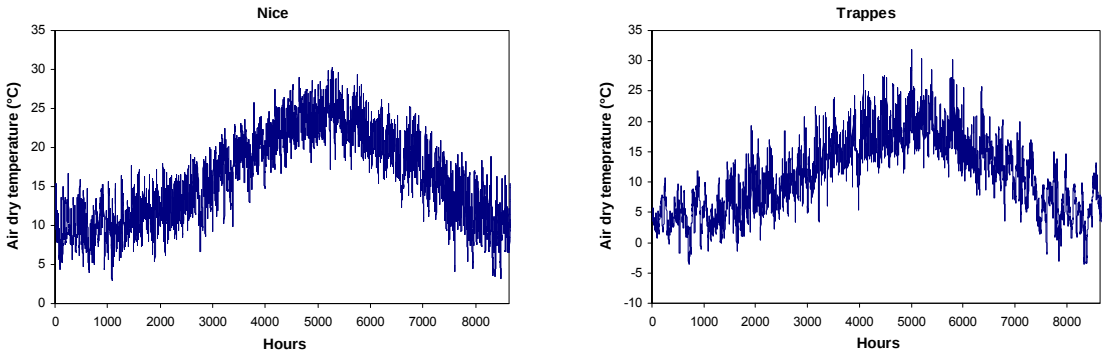

Figure 5.12 – RT2005 ambient temperature profiles.

The average annual global irradiance incidents on a solar collector surface inclined 45° are respectively 1023 kWh/m^2.year and 1498 kWh/m^2.year for Trappes and Nice. It can be seen in Figure 5.13 that the highest solar energy irradiance could reach 1400 W/m^2 for winter days (but for very short period of time) when the diffuse irradiances are largely high. However, in

summer the direct solar energy incidence represents the highest ratio of global solar energy incidence. Therefore it can be seen that the maximum solar irradiance in summer could go up to 1000 W/m^2 in Nice but in Trappes the diffuse solar energy has the major influence on the overall solar energy irradiance. The solar energy available in Nice is significantly larger than in Trappes. This will have a major impact on the performance and the total energy absorbed by the solar collectors.

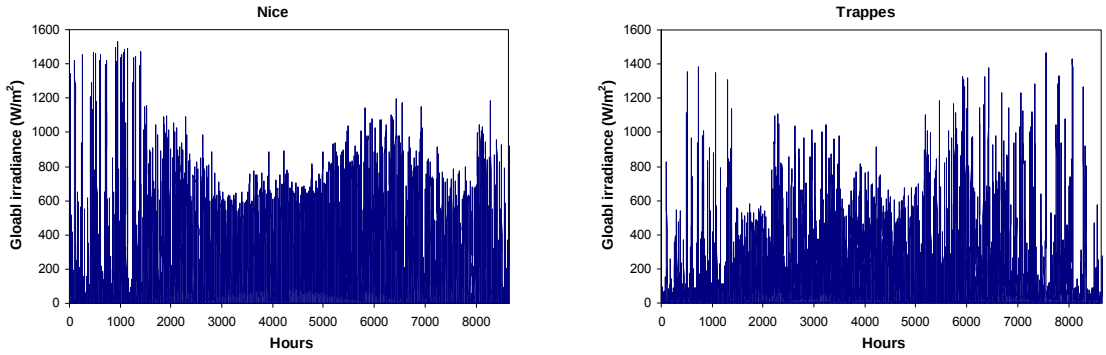

Figure 5.13 – Standard RT2005 global radiation data.

4.3 Domestic hot water model

The DHW consumption profile used in the present study is given in Appendix D. The energy required for hot water heating depends on the city water temperature. The city water temperature depends mainly on the location and the period. Therefore, a monthly average value has been considered for Nice and Trappes (see Figure 5.6). The main temperature varies from 5.7°C in February to a 15.3°C in August in Trappes. In Nice, the temperature fluctuates between 9.7 °C in February and 19.3°C in August. Considering that water is heated to a set point temperature of 55°C (Instantaneous DHW generation) in both Trappes and Nice, the annual hot water load is lower in Nice.

Table 5.5 –Cold water temperature (°C) for two climate zones.

Location	1	2	3	4	5	6	7	8	9	10	11	12
H3 (Nice)	9.7	9.7	11.0	13.2	15.8	18.0	19.3	19.3	18.0	15.8	13.2	11.0
H1 (Trappes)	5.7	5.7	7.0	9.2	11.8	14.0	15.3	15.3	14.0	11.8	9.2	7.0

A daily consumption of 180 L for a four-person family is considered. However, when designing a home with low-energy consumption as houses complying with the BBC-EFFINERGIE, a reduction in domestic hot water consumption is necessary to achieve lower primary energy consumption. Therefore, for houses with low-energy consumption, the annual domestic hot water consumption has been considered 90 L/day (a very optimistic assumption but it could be achieved with other technologies such as energy recovery available in the waste hot water [NEH08]. Figure 5.7 shows the hourly domestic hot water profile for the standard house and for the two climate zones. The peak domestic hot water demands are approximately 5 and 4.6 kW respectively for Trappes and Nice. For the BBC house, the peak loads will be respectively 2.5 and 2.3 kW.

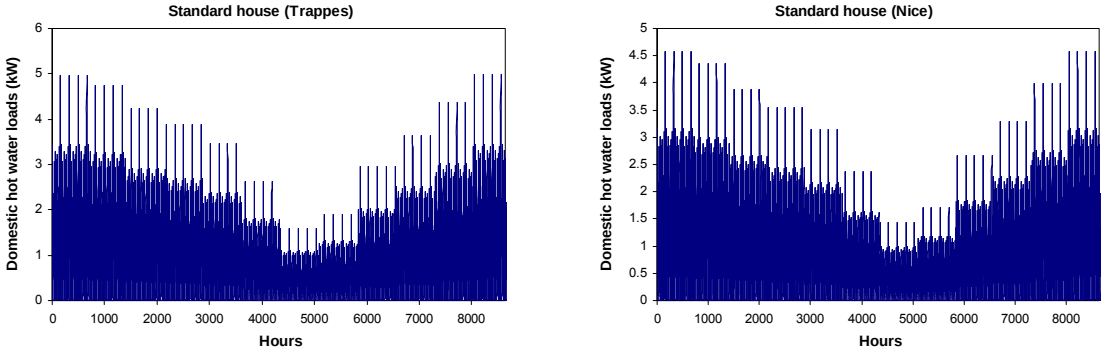

Figure 5.14 – Hourly domestic hot water load profiles.

The annual domestic hot water consumptions for the standard building are respectively 6854 and 6248 kWh for Trappes and Nice, and these values will be divided by two for low energy consumption buildings (BBC). Therefore, the domestic hot water consumption for the two houses will be respectively of 26 kWh/m^2.year and 24 kWh/m^2.year for Trappes and Nice; for the BBC houses the consumption will be divided by two.

4.4 Thermal simulation and heating loads

The two types of houses (BBC and RT2005) have been modeled and simulated using the thermal dynamic simulator COMFIE. As said before, COMFIE is a multi-zone simulation tool using a finite-volume method associated with a modal reduction technique [PEU90]. Thus, the simulator has modeled the energy loads in each building for heating periods and for the two different climate zones.

The results shown in this section are based on the two houses described in Table 5.3 and Table 5.4. Figure 5.15 shows the hourly heating needs for Nice and Trappes and for the two different types of buildings. Annual space heating energy required for the standard and the BBC buildings in Trappes are 19 876 and 6 194 kWh respectively. The peak heating load for the standard and the BBC buildings are 11.5 and 5.5 kW respectively. For Nice, the annual space heating energy for the standard and the BBC buildings are 4 775 and 366 kWh respectively and the peak heating loads are approximately 6.5 and 2.3 kW.

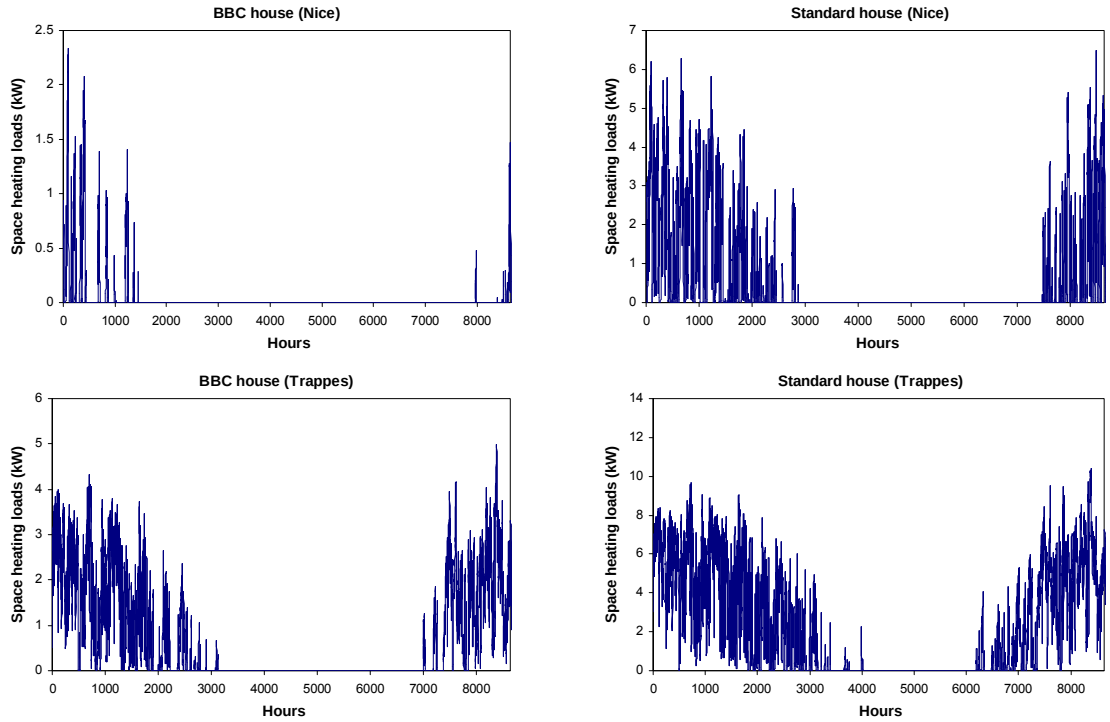

Figure 5.15 – Hourly space heating loads for Standard and BBC houses for two climate zones (Nice/Trappes).

Results of simulations for heating and domestic hot water generation are presented in Table 5.6. The total energy consumptions for the standard building are 101 and 41 kWh/m^2.year for Trappes and Nice respectively. Using the primary energy factor (1-kWh primary energy per kWh gas), the corresponding primary energy consumption would be respectively 101 kWh$_{pe}$ and 41 kWh$_{pe}$. Thus the standard building complies with the RT2005 (130 kWh$_{pe}$ and 80 kWh$_{pe}$ respectively for climate zones H1 and H3). The difference between values corresponds, in general, to the electrical consumption of auxiliaries. For the BBC house, the same calculation has been performed and the primary energy consumptions would be 36 kWh$_{pe}$ and 13 kWh$_{pe}$ respectively for Trappes and Nice. Thus, the passive design complies with the BBC-EFFINERGIE label, which implies to have primary energy

consumptions for new construction buildings lower than 50 kWh_{pe} and 40 kWh_{pe} respectively for zones H3 and H1.

Table 5.6 – The annual total energy consumption for space heating and DHW.			
Location and type	Peak energy consumption (W)	Annual total energy consumption (kWh)	Annual total energy consumption (kWh/m^2)
Trappes - Std	16500	26730	101
Trappes - BBC	8100	9621	36
Nice - Std	11100	11023	41
Nice – BBC	4600	3490	13

5. Optimum Rankine cycle design

The Organic Rankine cycle design depends mainly on components available on the market. Two different Rankine cycles are distinguished. The first cycle namely "Off-the-shelf Rankine cycle" that could be designed based on components currently available on the market (cf. Chapter 3). This system exhibits moderate energy performances since all components are not designed for optimum operating conditions. The second Rankine cycle namely "Advanced Rankine cycle" is composed of components that could be commercialized in the near future and present higher energy performances compared to available technologies.

5.1 Thermodynamic simulation and Rankine cycle electrical output

Rankine cycles could be distinguished according to working fluids. The first system, steam Rankine cycle, uses water as a working fluid with an oil-free scroll expander and has been tested previously. The second system, organic Rankine cycle, uses organic fluids with a scroll expander. The average heat to power ratio of the micro-CHP based on ORC is 9; to meet all heating needs in the buildings, a-1 kW_{el} electrical output power has been proposed in order to obtain fair comparison for both systems.

5.1.1 Off-the-shelf Steam Rankine cycle

The steam Rankine cycle (SRC) is composed of an oil-free scroll expander, a diaphragm pump, plate-heat exchangers for boiler, and condenser, evacuated tube solar collectors, and a wood-pellet boiler with an additional heat exchanger for preheating the cold water. The input data for the calculation of the SRC using mature technologies are listed in **Table 5.7**

Table 5.7 – Input data (Off-the-shelf steam Rankine cycle).	
Boiling temperature (°C)	100 to 190
Boiler pressure (kPa)	47 to 1255
Built-in volume ratio	3.18 – 4.1
Internal suction volume (cm^3/rev)	52 – 38
Superheating temperature (K)	25
Sub-cooling at the pump inlet (K)	10
Turbine efficiency (%)	50
Pump efficiency (%)	65

The main difference in the design of the SRC depends mainly on the selection of the expander. Therefore, two expanders have been considered in this study with different built-in volumes and internal suction volumes. The expansion ratio and the turbine suction volume have been selected for two oil-free scroll compressors available on the market, which have been previously tested in expander mode with vapor as working fluid. The first expander has an expansion ratio of 3.18 and an internal suction volume of 52 cm^3/rev. It is the same scroll expander as the one tested in Chapter 3, but with a larger internal suction volume selected to reach higher electrical output power. The second oil-free scroll expander has been previously tested by Lemort [LEM06]; its built-in volume ratio is 4.1 and the internal suction volume is 38 cm^3/rev.

Figure 5. presents the steam Rankine cycle (SRC) actual efficiency and electrical output power, calculated for several boiling temperatures, expansion ratios, and turbine suction volumes.

Results show that when the built-in volume ratio is kept constant, the SRC efficiency increases while increasing the boiler temperature. However, under a constant boiling temperature, the SRC efficiency increases when increasing the expansion ratio since the condenser temperature at which heat is rejected becomes lower. On the other hand, the electrical output power increases while increasing the boiling temperature.

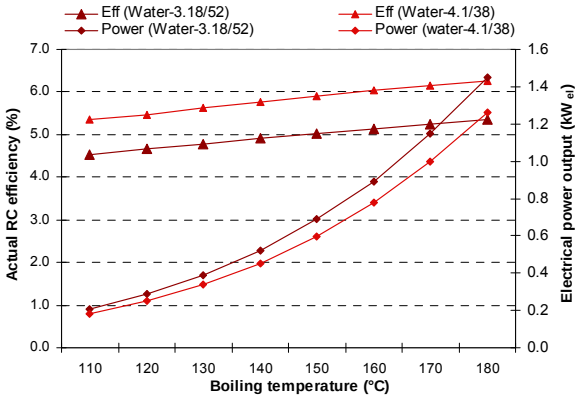

Figure 5.16 – Steam Rankine cycle actual efficiency and electrical output power.

The SRC efficiency reaches a maximum of 6.3 % when the boiling temperature and the expansion ratio are 180°C and 4.1 with an electrical output power of 1.26 kW. Therefore, a system generating 1 kWel could be designed with the two expanders existing on the market. However, the operating temperatures and pressures differ according to the selected expander. In Table 5.8, the two possible SRCs with the same electrical output power are presented with different operating conditions and their corresponding efficiencies. The system designed with the scroll expander used by Lemort et al. [LEM06] shows higher energy performances since the SRC efficiency is 6.13 % with a conversion efficiency of 4.2 % (wood-electricity) and 2.14 % (solar-electricity). The highest overall efficiency is reached by the scroll expander with the largest built-in volume ratio.

Table 5.8 – Off-the-shelf steam Rankine cycle optimum design.

Available and off-the-shelf technologies		
Built-in volume ratio	3.2	4.1
Discharge volume	52	38
Condensing temperature (°C)	118	113
Boiling temperature (°C)	165	170
Boiling pressure (kPa)	700	792
Electrical output power (kWel)	~1	
RC ideal efficiency (%)	10.43	12.35
RC actual efficiency (%)	5.06	6.01
Boiler capacity (kW)	19.77	16.64
Pre-heater capacity (kW)	2.13	1.87
Boiler thermal efficiency (%)	71.4	70
Boiler total efficiency (%)	79.4	78
Solar collector efficiency (%)	36.62	35.61
Total RC efficiency (wood) (%)	3.61	4.2
Total RC efficiency (solar) (%)	1.85	2.14
Power to hear ratio (PHR)	0.047	0.057

5.1.2 Off-the-shelf Organic Rankine cycle

The input data of the organic Rankine cycle designed with the off-the-shelf technologies are listedTable 5.9. Input parameters have been kept similar to the input data of the off-the-shelf steam Rankine cycle except the geometric specification of the expanders, the boiler pressure, and the superheat at the turbine inlet.

The boiling pressure of organic fluids is quite higher than the boiling pressure of water for the same boiling temperature, which is due to the thermodynamic properties of the organic

fluids. The working fluid at the turbine inlet is kept slightly superheated since the efficiency of the organic Rankine cycle decreases while increasing the superheat degree at the turbine inlet. The pressure ratio and the turbine inlet suction volume have been selected according to the available scroll expander. Two scroll expanders have been proposed in the literature. The first one was proposed by Kane [KAN02] with a built-in volume ratio of 2.3 and an internal suction volume of 23 cm^3/rev. The second one, a scroll expander has been proposed by Lemort et al. [LEM06] with a built-in volume ratio of 3.1 and an internal suction volume of 32 cm^3/rev designed originally for refrigeration application (R-404a). All other parameters are kept constant compared to the steam Rankine cycle.

Table 5.9 – Input data (Off-the-shelf Organic Rankine cycle).	
Boiling temperature (°C)	100 to 190
Boiler pressure (kPa)	143 to 3500
Built-in volume ratio	2.3 – 4.1
Turbine inlet suction volume (cm^3/rev)	23 – 32
Superheating temperature (K)	1
Sub-cooling at the pump inlet (K)	10
Turbine efficiency (%)	50
Pump efficiency (%)	65

Figure 5.17 and Figure 5.18 show the ORC actual efficiency and electrical output power respectively, calculated for several boiling temperatures, boiling pressures, pressure ratios, and turbine internal suction volumes. Obviously, the actual ORC efficiency decreases while increasing the boiling temperature and keeping a constant volume ratio; however, it can be seen that the electrical output power of the ORC increases. Therefore, high ORC efficiency with the same electrical output power could be achieved by selecting the most adapted working fluid.

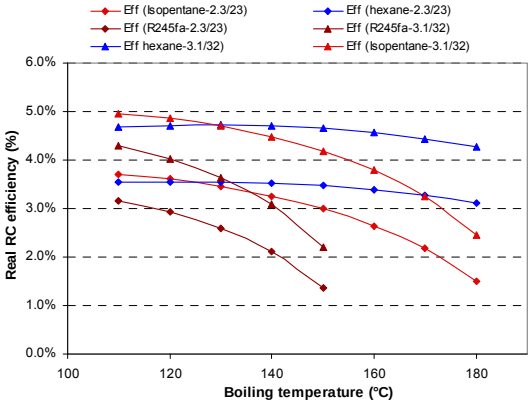

Figure 5.17 – Actual ORC efficiency.

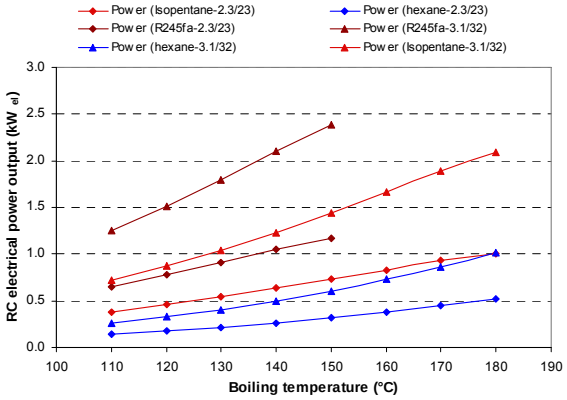

Figure 5.18 – Actual Rankine cycle electrical output power.

The ORC efficiency increases while increasing the volume ratio and keeping the boiler temperature constant, which is due to the lower condensing temperature at which the heat is rejected. The highest ORC efficiency (~ 4.9%) is reached when the boiler temperature is 110°C with isopentane as working fluid corresponding to an electrical output power of 0.6 kW_{el}.

Results show the possibility to design 1-kWel ORC system but the efficiency of the ORC will depend on the working fluid selected and the turbine size. Table 5.10 shows the different operating conditions and their corresponding efficiencies of possible 1-kWel ORC system that could be designed with the available scroll expanders. The highest actual efficiency (4.70%) is reached with isopentane, the operating boiler temperature is 128°C with the expander tested by Lemort et al. [LEM06]. The ORC conversion efficiency is 3.8 % (wood-electricity) and 2.3 % (solar-electricity).

Table 5.10 – Off-the-shelf organic Rankine cycle optimum design.			
Available and off-the-shelf technologies			
Working fluids	Hexane	Isopentane	R-245fa
Built-in volume ratio	3.1	2.3/3.1	2.3
Discharge volume	32	23/32	23
Condensing temperature (°C)	129	147/80	105
Boiling temperature (°C)	180	180/128	137
Boiling pressure (kPa)	1300	3020/1264	2664
Electrical output power (kWel)	1	1	1
RC ideal efficiency (%)	9.44	5.24/10.24	6.06
RC actual efficiency (%)	4.51	1.59/4.90	2.34
Boiler thermal capacity (kW)	21.9	62.7/20.4	42.8
Pre-heater capacity (kW)	2.1	6.2/1.05	1.3
Boiler thermal efficiency (%)	75.5	70/77.3	76.7
Boiler total efficiency (%)	82.7	77.8/81.3	81.3
Solar collector efficiency (%)	36.18	37.04/46.49	45.11
Total RC efficiency (wood) (%)	3.40	1.11/3.78	1.79
Total RC efficiency (solar) (%)	1.63	0.59/2.27	1.05
Power to heat ratio (PHR)	0.043	0.014/0.049	0.023

5.2 Near future Rankine cycle system thermodynamic simulation

The main objective of this section is to evaluate the potential of improving the efficiency and the power delivery of turbine technologies that could be commercialized in the near future. Turbines could be modified to increase their energy efficiency and improve their output power performances. The first option is to optimize the energy performance of the existing expanders, the main issue being a lower internal leakage of scroll turbines. In Chapter 3, the main losses have been described. This option is simulated in this section by increasing the turbine efficiency from 50% to 80% and to perform again calculations presented in the previous section with the new turbine efficiency.

The second option consists in designing a new turbine, which could be volumetric, axial or radial turbine. This new turbine will have the same efficiency as improved scroll expander (80%) but it can be designed to deliver a wide range of electrical output power depending on its design size (pressure ratio and internal built-in volume). This second option will be studied here by making thermodynamic simulations with an energy efficiency of 80% with several pressure ratios.

5.2.1 Near future steam Rankine system

Input data for the near future Rankine system are listed in Table 5.11. The global turbine efficiency is increased from 50% to 80% and its operating expansion ratio has been varied from 2.3 to 11.

Table 5.11 – Input data (Near future steam Rankine cycle).	
Boiling temperature (°C)	100 to 190
Condenser temperature (°C)	80
Boiler pressure (kPa)	47 to 1255
Pressure ratio	2.1 – 26
Superheating temperature (K)	1
Sub-cooling at the pump inlet (K)	10
Turbine efficiency (%)	80
Pump efficiency (%)	65

Table 5.12 shows the results from calculations for the same steam expanders presented below but with an efficiency of 80%. The Rankine cycle efficiency reaches 9.85 %. The conversion efficiencies from wood and solar to electricity are 6.9 % and 3.5 % respectively. The power to heat ratio of the system has been improved and it can be near 0.1 for the SRC operating with the scroll expander tested by Lemort et al. [LEM06]. This system presents an advantage compared to the off-the-shelf SRC, due to its higher power to heat ratio (PHR) that can improve the economic performance of the system.

Table 5.12 – Near future steam Rankine cycle optimum design.		
Near future technologies		
Built-in volume ratio	3.2	4.1
Discharge volume	52	38
Condensing temperature (°C)	118	113
Turbine efficiency (%)	80	
Boiling temperature (°C)	165	170
Boiling pressure (kPa)	700	792
Electrical output power (kWel)	~1	
RC ideal efficiency (%)	10.43	12.35
RC near future efficiency (%)	8.32	9.85
Boiler capacity (kW)	12	10.15
Preheater capacity (kW)	1.34	1.16
Boiler thermal efficiency (%)	71.4	70
Boiler total efficiency (%)	79.4	78
Solar collector efficiency (%)	36.62	35.61
Total RC efficiency NF (wood) (%)	5.94	6.9
Total RC efficiency NF (solar) (%)	3.04	3.50
Power to hear ratio (PHR)	0.08	0.096

Figure 5.19 shows results of calculations performed for the steam Rankine cycle with the advanced design. As it can be expected from the thermodynamic principles, increasing the boiler temperature while keeping the condenser temperature at 80°C will increase the SRC energy efficiency. As discussed previously, the thermal efficiencies of the solar collector and the wood-pellet boilers decrease while increasing the boiling temperature of the SRC. Results show that the conversion efficiency from wood energy to electrical energy increases while increasing the boiling temperature. The conversion efficiency from solar energy to electrical energy shows similar results since the efficiency increases also when increasing the boiling temperature. For the advanced steam Rankine cycle, the total efficiency for wood and solar energy is reached at the highest operating temperature (~190°C). To maintain a reasonable value of the HTF temperature at the exit of the wood-pellet boiler, the maximum boiling temperature will be fixed at 180°C. The corresponding efficiency of the Rankine cycle will be near 16%. The conversion efficiencies for wood and solar to electricity are 9.25% and 5.54% respectively.

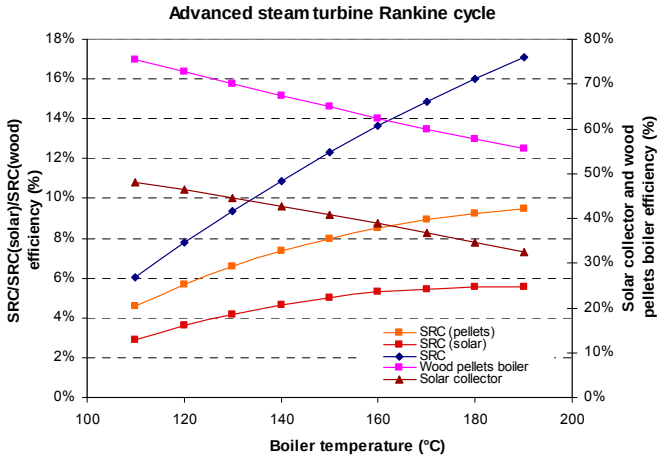

Figure 5.19 – SRC conversion efficiency for advanced turbine design.

5.2.2 Near future organic Rankine cycle

The same procedure as described before is performed to calculate the optimum operating conditions of the organic Rankine cycle for the two types of expanders. Input data for calculations are presented in Table 5.13.

Table 5.13 – Input data (Near future organic Rankine cycle).	
Boiling temperature (°C)	100 to 190
Condenser temperature (°C)	80
Boiler pressure (kPa)	240 to 3400
Pressure ratio	2.3 – 11
Superheating temperature (K)	1
Sub-cooling at the pump inlet (K)	10
Turbine efficiency (%)	80
Pump efficiency (%)	65

Table 5.14 shows the results for the four NFORC systems. As mentioned before, the system operating with isopentane presents the best conversion efficiencies of 5.95 % and 3.58 % for wood and solar respectively.

Table 5.14 – Near future Organic Rankine cycle optimum design.			
Near future technologies			
Working fluids	Hexane	Isopentane	R-245fa
Built-in volume ratio	3.1	2.3/3.1	2.3
Discharge volume	32	23/32	23
Condensing temperature (°C)	129	147/80	105
Boiling temperature (°C)	180	180/128	137
Boiling pressure (kPa)	1300	3020/1264	2664
Electrical output power (kWel)	1	1	1
RC ideal efficiency (%)	9.22	5.16/9.90	5.96
RC near future efficiency (%)	7.07	3.36/7.70	4.24
Boiler thermal capacity (kW)	14.1	29.7/13	23.58
Pre-heater capacity (kW)	1.35	3.3/0.66	1.41
Boiler thermal efficiency (%)	75.5	70/77.3	76.7
Boiler total efficiency (%)	82.7	77.8/81.3	81.3
Solar collector efficiency (%)	36.23	37.08/46.53	45.14
Total ORC efficiency NF (wood) (%)	5.33	2.35/5.95	3.25
Total ORC efficiency NF (solar) (%)	2.56	1.24/3.58	1.91
Power to heat ratio (PHR)	0.07	0.031/0.79	0.041

Figure 5.20 shows results of the NFORC with an advanced turbine. The conversion efficiency from wood and solar to electricity increases while increasing the boiling temperature. The working fluid (hexane) with the highest critical temperature shows the highest conversion efficiency. However, when working on solar energy, the conversion efficiency exhibits an optimum at high temperature and the optimum depends on the working fluids. The highest wood electricity conversion efficiency is about 9.8% while working with hexane at boiling temperature of 180°C. The solar electricity conversion efficiency is about 5.1%.

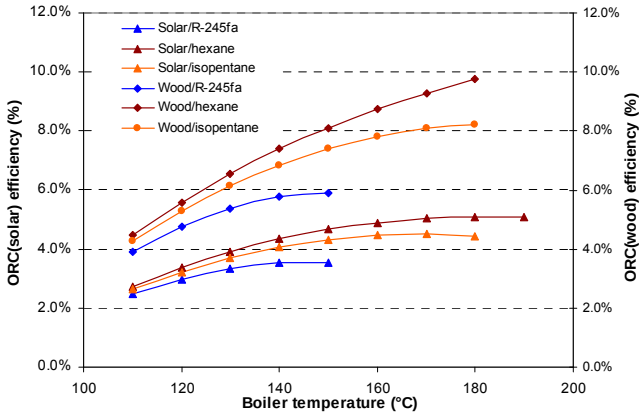

Figure 5.20 – ORC conversion efficiency of advanced turbine design.

5.3 Findings

Four systems have been selected and simulated. Two systems are available on the market with moderate performances and two other systems could be available in the near future with higher energy performances.

Characteristics of the selected Rankine cycle systems are presented in Table 5.15. The NFSRC presents the highest performances for the two heating sources: wood and solar. However, the NFORC presents lower energy performances compared to NFSRC but it has the lowest operating boiling temperature.

The NFSRC presents the highest performance because of its higher thermodynamic efficiency due to the large difference between the boiling and the condensing temperatures. As seen in Table 5.15, even when the boiling temperature is high, the total efficiency defined as the efficiency of the Rankine cycle multiplied by the thermal efficiency of the solar collector or the wood-pellet boiler remains higher for NFSRC compared to NFORC. Therefore, when operating in steady state the NFSRC will present better energy performance compared to NFORC. In dynamic operation mode, the energy performance of systems operating with lower temperatures could be higher since the thermal losses are also higher due to the higher operating temperatures of the solar collectors and the wood-pellet boiler, especially in standby.

Table 5.15 – Comparison between the OFSRC, OFORC, NFSRC, and NFORC.

	OFSFR	OFOFR	NFSRC	NFORC
Working fluid	Water	Isopentane	Water	Isopentane
Boiler temperature (°C)	170	128	180	128
Condenser temperature (°C)	113	80	80	80
Turbine inlet temperature (°C)	195	129	205	129
Volume ratio	4.1	3.1		3.1
Electrical output power (kW_{el})	~1			
Heat capacity (kW_{th})	17.55	20.45	11.36	12.66
Wood-electricity efficiency (%)	4.2	3.78	9.25	5.95
Solar-electricity efficiency (%)	2.14	2.27	5.55	3.58
Power to heat ratio (PHR)	0.057	0.049	0.088	0.079

Micro-CHP systems are designed to meet the maximum heat demand. Therefore, the dimensioning of the micro-CHP system depends on its thermal capacity and not on the electrical output power. When comparing systems generating similar thermal duty, the system with the highest PHR will be the most profitable because of the higher output power. The thermal duty, if associated with an adequate hot water storage can generate power at the peak demand period. The simulation will be conducted for systems representing several thermal capacities and PHRs in order to identify the optimum dimensioning for each building and thermal load.

The NFSRC will not be able to cover all heating needs of the standard building in Trappes since the heating peak load is near 16500 W and the maximum heating capacity that could be delivered by the NFSRC is about 11360 W. Therefore, for the standard building located in Trappes, the NFSRC simulation will not be performed.

6. Simulation results

All simulations presented in the previous sections, have been performed without considering the heat losses due to the transient operation of the CHP system. Therefore, the dynamic simulation program COGENSIM presented previously will be used to simulate the micro-CHP system operating performances to determine its energy performances in dynamic conditions.

The model has been developed to simulate the four micro-CHP systems operating on wood and solar energy under several operating conditions. As mentioned above, two types of buildings have been considered for two locations.

The main additional losses occurring in the system are due to the transient operation of the wood boiler and the solar collector due to heat dissipation during standby. To analyze the effect of the transient operation on the performance of the micro-CHP system, simulations have been performed for several heat storage tank volumes, space heat loads, domestic hot water loads, and global solar irradiances .

In a first step, the energy performances of the micro-CHP operating on wood will be analyzed, as a function of three variables: heat load, heat storage volume, and type of micro-CHP system. In a second step, one additional variable (solar surface area) will be included in the study to analyze the effect of the solar collector field on the performance of the micro-CHP system operating on hybrid mode solar and wood.

6.1 Micro-CHP operating on wood

In Chapter 4, it has been demonstrated that the PES is an adequate parameter to evaluate the micro-CHP system performance. This parameter depends mainly on the electrical and thermal efficiencies of the micro-CHP system. Therefore, in a first step the effects of the hot storage tank volume, heat load, and system design will be studied.

Figure 5.21 shows the annual electrical efficiency for several heat storage tank volumes, micro-CHP system design, and building types. The annual electrical efficiency increases when increasing the volume of the heat storage tank. When increasing the volume of the heat storage tank, the micro-CHP system will operate more continuously and extend its running time; therefore, the losses due to the transient operation will be minimized and the annual electrical efficiency will increase. The maximum electrical efficiency is reached when operating continuously over all the year (see Table 5.15). As it can be expected, the higher the annual electricity generation, the higher the system energy efficiency. For any micro-CHP system with the same heat storage volume, it can be seen that the highest electrical efficiency is obtained for building with the highest heat demand, because for a higher heat demand the system will operate a longer time.

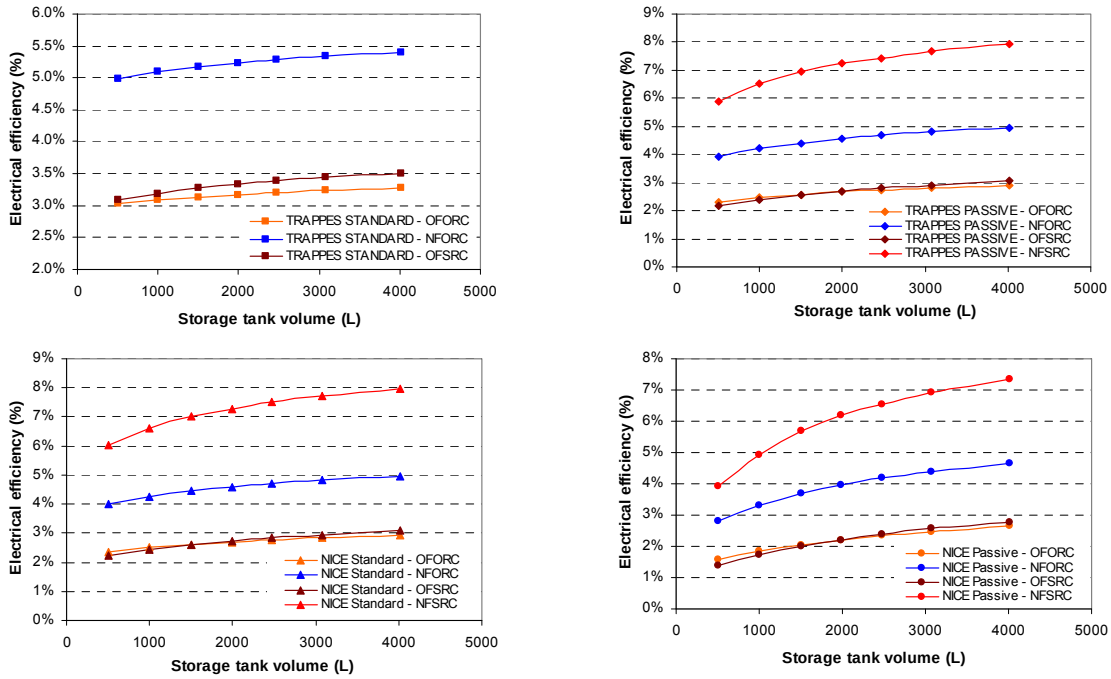

Figure 5.21 – Effect of the heat storage volume tank on the annual electrical efficiency of the micro-CHP system for the four micro-CHPs proposed systems and for buildings.

Figure 5.22 shows the annual thermal efficiency of micro-CHP systems for various storage tank volumes, types of micro-CHP systems, and buildings. The thermal efficiency of the micro-CHP system is defined by Eq. (5.13) where the building heat demand and the domestic hot water demand have been considered as the heat output of the micro-CHP system to take into consideration the heat losses that occur in the heat storage tank.

$$\eta_{th} = \frac{Q_{space\_heat} + Q_{DHW}}{Q_{comb}} \tag{5.13}$$

The thermal efficiency presents an optimum for the different case studies. A larger tank does not represent always the optimum solution, since when increasing the storage tank volume, the heat dissipated by convection losses increases and in most of the cases, for a larger storage tank the heat losses due to convection losses are much higher than the thermal capacity gained from a longer running time. Therefore, an optimum occurs for the thermal efficiency of the system. The optimum volume of the storage tank depends on the type of building, location, and the performance of the micro-CHP system. For each case, an optimum volume exists. This optimum does not represent the overall optimum, as seen in Figure 5.22, since the PES savings still increase while increasing the volume of the storage tank. The maximum volume has been limited in this study to 4000 L.

In addition, the annual thermal efficiency is higher for systems operating at lower boiling temperature, as NFORC and OFORC since the heat losses due to the standby operation are lower. The system annual thermal efficiency is higher when operating in buildings with higher energy consumption.

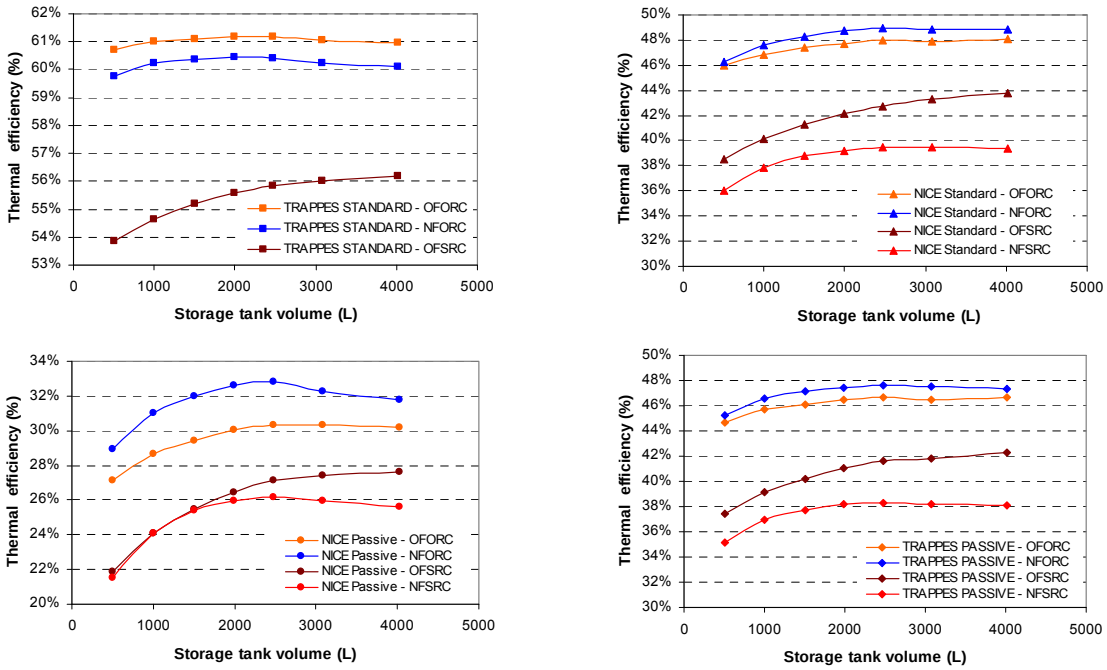

Figure 5.22 – Effect of the heat storage volume tank on the annual thermal efficiency of the micro-CHP system for the four micro-CHP systems and for buildings.

As presented above, the PES increases while increasing the storage tank volume. However, even if in these calculations no optimum has been found, an optimum exists for storage volume larger than 4000 L due to the increase of the annual electrical efficiency.

As presented before, the PES is also higher when operating in buildings with higher heating load demand as seen in Figure 5.23. In Nice, where the space heat load demand is negligible and only the domestic hot water demand is significant, the system could present negative primary energy savings since its thermal and electrical efficiencies are very low compared to the reference case.

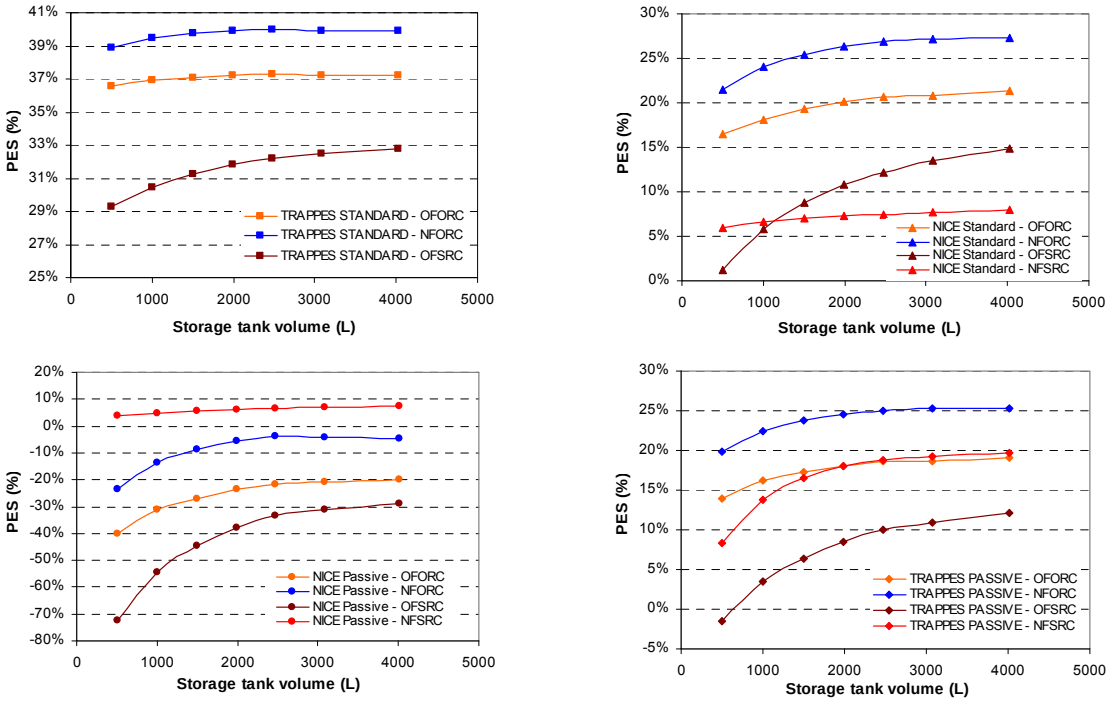

Figure 5.23 – Effect of the heat storage volume tank on the PES of the micro-CHP system for the four micro-CHP systems and for the different buildings ($\eta_{th,ref}$ = 0.7 and $\eta_{el,ref}$ = 1/2.58).

6.2 Dual fuel operation mode

The solar energy absorbed during the hybrid mode operation could be used in four ways:

- If the solar energy is available and the micro-CHP system is turned on; the solar energy will present part of the total generated energy (electricity and heat).
- If the solar energy is available and the micro-CHP system is turned off; the solar energy will be used to preheat the system to the set point operation.
    - o If the set point (tank temperature) is reached, the micro-CHP will be turned on and it will operate totally on solar mode.
    - o If the set point is not reached and the micro-CHP system is turned on because the hot storage tank is empty, the solar energy has been usefully used for pre-heating the system.
    - o If the set point is not reached and the hot storage tank remains full, the system will be cooled down and all the recovered solar energy will be lost to the surroundings.

The simulations performed for the different operating systems show that the solar energy share, which is used for producing electricity and heat or pre-heating the system, is negligible compared to the solar energy absorbed by the solar collectors. Most of the solar energy absorbed by the solar collectors has been dissipated to the surroundings, this being due mainly to the control strategy that is not optimized for dual mode operation.

First, results will be presented for the weak point where the control strategy is applied. Figure 5.24 shows the annual thermal efficiency of the solar collector under different operating conditions.

The performance of the solar collectors in Nice is higher compared to Trappes because the overall solar irradiance and the ambient temperature are higher in Nice. When comparing performances of the solar collectors for buildings situated in the same location with different energy consumption levels, the system with higher heat load demand shows a better performance compared to building with lower heat load demand, even if the thermal efficiency of the solar collectors will be lower when operating at higher temperatures. For the same building type and location, the thermal efficiency of the solar collectors is higher for ORC than for SRC. These results are related to the higher boiling temperature of SRC (170°C) compared to that of ORC (128°C).

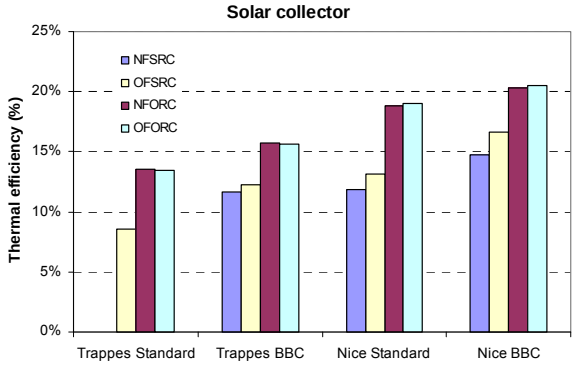

Figure 5.24 – Annual solar collector thermal efficiency for different types of CHP systems, for different building types, and locations (A_{sol} = 30 m^2).

Figure 5.25 shows the solar energy share defined by Eq. (5.14) for the different building types and locations. The useful solar energy is defined as the solar energy absorbed by the solar collectors when the micro-CHP is turned on. The useful boiler energy is defined as the total thermal energy produced by the wood-pellet boiler when the micro-CHP is turned on.

$$Solar\_energy\_share = \frac{Useful\_solar\_energy}{Useful\_boiler\_energy} \quad (5.14)$$

The solar energy share for Nice is higher than Trappes. These results are consistent because the annual solar energy available in Nice is higher than in Trappes and the thermal efficiency of the solar collectors shows higher energy performances when operating in Nice compared to Trappes. The micro-CHP systems operating with lower boiling temperature show higher solar energy share due to the higher thermal efficiency of the solar collectors when operating at lower temperatures.

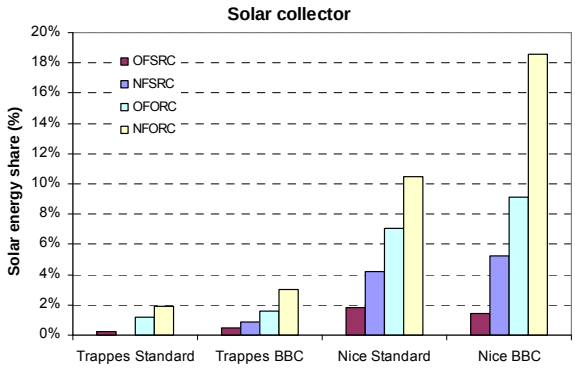

Figure 5.25 – Solar energy share for different types of CHP systems, for different building types, and locations (A_{sol} = 18 m^2).

Comparing the solar energy share of the proposed system with the solar energy absorbed by the solar collectors for the different systems, more than 80% of the solar energy absorbed is dissipated as heat losses to the surroundings due to the current control strategy. To optimize the solar energy share, a conventional control system could not be proposed due to the complexity of the system operation strategy. An advanced control system is the only solution to withstand the difficulties of the solar energy recovery at the right time. An adaptive predictive control algorithm could constitute a solution to this problem.

6.3 Future achievements

In order to evaluate the maximum possible improvements due to a predictive control, the potential solar energy share has been calculated by Eq. (5.15). The useful solar energy has been replaced by the solar energy absorbed by the solar collectors.

$$Solar\_energy\_share = \frac{Absorbed\_solar\_energy}{Useful\_boiler\_energy} \tag{5.15}$$

Results are presented in Figure 5.26. The potential solar energy share could be more than 100% of the heating and cooling needs of the building specifically when low space heat load is required such as the BBC building in Nice. The installation of hybrid systems is more suited in locations where solar energy is more abundant such as Nice. In addition, systems operating with lower boiling temperature could be more efficient in utilizing the available solar energy.

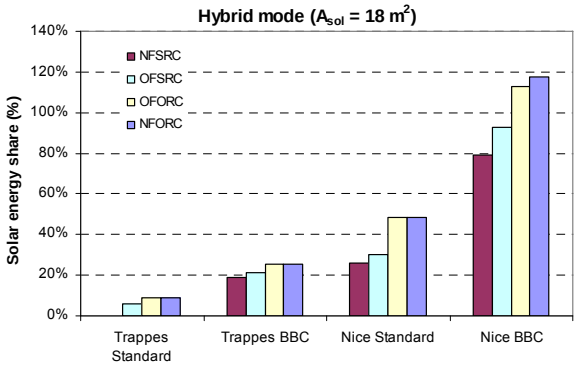

Figure 5.26 – Potential solar energy share for different types of CHP systems, for different building types, and locations.

7. Conclusions

In this chapter, series of simulations have been performed for different buildings coupled to a hybrid solar-wood micro-CHP system on annual basis.

Results have shown that for a 1-kW_{el} operating on wood, the micro-CHP system could achieve more than 40% of PES. The storage tank volume is a key parameter to optimize the system performance; however, this volume could be limited because it can affect slightly the economic performance of the system.

Four Rankine cycle systems have been studied. Results show that the system operating with turbines, that could be commercialized in the near future, presenting higher energy performances are necessary to achieve interesting return on investment.

Systems with lower boiling temperature could absorb more solar energy compared to systems operating with higher boiling temperature. The system with higher boiling temperature presents higher electrical efficiency and higher PHR. Therefore, a compromise should be defined to find a balance between the solar energy share and the system electrical efficiency. This conclusion leads to future research work for the development of an advanced control of the wood-solar CHP systems.

When operating in hybrid mode, results have shown that existing control systems cannot ensure a good operation strategy, since the highest energy solar share achieved with the conventional control system is 18%. However, the potential solar energy could be higher than the thermal needs. Therefore, it is necessary to optimize the operation in hybrid mode. An advanced control system “adaptive predictive control algorithm” should be developed to improve the system operation to take advantage of the available solar energy. The basis of this control is to integrate a prevision model of the solar energy availability and the required heating demand. From this prevision model and the state-of-charge of the hot storage tank, the control system will define the operating mode of the hybrid micro-CHP system in order to maximize the solar energy use.

References

[ARP66] *V.S. Arpaci, Conduction heat transfer, Addition-Wesley Pub., Reading, Mass, 1966.*

[BEJ96] *A. Bejan, G. Tsatsaronis, M. Moran, "Thermal design and optimization", WILEY INTERSCIENCE 1996.*

[BRU94] *S. Brunold, R. Frey, U. Frei, "a comparison of three collectors for process heat applications", SPIE, The International Society for Optical Engineering, 1994.*

[DIN02] *I. Dincer, M.A. Bejan, A. Bejan, "Thermal energy storage systems and application", Published by John Wiley and sons, 2002.*

[HOL88] *J.P. Holmann, Thermodynamics, fourth ed., McGraw-Hill Company,New York, 1988.*

[LEM06] *Lemort, V., Teodoreset, I., Lebrun, J., (2006), Experimental study of the integration of a scroll expander into a heat recovery Rankine cycle, Proc. of 18th Int. compressor eng. Conf. at Purdue: C105.*

[NOR04] *S. Nordlander, "TRNSYS model for type 210 Pellet stove with liquid heat exchanger", Documentation of model and parameter identification, Technical report ISRN DU-SERC-79-SE, Högskolan Dalarna, Borlänge, Sweden, 2003. Available at www.serc.sewww.serc.se, May 2004.*

[PER93] *B. Perers, B. Karlsson, "External reflectors for large solar collector arrays, simulation model and experimental results", J. Int. Solar energy Soc., 51, 327-337, 1993.*

[PEU90] *B. Peuportier, I. Blanc-Sommereux, "simulation tool with its expert interface for the thermal design of multizone buildings", Int. J*. Solar energy 8, 109-120, 1990.*

[REF06] *E.W. Lemmon and M.O. McLinden, "Reference fluid thermodynamic and transport properties", NIST standard reference Database 23, Version 7, Beta version 21/13/02.*

[SIM04] *Simbad, 2004. SIMBAD Building and HVAC Toolbox, CSTB. http://ddd.cstb.fr/simbad*

General conclusion and perspectives

Because of the large abundance of the solar and biomass energy in the world, a micro-CHP system operating on solar and biomass energy has been described in this thesis. First, it was demonstrated that the ORC is the best-suited thermodynamic cycle that could be used for micro-CHP system while operating with renewable energies available at low temperature (from 100 to 200 °C).

Micro-CHP systems present many advantages compared to conventional heating systems since they can present higher primary energy and lower CO_2 emissions. However, when the reference system of electrical generation presents low level of CO_2 emissions as in France, conventional micro-CHP systems could not be justified from an environmental point of view. Therefore, micro-CHP systems operating on renewable energies could constitute an alternative option compared to conventional micro-CHP systems that could present many advantages by saving energy and reducing CO_2 emissions while producing electricity.

In order to develop a safe and efficient system, the selection of working fluids is one of the most important issues to reach energy-efficient ORC. A general method has been elaborated for comparing different working fluids for the Rankine cycle operating with low-grade heat. The elaborated comparison criteria do not include only performance criteria, but also safety and environmental criteria. In addition, special tools have been developed to analyze the effect of the different working fluids on the design and sizing of the ORC system components and their impact on costs.

Four different working fluids: water, hexane, isopentane, and R-245fa have been identified as potential working fluids. Each of this working fluid presents advantages and drawbacks. It was demonstrated that a compromise has to be made by the designer to choose the best working fluid according to each application.

The different technologies, which could be used for the manufacturing of micro-CHP system, have been identified. Some of the components are off-the-shelf and other components could be converted from available technologies with minor modifications. However, for reaching higher energy performances, it is important to conduct R&D studies for the development of new technologies of expanders able to deliver the specific electrical capacity with higher efficiency.

Except Rankine turbines, all Rankine components could be found on the market, and meet a wide range of capabilities. The Rankine expander could be converted from available volumetric compressors (scroll, screw, vane…). Designing a completely new turbine, presenting a higher global efficiency and meeting exactly the desired operating range, is also an option, but requires significant means.

A test bench has been designed to test an oil-free scroll compressor that has been converted to operate as an oil-free vapor scroll expander. The maximum volumetric and isentropic efficiencies measured are 60% and 48% respectively. Results of the tested expander have shown moderate efficiency; however, some improvements could be made to achieve higher efficiencies with different power output capabilities.

After evaluating the different technical barriers to be overcome for improving the performance of the system, an economical study has been performed to identify the different economic incentives, which should be imposed by the government to help and encourage the development of these systems. Results show that a LEC of 40 to 60 c€/kWh_{el} should be applied for systems operating only on wood energy. However, when operating in hybrid mode with solar collectors added to the system, higher LEC should be applied depending on the solar energy share. This economic analysis shows that the LEC is very sensitive to the cost of heat avoided and it will be more economical to introduce these systems to the market when the price of energy used in conventional heating system is higher.

A dynamic simulation tool COGENSIM has been developed to simulate the annual performance of the system operating on wood only and on hybrid mode for different building types, climate conditions, and operating parameters. Four different micro-CHP systems have been proposed representing different energy performances and operating parameters depending on the working fluid used, operating temperatures, and expander type.

The simulation results show that the micro-CHP system operating with steam presents the highest efficiency compared to the Organic Rankine cycle. On the other hand, when operating at lower boiling temperature, which is the case with Organic Rankine cycle, the system annual efficiency could be higher than that of systems operating at high boiling temperatures since the heat losses in transient phases and standby operation could be minimized.

Simulations have shown that building with higher thermal needs is more suitable for the integration of micro-CHP system. Therefore, when the building becomes more thermally efficient, the economical feasibility of the micro-CHP system decreases. To overcome this economical difficulty, low energy collective buildings will be the best option to integrate these systems.

The systems operating in hybrid mode could be interesting in terms of primary energy savings when solar energy is abundant especially in the Mediterranean climate. Moreover, to recover more efficiently the available solar energy, a special predictive adaptive control system should be developed.

Appendices

Appendix A

- Law of 13 July 2005 [LOI05]: Increase of 50% in the production of electricity from renewable energy sources by 2010.
- Incentive and fiscal measures: Payments of half the cost of pellets boiler purchased for private individual application.
- French thermal regulation "RT2005" [RTH05]: The primary energy consumption for heating, cooling, lighting, ventilation, and domestic hot water of the buildings complying with the "RT2005" are set between 80 and 250 kWh_{pe}/m^2.year according to energy sources, architecture shape, and climate zones.
- Decree of 15 September 2006 [ARR06a]: Reduction of energy consumption by the introduction of energy efficiency certificates (see Figure 1). This energy certificate will encourage the owner to improve the energy performance of its building.

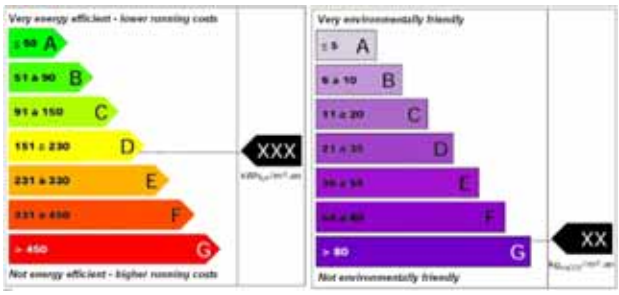

Figure 1 – Home energy performance rating charts.

Appendix B

Cost data

The cost data of the different components of the hybrid solar/wood micro-CHP system is derived from the different costs given by the components suppliers. Table 1 shows the correlations used for the cost calculations of the different components.

Table 1 – Cost data.

Component	Correlation	Constant
Wood pellet boiler	$C_{pellets,boiler} = C_{1,pellets,boiler} * P_{pellets,boiler} + C_{2,pellets,boiler}$	$C_{1,pellets,boiler} = 56.59$, $C_{2,pellets,boiler} = 7984$
Plate heat exchanger	$C_{PHX} = C_{1,PHX} * \ln(A_{PHX}) + C_{2,PHX}$	$C_{1,PHX} = 377$, $C_{2,PHX} = 908$
Turbine (scroll expander)	$C_{exp,Y} = C_{exp,X} * ((V_Y/V_x)(Pr_Y/Pr_X))^{0.6}$	$C_{exp,X} = 4000$, $V_x = 31.5\ cm^3/rev$, $Pr_x = 3.18$
Pump	$C_{pump} = C_{1,pump}$	$C_{1,pump} = 2000$ €
Solar collectors	$C_{solar} = C_{1,sol} * A_{sol}$	$C_{1,sol} = 500$ €
Recuperator	$C_{rec} = C_{1,rec} * (Q_{rec}/DT_{lm})$	$C_{1,rec} = 6.23$ €/(W/K)

Appendix C

Combustion Model

- **Heat of combustion (HOC)**

The combustion heat is calculated from the weight and the lower heating value of the pellet.

$$\dot{Q}_{comb} = LHW\dot{m}_{pell}$$

Where LHV is the lower heating value of the pellets and m_{pell} is the mass flow rate of consumed pellet. The lower heating value is delivered by the wood pellets suppliers. For the calculation, the moisture of the wood pellets has been set to 6% and the LHV is 18 MJ/kg.

To calculate the moisture content of the fuel, $m_{H2O,fuel}$ is given per kg of humid wood pellet, thus the following correlation is valid.

$$\dot{m}_{H_2O,\,fuel} = Y_{H_2O,\,fuel}\, m_{fuel,h}$$

Solving for $m_{H20,fuel}$ gives the following expression

$$\dot{m}_{H_2O,\,fuel} = \frac{Y_{H_2O,\,fuel}\dot{m}_{fuel,dry}}{1 - Y_{H_2O,\,fuel}}$$

The composition (mass fraction) of the dry wood pellet is given in Table 1

Table 1 – Wood pellets composition.		
		Y [%]
Carbon	C	51.3
Hydrogen	H_2	6.2
Nitrogen	N_2	<0.1
Oxygen	O_2	42.2
Ashes		0.25

Combustion reaction

For a fuel containing C (Carbon), H_2 (hydrogen), N_2 (Nitrogen), O_2 (Oxygen), and A, the chemical reactions for the combustion (oxidation) can be written

$$C + O_2 \rightarrow CO_2$$

$$H_2 + \frac{1}{2}O_2 \rightarrow H_2O$$

Here we assume that no CO (Carbon monoxide) or NOx is produced. Usually the concentration of NOx and CO in the flue gases is far below 1000 ppm (1%) for wood pellet boilers so the influence on the energy efficiency is small.

From the chemical reaction in Equations 2 and 3, an expression for the required amount of oxygen for stoichiometric combustion can be derived. The oxygen in the fuel is used during the combustion and the oxygen demand is therefore reduced by the oxygen content in the fuel. Stoichiometric combustion is complete combustion with minimum required amount of oxygen. Ashes do not take part in the reactions.

$$N_{O_2,stoic} = \frac{m_{C,fuel}}{MW_C} + \frac{m_{H_2,fuel}}{2MW_{H_2}} + \frac{m_{O_2,fuel}}{MW_{O_2}}$$

The amount of air is assumed to be 4.773 times the amount of oxygen for stoichiometric combustion because the air has been assumed to be composed respectively of 0.79 and 0.21 for N_2 and O_2 in molar fraction.

$$N_{air,stoic} = 4.773\left(\frac{m_{C,fuel}}{MW_C} + \frac{m_{H_2,fuel}}{2MW_{H_2}} + \frac{m_{O_2,fuel}}{MW_{O_2}}\right)$$

The number of moles of Nitrogen in the combustion air can also be calculated separately in relation to the stoichiometric O_2 demand as follows:

$$N_{N_2,stoic,air} = 3.73N_{O_2,stoic}$$

Therefore, the necessary amount of air is calculated as follows:

$$N_{air,stoic} = N_{O_2,stoic} + N_{N_2,stoic,air}$$

The total amount of dry flue gases is calculated from the sum of N_2 and CO_2 in the flue gases.

$$N_{flue,stoic} = N_{CO_2,stoic} + N_{N_2,stoic}$$

The molar concentration of species I in a mixture of species can be calculated by

$$\chi_i = \frac{N_i}{N_{tot}}$$

And mass fractions can be calculated by

$$Y_i = \frac{m_i}{m_{tot}} = \frac{\chi_i MW_i}{MW_{mix}}$$

The air factor λ is defined as the rate between real dry air consumption and the theoretical amount of dry air required achieving stoichiometric combustion.

$$\lambda = \frac{N_{air}}{N_{air,stoic}}$$

This relation can be used to calculate the amount of excess air in the combustion, which is the additional air that is not used in the combustion. The dry amount of excess air can be calculated.

$$N_{air,exc} = N_{air} - N_{air,stoic} = (\lambda - 1)N_{air,stoic}$$

From the knowledge of the consumed wood pellet, the amount of stoichiometric air and excess air the total mass of the flue gases can be calculated

$$m_g = m_{fuel} + m_{H_2O,fuel} - m_{ashes} + m_{air,stoic} + m_{H_2O,air,stoic} + m_{air,exc} + m_{H_2O,air,exc}$$

The total mass can also be calculated from the components in the flue gas as

$$m_g = N_{H_2O} MW_{H_2O} + N_{CO_2} MW_{CO_2} + N_{N_2} MW_{N_2} + N_{O_2} MW_{O_2}$$

From the chemical reactions and from the stoichiometric air consumption N_2/O_2stoic, the number of moles of the carbon dioxide at stoichiometric conditions can be calculated. The non-burning components in the fuel, nitrogen and ashes, are assumed to have negligible impact on the flue gases. Also the relatively low production of CO and NO_x is ignored.

$$N_{CO_2,stoic} = \frac{m_{C,fuel}}{MW_C}$$

CO_2 contained in the flue gases comes from the combustion of the carbon in the wood pellets.

$$N_{N_2} = \frac{m_{N2,fuel}}{MW_{N2}} + \frac{\chi_{N_2,air} N_{O_2,stoic}}{\chi_{O_2,air}} + N_{air,exc} \chi_{N_2,air}$$

$$N_{O_2} = N_{air,exc} \chi_{O_2,air}$$

The water in the flue gases comes from the oxidation of hydrogen in the fuel, from the humidity in the fuel, and from the humidity in the combustion air, and can be expressed as

$$N_{H_2O} = \frac{m_{H_2,fuel}}{MW_{H_2}} + \frac{m_{H_2O,fuel}}{MW_{H_2O}} + \frac{\chi_{H_2O,air} N_{air,stoic} MW_{air}}{MW_{H_2O}} + \frac{\chi_{H_2O,air} N_{air,exc} MW_{air}}{MW_{H_2O}}$$

Heat capacity of the flue gases

The capacity of the flue gases is estimated by weighting the heat capacity for the different species by the mass fractions.

$$c_{p,g} = Y_{H_2O} c_{p,H_2O} + Y_{CO_2} c_{p,CO_2} + Y_{N_2} c_{P,N_2} + Y_{O_2} c_{p,O_2}$$

The heat duty has been calculated by regression function depending on the temperature of the flue gases.

Appendix D

Boiler Model

The heat duty of the flue gases can be calculated as follows

$$\dot{Q}_g = \dot{m}_g c_{p,g} \left(T_{comb} - T_{out} \right)$$

The mass flow rate of the flue gases are calculated from the composition of the different species as described in Appendix C and $c_{p,g}$ is evaluated at the average temperature of T_{comb} and T_{out}. On the other hand, T_{comb} represents the adiabatic combustion temperature, calculated depending on the LHV, MFR of the wood pellets, and the excess of air.

To calculate the outlet temperature of the gases and the HTF at the exit of the wood pellets boiler, the equation of the thermal energy balance will be solved simultaneously for the gases and the HTF as written below

$$\dot{Q}_g = \dot{m}_g c_{p,g} \left(T_{comb} - T_{g,out} \right) = UA_{\text{int}} \left(T_{comb} - T_{htf,out} \right)$$

$$\dot{Q}_g = \dot{m}_{htf} c_{p,htf} \left(T_{htf,out} - T_{htf,in} \right) = UA_{\text{int}} \left(T_{comb} - T_{htf,out} \right) + UA_{ext} \left(T_{htf,out} - T_{amb} \right) + M_{htf} C_{p,htf} \frac{dT_{htf,out}}{dt}$$

The exterior heat transfer coefficient U_{ext} is assumed to be 0.2 W/m^2.K and the interior heat transfer coefficient is calculated at the rated power from the different parameters given by the wood boiler supplier.

Appendix E

Domestic hot water production

Hourly profile. Coefficients α_i $\left(\sum \alpha_i = 24\right)$			
Period	**J1**	**J2**	**J3**
0 à 1 h	0.02	0.06	0.05
1 à 2 h	0.02	0.04	0.05
2 à 3 h	0.01	0.02	0.02
3 à 4 h	0.01	0.02	0.02
4 à 5 h	0.02	0.01	0.02
5 à 6 h	0.20	0.05	0.02
6 à 7 h	1.60	0.35	0.04
7 à 8 h	3.30	1.07	0.36
8 à 9 h	1.80	2.21	1.28
9 à 10 h	1.50	2.59	2.63
10 à 11 h	1.23	2.63	3.53
11 à 12 h	0.90	1.83	2.94

Hourly profile. Coefficients α_i $\left(\sum \alpha_i = 24\right)$			
Period	**J1**	**J2**	**J3**
12 à 13 h	1.10	1.50	1.74
13 à 14 h	1.42	1.94	1.38
14 à 15 h	0.80	1.72	1.56
15 à 16 h	0.50	**1.06**	1.00
16 à 17 h	0.54	0.73	0.74
17 à 18 h	0.85	0.89	0.68
18 à 19 h	1.65	1.38	1.30
19 à 20 h	1.90	1.34	1.59
20 à 21 h	2.25	1.19	1.59
21 à 22 h	1.30	0.60	0.68
22 à 23 h	0.78	0.44	0.59
23 à 24 h	0.30	0.33	0.19

J1: (Monday, Tuesday, Wednesday, Thursday, Friday) J2: (Saturday) J3: (Sunday)

Weekly profile. Coefficients c_i $\left(\sum c_i = 7\right)$						
Monday	**Tuesday**	**Wednesday**	**Thursday**	**Friday**	**Saturday**	**Sunday**
0.96	0.86	0.92	0.87	0.90	**1.19**	1.30

Monthly profile. Coefficients c_m $\left(\sum c_m = 12\right)$											
January	February	March	April	Mai	June	July	August	September	October	November	December
1.26	**1.20**	1.10	1.06	1.00	0.80	0.50	0.60	0.90	1.05	1.15	1.40

Cold water temperature [°C] for each climate zone						
Zone	**January**	**February**	**March**	**April**	**Mai**	**June**
H1	5.7	5.7	7.0	9.2	11.8	14.0
H2	7.2	7.2	8.5	10.7	13.3	15.5
H3	9.7	**9.7**	11.0	13.2	15.8	18.0

Cold water temperature [°C] for each climate zone						
Zone	**July**	**August**	**September**	**October**	**November**	**December**
H1	15.3	15.3	14.0	11.8	9.2	7.0
H2	16.8	16.8	15.5	13.3	10.7	8.5
H3	19.3	19.3	18.0	15.8	13.2	11.0

Domestic hot water needs (L/day) at 60°C					
Number of room	1	2	3	4	5
DHW needs (L/day)	75	105	150	180	240